Modulation of parathyroid hormone 1 receptor (PTH1R) signaling by receptor activity-modifying proteins (RAMPs)

Regulierung der Signalübertragung des Parathormon 1-Rezeptors (PTH1R) durch Rezeptoraktivitäts-modifizierende Proteine (RAMPs)

Doctoral thesis for a doctoral degree
at the Graduate School of Life Sciences,
Julius-Maximilians-Universität Würzburg,
Section Biomedicine
Submitted by

Katarina Nemec
from Murska Sobota, Slovenia

Berlin **2022**

Modulation of parathyroid hormone 1 receptor (PTH1R) signaling by receptor activity-modifying proteins (RAMPs)

Regulierung der Signalübertragung des Parathormon 1-Rezeptors (PTH1R) durch Rezeptoraktivitäts-modifizierende Proteine (RAMPs)

Doctoral thesis for a doctoral degree
at the Graduate School of Life Sciences,
Julius-Maximilians-Universität Würzburg,
Section Biomedicine
Submitted by

Katarina Nemec
from Murska Sobota, Slovenia

Berlin **2022**

Submitted on:

Members of the Promotionskomitee:

Chairperson: **Prof. Dr. Peter Jakob**

Primary Supervisor: **Prof. Dr. Martin J. Lohse**

Supervisor (Second): **Prof. Dr. Manfred Schartl**

Supervisor (Third): **Prof. Dr. Kathleen Caron**

Supervisor (Fourth): **Dr. Isabella Maiellaro**

Date of Public Defence:

Date of Receipt of Certificates:

AFFIDAVIT

I hereby confirm that my thesis entitled **"Modulation of parathyroid hormone 1 receptor** (**PTH1R**) **signaling by receptor activity-modifying proteins** (**RAMPs**)**"** is the result of my own work. I did not receive any help or support from commercial consultants. All sources and / or materials applied are listed and specified in the thesis.

Furthermore, I confirm that this thesis has not yet been submitted as part of another examination process neither in identical nor in similar form.

Place, Date Signature

EIDESSTATTLICHE ERKLÄRUNG

Hiermit erkläre ich an Eides statt, die Dissertation **„Regulierung der Signalübertragung des Parathormon 1-Rezeptors** (**PTH1R**) **durch Rezeptoraktivitäts-modifizierende Proteine** (**RAMPs**)**"** eigenständig, d.h. insbesondere selbständig und ohne Hilfe eines kommerziellen Promotionsberaters, angefertigt und keine anderen als die von mir angegebenen Quellen und Hilfsmittel verwendet zu haben.

Ich erkläre außerdem, dass die Dissertation weder in gleicher noch in ähnlicher Form bereits in einem anderen Prüfungsverfahren vorgelegen hat.

Ort, Datum Unterschrift

Modulation of parathyroid hormone 1 receptor (PTH1R) signaling by receptor activity-modifying proteins (RAMPs)

Doctoral thesis by
Katarina Nemec

ABSTRACT

The receptor activity-modifying proteins (RAMPs) are ubiquitously expressed membrane proteins that interact with several G protein-coupled receptors (GPCRs), the largest and pharmacologically most important family of cell surface receptors. RAMPs can regulate GPCR function in terms of ligand-binding, G-protein coupling, downstream signaling, trafficking, and recycling. The integrity of their interactions translates to many physiological functions or pathological conditions.

Regardless of numerous reports on its essential importance for cell biology and pivotal role in (patho-)physiology, the molecular mechanism of how RAMPs modulate GPCR activation remained largely elusive.

This work presents new insights that add to the common understanding of the allosteric regulation of receptor activation and will help interpret how accessory proteins - RAMPs - modulate activation dynamics and how this affects the fundamental aspects of cellular signaling. Using a prototypical class B GPCR, the parathyroid hormone 1 receptor (PTH1R) in the form of advanced genetically encoded optical biosensors, I examined RAMP's impact on the PTH1R activation and signaling in intact cells. A panel of single-cell FRET and confocal microscopy experiments as well canonical and non-canonical functional assays were performed to get a holistic picture of the signaling initiation and transduction of that clinically and therapeutically relevant GPCR. Finally, structural modeling was performed to add molecular mechanistic details to that novel art of modulation.

I describe here that RAMP2 acts as a specific allosteric modulator of PTH1R, shifting PTH1R to a unique pre-activated state that permits faster activation in a ligand-specific manner. Moreover, RAMP2 modulates PTH1R downstream signaling in an agonist-dependent manner, most notably increasing the PTH-mediated Gi3 signaling sensitivity and kinetics of cAMP accumulation. Additionally, RAMP2 increases PTH- and PTHrP-triggered β-arrestin2 recruitment to PTH1R and modulates cytosolic ERK1/2 phosphorylation. Structural homology modeling shows that structural motifs governing GPCR-RAMP interaction originate in allosteric hotspots and rationalize functional modulation. Moreover, to interpret the broader role of RAMP's modulation in GPCRs pharmacology, different fluorescent tools to investigate RAMP's spatial organization were developed, and novel conformational biosensors for class B GPCRs were engineered. Lastly, a high throughput assay is proposed and prototyped to expand the repertoire of RAMPs or other membrane protein interactors.

These data uncover the critical role of RAMPs in GPCR activation and signaling and set up a novel platform for studying GPCR modulation. Furthermore, these insights may provide a new venue for precise modulation of GPCR function and advanced drug design.

CONTENT

LIST OF FIGURES

LIST OF TABLES

ABBREVIATIONS

β_2AR	β2 adrenergic receptor
β-arr	β-arrestin
aa	amino acid
AC	adenylyl cyclase
ACKR	atypical chemokine receptor
AB	acceptor bleaching
AM	adrenomedullin (receptor)
AMY	amylin
ATP	adenosine triphosphate
B1 GPCR	secretin-like family G protein-coupled receptor
B2 GPCR	adhesion family G protein-coupled receptor
BRET	bioluminescence resonance energy transfer
BSA	bovine serum albumin
CaSR	calcium-sensing receptor
cAMP	cyclic adenosine monophosphate
camps	cyclic adenosine monophosphate sensor
CFP	cyan fluorescent protein
CHO	chinese hamster ovary
CNBD	cyclic nucleotide-binding domain
CRF	corticotropin-releasing factor
CT	calcitonin
CRLR	calcitonin receptor-like receptor
CTR	Calcitonin receptor
DAG	diacylglycerol
DMEM	Dulbecco's modified Eagle medium
DMSO	dimethylsulfoxide
dNTPs	deoxyribonucleotides
DPBS	Dulbecco's phosphate buffered saline
EC_{50}	half maximal effective concentration
ECD	extracellular domain
ECL	extracellular loop
EDTA	ethylenediaminetetraacetic acid
EM	electron microscopy
E_{max}	maximum effect
Epac	exchange protein directly activated by cyclic adenosine monophosphate
ER	endoplasmic reticulum
ERK	extracellular signal-regulated kinase
EYFP	enhanced yellow fluorescent protein
FACS	fluorescence-assisted cell sorting
FBS	fetal bovine serum
FDA	food and drug administration

FP	fluorescent protein
FRET	fluorescence resonance energy transfer
Fsk	forskolin
$GABA_{B1}$	gamma-aminobutyric acid receptor B1
GAP	GTPase-activating protein
GCGR	glucagon receptor
GDP	guanosine diphosphate
GEF	guanine nucleotide exchange factor
GFP	green fluorescent protein
GIPR	gastric inhibitory polypeptide receptor
GIRK	G protein-coupled inwardly rectifying potassium channel
GLP1	glucagon-like peptide 1
GPCR	G protein-coupled receptor
GRK	G protein-coupled receptor kinase
GTP	guanosine triphosphate
h	hours
HEK	human embryonic kidney
HDX-MS	hydrogen-deuterium exchange - mass spectrometry
HTS	high throughput screening
GLP1R	glucagon-like peptide 1 receptor
IBMX	3-Isobutyl-1-methylxanthine
IC_{50}	half maximal inhibitory concentration
ICL	intracellular loop
IP3	inositol triphosphate
IRES	internal ribosomal entry site
JMC	Jansen's metaphyseal chondrodysplasia
kDa	kilo Dalton
LB	lysogeny broth
LH	luteinizing hormone
MAPK	mitogen activated protein kinase
mC	mCitrine
mem	membrane
min	minutes
ms	milliseconds
mT2	mTurquoise2
NFκB	nuclear factor kappa-light-chain enhancer of activated B cells
Nluc	nanoluciferase
nm	nanometer
NMR	nuclear magnetic resonance
ns	not significant
p	probability value
PACAP	pituitary adenylate cyclase-activating polypeptide
PCR	polymerase chain reaction
PDE	phosphodiesterase
PDL	poly-D-Lysine

PI3K	phosphoinositide 3-kinase
PIP2	phosphatidylinositol-4,5-bisphosphate
PKA	protein kinase A
PKC	protein kinase C
PLC	phospholipase C
POI	protein of interest
POPDC	Popeye domain containing protein
PPI	protein - protein interaction
PTH	parathyroid hormone
PTH1R	parathyroid hormone 1 receptor
PTH2R	parathyroid hormone 2 receptor
PTHrP	parathyroid hormone-related peptide
R	receptor
RAMP	receptor activity-modifying protein
RFP	red fluorescent protein
RGS	regulator of G protein signaling
ROI	region of interest
RPM	rounds per minute
s	seconds
SD	standard deviation
SEM	standard error of mean
TAE	tris acetate buffer
TIP	tuberoinfundibular peptide
TIRF	total internal reflection fluorescence
TM	transmembrane domain
TR FRET	time-resolved FRET
TSB	transformation storage buffer
UAA	unnatural amino acid
VIP	vasointestinal peptide
YFP	yellow fluorescent protein

1. INTRODUCTION

1.1 G protein-coupled receptors

Characterized by their seven helices, embedded in the membrane's lipid bilayer, seven-transmembrane receptors (7TM), or more commonly, G protein-coupled receptors (GPCRs) constitute the most extensive family of membrane proteins in the human body. As of now, more than 800 genes are known which encode for a group of surface proteins that are the critical signal transducers in our body. GPCRs transduce signals from extracellular space to the cell interior in the process of receptor activation. The engagement of receptors with the various stimuli initiates allosteric rearrangements in the structural core, enabling intracellular transducers' binding. The primary transducer – guanine nucleotide-binding protein or simpler G protein gave the name to this superfamily of receptors since most of the GPCRs couple to one of their subtype proteins. Transducers and further downstream effectors induce a multitude of signaling pathways, which later modulate various cellular responses, gene expression, and transcription regulation. GPCRs are involved in vision, gustation, regulation of ion homeostasis, embryonic development, and growth of the organs. Since those receptors comprise a myriad of functions, is the knowledge about their activation and signaling of the utmost importance for medicine and, subsequently, drug discovery. Approximately 1/3 of therapeutics target GPCR-related signaling cascades, and hence, GPCRs represent the most important and studied pharmacology scope (Pierce *et* al., 2002; Hill, 2006; Rosenbaum *et* al., 2009; Hilger *et* al., 2018; Hauser *et* al., 2018).

1.1.1 GPCR structural characteristics and classification

GPCRs are characterized by their seven transmembrane helices (TM1-TM7), nested in the membrane's lipid bilayer. Seven helices are connected by three intracellular loops (ICL-1, ICL-2, and ICL-3), and three extracellular loops (ECL-1, ECL-2, and ECL-3). Amino-terminus (N-terminus) is positioned in the extracellular and carboxy-terminus (C-terminus) in the intracellular space (**Figure 1A**). Helices are organized in a circular way within the membrane's lipid bilayer (**Figure 1B**). The cavity between TM3, TM5, TM6, and TM7 creates an orthosteric ligand-binding pocket, although growing evidence suggests that certain agonists can also bind intracellularly (Ortiz Zacarías *et* al., 2018). Helices are generally made of 20 – 27 amino acids, whereas other parts, C- and N-terminal domains and loops, display great variety within and between classes and receptors. ECLs are additionally often stabilized with disulfide bonds. Helix-8 is a prolongation of TM7 and spans into the intracellular space. Different numbering systems are used to identify similar residues across the receptor structures (Isberg *et* al., 2015). For class A GPCRs is mostly used Ballesteros-Weinstein numbering system, for class B GPCRs Wootten, for class C GPCRs Pin, and for class F GPCRs Wang numbering. In brief, the first number represents helix (TM1-7), and the second residue the placement relative to the most conserved residue, Pro 5.50, which gets the number 50. Since all schemes use similar formatting, it is helpful to add a class name to identify which classification is used (*e.g.*, 5.40a stands for residue, located in TM5, ten residues before the most conserved residue, Pro 5.50). “a” symbolizes that it refers to class A of GPCRs and hence Ballesteros-Weinstein numbering.

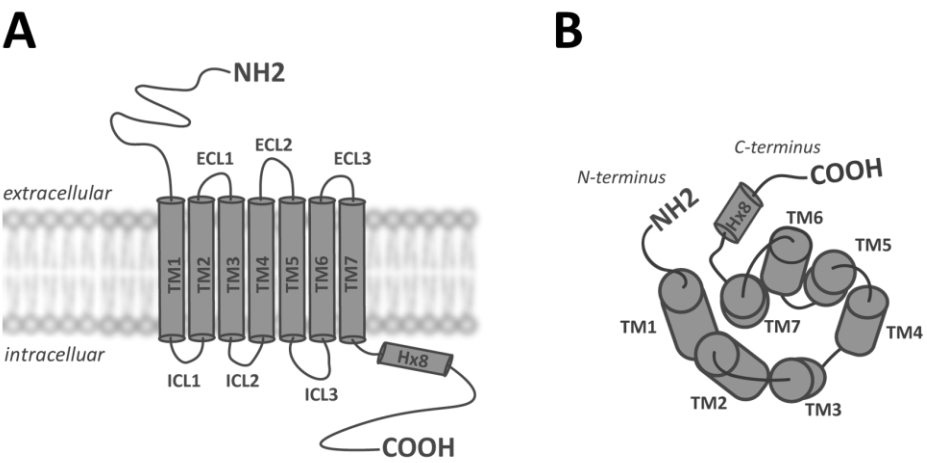

Figure 1: GPCR architecture.
*Seven transmembrane helices (7TM) embedded in the lipid bilayer of the membrane are connected with three extracellular (ECL) and three intracellular loops (ICL) (**A**). Helices are organized in a circular way (**B**).*

Two different classification systems emerged over the years to organize this superfamily of receptors. A newer system is the GRAFS classification, relying on phylogenetic analysis of GPCR sequences and classifies GPCRs into five classes (**Table 1, Figure 2**). Some GPCRs remain outside this classification, particularly a few orphan receptors (Fredriksson *et* al., 2003).

An older classification, classifying GPCRs into A to T classes, is based on structural characteristics: functional similarity and sequence homology (**Table 1**), includes all GPCRs of vertebrates and invertebrates, although some of the included GPCRs are not expressed in the human body (classes D and E) (Attwood & Findlay, 1994; Kolakowski, 1994).

Classes overlap; the main difference is a further division of class B in GRAFS classification, divided into secretin-receptor and adhesion receptor families.

GRAFS	
Basis	Phylogenetic tree
Class	**Family**
G	**G**lutamate
R	**R**hodopsin
A	**A**dhesion
F	**F**rizzled/Taste2
S	**S**ecretin

Homology and structural properties classification	
Basis	Homology and structural properties
Class	**Family**
A	Rhodopsin-like
B	Secretin (B1) and Adhesion (B2)
C	Metabotropic glutamate
D	Fungal mating pheromone (D1)
E	Cyclic AMP
F	Frizzled/Smoothened
T	Taste

Table 1: GRAFS and homology and structural properties classification systems for GPCRs.

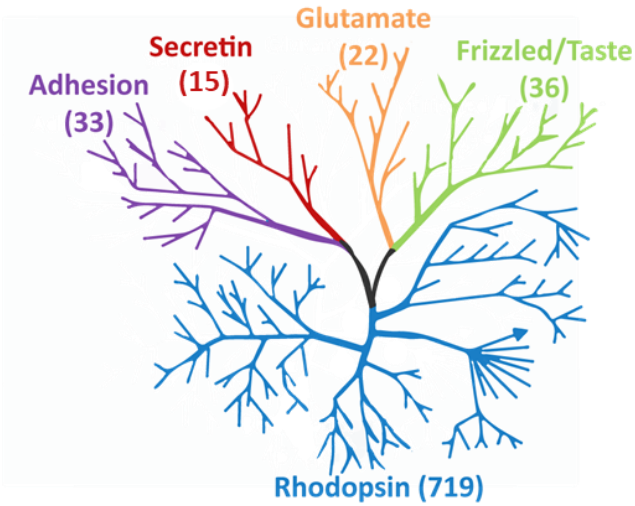

Figure 2: GRAFS classification of GPCRs and number of associated receptors.

1.1.2 GPCR activation

In the process of receptor activation, a GPCR translates extracellular signals through allosteric conformational changes into the intracellular space. After the association of GPCRs with its cognate agonist, conformational changes commence in the process of ligand-binding. After allosteric spread through the receptor core to induce the opening of an intracellular cavity to accommodate intracellular effectors – G proteins or arrestins.

GPCRs make an allosteric transition from the inactive to the active state through many intermediate conformations (Latorraca *et* al., 2017; Hilger *et* al., 2018). Recent crystallographic work, cryogenic electron microscopy (cryo-EM), nuclear magnetic resonance (NMR) structures, and single-molecule fluorescence techniques help to understand the extent of conformational dynamics that GPCRs adopt during the activation process. The number of structures available is growing immensely, and with it, the understanding of their activation mechanism (Manglik *et* al., 2015; Manglik & Kruse, 2017; Latorraca *et* al., 2017; Hauser *et* al., 2021).

The activation process of GPCRs commences with ligand-binding into orthosteric binding pockets, located at different positions in diverse receptor classes. The classical ligand-binding place is in the middle of the TM helices (TM3, TM5, TM6, and TM7) in class A. The class C binding pocket is in the extracellular domain, and in classes B and F, big peptidic ligands bind with a two-step binding mechanism to both – extracellular domains and between TMs. Ligands and receptors differ significantly between classes, but with a subset of common activation mechanisms, it is possible to outline receptor activation in a few critical points (Hauser *et* al., 2021; Kooistra, Munk, *et* al., 2021).

Figure 3 visualizes the activation process of a prototypical GPCR. Following ligand-binding, rotation and significant outward movement of TM6 represent the most common features of the activation process (3 - 20 Å for different classes and different G protein partners), which opens an intracellular cavity for the binding of the G protein. Slight inward rotations and movement of TM5 and TM7 can be seen while the binding site packs the ligand, contributing to the high-affinity binding and efficient engagement of the ligand with the receptor core. The activation process is facilitated by newly made or dissociated intramolecular interactions: salt bridges, hydrophobic interactions, and hydrogen bonds. Water molecules promote the stabilization of the ligand in the binding pocket. The process enables the binding of intracellularly located G protein: the C-terminus of the Gα subunit anchors into the receptor core near the GPCRs' IL2, which further stabilizes the fully active state (Mahoney & Sunahara, 2016; Manglik & Kruse, 2017).

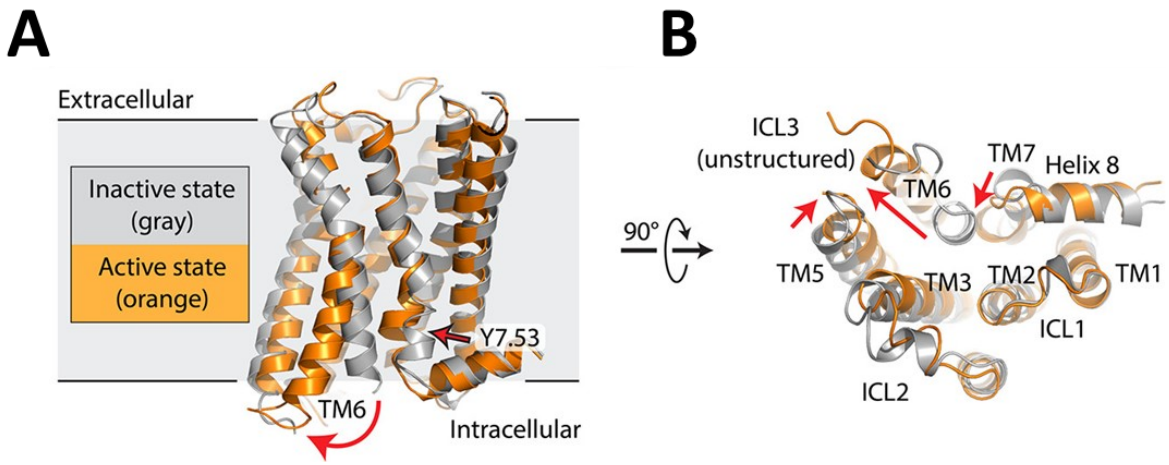

Figure 3: Comparison of active and inactive states for a prototypical GPCR.

(A) *Inactive-state (gray, PDB entry 3UON) and active-state (orange, PDB entry 4MQS) structures of the human M2 muscarinic acetylcholine receptor are shown in a side view, parallel to the membrane plane. Red arrows indicate conformational changes upon activation. (**B**) Same structure, viewed from the intracellular side. Adapted with permission from (Manglik & Kruse, 2017). Copyright 2017 American Chemical Society.*

Structural diversity between the receptor classes also directs different activation processes, and most described are patterns that drive class A (Deupi & Kobilka, 2007; Hilger *et* al., 2018), B (Hilger *et* al., 2020; Qiao *et* al., 2020; Cong *et* al., 2022), C (Kunishima *et* al., 2000; Hlavackova *et* al., 2012; Grushevskyi *et* al., 2019), F (Qi *et* al., 2019; Kowalski-Jahn *et* al., 2021; Wright *et* al., 2019; Schihada *et* al., 2021; Turku *et* al., 2021) and very recently also adhesion class of GPCRs (Barros-Álvarez *et* al., 2022; Ping *et* al., 2022; Qu *et* al., 2022; Xiao *et* al., 2022).

Comparing multiple inactive and active structures allowed recognition of critical structural motifs governing the receptor activation process. The active structure is maintained with polar interactions between NPxxY and CWxP motifs located at TM6 and TM7, respectively. The inactive structure is mainly maintained via a salt bridge between the DRY motif residues, located at TM3 (or related in other subclasses). If residues around this motif are mutated, a receptor can display the constitutively active phenotype (Schipani *et* al., 1995, 1999, 2009). Further **microswitches** induce activation, which was recently described in detail by Venkatakrishnan *et* al. and Hauser *et* al. (Venkatakrishnan *et* al., 2016; Hauser *et* al., 2021). Those microswitches are located at similar receptor areas and are more conserved within the classes. In class A, key microswitches are: the DRY (TM3), the CWxP (TM6), the NPxxY (TM7), PIF or PAF motif, and Na^+ pocket (Nygaard *et* al., 2009; Zhou *et* al., 2019). In class B1, similarly important microswitches are: HETX, NPGQ, and P6.47xxG6.50 motif (TM6) (Yin *et* al., 2017; L.-H. Zhao *et* al., 2019; Cong *et* al., 2022). For class B2, HETX motif, central ionic lock between H2.50b and E3.50b, and intracellular ionic lock between R2.46b and E8.49b (Arimont *et* al., 2019) represent the critical microswitches. In class F, two important microswitches were identified - R/K6.32f (Wright *et* al., 2019) and P6.43f (TM6) (Turku *et* al., 2021).

Another hallmark of the GPCR activation process is that different ligands use slightly different residues to exert activation of the receptor and, through them, stabilize diverse receptor conformations, which may dictate specific downstream signaling pathways (Flock *et* al., 2017; Gregorio *et* al., 2017; Hauser *et* al., 2021; Heydenreich *et* al., 2021). Such described conformational selection is a mechanistic explanation for biased signaling. Today we know that the binding of various transducers to GPCRs triggers diverse responses of downstream signaling pathways. **Biased signaling** is the ligand-dependent activation of certain pathways over

others, and can lead to a **functionally selective response** (definition from Kolb *et* al). It is accepted in the community after years of evidence showing that the rank order of ligands by potency could be different for different pathways engaged by a single receptor (Roth & Chuang, 1987; Spongier *et* al., 1993) or inversion of the ligand modality (Azzi *et* al., 2003; Baker *et* al., 2003). The binding of specific ligand can trigger **temporally** (primary and secondary waves of signaling (Grundmann & Kostenis, 2017)), **spatially** (signaling in different parts of the cell surface or intracellular vesicles (Mohammad Nezhady *et* al., 2020; A. D. White *et* al., 2021)) and **functionally** different patterns (diverse functional outcomes (Urban *et* al., 2007)) (Lohse & Calebiro, 2013). Extensive guidelines and terminology were recently published to decrease poor reproducibility and facilitate descriptions of bias in the field (Kolb *et* al., 2022).

The vision for the drugs of the future is that ligand will use only the desired type of active receptor form, which will trigger a cascade of predicted signaling. Therefore, developing better drugs with higher efficacy and fewer adverse effects is of high interest in the field (Kenakin & Christopoulos, 2013; Kenakin, 2019). Nevertheless, only very recently first biased agonist, oliceridine, was approved by Food and Drug Administration (FDA) Agency for moderate to severe acute pain in adults (Mullard, 2020).

Sequence (Thompson *et* al., 2014; Hauser *et* al., 2018), expression profile (Kenakin, 2019), and functionally diverse GPCR isoforms (Marti-Solano *et* al., 2020) also contribute to signaling diversity and orchestrate the ability of GPCRs to respond to a variety of stimuli and transduce them into different signaling patterns in distinct physiological systems. Accumulated knowledge about mentioned areas helps us to understand how GPCRs as “allosteric microprocessors“ through simple switches exert numerous biological roles (Smith *et* al., 2018).

1.1.3 GPCR signaling

Different activation patterns can induce different signaling patterns (**Figure 4**). Previous understanding of canonical GPCR signaling proposed that GPCRs can (only) induce G protein-related signaling, routing their signaling cascade according to the interacting G protein alpha subunit (Gs, Gi, Gq, G11/12, G13, …). Some of the receptors decide exclusively for one coupler, whereas others pleiotropically couple to more downstream effectors to induce diverse signaling patterns (Flock *et* al., 2017; Hauser *et* al., 2022). Moreover, although being called G protein receptors, increasing evidence suggests that some of the GPCRs are actually (also) β-arrestin coupled receptors (Lefkowitz *et* al., 2006; Shukla *et* al., 2008; Gesty-Palmer *et* al., 2009; Reiter *et* al., 2012; Pandey *et* al., 2021), and induce signaling profiles downstream of those effectors, which were traditionally viewed as responsible for receptor desensitization (Benovic *et* al., 1987a). A multitude of intracellular partners and various functions that regulate signaling were visualized by Apostolakou *et* al. in a freely available web application that enables exploration of the human GPCR network in a cell-type-specific manner (Apostolakou *et* al., 2020).

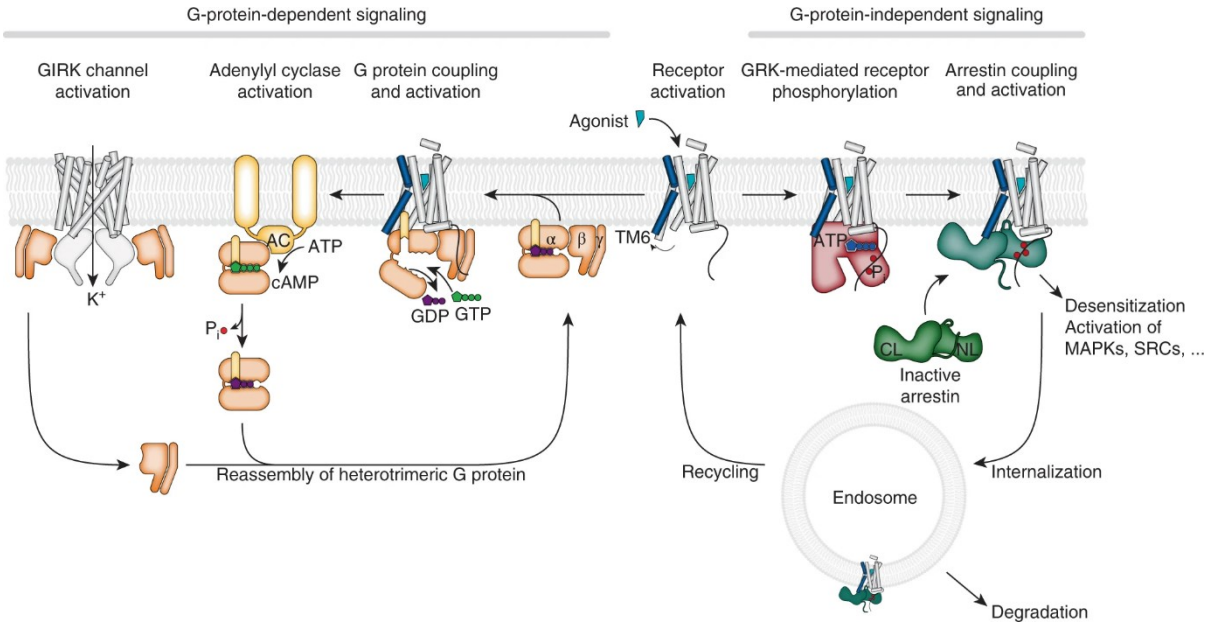

Figure 4: GPCRs and their signal transduction.
Reprinted by permission 5282031368877 from Springer Nature: Nature Structural & Molecular Biology, Structure and dynamics of GPCR signaling complexes, Daniel Hilger et al., Copyright © 2018, Springer Nature (2018).

1.1.3.1 G protein-dependent signaling

Ligand-stimulated activation of GPCRs mainly initiates G protein signaling (Lefkowitz, 2000; Pierce *et* al., 2002; Rasmussen *et* al., 2007; Flock *et* al., 2017; Liu *et* al., 2019). Heterotrimeric G proteins consist of three subunits: Gα, Gβ, and Gγ (Rodbell *et* al., 1971; Ross & Gilman, 1977; Gilman, 1987). There are 38 known Gα subunits (21 in humans), 5 Gβ, and 12 Gγ subunits (Downes & Gautam, 1999; McCudden *et* al., 2005; Hauser *et* al., 2022), which creates a vast number of different combinations, which is expected to be tissue-dependent and thus, regulating numerous intracellular roles (Hauser *et* al., 2022). The α subunit gave the name to the four families which share homology and downstream signaling pathways: **Gs** (G_s and G_{olf}) (Northup *et* al., 1980), **Gi/o** (G_{i1}, G_{i2}, G_{i3}, G_o, G_z, G_{t1}, G_{t2}, and G_{gust}) (Codina *et* al., 1984; Bokoch *et* al., 1984), **Gq/11** (G_q, G_{11}, G_{14}, and G_{15}) and **G12/13** (G_{12} and G_{13}) (Downes & Gautam, 1999). According to a recent metastudy, most of the GPCRs couple to $G_{i/o}$ family (64 %), followed by G_s (55 %), $G_{q/11}$ (50 %), and least to $G_{12/13}$ (25 %) (Hauser *et* al., 2022). **Figure 5** portrays G protein families and their regulation of downstream signaling.

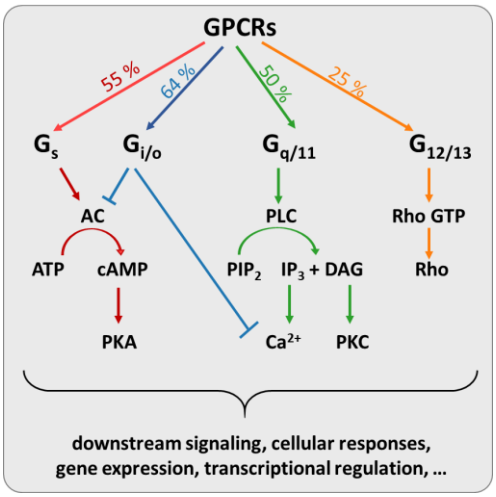

Figure 5: G protein-mediated signaling pathways.

The basal state of a G protein is characterized by the heterotrimeric complex Gαβγ and guanosine diphosphate (GDP) bond to the Gα subunit. Ligand-induced receptor activation leads to structural changes in the receptor core (**Chapter 1.1.2**) and the opening of an intracellular cavity of GPCRs for the binding of the G protein – the α5-helix of Gαs docks into a cavity formed on the intracellular side of the receptor by opening TM5 and TM6.

Agonist-bound GPCRs act as guanine nucleotide exchange factor (GEF), and facilitate switching from an inactive, GDP-bound state to an active GTP-bound state. This leads to conformational changes in the α-subunit, which then separates from the βγ-subunit – and both signaling modules can regulate the activity of effector proteins (Milligan & Kostenis, 2006; Pierce *et* al., 2002; Rasmussen *et* al., 2007; Smrcka, 2008). Activation of G proteins is terminated by the nucleotide guanosine triphosphate hydrolase (GTPase) activity of the α-subunit (Cassel & Selinger, 1976), which induces hydrolysis of one phosphate of GTP and leads to Gβγ reassociation with GDP-bound Gα subunit and, thus, a recreation of the inactive form of GDP-bond heterotrimeric complex Gαβγ. For *de novo* activation, new interaction with the receptor is necessary. The GTPase process can be modulated by the GTPase-accelerating protein (GAP) activity of the regulator of G protein signaling (RGS) proteins (Lambert *et* al., 2010).

Subunits in the heterotrimeric GαβɣX proteins have different roles; the Gα subunit is responsible for GTP and GDP binding and GTP hydrolysis, and further activation of enzymes or downstream effectors, whereas the Gβγ subunit represents a stable complex and also acts as independent signaling modality (Milligan & Kostenis, 2006; Smrcka, 2008).

Coupling of GPCR to Gs leads to the dissociation of Gβγ away from Gα, which binds to and activates an enzyme adenylyl cyclase (AC), that catalyzes the conversion of adenosine triphosphate (ATP) into cyclic adenosine monophosphate (cAMP), one of the leading second messengers in the cell (Ross & Gilman, 1977). An increased level of cAMP in the cell stimulates the activity of cAMP effector proteins: cyclic nucleotide-gated ion channels, exchange proteins activated by cAMP (EPAC), popeye domain-containing proteins (POPDC), or the enzyme protein kinase A (PKA). PKA can further phosphorylate many different proteins, including enzymes, receptors, or transcription factors (Rosenbaum *et* al., 2009, p.; Weis & Kobilka, 2018).

Contrary, $G_{i/o}$ proteins inhibit AC activity and its downstream consequences (Codina *et* al., 1984; Bokoch *et* al., 1984).

Coupling to Gq activates phospholipase C (PLC), which catalyzes the conversion of phosphatidylinositol 4,5-bisphosphate (PIP_2) into inositol-1,4,5-trisphosphate (IP_3) and diacylglycerol (DAG). It leads both to Ca^{2+} release (second crucial second messenger in the cell) as well to the activity of protein kinase C (PKC) (Mizuno & Itoh, 2009). Recent studies suggest that it can also regulate G protein-coupled receptor kinase (GRK) signaling (Kawakami *et* al., 2022).

The last group, $G_{12/13}$ proteins, regulate the activity of Rho GTPases, which modulate intracellular kinase activity; they induce activation of Rho A or GRKs (Milligan & Kostenis, 2006).

G protein βγ subunit can function as a separate signaling entity; most prominently, it recruits GRKs to the membrane and regulates the activity of specific channels (*e.g.*, G protein-coupled, inwardly rectifying K+ (GIRK) channels or Ca^{2+} channels) (Smrcka, 2008).

Although the conventional view of GPCR signaling suggests that GPCR – G protein interaction happens and ends on the cell surface, is now already well established that as class A as well class B GPCR can induce prolonged signaling from endosomal compartments (Ferrandon *et* al., 2009; Calebiro *et* al., 2009; Irannejad *et* al., 2013; Kuna *et* al., 2013; Merriam *et* al., 2013; Feinstein *et* al., 2013; Andreassen *et* al., 2014; Lyga *et* al., 2016; Yarwood *et* al., 2017) and trans-Golgi network (Godbole *et* al., 2017). The mechanism of prolonged signaling is described in detail in **Chapter 1.2.4.2** for the parathyroid hormone 1 receptor.

1.1.3.2 G protein-independent signaling

To turn off the continuous stimulus of active GPCRs and in the same moment to signal through G protein independent cascades, GRKs prepare GPCRs for arrestin binding while they phosphorylate serines and threonines, located in the intracellular part of GPCRs (in ICL3 and C-terminus) (Tesmer *et* al., 2005; Krasel *et* al., 2005; Komolov & Benovic, 2018; Q. Chen *et* al., 2021; Drube *et* al., 2022a). This process is regulated via distinct "phosphorylation barcodes," influenced by ligand, GPCR type, as well depending on one of the seven GRKs isoforms. "Phosphorylation barcodes" dictate different patterns of β-arrestin conformations, efficiencies, and amplitudes of recruitment and, hence, a continuation of signaling or its termination (Luttrell & Lefkowitz, 2002; Tobin, 2008; Nobles *et* al., 2011; Liggett, 2011; Shukla *et* al., 2013; Nuber *et* al., 2016; Mayer *et* al., 2019; Latorraca *et* al., 2020). Independently of β-arrestin-mediated desensitization, other downstream-activated kinases such as PKA and PKC can phosphorylate and desensitize receptors (Hausdorff *et* al., 1989; Lohse, 1993; Tobin *et* al., 2008).

As it has become clear that β-arrestin binding does not only terminate signaling but also serves as a signaling unit, more and more downstream effectors are being identified that sense β-arrestin activation: Src kinases, mitogen-activated protein kinases (MAPK) (*e.g.,* extracellular-regulated kinases (ERKs)), p38 MAPK, and C-Jun N-terminal kinase (JNK) 3 (Luttrell & Lefkowitz, 2002; Gurevich & Gurevich, 2019).

It is highly debated if β-arrestin signaling can also exist independent of G proteins and thus create biased signaling profiles (Reiter *et* al., 2012). Recent studies in β-arrestin knock-out cell lines denied such G protein-independent, β-arrestin-dependent signaling (Alvarez-Curto *et* al., 2016; Grundmann *et* al., 2018), but the saga continues as some labs started to identify GPCR-like receptors which are (solely) β-arrestin-coupled (ACRs) (Pandey *et* al., 2021).

β-arrestin functions go beyond this. Most prominently, β-arrestin induces internalization via a dynamin-dependent process into clathrin-coated vesicles, directs GPCRs to different locations across the cell, or forwards them for de-/ubiquitination and degradation. In addition, internalized GPCRs can be dephosphorylated and recycled back to the membrane (Luttrell & Lefkowitz, 2002; Lefkowitz *et* al., 2006) or, in some cases, continue signaling from endosomes (Ferrandon *et* al., 2009; Mullershausen *et* al., 2009; Calebiro *et* al., 2009; Vilardaga *et* al., 2012; Kuna *et* al., 2013; Wehbi *et* al., 2013; Merriam *et* al., 2013; Andreassen *et* al., 2014; Godbole *et* al., 2017; Yarwood *et* al., 2017; Nguyen *et* al., 2019).

Of four different genes that encode arrestin proteins, two exist only in photoreceptors and are thus called visual arrestins, arrestin1 and arrestin4 (Benovic *et* al., 1987a; Craft *et* al., 1994). Non-visual arrestins or β-arrestins are ubiquitously expressed β-arrestin1 (arrestin2) and β-arrestin2 (arrestin3) (Lohse *et* al., 1990; Attramadal *et* al., 1992), which serve as multifunctional proteins for all non-visual GPCRs. They got their name after first identified interacting partner in the non-visual system, β-adrenergic receptor, thus β-arrestins (Lohse *et* al., 1990).

1.2 Class B1 GPCRs

Class B GPCRs are divided into **class B1 (secretin-like family)** and **class B2 (adhesion family)**. Class B1 GPCRs consist of 15 members, phenotypically further divided into five subclasses: calcitonin (CT) family, corticotropin-releasing factor (CRF) family, glucagon family, parathyroid hormone (PTH) family, and vasointestinal peptide (VIP) and pituitary adenylate cyclase-activating polypeptide (PACAP) family (**Figure 6**).

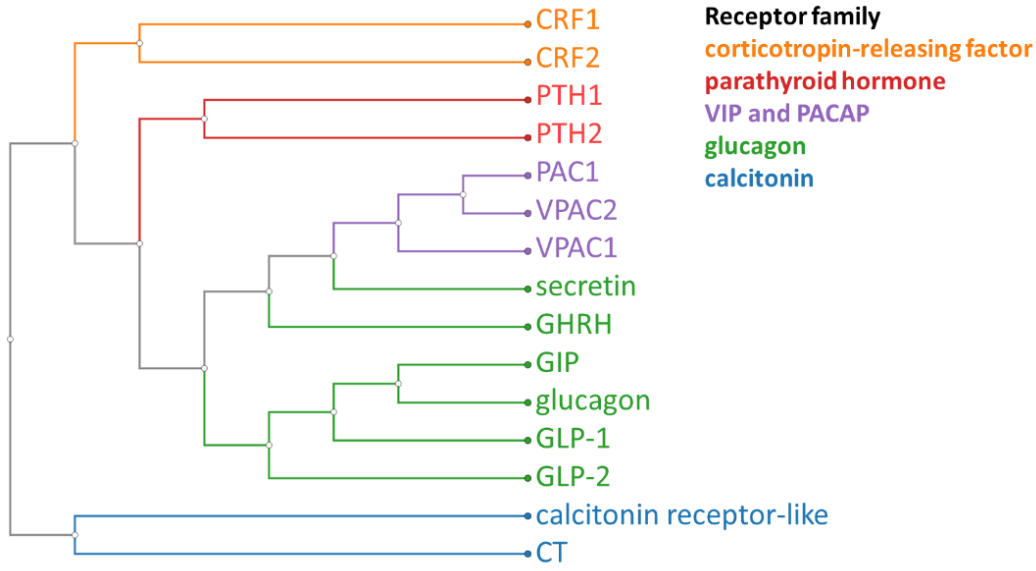

Figure 6: Phylogenetic tree of class B GPCRs.

The phylogenetic tree was created with the GPCRdb tool "sequence comparison" followed by the phylogenetic tree. Structurally conserved sequence segments were selected, and a phylogenetic tree was visualized as a horizontal dendrogram (Isberg et al., 2016; Kooistra, Mordalski, et al., 2021; Pándy-Szekeres et al., 2022).

Most of the ligands for those receptors can be assigned through receptor family names and are structurally polypeptide hormones, governing critical physiological functions (**Table 2**). Their actions are primarily transduced via the Gs signaling pathway, and some of them display prolonged signaling from endosomes: PTH1R (Ferrandon *et* al., 2009), glucagon-like peptide 1 receptor (GLP1R) (Kuna *et* al., 2013), PAC1R (Merriam *et* al., 2013), CTR (Andreassen *et* al., 2014), CRLR (Yarwood *et* al., 2017). Interestingly, an increasing number of studies suggest that internalized receptors modulate some vital physiological functions such as glucose-stimulated insulin secretion in pancreatic β-cells (Kuna *et* al., 2013), pain transmission (Yarwood *et* al., 2017), and synthesis of rate-limiting amount of enzymes (A. D. White *et* al., 2021).

Structurally, class B1 GPCRs consist of an extensive N-terminal ECD, which is highly mobile and involved in a two-step ligand-binding process (Hollenstein *et* al., 2014; Cong *et* al., 2022). In the first step of the binding process, the C-terminal part of the peptide contacts the N-terminus of receptors ECD in rapid ~140 ms long action, which is followed by slower insertion of the N-terminal domain of peptide deep into the conserved orthosteric binding pocket, which coincides with receptor conformational switch and lasts for ~1 s (Vilardaga *et* al., 2003a; Castro *et* al., 2005). Most class B receptors bind their receptors in extended helical conformation, except CTR and CRLR, where C-terminal parts are unfolded, to accommodate receptor accessory protein (RAMP) binding (Liang, Belousoff, Zhao, *et* al., 2020; Sutkeviciute & Vilardaga, 2020). Note, since only shorter versions of peptides were used for recent structures (*e.g.*, LA-PTH, ePTH), it might be that the C-terminal part, in reality, adapts to the unfolded form. In comparison to class A, during the activation process, TM6 moves for

as much as 20 Å (6–14 Å in class A GPCRs) to create a V-shaped cavity for the binding of the α5 helix of the G protein. This displacement is supported by the conserved NPGQ motif (TM6). Interestingly, ligand-dependent bias and allosteric modulation play an important role in the receptor's ECD/ECL conformations. For example, for GLP1R, the nonpeptidic biased agonist TT-OAD2 binds at a higher level in TMD and thus increases ECD mobility, which is, in related studies, correlated with Gs protein activation kinetics (P. Zhao *et* al., 2020; Deganutti *et* al., 2022). For PTH1R, engagement with different ECL2 results in biasing receptor phenotype; ECD-binding antibody fragment can abolish β-arrestin recruitment with unaffected Gs signaling (Sarkar *et* al., 2019), and specific ligand can, while engaging with ECL2, induce structure-encoded allosteric coupling, regulating key interactions between PTH1R's ICL3 and β-arrestins (L. J. Clark *et* al., 2020a). Moreover, ECD/ECL conformations can be modulated by RAMPs; in CRLR and CTR, RAMPs influence the dynamics of ECD in a RAMP-dependent manner (Liang, Belousoff, Fletcher, *et* al., 2020; Cao *et* al., 2022).

Receptor	Agonists	Antagonists	Physiological role	Disease	Drugs (mode of action, clinical phase/marketed)
CRF1	CRF	astressin	response to stress	depression, PTSD, alcoholism	Verucerfont (non-peptide antagonist, II)
	Ucn1	CP 154,526		cerebral edema	Corticorelin (ovine CRF, agonist, phase III)
CRF2	CRF	antisauvagine	response to stress	depression	
	Ucn1	astressin	cardiac contractility		
	Ucn2				
PTH1	PTH	TIP39 (7-39)	calcium and phosphate homeostasis, bone growth, skeletal development	osteoporosis, hypo/hyperparathyroidism, metaphyseal Jansen chondrodysplasia, Blomstrand chondrodysplasia, Eiken syndrome, dental ankylosis, Ollier enchondromatosis, primary failure of tooth eruption	Teriparatide (PTH analog, agonist, marketed) Abaloparatide (PTH-PTHrP chimera, agonist, marketed)
	PTHrP				
PTH2	TIP (1-39), PTH	TIP39 (7-39)	hypothalamic secretion, calcium transport, nociception mediation, wound healing	osteoarthritis, syndromic short stature	
PAC1	PACAP-27, ACAP-27, PACAP-38	PACAP (6-38)	neuroendocrine	migraine	AMG301 (antibody, antagonist, phase II)
VPAC1	VIP, PACAP-27, PACAP-38	PG (97-269)	vasodilation		
VPAC2	VIP, PACAP-27, PACAP-38	PG (99-465)	vasodilation	Sjögren's syndrome	
GHRH	GHRH	JV (1-37)	growth hormone release	HIV-associated lipodystrophy	Tesamorelin (GHRH analog, agonist, marketed)
GIP	GIP		insulin secretion		
GLP-1	GLP-1, GLP-1(7-36)	exendin-(9-39)	insulin secretion	type 2 diabetes	Exenatide (GLP-1 analog, agonist, marketed), Liraglutide (GLP-1 analog, agonist, marketed), Lixisenatide (GLP-1 analog, agonist, marketed), Albiglutide (GLP-1 albumin fusion, agonist, phase III), Dulaglutide (GLP-1 Fc fusion agonist, phase III), TTP-054 (modified-peptide agonist, phase I), …
GLP-2	GLP-2	GLP-2(3-33)	gut mucosal growth	short bowel syndrome	Teduglutide (GLP-2 analog, agonist, marketed), Apraglutide (GLP-2 analog agonist, phase II)
				chemotherapy-induced diarrhea	Elsiglutide (peptide agonist, phase III)
GCGR	glucagon	des-His1-[Leu4-Glu9]-glucagon-NH2	glucose homeostasis	type 2 diabetes	LY-2409021 (non-peptide antagonist, phase I), TT-401 (peptide agonist, phase I), ZP-2929 (peptide agonist, phase I)
Secretin	secretin		pancreatic secretion		Secretin synthetic porcine (agonist, phase II)
CT	CT	CT (8-32) salmon	calcium homeostasis	osteoporosis, hypercalcemia, Paget's disease	Miacalcitonin (salmon agonist, agonist, marketed), Elcatonin (calcitonin, agonist, marketed)
AMY1 (CT, RAMP1)	amylin	a-CGRP (8-37)	vasodilation	types 1 and 2 diabetes	Pramlintide (amylin analog, agonist, marketed)
AMY2 (CT, RAMP2)	amylin	a-CGRP (8-37)	vasodilation		
AMY3 (CT, RAMP3)	amylin	a-CGRP (8-37)	vasodilation		
CGRP (CRLR, RAMP1)	a-CGRP	a-CGRP (8-37)	vasodilation	Migraine	Erenumab (CGRP receptor antibody, antagonist, marketed), Rimegepant (non-peptide antagonist, marketed), Ubrogepant (non-peptide antagonist, marketed), Eptinezumab (CGRP antibody, marketed), Galcanezumab (CGRP antibody, phase III), Fremanezumab (CGRP antibody, antagonist, marketed), Atogepant (CGRP antibody, antagonist, marketed), …
	b-CGRP				
AM1 (CRLR, RAMP2)	adrenomedullin	AM (22-52)	vasodilation	cancer	
AM2 (CRLR, RAMP3)	intermedin	AM (22-52)	vasodilation		

Table 2: Human class B1 GPCRs and their ligands, physiological roles, associated diseases, and current and prospective drugs.

Adapted after ***(Hollenstein et al., 2014; Alexander et al., 2015; Fahrenkrug et al., 2019; Serafin et al., 2020; Bisello et al., 2021; D. Hay et al., 2021)****. Reprinted from Trends in Pharmacological Sciences, 35/1, Kaspar Hollenstein, Chris de Graaf, Andrea Bortolato, Ming-Wei Wang, Fiona H. Marshall, Raymond C. Stevens, Insights into the structure of class B GPCRs, 11, Copyright 2014, with permission 5282420154966 from Elsevier.*

1.2.1 Parathyroid hormone 1 receptor

Parathyroid hormone 1 receptor (PTH1R) is a secretin-like receptor, a member of class B1 GPCRs, first cloned from opossum (*Didelphis virginiana*) kidney cell cDNA (Jüppner *et* al., 1991). Gene *PTH1R* on chromosomal position 3p21.1-p24.2. encodes for a protein of 593 amino acids (aa) and ~ 80 kDa (Gelbert *et* al., 1994). Its endogenous ligands and signaling cascade are described in **Chapters 1.1.4.1** and **1.1.4.2**, respectively.

The extracellular part of PTHR consists of 190 aa, where the first 22 aa code for signal peptide cleaved during receptor maturation (Shimada *et* al., 2002). Four putative N-glycosylation sites are asparagine 151, 161, 166, and 176 (Jüppner *et* al., 1991; Bisello *et* al., 1996). Disulfide bridges between cysteines (48 and 117, 131 and 170, and 108 and 148) help to structure ECD in three layered α-β-β-α conformations and create a unique "extracellular vestibule" called "hot dog in a bun" for ligand-binding (Grauschopf *et* al., 2000; Pioszak & Xu, 2008; Pioszak *et* al., 2009; Ehrenmann *et* al., 2018; L.-H. Zhao *et* al., 2019). As classical GPCR, the PTH1R structure contains seven TMs, three ECLs, and three ICLs, followed by a long C-terminus that spans into intracellular space. The C-terminus contains nine serines or threonines (Ser489–Ser495 and Ser501–Thr506), which GRKs phosphorylate after receptor activation (Dicker *et* al., 1999; Malecz *et* al., 1998; Zindel *et* al., 2016; Drube *et* al., 2022a). Further phosphorylation sites in ICL3 were shown to be decisive for β-arrestin recruitment, whereas C-terminus sites help stabilize the PTH1R-β-arrestin complex (Vilardaga *et* al., 2002; A. D. White *et* al., 2021). **Figure 7** shows a "snake plot" of PTH1R.

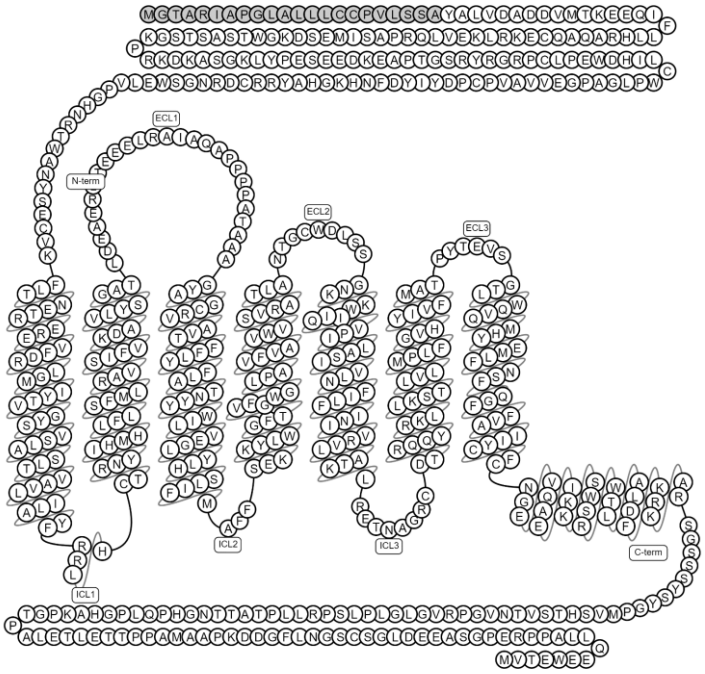

Figure 7: Snake plot of PTH1R.

Snake plot was created with GPCRdb, receptor page. The grey area indicates the position of the signal peptide (first 22 amino acids) (Kooistra, Mordalski, et al., 2021).

PTH1R is expressed at high levels in PTH target tissues, kidneys, and bones, to a medium extent in the respiratory system, female tissues (fallopian tube, uterus, placenta, mamma), cardiac and skeletal muscle, skin, liver, and male tissues (testis) (Ureña *et* al., 1993; Uhlen *et* al., 2010; Uhlén *et* al., 2015). In those locations, PTH1R mediates the biological roles of two endogenous ligands, parathyroid hormone (PTH) and parathyroid

hormone-related protein (PTHrP), which action translates into different biological functions (Jüppner *et* al., 1991; Cheloha *et* al., 2015a). PTH regulates blood levels of calcium and phosphate in an endocrine manner, whereas PTHrP acts in a paracrine manner within developing tissues and is secreted in certain cancers. Besides their biological roles, their biochemical way of functioning is also distinct – PTH can induce prolonged signaling, which originates from the membrane and from endosomes, while PTHrP signals exclusively from the membrane (Ferrandon *et* al., 2009; Vilardaga *et* al., 2011). It is known that PTHR1 signaling is highly context-dependent and can be modulated by various ligands, allosteric partners, or cellular backgrounds (Ferrandon *et* al., 2009; Cheloha *et* al., 2015a; A. D. White *et* al., 2019; Chang *et* al., 2020; L. J. Clark *et* al., 2020a; Bisello *et* al., 2021; A. D. White *et* al., 2021).

1.2.1.1 Parathyroid hormone and parathyroid hormone related peptide

Figure 8 illustrates the molecular life of PTH. The precursor of PTH is synthesized by ribosomes as Pre-Pro-PTH of 115 aa and gets cleaved by signal peptidase during translocation in the endoplasmic reticulum, yielding a 90 aa long Pro-PTH. The remaining six aa are cleaved in the Golgi apparatus, and PTH(1-84) is enveloped by secretory granules and stored. The secretion of PTH is dependent on extracellular Ca^{2+} levels. Decreased calcium levels cause activation of the calcium-sensing receptor (CaSR), a GPCR located on the surface of the parathyroid gland cells. A Gq-mediated release of intracellular Ca^{2+} triggers the exocytosis of the hormone from the secretory granules.

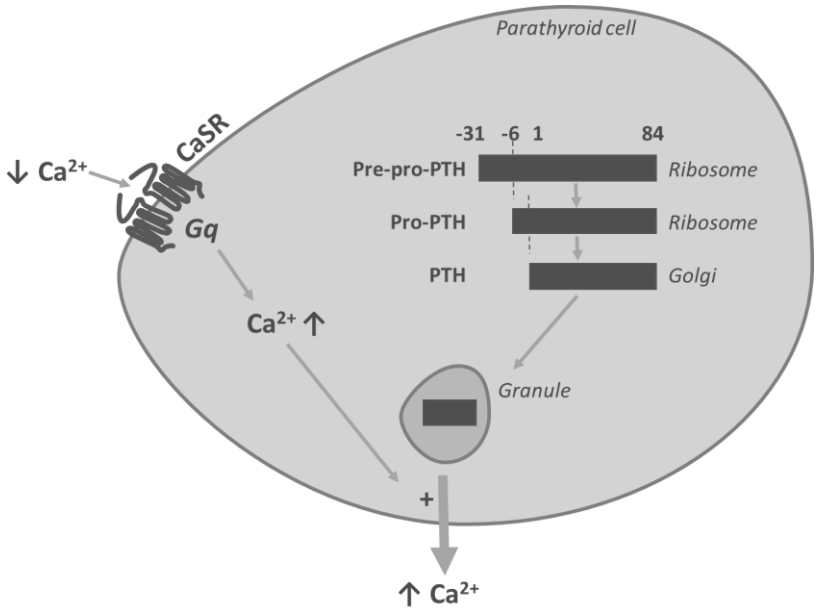

Figure 8: Ca^{2+} regulates PTH secretion.

PTH is synthesized as a precursor hormone, Pre-Pro-PTH, cleaved in the parathyroid gland to Pro-PTH and then to PTH. Secretion of PTH(1-84) is regulated by a negative feedback loop with extracellular Ca^{2}. Most PTH is secreted in this form and then cleaved in the liver into N- and C-terminal fragments.

In addition to the PTH, another polypeptide binds to the PTH1R. The neuroendocrine peptide PTHrP exists in two different isoforms; a 139 aa and a 173 aa long version, where the N-terminal part PTHrP (1-36) represents a bioactive form that binds to PTH1R with similar affinity and efficacy as PTH (Jüppner *et* al., 1991; Sato *et* al., 2021). PTHrP is secreted from mesenchymal stem cells, bone marrow, gastric cells, keratinocytes, and cancer cells and acts as an endocrine, autocrine, paracrine, and intracrine hormone. Most notably, it plays a vital role in fetal development by regulating endochondral bone development and epithelial-mesenchymal interactions

during the mammary glands formation and teeth growth (Weckmann *et* al., 1997; Hens & Wysolmerski, 2005; Soki *et* al., 2012; Lyu *et* al., 2021). PTHrP is also secreted by various tumors (breast, bone, and some lung tumors), which causes hypercalcemia and hypercalciuria (Ralston, 1987). The C-terminal fragment of PTHrP is called osteostatin and is a different hormone regulating bone formation and keratinocyte proliferation. Both PTHrP (107–111) and the entire domain PTHrP (107–139) exert inhibitory effects on osteoclast activity *in vitro* and *in vivo* (Fenton *et* al., 1991; Fenton *et* al., 1991; Zheng *et* al., 1994).

1.2.1.2 PTH1R activation and signaling

Both endogenous agonists, PTH and PTHrP, and their bioactive N-terminal sections, PTH (1-34) and PThrP (1-36), can bind and efficiently activate PTH1R (Jüppner *et* al., 1991; Vilardaga *et* al., 2003b; Ferrandon *et* al., 2009; Sato *et* al., 2021). The initiation of the signaling cascade of PTH1R consists of two steps; initial rapid ligand-binding (τ = 140 ms) is followed by slower receptor activation (τ = 1 second) (Vilardaga *et* al., 2003b; Castro *et* al., 2005). Critical for activation is the interaction of the N-terminus of the ligand (aa 1-16), which penetrates the binding pocket of the receptor formed by all TM, except TM4, supported by ECL2 and ECL3 (Carter *et* al., 1999; Ehrenmann *et* al., 2018; L.-H. Zhao *et* al., 2019). In the complex, LA-PTH binds as a single continuous helix and forms extensive hydrophobic and hydrogen bonds with neighboring residues, giving rationale for older structure-activity relationship studies of PTH-like ligands (Gardella & Vilardaga, 2015). LA-PTH, a modified PTH/PTHrP chimera, was used for the recent cryo-EM structure. Due to higher affinity enabled stabilization of the particles for the successful acquisition of the receptor-Gs complex (Shimizu *et* al., 2016; L.-H. Zhao *et* al., 2019). Studies of PTH identified that aa at positions 10, 11, 12, and 14 are particularly important for enhanced affinity (L.-H. Zhao *et* al., 2019) and first 1-3 aa for agonist response since PTH fragments (3-34), PTH (7-34), PTHrP (7-34), TIP39 (7-39) bind to the receptor and act as competitive antagonists (Rosenblatt *et* al., 1977; Jüppner *et* al., 1994; Hoare & Usdin, 2000; Jonsson *et* al., 2001).

Interestingly, certain parts of the peptide can differentiate between signaling pathways; PTH (1–31) would fully stimulate AC but not PKC, while a fragment of PTH, only four aa long PTH (29-32) surprisingly induces PKC pathway (Jouishomme *et* al., 1994). Furthermore, newer studies suggest that His7 in PTH plays an important role in β-arrestin binding (Clark *et* al., 2020) since it engages with the ECL2 region of the PTH1R, where binding of an antibody can also prevent PTH1R-induced β-arrestin recruitment (Sarkar *et* al., 2019).

It was recently shown that PTH7d peptide inhibited β-arrestin coupling to PTHR and induced sustained cAMP production at the cell surface. Comparison of cellular and organismal responses to wild-type PTH, PTH7d, and LA-PTH resulted in different biological outcomes and thus spatial bias: PTH and LA-PTH could induce the synthesis of active vitamin D via α-hydroxylase while PTH7d could not. In this way have, PTH ligands, inducing endosomal productions, a decisive impact on vitamin D-regulated Ca^{2+} concentrations. The plasma membrane of the PTH1R-related Gs-signaling pool presumably regulates phosphate import through Na^{+}-dependent phosphate cotransporter 2A (A. D. White *et* al., 2021).

Engagingly, Ca^{2+}, which is regulated through PTH1R activity, can *per se* act as a positive allosteric modulator while binding into acidic clusters within the ECL1 of PTH1R. Along these lines can enhance signaling by inducing a prolonged duration of PTH1R activation and cAMP signaling (White *et* al., 2019).

Recent crystallographic, cryo-EM, and AlphaFold structures, visualized in **Figure 9,** added substantially to the understanding of the activation mechanism of PTH1R (Ehrenmann *et* al., 2018; Jumper *et* al., 2021; Varadi *et* al., 2022; L.-H. Zhao *et* al., 2019).

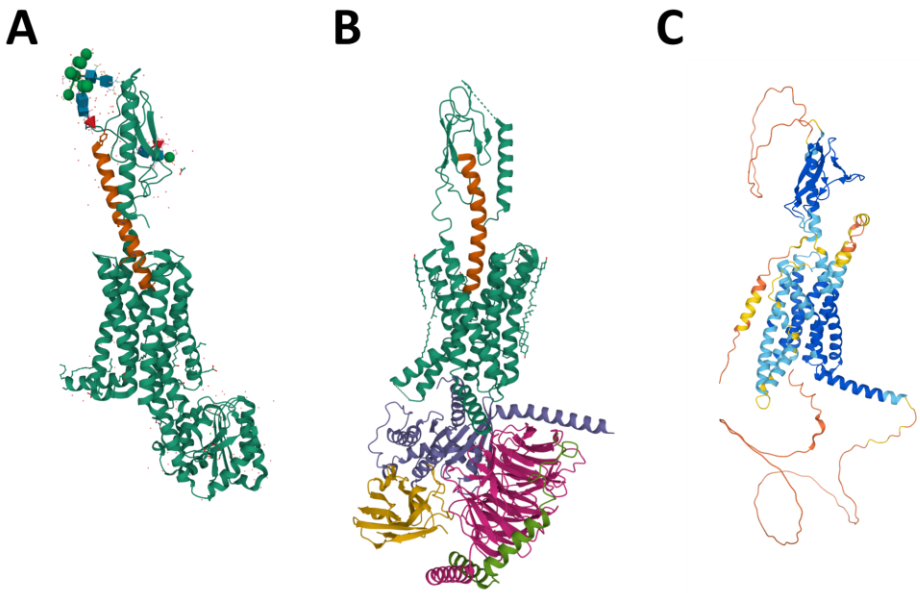

Figure 9: Structural models of PTH1R.

(**A**) High-resolution crystal structure of parathyroid hormone 1 receptor in complex with a peptide agonist (PDB number 6FJ3) *(Ehrenmann et al., 2018)*.

(**B**) Cryo-EM structure of parathyroid hormone receptor type 1 in complex with a long-acting parathyroid hormone analog and G protein (PDB number 6NBF) *(L.-H. Zhao et al., 2019)*.

(**C**) PTH1R model was downloaded from the Alpha Fold Database *(Jumper et al., 2021; Varadi et al., 2022)*

Pleiotropic in its signaling (**Figure 10**), PTH1R couples primarily to Gs and Gq (Abou-Samra *et* al., 1992) but also to G12/13 (Singh *et* al., 2005a), Gi (Miyauchi *et* al., 1990) and can interact with and signals via β-arrestins (Syme *et* al., 2005; Gesty-Palmer *et* al., 2006). Gs activation causes activation of PKA and is the primary PTH- and PThrP-induced mechanism for the regulation of serum Ca^{2+} and bone remodeling (**Figure 10 A, 1**) (Jüppner *et* al., 1991; Jüppner, 1994; Goltzman, 1999). In addition, via Gq, it stimulates PLC, which induces DAG and IP_3 release and the subsequent activation of PKC and the release of intracellular Ca^{2+} from the endoplasmic reticulum (Dunlay & Hruska, 1990; Offermanns *et* al., 1996; Pines *et* al., 1996) (**Figure 10 A, 2**). It was recently revealed that Gs and Gq/11-induced Gβγ signaling, contribute to sustained waves from endosomes (Ferrandon *et* al., 2009; A. D. White *et* al., 2020) (**Figure 10 B**).

Sustained signaling is the hallmark of PTH1R activation since it was initially described for that receptor by Ferrandon *et* al.. The ternary complex of PTH1R–β-arrestin–Gβγ is internalized in early endosomes **(Figure 10 B, 5**). While β-arrestin-induced ERK1/2 inhibits PDE4 (**Figure 10 C, 7**), cAMP continues to be synthesized and diffuses into the nucleus, where it activates nuclear PKA (**Figure 10 C, 8**). Termination of sustained signaling is PKA-induced activation of the H+ pump v-ATPase (**Figure 10 C, 9**), which acidifies endosomes, and parts of the ternary complex are disassembled. Retromer couples to PTH1R and facilitates recycling back to the membrane or redistribution to Golgi (**Figure 10 C, 10**). Dysregulation of this complex signaling cascade (**Figure 10**) can lead to various diseases, summarized in **Table 3**.

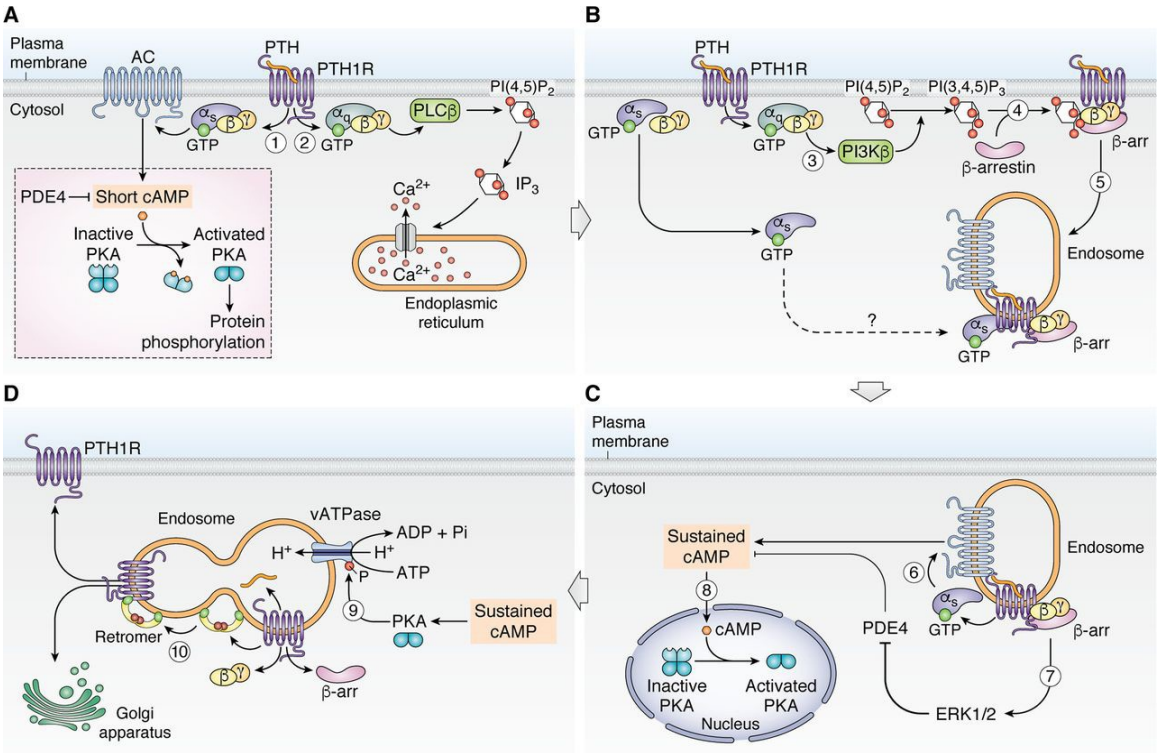

Figure 10: Mechanism of PTH1R signaling.

(A) *Upon PTH binding, PTH1R couples and activates heterotrimeric Gs (1) and Gq (2) proteins at the plasma membrane. Gs activates AC, leading to acute cAMP synthesis and activation of PKA. The cAMP activation is short due to the inactivation by phosphodiesterases (PDE) (pink box). Gq activates PLCβ, which cleaves phosphatidylinositol 4,5-bisphosphate (PI(4,5)P2) into IP3. IP3 diffuses through the cytosol to activate IP3-gated Ca^{2+} channels, releasing stored Ca^{2+}.*

(B) *Gβγ and Gαg subunits dissociation promote phosphoinositide 3-kinase (PI3Kβ)-dependent generation of PI(3,4,5)P3 (3), which induces β-arrestin recruitment to the PTH1R (4) and formation of ternary PTH1R–β-arrestin–Gβγ complex that remains active following internalization and redistribution to early endosomes (5). Reassembly of the ternary PTH1R complex with Gαs is thought to be dependent on Gαs diffusion. Besides Gαs, also Gαq can sustain this complex.*

(C) *Prolongedoged cAMP production (6) is due to the inhibition of ERK1/2 on PDE4 (7), and cAMP can efficiently diffuse to the nucleus to activate nuclear PKA (8).*

(D) *A negative feedback loop initiates termination of endosomal cAMP signaling, where PKA-dependent activation of the H^+ pump v-ATPase increases endosomal acidity (9), which sequentially disassembles the ternary PTHR–arrestin–Gβγ signaling complex and engages retromer coupling to PTH1R (10) and its recycling to the cell surface or redistribution in the Golgi apparatus.*

Adapted from JBC. Structural insights into emergent signaling modes of G protein–coupled receptors (Sutkeviciute & Vilardaga, 2020) under Creative Commons CC-BY license. This research was originally published in (Sutkeviciute et al., 2019; A. D. White et al., 2020)

After activation of PTHR, various kinases phosphorylate receptor – besides GRKs also second messenger-induced kinases (PKA, PKC) (Malecz *et* al., 1998; Dicker *et* al., 1999; Zindel *et* al., 2016; Drube *et* al., 2022a). The phosphorylation barcode should be decisive for the subsequent interaction with β-arrestin (Matthees *et* al., 2021; Drube *et* al., 2022b). Different conformations of PTH1R are required for interaction with G proteins and β-arrestin (Vilardaga *et* al., 2001). Still, initial engagement with β-arrestin is believed to proceed even without the phosphorylation step since phosphorylation-independent inhibition of PTH1R signaling has been described (Dicker *et* al., 1999).

A stable interaction of PTH1R with β-arrestin1 or β-arrestin2 leads to desensitization of signaling plus internalization of the receptors into endosomes (Malecz *et* al., 1998; Ferrari *et* al., 1999) – after this, receptors can either 1) undergo dephosphorylation and recycle back to the membrane, 2) undergo lysosomal

degradation or 3) sustain prolonged signaling from endosomes (Ferguson *et* al., 1998; Luttrell & Lefkowitz, 2002; Lefkowitz *et* al., 2006; Nguyen *et* al., 2019).

Highlighted by many studies from Lefkowitz´s, Luttrell´s, and Ferrari´s labs, β-arrestin2-mediated signaling plays a significant role in PTH-mediated effects in bone. Intermittent PTH administration resulted in significantly weaker bone formation in β-arrestin2 KO mice than continuous PTH administration. Although the rate of new bone formation was the same in both groups, there was a concomitant increase in the rate of bone resorption in the KO animals, resulting in a net reduction in bone mass (Bouxsein *et* al., 2005; Ferrari *et* al., 2005). Those effects of β-arrestin2 might be mediated by a distinct pool of ERK1/2 activation, where β-arrestin2-mediated activation increases specifically cytosolic phospho-ERK1/2 amounts. The increase in cytosolic ERK1/2 should lead to decreases in Elk1 reporter transcription, regulation of genes such as p38, and nuclear factor kappa-light-chain enhancer of activated B cells (NFκB) signaling pathways, which suppress the maturation of osteoclasts (Tohgo *et* al., 2003; Ferrari *et* al., 2005; Gesty-Palmer *et* al., 2006, 2009; Bianchi & Ferrari, 2009; Gesty-Palmer & Luttrell, 2011). The proposed mechanism is illustrated in **Figure 11**.

Therefore, it appears crucial to develop therapeutics targeting the PTH1R-β-arrestin branch of signaling, particularly in osteoporosis management. In addition to osteoporosis, malfunction of the PTH1R complex signaling cascade can cause many diseases, which are, together with their current and prospective treatment, summarized in the **Table 3**.

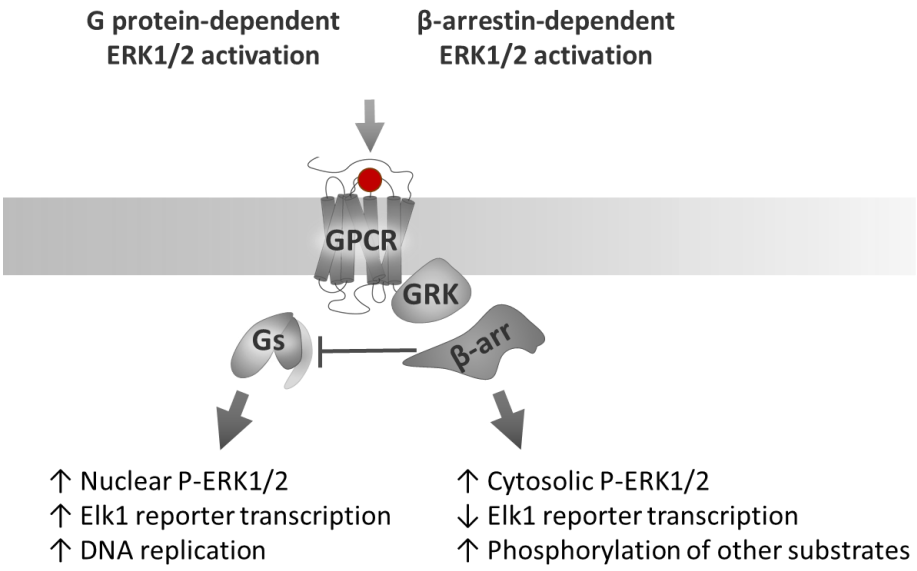

Figure 11: Mechanism of G protein-dependent and β-arrestin-dependent ERK1/2 activation in GPCR signaling.

Adapted after (Tohgo et al., 2003).

Disease	Biological cause	Physiological manifestation	Current treatment	Prospective treatment
Blomstrand's lethal achondroplasia	Abrogation of PTHR1 function by homozygous mutation in PTHR1 (Pro132Leu or nonsense mutation)	Advanced endochondral bone formation, Prenatal mortality	None	None
Ollier's disease	Heterozygous expression of inactive PTHR1 variants (Arg150Cys and other variants)	Development of cartilaginous lesions and tumors in and around the bone	None	None
Familial primary failure of tooth eruption	Heterozygous expression of inactive PTHR1 variants (Pro132Leu, Arg174Cys, and other variants)	Premature ceasing of posterior tooth eruption in children and adolescents	None	None
Jansen's metaphyseal chondrodysplasia	Constitutive cAMP signaling at PTHR1 from a heterozygous mutation in PTHR1 yields receptor variants with mutations in transmembrane helices 2, 6, or 7 (His223Arg, Thr410Pro, or Ile458Arg, respectively)	Short limbed dwarfism Hypercalcemia Hypophosphataemia	None	Inverse agonists of constitutive PTHR1 signaling
Eiken syndrome	Alteration in PTHR1 function by a homozygous nonsense mutation in PTHR1 (Arg485stop)	Retarded ossification Epiphyseal dysplasia	None	Inverse agonists of constitutive PTHR1 signaling
Primary hyperparathyroidism	Oversecretion of PTH by parathyroid glands causes excessive PTHR1 activation	Hypercalcemia Kidney stones	Surgical removal of offending PTH gland	Competitive antagonists of PTHR1 signaling
Humoral hypercalcemia of malignancy	Oversecretion of PTHrP by cancer cells causes excessive PTHR1 activation (observed in 20–30% of patients with cancer)	Hypercalcemia Cachexia	Bisphosphonates Denosumab in bisphosphonate-resistant cases	Neutralizing PTHrP antibodies Competitive PTHR1 antagonists
Brachydactyly type E	Heterozygous mutation of PTHLH resulting in expression of PTHrP variants (Leu44Pro and Leu60Pro, corresponding to positions 8 and 24 of mature PTHrP) with reduced activity	Short metacarpals and metatarsals resulting in small hands and feet	None	None
Hypoparathyroidism	Surgical damage to or removal of parathyroid glands, a mutation in calcium-sensing receptor expressed on parathyroid glands, defective PTH precursor processing	Hypocalcemia Tetany Numbness	Oral calcium, Vitamin D Daily PTH (can be administered separately or together)	Long-acting PTH derivatives
Osteoporosis	The imbalance between bone resorption and bone-building processes	Reduction in BMD, alterations in the skeletal architecture, and increased fracture frequency	Bisphosphonates Denosumab PTH	Analogs of PTHR1 ligands with weak calcium mobilization activity (PTHrP, abaloparatide)

Table 3: Diseases associated with PTHR1.

1.3 Modulators of G protein-coupled receptors

The activity of GPCRs can be modulated by different stimuli or biomolecules, which are of endogenous or exogenous origin. Compared to the traditional belief of receptor signaling, where ligand-receptor interaction triggers the transduction of a specific response, the contemporary view acknowledges there might be many ligands or biomolecules that act as allosteric modulators and thus affect signaling cascades (Jeffrey Conn *et* al., 2009; Gentry *et* al., 2015). Furthermore, such modulators are increasingly appreciated as potential therapeutic agents or co-targets since they usually possess biased preference or spatio-temporal selectivity in the activation process (bias described in **Chapter 1.1.2**). Hence, not all modulators are expressed at all times or in all tissues or modulate the receptor's conformation only at a specific time point. Future drugs will be engineered to multimodal targets, resulting in very precise effects (George *et* al., 2002). **Figure 12** visualizes possible mechanisms of GPCR modulation.

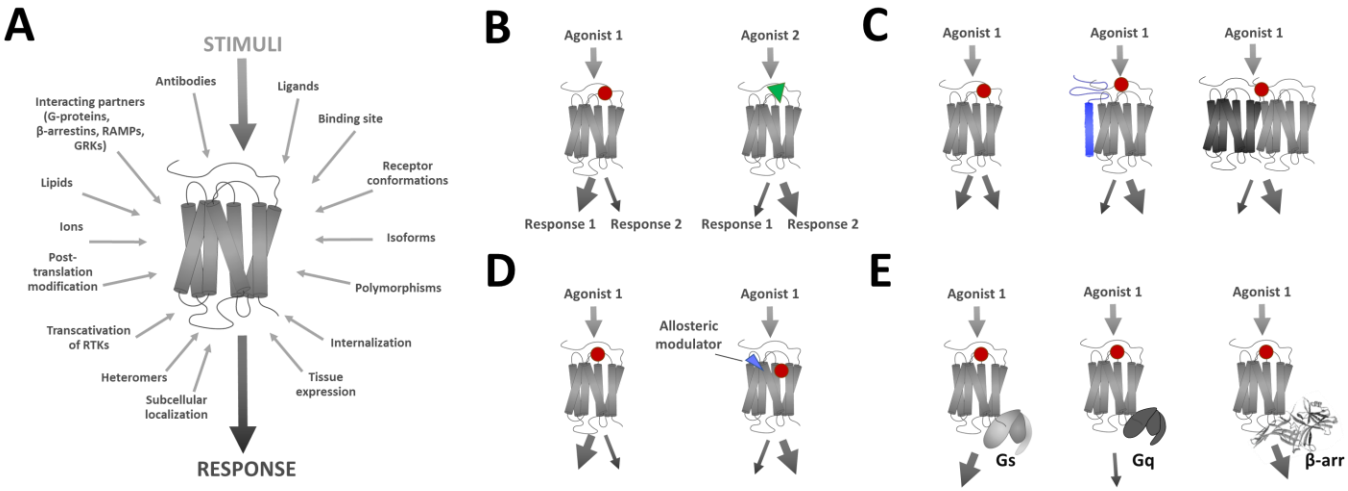

Figure 12: Mechanisms of GPCR modulation.

*(**A**)The current understanding of GPCRs receptor signaling incorporates many interacting proteins and processes, which modulate receptor activation and signaling and, subsequently, receptor functions.*

*(**B**) Ligand (agonist) bias: agonist-dependent preferential receptor activation so that one over other transducer pathways in a given cellular system and relative to a reference agonist is induced (according to the terminology of Community guidelines for GPCR ligand bias: IUPHAR review 32 (Kolb et al., 2022)).*

*(**C**) Homo and heterodimerization with the same or different GPCRs and accessory proteins.*

*(**D**) Allosteric interactions: receptor function can be influenced by interactions with other proteins (e.g., RAMPs) or other allosteric ligands or ions (e.g., Ca^{2+}).*

*(**E**) Biased signaling through different G proteins and other non-G proteins effectors, such as β-arrestins.*

Adapted after (Foster et al., 2015; Westhuizen et al., 2015).

1.3.1 Receptor activity-modifying proteins

Receptor activity-modifying proteins, or RAMPs, are ubiquitously expressed accessory proteins that have globally coevolved with GPCRs (Barbash *et* al., 2017, 2019) and regulate their function. This family of proteins was initially discovered because of their essential oligomerization with the calcitonin receptor-like receptor (CRLR), which can neither reach the cell surface without interacting RAMPs nor create a fully functional receptor phenotype (McLatchie *et* al., 1998). Since then, plentiful studies have expanded the GPCR-RAMP interactome to first secretin-like GPCRs, and recently GPCRs from class A (chemokine subgroup) and class C (CaSR) were identified as interacting partners. As of now, there are more than 40 GPCRs described to interact with RAMPs (Christopoulos *et* al., 2003; Lorenzen *et* al., 2019; Mackie *et* al., 2019; Serafin *et* al., 2020; Harris *et* al., 2021a). Moreover, bioinformatics-aided studies showed that GPCRs and RAMPs share orthologs in the same species and have correlated phylogenetic trees. Latter and high expression correlations suggest a broader role of RAMPs in GPCR pharmacology (Barbash *et* al., 2017, 2019).

RAMP1,2,3 are of similar size, located in the cell interior, especially when they are not in complex with the interacting receptor. Structurally, they display three regions: a large extracellular N-terminus (91 – 95 aa) continues into a membrane-embedded single TM helix and reaches intracellular space with a short intracellular C-terminus (9 or 10 aa) (**Figure 13**). In the absence of interacting GPCRs, RAMPs form 30-32 kDa disulfide-linked homodimers in the ER/Golgi, which are resistant to denaturation and reducing agents.

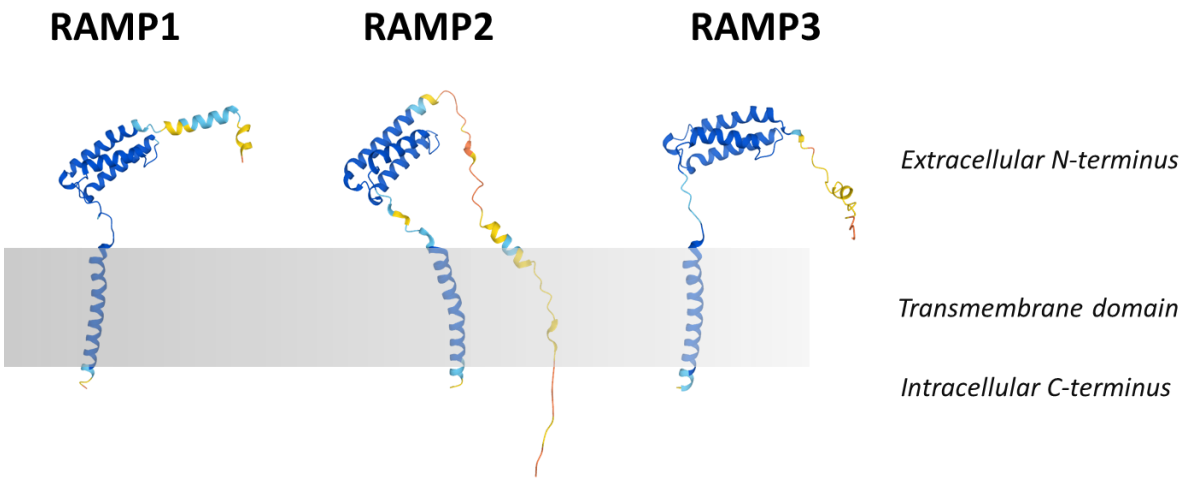

Figure 13: Structural models of RAMP1, RAMP2, RAMP3 as predicted by Alpha Fold SB.
(Jumper et al., 2021; Varadi et al., 2022)

RAMP1 consists of 148 aa, in mature form, presents a 122 aa big, non-glycosylated protein of 14-18 kDa, depending on the presence/absence of disulfide bonds. RAMP1 is expressed at high levels in the endometrium, gastrointestinal tract, cardiomyocytes, neurons, vascular smooth muscle cells, pancreas, and less in various other tissues (McLatchie *et* al., 1998). The most prominent pathophysiological function of RAMP1 is in migraine pathology – where cocreates the Calcitonin gene-related peptide (CGRP) receptor, overexpressed in the central and peripheral nervous system, where CGRP acts as a potent vasodilator and nociception transmitter and enables neurogenic inflammation (Brain *et* al., 1985; Noseda & Burstein, 2013).

RAMP2 is the biggest of all RAMPs, with 175 aa, and in a mature state, 133 aa, forms a 17 kDa big glycoprotein. Compared to RAMP1 and RAMP3, possesses a longer extracellular N-terminus. It is expressed abundantly in cardiomyocytes, placenta, lung, vascular smooth muscle cells, endothelium, adipose tissues, and less in various brain regions and other tissues (McLatchie *et* al., 1998). A higher expression was also detected in certain cancers and appeared to drive its aggressiveness (Larráyoz *et* al., 2014; Larrue *et* al., 2021; Vázquez *et* al., 2021). RAMP2 knockout is lethal due to abnormal vascular development; heterozygous mice survive but develop dilated cardiomyopathy (Kadmiel *et* al., 2011a; Kechele *et* al., 2016; Kadmiel *et* al., 2017).

RAMP3 is the only RAMP that can reach the cell surface without interacting receptors. RAMP3 compromises 148 aa, in mature form 125 aa large glycoprotein of 20-26 kDa. Its C-terminus forms a type-1 PSD-95/Discs-large/ZO-1 homology (PDZ-1) recognition motif. PDZ-1 motif can lead to interactions with the Na^+/H^+ exchange regulatory factor (NHERF) or N-ethylmaleimide-sensitive factor (NSF) and influences receptor internalization and recycling (McLatchie *et* al., 1998; Bomberger, Spielman, *et* al., 2005; Bomberger, Parameswaran, *et* al., 2005). Expressed in the lung, kidney, cardiomyocytes, skeletal muscle cells, pancreas, thyroid glands, female and adipose tissues, it conveys cardioprotection in a sex-dependent manner (McLatchie *et* al., 1998; Lenhart *et* al., 2013b). Different physiological and pathophysiological roles of RAMPs were extensively reviewed in Serafin *et* al. (Serafin *et* al., 2020).

There are many ways in which RAMPs can modulate the functionality of GPCRs, as visualized in **Figure 14**.

1. **Chaperone**

RAMPs facilitate correct conformational folding and assembly of GPCRs in ER and their transport to the cell surface, presumably due to the stabilization of the proteins in the complex (McLatchie *et* al., 1998; Christopoulos *et* al., 2003).

2. **Pharmacological switch**

RAMPs bind to GPCRs and form either required or optional heterooligomers. The most prototypical example and described oligomer with GPCR, CRLR, requires RAMPs as their obligate partners: RAMP1 is necessary for CGRP binding, and RAMP2,3 promote adrenomedullin (AM) and adrenomedullin 2/intermedin (AM2) binding (McLatchie *et* al., 1998). The pharmacology of many receptors is RAMP- and ligand-dependent, which suggests that RAMPs can modulate very subtle changes in GPCRs pharmacology. For example, CTR can bind CT and endocrine hormone amylin (AMY). The affinity of AMY varies between three amylin receptor subtypes (AMY1-3), each formed by a different interacting RAMP. Interestingly, RAMP can enhance but also prevent ligand-binding or act as a negative allosteric modulator (Weston *et* al., 2015).

3. **Signaling switch**

RAMPs can switch preference of coupling on specific GPCRs; or favor β-arrestin recruitment and signaling. As in the case of pharmacological switching, also signaling switch happens in dependence of RAMP and ligand. For example, RAMP2 decreased the efficiency of glucagon receptor-Gαi coupling when stimulated with glucagon. When oxyntomodulin was used as a ligand, RAMP2 potentiated the Gαs activity. RAMP3 can induce higher β-arrestin recruitment of gastric inhibitory polypeptide on its cognate receptor (GIPR) – similar was described for some amylin receptors (Weston *et* al., 2015; Harris *et* al., 2021a; Shao *et* al., 2021; Pearce *et* al., 2022).

4. **Trafficking switch**

RAMPs, particularly RAMP3, due to their PDZ recognition motif, can interact with PDZ protein NSF and enable rapid recycling and resensitization of CRLR or atypical chemokine receptor (ACKR3) (Bomberger, Parameswaran, *et* al.,

2005; Mackie *et* al., 2019). Moreover, for ACKR3, it was shown that RAMP3 directed internalization into Rab4- and not Rab7-positive vesicles. Rab4 vesicles subsequently sorted receptors towards recycling, in contrast to lysosomal degradation, which would be their path through Rab7-dependent mechanism (Mackie *et* al., 2019).

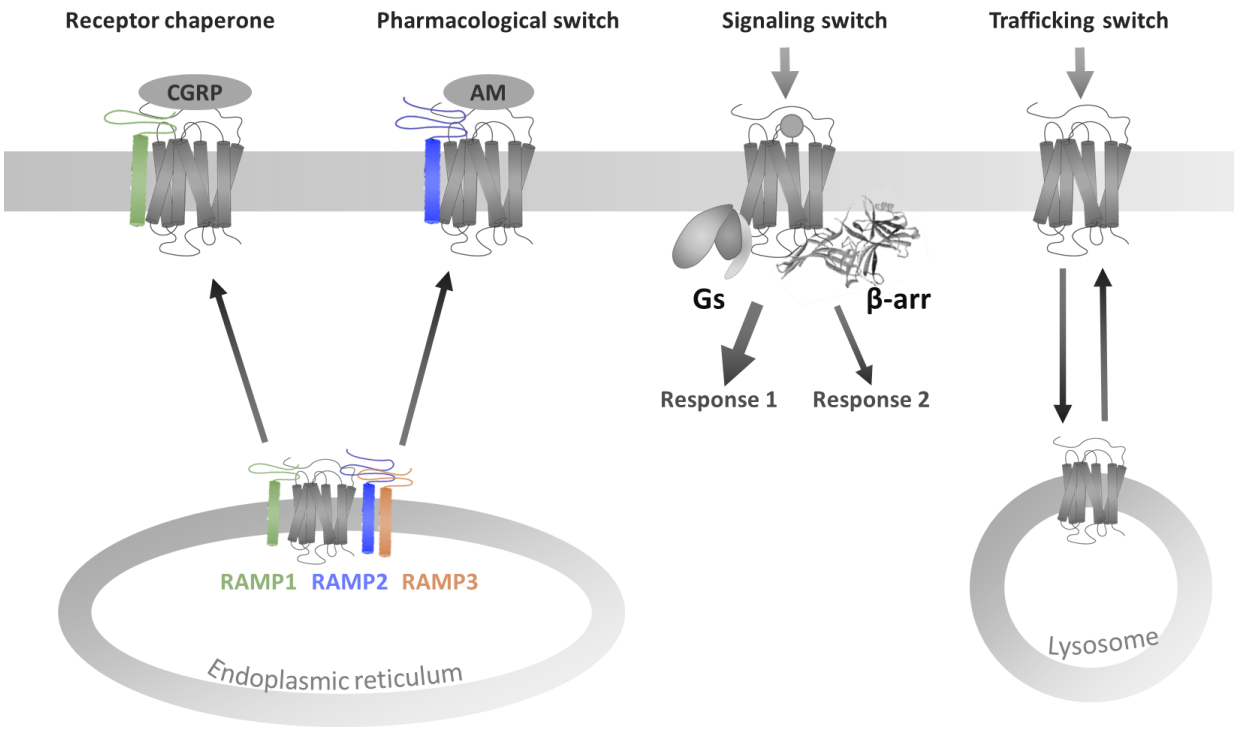

Figure 14: Mechanisms of RAMPs modulation.

RAMPs can act as receptor chaperons modulate ligand specificity and functional selectivity, and direct receptors towards recycling or degradation.

1.3.1 Structural basis of GPCR-RAMP interaction

Structurally, RAMPs are tightly packed with their interacting GPCR partner, being placed adjacent to TM3, TM4, TM5 and making contacts with ECL2 of the receptors (Liang, Belousoff, Fletcher, *et* al., 2020; Josephs *et* al., 2021; Cao *et* al., 2022). The specificity of GPCR-RAMPs interaction originates from various areas across the oligomer interface, particularly from the RAMP linker, which interacts with ECL2, but also from mobility and, subsequently stability of their ECD (Booe *et* al., 2015; J Gingell *et* al., 2016a; Liang, Belousoff, Fletcher, *et* al., 2020b).

Structural studies postulated that RAMP changes specify for different ligands in two ways: 1) RAMPs allosterically reshape ligand-binding pockets, and 2) they enable different contact sites for ligands to emerge as a consequence of RAMP remodeling (Booe *et* al., 2015). Cryo-EM and molecular simulations revealed that RAMP association with CRLR and CTR induces subtle changes in GPCR conformation that allosterically alter the CRLR binding pocket. Although there are minimal direct contacts between ligands and RAMPs (at distant C-terminal of peptides), their binding is allosterically impacted by the oligomerization between GPCR and RAMP. Thus, ligand-binding specificity is different for every receptor-RAMP combination (Booe *et* al., 2015; Liang, Belousoff, Fletcher, *et* al., 2020; Cao *et* al., 2022).

1.3.2 PTH1R and RAMPs

Previous studies established interaction between PTHR1 and RAMPs, showing that coexpression of PTH1R enabled RAMP2, but not RAMP1 or RAMP3 translocation to the cell surface and increased total RAMP2 cellular levels (Christopoulos *et* al., 2003). However, newer experiments suggested that PTH1R can interact with RAMP2 and RAMP3 (Harris *et* al., 2021a) or even all three RAMPs (Lorenzen *et* al., 2019).

Recent studies from mouse models showed that the haploinsufficiency of RAMP2 reduced fertility and caused hyperprolactinemia, skeletal abnormalities, and endocrine dysfunction (Kadmiel *et* al., 2011a). RAMP2-specific endothelial restoration rescued lethality, but survivors developed dilated cardiomyopathy (Kechele *et* al., 2016). Most prominently, the loss of RAMP2 caused placental dysfunction and altered PTH1R regulation (Kadmiel *et* al., 2017). Regardless of established physiological relevance, little is known about the molecular mechanism of PTHR1-RAMPs interaction and its consequences for various aspects which RAMPs were shown to modulate; ligand specificity, functionally selectivity, or trafficking of the PTH1R. I will try to answer some of those open questions in the Results and discussion chapter.

2 RESEARCH OBJECTIVES

GPCRs - a family of membrane proteins with tremendous molecular diversity encompasses more than 800 members and coordinate essentially all cellular functions. GPCR´s signaling orchestrates crucial (patho-)physiological processes and therefore, their members represent key targets in modern drug discovery. For example, the main target for osteoporosis and an essential regulator of ion homeostasis and bone metabolism is PTH1R.

Some of the GPCRs, also PTH1R, oligomerize with accessory proteins, named RAMPs. Three members of the group RAMP1,2,3 are ubiquitously expressed in the human body and are known to switch receptor functions and phenotypes. Structural studies suggest that GPCRs and RAMPs exist in heterooligomeric complexes. Still, the dynamic and kinetic properties of the association, ligand-induced activation, and functional outcomes of those complexes remain poorly understood.

A widely appreciated methodology for researching protein inter- and intramolecular interactions currently relies on imaging and the use of biophysical methods. One of them, resonance energy transfer (RET) technology, enables real-time monitoring of interaction and activation in the intact cells. For this purpose, RET methods are used together with optical devices with a superb temporal resolution to quantify the subsecond processes in real-time.

In this work, I will study the effect of RAMPs in shaping the dynamics of GPCR activation and signaling. The physiologically and therapeutically important PTH1R will be used as exemplary GPCR.

For this objective, various optical biosensors and tagged proteins, based on RET principles will be engineered, optimized, and used in intact cells with high spatiotemporal precision to:

1. Determine preference of interactions between PTH1R and RAMPs.
2. Describe the PTH1R activation process using FRET and a single fluorophore-based conformational biosensor. Analyze the role of accessory protein RAMP2 in shaping both basal and ligand-stimulated conformations.
3. Investigate RAMP's effect on G protein-dependent signaling cascade by assessing activation of G proteins and cAMP accumulation.
4. Evaluate RAMP's effect on non-G protein-dependent signaling cascade: GRK recruitment, β-arrestin recruitment, and ERK phosphorylation.
5. Describe the structural basis of PTH1R-RAMP2 interaction.

Moreover, to interpret the broader role of RAMPs modulation in GPCRs pharmacology:

6. Different fluorescent tools to investigate RAMP's spatial organization will be engineered.
7. Novel activation biosensors for class B GPCRs will be made.
8. A high throughput assay for expanding the repertoire of RAMP interactors will be developed.

3 MATERIALS AND METHODS

3.1 Materials

3.1.1 Cell lines

- Human embryonic kidney (HEK)-293 cells; termed HEK293 in the thesis (ECACC #85120602, CRL-1573, ATCC)
- HEK-TSA cells (ECACC #96121229, Sigma-Aldrich)
- HEK293A (#R70507, Fisher Scientific)
- ΔGα HEK293A cells (Inoue *et* al., 2019)
- Chinese Hamster Ovary cells (CHO)-K1 cells (ATCC)
- Clonal line stably expressing hPTH1R$_{FRET}$ generated from HEK293 cells (this work)
- Clonal line stably expressing hPTH2Ra$_{BRET}$ generated from HEK293 cells (this work)
- Clonal line stably expressing hPTH2Rb$_{BRET}$ generated from HEK293 cells (this work)

3.1.2 Cell culture media and supplements

- Dulbecco's modified Eagle medium (DMEM) 4.5g/L Glucose, w/o: L-glutamine, w: Sodium pyruvate, w: 3.7 g/L NaHCO3 (#P04-03600, PAN Biotech GmbH)
- Opti-MEM I Reduced Serum Medium, no phenol red (#11058021, Life Technologies GmbH)
- Ham's F12 Medium, without L-glutamine, with 1,176 g/l NaHCO3 (#P04-14550, PAN Biotech GmbH)
- DMEM/F12, no phenol red (#21041033, Life Technologies GmbH)
- Dulbecco's phosphate-buffered saline (DPBS), calcium, magnesium (#14040091, Life Technologies GmbH)
- Penicillin/Streptomycin 10.000 E/10.000 µg/mL (#A2213, Biochrom GmbH)
- L-Glutamine 200 mM (#P04-80050, PAN Biotech GmbH)
- Trypsin 0,05 %/EDTA 0,02 % in PBS, without Ca2+ and Mg2+ (#P10-023100, PAN Biotech GmbH)
- Fetal bovine serum (FBS, #F7524-500ML, Sigma Aldrich Chemie GmbH)
- Dimethylsulfoxide for cell culture (DMSO, #A994.1, Carl Roth GmbH & Co. KG)
- Poly-D-Lysine hydrobromide (PDL, #P0899-100 mg, Sigma Aldrich Chemie GmbH)
- G418 disulfate salt (#G5013-250MG, Sigma Aldrich Chemie GmbH)

3.1.3 Plasmids

Plasmid	Source
pcDNA3	Institute of Pharmacology and Toxicology Würzburg
GRK2-YFP in pcDNA3 (Wolters *et* al., 2015)	Institute of Pharmacology and Toxicology Würzburg
HA-PTH1R-CFP-YFP in pcDNA3	Institute of Pharmacology and Toxicology Würzburg
HA-PTH1R-wt in pcDNA3	Institute of Pharmacology and Toxicology Würzburg

HA-PTH1R-cpGFp in pCMV Twist vector	this work; synthesized by Twist Bioscience
HA-PTH1R-mCitrine in pcDNA3	this work; Nemec K.
HA-PTH1R-mTurquoise2-mCitrine in pcDNA3	this work; Nemec K.
HA-PTH1R-mTurquoise2-mCitrine H223R in pcDNA3	this work; Nemec K.
HA-PTH1R-NanoLuc in pcDNA3	this work; Zabel U.
CAAX-mCitrine in pcDNA3	this work; Zabel U.
CAAX-mTurquoise2 in pcDNA3	this work; Zabel U.
β_2AR-mCitrine in pcDNA3	this work; Zabel U.
RAMP1-mTurquoise2 in pcDNA3	this work; Zabel U.
RAMP2-mTurquoise2 in pcDNA3	this work; Zabel U.
RAMP2-SNAP-tag in pcDNA3	this work; Zabel U.
RAMP2-wt in pcDNA3	this work; Zabel U.
RAMP3-mTurquoise2 in pcDNA3	this work; Zabel U.
RAMP1-wt, RAMP2-wt, RAMP3-wt in pVitro2 (Schonauer *et* al., 2015)	Gift from Annette Beck-Sickinger (University of Leipzig, Leipzig, Germany)
β_2AR-NanoLuc in pcDNA3	Annibale P.
G_s BRET biosensor (Gβ_1-2A-cpVenus-Gγ_1-IRES-Gαs-NanoLuc) in T2A-IRES vector	Schihada H.
G_q BRET biosensor (Gβ_3-2A-cpVenu-Gγ_9-IRES-Gαq-NanoLuc) in T2A-IRES vector	Schihada H.
Gi_3 BRET biosensor (Gβ_1-2A-cpVenu-Gγ_2-IRES-Gαi3-NanoLuc) in T2A-IRES vector	Schihada H.
G_{13} BRET biosensor (Gβ_3-2A-cpVenu-Gγ_9-IRES-Gα13-NanoLuc) in T2A-IRES vector	Schihada H.
Lyn-HaloTag-SAH60-HaloTag-CAAX in pcDNA3	Schihada H.
β-Arrestin2-mVenus in pcDNA3	Isbilir A.
R-Flinc A in pcDNA4 (Ohta el al., 2018)	Gift from Kazuki Horikawa (Department of Optical Imaging, The Institute of Biomedical Sciences, Tokushima University, Tokushima City, Japan)
Epac-S^{H187} in pcDNA3 (Klarenbeek *et* al., 2015)	Gift from Kees Jalink (The Netherlands Cancer Institute, Amsterdam, Netherlands)
SNAP-tag-$GABA_{B1}$ (Maurel *et* al., 2008)	Gift from Jean-Philippe Pin (Institut de Génomique Functionnelle, Montpellier, France)
pFC14K HaloTag® CMV Flexi® Vector	Promega (#G966A)
pFC32K Nluc CMV229 neo Flexi® Vector	Promega (#N1331)
ERK_{cyto} and ERK_{nucl} biosensors in pcDNA3 (Harvey *et* al., 2008)	Addgene (#18682)

Table 4: Plasmids used in the course of this study.

All plasmids were generated with human gene isoforms. The sequences of all constructs were validated through Sanger sequencing by Eurofins Genomics or LGC Genomics.

3.1.4 Primers

All primers used for the generation and amplification of cDNA were synthesized by Eurofins Genomics or BioTeZ GmbH.

3.1.5 TaqMan® Gene Expression Assay probes

- RAMP1 (Hs00195288_m1, #4331182, Fisher Scientific)
- RAMP2 (Hs00237194_m1, #4331182, Fisher Scientific)
- RAMP3 (Hs00389131_m1, #4331182, Fisher Scientific)
- TaqMan™ Universal PCR Master Mix (#4304437, Applied Biosystems™)

3.1.6 Cloning enzymes

All restriction enzymes, polymerases ligases, and nucleotides employed for the generation of new plasmid cDNA were purchased from New England Biolabs.

3.1.7 Fluorescent SNAP-tag® and HaloTag® dyes and luciferase substrate

- SNAP-Cell® 647-SiR (#S9102S, NEB)
- HaloTag® NanoBRET™ 618 Ligand (#G980A, Promega)
- NanoBRET™ Nano-Glo® Substrate - furimazine (#N157A, Promega)

3.1.8 Antibodies and HRP substrate

- Anti HA-tag (#ab9110, Abcam)
- Anti-rabbit IgG, HRP-linked antibody (#7074P2, Cell Signalling)
- 3,3',5,5'-Tetramethylbenzidine – TMB (#T8665, Sigma-Aldrich)

3.1.9 Ligands

- (D-Trp12,Tyr34)-pTH (7-34) amide (bovine) Trifluoroacetate (#H-9115, Bachem)
- (Tyr34)-pTH (7-34) amide (bovine) Trifluoroacetate (#N-1110, Bachem)
- pTH-Related Protein (7-34) amide trifluoroacetate (#H-9100, Bachem)
- pTH (1-31) amide (human) (#H-3408, Bachem)
- pTH (3-34) (bovine) Trifluoroacetate (#H-3088, Bachem)
- pTH (1-34) (human, #H-4835-GMP, Bachem)
- pTHrP (1-34) (human, mouse, rat, #H-6630, Bachem)
- TIP-39 trifluoroacetate salt (#H-4878, Bachem)
- TIP (7-39) (Human, Bovine, #056-52, Phoenix Pharmaceuticals)
- Forskolin (Fsk) (#F3917, Sigma-Aldrich),

- 3-Isobutyl-1-methylxanthine (IBMX, #I5879, Sigma-Aldrich),
- (-)-Isoproterenol x HCl (#I6504, Sigma-Aldrich)

All vials were initially stored at -20°C and shortly centrifuged before opening. Fluorescent dyes were reconstituted in DMSO. Antibodies were diluted in 1 % (wt/vol) BSA/PBS.
All peptide ligands were reconstituted in RET imaging buffer containing 0.1 % (w/v) BSA. Fsk and IBMX were reconstituted in DMSO. Isoproterenol was freshly prepared in RET imaging buffer right before the measurements due to its instability in the solution. After reconstitution, aliquots were stored at -20°C, avoiding freezing-thawing cycles. Furimazine and all ligands were diluted in RET imaging buffer containing 0.1 % (w/v) BSA before the experiments.

3.1.10 Commercially available kits and reagents

- Effectene Transfection Reagent - 4 x 1 mL (#301427, Qiagen GmbH)
- Lipofectamine 2000 Transfection Reagent - 0.3 mL (#11668030, Life Technologies GmbH)
- Lipofectamine 3000 Transfection Reagent - 1.5 mL (#L3000015, Life Technologies GmbH)
- Gibson Assembly Master Mix (#E2611L, New England Biolabs GmbH)
- Q5® Site-Directed Mutagenesis Kit (#E0554S, New England Biolabs GmbH)
- Phusion™ High-Fidelity DNA Polymerase (2 U/µL) (#F530S, Fisher Scientific)
- Monarch™ Plasmid Miniprep Kit (#T1010L, New England Biolabs GmbH)
- Monarch™ DNA Gel Extraction Kit (#T1020L, New England Biolabs GmbH)
- QIAGEN Plasmid Plus Midi Kit (#12945, Qiagen GmbH)
- MycoAlert™ Mycoplasma Detection Kit (#LT07-118, Lonza)
- NanoBRET Nano-Glo Detection System (#N1663, Promega)
- GeneRuler 1 kb DNA Ladder (#SM0313, Fisher Scientific)

3.1.11 Other consumables

- TC-Platte 6 Well, Standard F (#833,920,005, SARSTEDT)
- TC-Schale 100, Standard (#833,902, SARSTEDT)
- TC-Platte 96 Well, Standard F (#833,924,005, SARSTEDT)
- TC-Schale 60, Standard (#833,901 SARSTEDT)
- Coverslips 24 mm Ø (#0111640, Paul Marienfeld GmbH)
- Millipore® Millex-MP filter 0.22 µm (#10074590, Merck)
- 96-well plates, black-walled, black bottomed (#BR781968, Brand GmbH)
- 96-well plates, white-walled, white bottomed (#BR781965, Brand GmbH)
- 96-well plates, transparent (#BR781962, Brand GmbH)
- Reagent Reservoir 25 mL divided (#11475748, Fisher Scientific)
- Attofluor™ chamber (#A7816, Fisher Scientific)

3.1.12 Software

- SNAPgene 5.0.8 (GSL Biotech LLC, San Diego, California, USA)
- Microsoft Excel 2016 (Microsoft, Washington, USA)
- GraphPad Prism software 8.1.2 (GraphPad Software, California, USA)
- OriginPro 2018 software (OriginLab, Massachusetts, USA)
- Visiview 4.0 imaging software (Visitron Systems)
- LAS X microscope control software (Leica, Germany)
- Gen5 Data Analysis (BioTek Instruments, Vermont, USA)
- OctaFlow II ™ (ALA Scientific Instruments, USA)

3.1.13 Devices

- **Brightfield fluorescence microscope:**
  Leica DMi8 inverted microscope (Leica Microsystems, Wetzlar, Germany), equipped with an oil-immersion objective (HC PL APO 63×/1.40-0.60 oil, Leica Microsystems), dichroic beamsplitter T505lpxr (Visitron Systems, Puchheim, Germany), and Xenon lamp coupled with a continuously tunable Visichrome high-speed polychromator (Visitron Systems). sCMOS camera (Prime 95B, Teledyne Photometrics, USA) with a dual image splitter (OptoSplit II, Cairn Research, UK).
  Filters: 470/24 *et* Bandpass (#F49-469, Chroma, Bellows Falls, Vermont, USA), 535/30 *et* Bandpass (#F47-535, Chroma), 520/35 BrightLine HC (#F37-520, IDEX Health & Science, Rochester, NY, USA).
- **Rapid superfusion system:**
  OctaFlow II ™ ALA-VM8 with Quartz MicroManifold® 8 to 1 channel 100 µm (or 200 µm) tubing and tip (ALA Scientific Instruments, Farmingdale, USA).
- **Confocal setup:**
  Leica confocal laser-scanning microscope TCS SP8 with an oil immersion objective (HC PL APO (HC PL APO CS2 40x/1.3 NA), a 1.5 mW white light laser, and HyD photon-counting detectors.
- **TIRF-microscope**
  Nikon ECLIPSE Ti2 microscope body with TIRF module for angle control in multiple color imaging with different layers/ penetration-depths. Acal BFi three Twincams to divide the emission signal in four different wavelengths. Four Andor iXon Ultra 897 EMCCD cameras with filter sets for DAPI, GFP, Cy3, and Cy5. Microscope can be used with two lightsources. 1: Nikon laserbox with 405 nm, 488 nm, 561 nm, 647 nm wavelength Laser-diodes. 2: CoolLED LED-based light source with 16 different wavelengths (within 405 nm – 770 nm). Objective: Nikon CFI HP Plan Apochromat TIRF 100x Oil / NA:1.49/ WD:0.12.
- **Plate reader:**
  Synergy Neo2 (BioTek) equipped with filters and monochromator optics. Filters: #13 420/50 nm excitation filter, #14 485/20 nm excitation filter, #43 485/20 - 540/25 nm dual emission filter, #46 516/20 nm – 590/35 nm dual emission filter, #255 460/40 – 520/20 nm dual emission filter, #74 450/50 and 610LP nm dual emission filter.
- **Thermal Cycler:**

Biometra TRIO (Analytik Jena, Jena, Germany)

- **Electrophoresis System:**
  Mini-Sub Cell GT Horizontal Electrophoresis System and PowerPac Basic Power Supply by Bio-Rad (Bio-Rad, Hercules, California, USA)
- **Spectrophotometer/Fluorometer:**
  NanoDrop ™ DS-11 (Denovix Inc., Wilmington, Delaware, USA)
- **Cell counter:**
  Countess 3 Automated Cell Counter (Invitrogen, Fisher Scientific)

3.2 Methods

3.2.1 Molecular biology

Cloning technique

The cloning of the constructs was executed by following the steps:

1. Design of the constructs
2. Amplification of fragments´ cDNA via PCR
3. Gel electrophoresis and cDNA extraction
4. cDNA adjustment and Gibson assembly
5. Transformation of chemically competent *Escherichia coli* cells
6. Extraction and purification of plasmids
7. Mini/Midi plasmid preparation
8. Concentration adjustment and verification

To express the protein of interest (POI), its cognate cDNA needed to be incorporated into the expression plasmid vector. To combine different parts into one plasmid vector, specific primers for the insert and the vector part were designed. A complementary overhanging sequence was introduced into each fragment during the design with suitable cloning software (*e.g.*, SNAPgene) (**Figure 15**). All fragments were PCR amplified, and the cDNA was separated and extracted from an agarose gel. DNA concentration was measured using a UV/Vis- -Spectrophotometer. Fragments were combined in a suitable ratio and mixed with the Gibson assembly mix. The mixture was put in a Thermal cycler, and the resulting cyclized plasmid was transformed into competent *Escherichia coli (E. coli) cells*. The next day, single clones were picked, and plasmids were amplified in a lysogeny broth (LB) medium with suitable antibiotics. Plasmids were purified using a mini or midi plasmid preparation protocol. Each clone was tested by DNA sequencing or control digestion to assure the fragments were combined appropriately, without mutations or frameshifts.

Design of the constructs

PcDNA3(+), pCMV Twist, and T2A-IRES plasmid vectors were used for high expression of POI in mammalian cell lines. Plasmids were either created by molecular restriction cloning or the Gibson Assembly technique. **Figure 15** shows the typical appearance of primer design.

All PTH1R-based constructs were cloned from full-length human PTH1R. HA-PTH1R$_{mTurquoise/mCitrine}$ (PTH1R$_{FRET}$) and HA-PTH1R$_{mCitrine}$ were modified from previously described biosensors. For HA-PTH1R$_{NanoLuc}$, NanoLuc was fused to the C-terminal of HA-PTH1R$_{wt}$.

PTH1R$_{cpGFP}$ biosensor was cloned into pCMV Twist vector and designed according to the previously described dLight1 cpGFP biosensor and synthesized by Twist Bioscience, California, USA. Influenza A signaling peptide (MKTIIALSYIFCLVFADYKDDDDA) was fused to the N-terminus of PTH1R, and LSSLI-cpGFP-NHDQL was inserted between Lys388 and Arg400 in the third intracellular loop.

RAMP$_{mCitrine}$ and RAMP$_{SNAP}$ were generated by fusing mCitrine or SNAP-tag to the C-termini of RAMPs. SNAP-tag sequence was amplified from a SNAP-tag-GABA$_{B1}$ receptor template. The C-terminus of the CAAX sequence was

tagged with mCitrine or mTurquoise2. For $\beta_2AR_{mCitrine}$ and $\beta_2AR_{NanoLuc}$, mCitrine and NanoLuc were fused to the C-terminus of β_2AR, respectively. β-arrestin2$_{mVenus}$ was modified from previously described β-arrestin2$_{EYFP}$[62] by exchanging EYFP for mVenus.

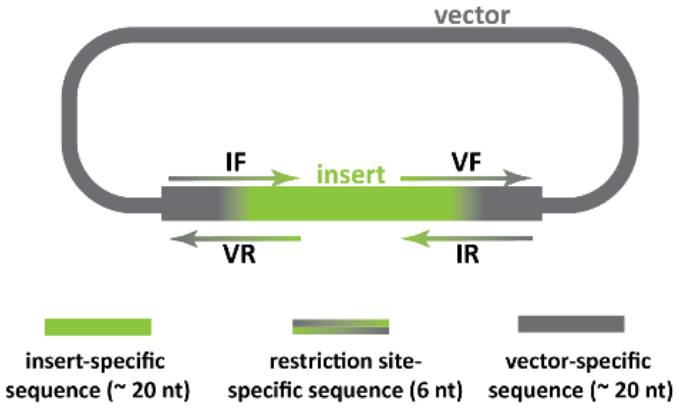

Figure 15: Design of primers for amplifying cDNA.

Insert-forward primer (IF) compromises part of the vector-specific sequence, followed by the insert-specific sequence. Vector-forward primer (VF) is built from the insert-specific sequence, followed by the vector-specific sequence. Vector-reverse (VR) and insert-reverse (IR) primers are reverse complementary to IF and VF, respectively. If required, a restriction site-specific sequence is inserted between the insert and vector part for easier digestion in future cloning procedures.

Amplification of insert and fragment DNA via PCR

Polymerase-chain-reaction (PCR) was used to amplify cDNA fragments, expressed in plasmid vectors. During the PCR reaction, fragment-specific primers determined the start (forward primer) and endpoint (reverse primer) of the desired fragment. The sequence was elongated by DNA polymerase at the 3' end while building in suitable deoxyribonucleotides (dNTPs), corresponding to the complementary DNA strand. Content of the amplification PCR mix (**Table 5**) was combined on ice and incubated in a Thermal cycler according to the PCR Program (**Table 6**). The annealing temperature and length of each step were optimized for specific fragments.

Amplification PCR mix
20 ng DNA template
1 µl 10 mM dNTP mix (200 µM)
2.5 µL 10 µM forward primer (0,5 µM)
2.5 µL 10 µM reverse primer (0,5 µM)
0.5 µl Phusion polymerase (1 U/50 µL PCR)
10 µl 5X Phusion HF buffer
1.5 µL 100% DMSO (3%)
ad 50 µl ddH2O

Table 5: Ingredients for amplification PCR.

PCR Program		
Step	**Temperature**	**Time**
Initial denaturation	98 °C	30 s
30 cycles: Denaturation Annealing Extension	 98°C **X°C** 72°C	 15 s 15 s **Y min**
Final extension	72°C	5 min
Cooling	4°C	hold
X – Annealing temperature is primers-specific. Y – Extension time is fragment-specific ~ 1kb/min		

Table 6: Amplification PCR procedure.

Gel electrophoresis and DNA extraction

Amplified PCR product from the Thermal cycler was examined and purified on an agarose gel. 0.8 – 1 % (w/v) gels were prepared by dissolving an appropriate amount of agarose powder in 1X tris-acetate (TAE) buffer (**Table 7**), boiling the solution, and subsequently adding 0.06% Ethidium Bromide. The solution was poured into a chamber; combs were added to create holes, and the solution was let to harden at room temperature for 30 min. The gel was put to an electrophoresis chamber, and 1xTAE buffer was added. PCR product was mixed with 10x DNA loading buffer (**Table 7**) and slowly inserted into the gel holes. One hole was loaded with 1 kb DNA ladder to compare the size of other DNA strands. Electrophoresis was executed at 120 V for 30 min.

Electric field, which was created in the electrophoresis chamber, allowed negatively charged DNA to move towards the positive electrode. DNA was separated according to size, and DNA-binding dye was used to visualize DNA bands of different sizes. DNA-binding dye Ethidium Bromide intercalates between the DNA bases, and DNA can be visualized upon excitation under UV light. Separated DNA bands can be examined, excised, and further extracted from the agarose gel with Monarch™ DNA Gel Extraction Kit according to the manufacturer's protocol.

TAE buffer (50x)
10 mM EDTA
50 mM sodium acetate
400 mM Tris-HCl
H_2O, adjust pH=8.0

DNA loading buffer (10x)
0.25% (m/v) bromophenol blue
50% glycerol
100mM EDTA
H_2O

Table 7: Ingredients for TAE buffer and DNA loading buffer.

DNA adjustment and Gibson assembly

DNA concentration was measured at 260 nm using a microvolume UV/Vis-Spectrophotometer. Appropriate amounts of fragments were calculated according to ***Equation 1*** and adjusted to combine them in a suitable ratio. A total amount of 0.03 pmol was used, and there was triple excess of small fragments. Gibson assembly mix (**Table 8**)

was put into a Thermal cycler, and a suitable, very conveniently short PCR program was executed (**Table 9**). 2 µl of the resulting cyclized plasmid was used for transformation in competent *E. coli*.

Equation 1: $Amount\ fragment\ (ng) = \frac{0.03\ pmol\ x\ size\ [bp]\ x\ 650\ daltons}{1000}$

Gibson assembly mix
The total amount of fragments (0.03 pmol)
10 µL Gibson assembly master mix (2x)
H_2O ad 20 µL

Table 8: Ingredients for Gibson assembly.

PCR Program		
Step	**Temperature**	**Time**
Assembly	50 °C	15 - 60 minutes

Table 9: PCR Program for Gibson assembly.

Transformation of chemically competent E. coli cells

For transformation, *E. coli* competent cells of strain DH5α were used. Bacterial cells have been made competent – porous to be capable of DNA uptake. During the transformation, competent cells were taking up the plasmid and, with its machinery, amplifying the cDNA. 100 µL of the bacterial suspension was slowly defrosted on ice, mixed with 100 µL KCM buffer (**Table 10**) and either 1 µL of plasmid DNA (1 µg/µL) or 5-10 µL PCR product of Gibson assembly. The mixture was incubated for 20 minutes on ice, afterward put for 1 minute on 42°C and 5 minutes on ice for heat shock. 1 mL of antibiotic-free LB medium (**Table 10**) was added, and the mixture was further incubated with shaking for 60 minutes (37 °C, 500 RPM). To isolate the transformed bacteria, the mixture was centrifuged (5 min, 5000 RPM), LB medium slowly aspirated, and the pellet was re-suspended in 100 µL of fresh LB medium.

KCM buffer
100 mM KCL
30 mM $CaCl_2$
50 mM $MgCl_2$
H_2O, sterile filtered 0.2 µm

LB medium
1% (w/v) Trypton
0.5% (w/v) yeast extract
1% (w/v) NaCl
H_2O, autoclave

Table 10: Ingredients for KCM buffer and LB medium.

Extraction and purification of the plasmids

Suspension of the freshly resuspended pellet was plated on antibiotic-containing agar plates (**Table 8**) and kept overnight in a bacterial incubator at 37°C, 5 % CO_2. On the next day, single colonies were picked and inoculated in 5 mL (for mini preparation) or 50 mL (for midi preparation) of LB medium containing selection antibiotic (*e.g.*, 100 µg/ml Ampicillin). The suspension was kept at 37°C, 5 % CO_2 in a circulatory shaker (150 RPM) overnight or until the

optical density of the suspension measured at 595 nm reached 0.5 – 0.6. The next day, 500 µL of suspension was mixed with 500 µL 50 % glycerol to create bacterial glycerol stock (**Table 11**), which can be kept at -80°C for many years. The rest of the suspension was centrifuged for 10 minutes at 3500 RPM and 4°C. The medium was aspirated in pellet resuspended in appropriate Mini or Midi preparation buffer according to the manufacturer's protocol.

LB agar plates
1% (w/v) agar in LB-medium
Selection antibiotic: *Ampicillin 100 µg/mL*, or *Kanamycin 50 µg/mL*

Bacterial Glycerol Stocks
50% bacterial suspension
25% glycerol
25% ddH20

Table 11: Ingredients for LB agar plates and bacterial glycerol stocks.

Extraction and purification of DNA plasmids

For mini and midi preparation, Monarch™ Plasmid Miniprep Kit and QIAGEN Plasmid Plus Midi Kit were used, respectively, and procedures were executed according to the manufacturer's protocol.

Concentration adjustment and verification

After purification with the appropriate kit, the concentration of cDNA was measured at 260 nm using a microvolume UV/Vis-Spectrophotometer NanoDrop ™ DS-11. Quality of purified cDNA was controlled with the simultaneous measurement at 280 nm, and absorption ratio (AR) at 260 nm/280 nm was controlled to be greater than or equal to 1.8. Samples with smaller AR were probably contaminated with proteins. DNA concentration was adjusted to 1 µg/µL for long term storage at -20°C and 50-100 ng/µL for verification with sequencing.
Verification of DNA was performed with Sanger sequencing by Eurofins or LGC Genomics. Alternatively, verification with restriction digest with unique restriction enzymes could be done.

3.2.2 Cell biology

Cell maintenance

Different clones of human embryonic kidney cells (HEK293) were employed. HEK293 was used to generate a stable cell line, HEK293T for most experiments, and HEK293A for plate reader experiments of G protein activation and internalization. They are termed HEK293 in the Result section and corresponding experimental details are described in the Methods section.
Cells were grown in cell culture medium (**Table 12**), constituted from DMEM (HEK293 cells) or DMEM/F12 (CHO cells) medium, further supplemented with 2 mM L-glutamine, 10 % fetal calf serum, 100 µg/mL streptomycin, and 100U/mL penicillin, at 37°C with 5 % CO_2. Cells were routinely passaged every 2-3 days when reaching 80 % confluency. The old medium was aspirated, and cells were carefully washed with PBS. 0.05 %/0.02 % Trypsin/EDTA solution was added, flown over the whole dish, and aspirated a few seconds later. After detaching, for approximately 1 minute, cells were resuspended in a fresh culture medium, and an aliquot was transferred to a new dish. Passages between 4-25 were used for experiments.

Cells were routinely tested for mycoplasma infection using MycoAlert™ Mycoplasma Detection Kit, and cells were not contaminated with mycoplasma.

Cell culture medium
DMEM 4.5 g/L glucose (HEK293) or phenol red-free DMEM/F12 (CHO)
10 % (v/v) FBS
100 U/mL penicillin, 100 µg/mL streptomycin
Two mM L-glutamine, sterile filtered 0.2 µm

Table 12: Ingredients for cell culture medium.

Freezing and thawing of cell lines

For long-term storage in liquid nitrogen, cells were harvested according to the before-mentioned protocol and resuspended in 1 mL of freezing medium (**Table 13**). Cells were aliquoted into cryo-vials and stored for one night in Nalgene® Mr. Frosty® Cryo 1°C Freezing Container at -80°C to ascertain a cooling rate of -1°C/minute. On the next day, the cryovials were transferred to liquid nitrogen tank for the extended storage.

To thaw frozen cells, a cryo-vial was thawed quickly in a water bath at 37°C, resuspended in a warm culture medium, and centrifuged for 3 minutes at 800 RPM. The medium was aspirated to remove DMSO, and cells were re-suspended in fresh culture medium and plated on cell culture dishes.

Freezing medium
85 % (v/v) cell culture medium
10 % (v/v) FBS (*or more*)
10 % (v/v) DMSO

Table 13: Ingredients for freezing medium.

Creation and maintenance of stable cell lines

HEK293 cells were used to develop a stable cell line. Cells seeded into 100 mm dishes were transfected at a confluence of 60 % with 2 µg of desired biosensor cDNA with Lipofectamine 3000, according to the manufacturer´s protocol. Transfected clones were selected with 600 µg/mL G418 and sorted with a fluorescence-assisted cell sorting (FACS) into transparent 96-well plates. Monoclonal single clones were grown in DMEM supplemented with 200 µg/mL G418. For further experiments, the best clone was selected based on the brightness and amplitude of the saturating agonist stimulation of the desired biosensor in a plate reader experiments.

3.2.3 Plating and transfection

Microscopy experiments:

Coverslips were covered with PDL for 30 min, washed twice with PBS, and left to dry before seeding.

2×10^5 HEK293T cells were seeded onto 25 mm coverslips into a 6-well plate. After 24 hours, cells were transfected with Lipofectamine 3000, according to the manufacturer´s protocol. For all transfections, PTH1R:pcDNA3/RAMP ratio was 1:1, unless otherwise noted. The empty backbone of pcDNA3 was used throughout to maintain a consistent level of total cDNA.

Plate reader experiments:

1.5 or $3x10^6$ HEK293T cells were seeded into 55- or 100-mm dishes and transfected 24 hours after at a confluence of 80 % with 2 or 6 µg of total cDNA with Lipofectamine 3000, respectively.

For FRET experiments, cells were transfected with the combination of $PTH1R_{FRET}$/$PTH1R_{cpGFP}$ and pcDNA3/$RAMP2_{wt}$/$RAMP2_{SNAP}$ or $PTH1R_{wt}$, H187/EKAR biosensor, and pcDNA3/$RAMP2_{wt}$/$RAMP2_{SNAP}$. Combinations were transfected at a ratio of 1:1 or 1:1:1, respectively.

For BRET experiments, cells were transfected with $GRK2_{EYFP}$, $PTH1R_{NanoLuc,}$ and pcDNA3/$RAMP2_{wt}$; β-$arrestin2_{mVenus}$, PTH1RNanoLuc and pcDNA3/$RAMP2_{wt}$ or G protein BRET biosensor, $PTH1R_{wt}$ and pcDNA3/$RAMP2_{wt}$ at an of ratio 1:1:1.

The medium was removed after 12 hours, and after 24 hours, cells were trypsinized and seeded into a PDL-precoated, black-wall, black-bottomed or white-wall, white-bottomed 96-well plates (50,000 -70,000 cells/well).

Plate reader experiments of G protein activation and internalization:

HEK293A cells were transfected in suspension with a combination of the constructs, at a ratio of 1:1:1 ($PTH1R_{wt}$, G protein BRET biosensor, and pcDNA3/$RAMP2_{wt}$ - G protein activation) or 1:4:2.5 ($PTH1R_{NanoLuc}$, Lyn-Halo-SAH60-Halo-CAAX, and pcDNA3/$RAMP2_{wt}$ - internalization). Cells were transfected with Lipofectamine 2000 (2 µl transfection reagent/1 µg total cDNA) according to the manufacturer's protocol and seeded into a PDL-precoated, white-wall, white-bottomed 96-well plates (30,000 cells/well).

3.2.4 Labeling

Cells were labeled and kept in the dark during the incubation, at 37°C and 5 % CO_2.

SNAP-tag labeling:

Before experiments, cells expressing a combination of $PTH1R_{FRET}$ and $RAMP2_{SNAP}$ were labeled with 1 µM SNAP-Cell 647-SiR in serum-free Fluorobrite™ DMEM for 30 min. Excessive dye was washed by exchanging medium three times every 10 minutes, and imaging was performed in RET buffer (**Table 14**).

HaloTag labeling:

12-24 hours before the experiment, 100 nM HaloTag® NanoBRET 618 was added to the cells during plating in 96-well plates. A minimum of 4 wells remained unlabeled to correct donor bleedthrough (unlabeled control).

Furimazine substrate addition

Before BRET experiments, cells in 96-well plates were washed with RET buffer and incubated with 90 µL of a 1:1000 (vol: vol) stock solution of furimazine in RET buffer (**Table 14**). After 3 minutes of incubation, measurement was started.

RET buffer
0.1 % (wt/vol) BSA
20 mM HEPES
137 mM NaCl
5 mM KCl
1 mM $MgCl_2$
1 mM $CaCl_2$
H_2O, pH=7.4

Table 14: Ingredients for RET buffer.

3.2.5 Assessment of PTH1R$_{FRET}$ surface expression through live-cell ELISA

3×10^6 HEK293T cells were seeded into 100 mm dishes and transfected 24 hours later with a combination of PTH1R$_{FRET}$ and pcDNA3/RAMP2$_{wt}$/RAMP2$_{SNAP}$ or PTH1R$_{cpGFP}$ and pcDNA3 (no HA-tag control) at a ratio of 1:1. The medium was exchanged after 12 hours, and 24 hours after the transfection, the cells were transferred to PDL-precoated transparent 96-well plates at a density of 70,000 cells/well. 48 hours later, cells were washed twice with washing buffer (**Table 15**). Subsequently, cells were incubated for 1 hour at 4 °C with rabbit anti-HA tag antibody (1:1000) in antibody buffer (**Table 15**). Following incubation, cells were washed four times with washing buffer and incubated for 1 hour at 4 °C with goat anti-rabbit IgG, HRP-linked antibody (1:4000) in antibody buffer. Finally, cells were washed three times with washing buffer, and 50 µL of the peroxidase substrate TMB was added. Following 30 minutes of incubation and development of a blue product, absorbance was recorded at 665 nm using a Neo2 plate reader. Subsequently, the cells were incubated for 20 minutes, and 50 µl of 2 M HCl was added. The absorbance was read at 450 nm using a Neo2 plate reader.

Washing buffer
0.5 % (wt/vol) BSA/PBS

Antibody buffer
1 % (wt/vol) BSA/PBS

Table 15: Ingredients for washing and antibody buffer.

3.3 Biophysical methods

Principe of the used method is in detail described at their corresponding Results section and here I present detailed protocol.

3.3.1 FRET kinetic experiments

Cells were imaged 36 - 48 hours after the transfection. Coverslips were washed once with RET buffer and kept in buffer at room temperature throughout the experiment. Coverslips were mounted onto an Attofluor™ chamber and washed once with RET buffer. The chamber was mounted onto an inverted Zeiss Axiovert microscope equipped with an oil-immersion 63x objective lens and a dual-emission photometric system. Image sequences had 40 ms acquisition intervals and were recorded with the VisiView 4.0 software.

For FRET experiments, cells expressing $PTH1R_{FRET}$ were excited with a 445 nm laser, and fluorescence emission was simultaneously recorded at 470/24 nm and 535/30 nm. Cells expressing $PTH1R_{cpGFP}$ were excited at 483 nm, and fluorescence emission was recorded at 506 nm.

3.3.2 Ligand application for kinetic experiments

Ligand application was performed using a high-speed solenoid valves perfusion system with a 100 µm inner diameter 8 to 1 channel manifold-tip. Valves were controlled with Octaflow II, and pressure was set to 60 mbar. Before the experiment, pressurized syringe reservoirs were washed with ddH_20 and filled with ligand solution in RET buffer. After the experiments, reservoirs were washed three times with ddH_20 and kept till subsequent usage with a small amount of ddH_20.

3.3.3 FRET acceptor photobleaching

Cells were imaged 36 hours after transfection. Coverslips were mounted onto the Attofluor™ chamber and washed once with RET buffer. Cells were kept in a FRET buffer at room temperature throughout the experiment.
The chamber was mounted onto a Leica SP8 confocal laser-scanning microscope, equipped with an oil immersion objective. LAS X microscope control software and the Leica FRET-AB wizard tool were used to perform experiments. A 1.5 mW white light laser was set to 1 % power, and a 431 nm laser line was used at 1 % power for donor imaging. For acceptor imaging, a 512 nm laser line at 1 % power was used, and for the bleaching, step increased to 100 % for ten frames. 512 × 512-pixel images were acquired with a hybrid detector in standard mode. Emission of donor channel was recorded within 440 – 512 nm, and emission of acceptor channel was recorded within 517 – 620 nm. The zoom factor was set to 5.5 x, resulting in a pixel size of 103 nm, and the laser scanning speed was set to 400 Hz. Fixed-size regions of interest (ROI) were selected on the cell membrane. For intramolecular FRET-AB experiments, ROIs expressing both $PTH1R_{FRET}$ and $RAMP2_{SNAP}$ were chosen.
FRET efficiencies were calculated with the manufacturer's Wizard tool, based on the provided ***Equation 2***, where I = fluorescence emission:

$$\textbf{\textit{Equation 2}}: FRET\ efficiency\ (\%) = \frac{I\ donor\ (postbleach) - I\ donor\ (prebleach)}{I\ donor\ (postbleach)}$$

A maximum of 4 cells was taken for analysis per image. To ensure coexpression integrity and enough bleaching of the acceptor, only cells with initial emission ratios (mCitrine/mTurquoise2) within 0.25 and 4, and bleaching > 20 %, were considered for statistical analysis.

3.3.4 Confocal microscopy

Coverslips were prepared for imaging as described before. Excitation and emission settings for imaging were: a 1.5 mW white light laser was set to 1 % power, and a 431 nm laser line was used at 2-5 % power for donor imaging. For acceptor imaging, a 512 nm laser line at 2 - 5 % power was used. Emission of donor channel was recorded within 440 – 512 nm, and emission of acceptor channel was recorded within 517 – 620 nm. The zoom factor was set

to 2-10 x, and the laser scanning speed was 200 - 400 Hz. 1024 × 1024-pixel images were acquired with a hybrid detector in sequential scan mode to avoid bleed through.

3.3.5 Total internal reflection fluorescence microscopy

Total internal reflection fluorescence microscopy (TIRFM) was performed by dr. Jan Möller. Briefly, CHO cells, expressing HaloTag-RAMP2 were labeled with 1 µM Janelia Fluor® 646 HaloTag® ligand for 15 minutes, followed by three subsequent washing steps for 5 minutes. Cells were imaged on the above described TIRF-microscope by using 100x objective and the Cy5-emission channel. More details are presented in the works of other lab members (Işbilir *et* al., 2020a; Möller *et* al., 2020a; Möller, 2020).

3.3.6 Microplate photometry

96-well plates were taken from the incubator, the medium was removed, and cells were washed once with RET buffer and incubated with 90 µL of RET buffer (for FRET experiments) or 90 µL of a 1:1000 (vol: vol) stock solution of furimazine in RET buffer (for BRET experiments). After 5 minutes, basal reads were recorded for four minutes and subsequently, 10 µL of 10-fold ligand solution or RET buffer was applied to each well, and the simulated reads were further recorded.

RET measurements were performed at 37 °C using a Synergy Neo2 Plate Reader with a monochromator optics or filter sets. FRET experiments were performed with ten excitation flashes per data point. For FRET constructs-expressing cells, 420/50 nm excitation filter and 485/20 nm and 540/25 nm dual emission filter were used. For $PTH1R_{cpGFP}$-expressing cells, 485/20 nm excitation and 516/20 nm emission filters were used. For the fluorescence emission spectrum of $PTH1R_{cpGFP}$, cells were excited at 455/10 nm, and fluorescence emission was recorded with 1 nm resolution within 500 - 660 nm.

For the $PTH1R_{FRET}$, EKAR, or H187 biosensor-expressing cells, expression levels were measured with a monochromator optics. Cells were excited at 510/20 nm, and fluorescence emission was recorded at 560/20 nm.

BRET experiments were performed with the NanoBRET filter set - 450/50 and 610LP nm dual emission filter or 516/20 nm and 590/35 nm double emission filter, integration time per data point was set to 0.3 s and gain to 100/120 (GRK2 recruitment) or 90/110 (β-arrestin2 recruitment, Gs activation). $GRK2_{YFP}$- and β-arrestin2-expressing cells were excited at 510/20 nm, and fluorescence emission was recorded at 560/20 nm for quantification of expression level.

3.4 Data analysis and statistics

3.4.1 Microscopy

For microscopic FRET experiments, fluorescence emission time courses of both FRET donor and acceptor were routinely corrected for background and spectral bleed-through, and the FRET ratio was calculated as described earlier (Vilardaga *et* al., 2003b; Börner *et* al., 2011). Briefly, corrected FRET was calculated: $\boldsymbol{FRET_{Cor} = Ch_{FRET} - f \times Ch_{mTurquoise2}}$. Ch_{FRET} and $Ch_{mTurquoise2}$ were the emissions in the FRET and mTurquoise2 channels,

respectively, and f was previously calculated bleed-through coefficient, estimated to 1,13. Corrected FRET ratio was calculated as ***FRET ratio*** $= \frac{\boldsymbol{FRET\ Cor}}{\mathbf{Ch\ mTurquoise2}}$. The bleedthrough of mCitrine into the 480-nm channel was negligible.
ΔFRET values were calculated as normalized differences between basal and stimulated FRET ratios.
For calculating time constant τ (s), agonist-independent changes in FRET due to photobleaching were subtracted. The decrease in FRET ratio was fitted with the one-phase decay function ***Equation 3;***

$$\textbf{\textit{Equation 3:}}\ Y = (Y0\ -\ Plateau) - e^{(-K*X)}) + Plateau$$

Y_0 is the Y value when X (time) is zero. Plateau is the Y value at infinite times. K is the rate constant, and time constant τ (s) is computed as the reciprocal of K. X_0 was constrained to the starting time of the decay during the curve fitting procedure.

3.4.2 Microplate photometry

For microtiter plate experiments, the data were analyzed in Microsoft Excel and if needed, wells out of the fluorescence range of plate readers were excluded. For FRET and BRET experiments, raw RET ratios were defined as acceptor emission/donor emission (Börner *et* al., 2011; Schihada, 2021). RET ratios before ligand/buffer addition were averaged and defined as RETbasal. To quantify ligand-induced RET changes, ΔRET was calculated for each well and time point as percent over basal with ***Equation 4.***

$$\textbf{\textit{Equation 4:}}\ \Delta RET\ (\%) = 100 * \frac{RETstim - RETbasal}{RETbasal}$$

Subsequently, the average ΔRET of buffer-treated control wells was subtracted. To reduce the fluctuation of the BRET ratio, three consecutive BRET ratios were averaged before and after ligand addition. Concentration-response curve experiments were fitted using a three or four-parameters logistic curve fit as stated in corresponding figure legends.
Statistical differences were evaluated using a one-way ANOVA test followed by Tukey multiple comparisons, Brown-Forsythe ANOVA, followed by Dunnett T3's multiple comparisons test, Student's t-test, Mann Whitney test, or extra-sum-of squares F-test. Each figure legend contains a description of statistical treatment. Differences were considered significant for values of $p < 0.05$. The data were analyzed and visualized using Microsoft Excel 2016 (Microsoft, Washington, USA), GraphPad Prism software 8.1.2 (GraphPad Software, California, USA), and OriginPro 2018 software (OriginLab, Massachusetts, USA).

4 RESULTS AND DISCUSSION

4.1 RAMPs – characterization and tools

4.1.1 Characterization of endogenous expression levels of RAMPs in the experimental model system

The characterization of endogenous RAMPs abundance was performed in-house cell lines to ensure that our experimental design and our observations are not confounded by observational bias (*e.g.*, assay, cell background) (Kolb *et* al., 2022) lines.

The most direct and obvious way to test for the presence of RAMPs in cell lines would be via Western Blot experiments to detect protein expression in the samples. Unfortunately, antibodies for RAMPs are non-specific, and their usage is highly contested by the established laboratories working with RAMPs (D. L. Hay & Pioszak, 2016a). After a few unspecific and unreproducible experiments, where many unspecific bands were observed, or antibodies could not reproduce the effect, although used with the same sample, it was decided not to use them. Instead, RT-PCR experiments with the adjacent functional assays were recognized as a more reliable indicator of the cellular background in in-house cell lines.

First, it was made sure that RAMPs can be efficiently transfected in our cell lines to study their modulation effect. For this reason, different transfection reagents and protocols were tested (**Figure 16**), and the amount of $RAMP2_{CFP}$ was visualized through the emission of its C-terminally fused CFP tag. Finally, the transfection method with Lipofectamine 3000 was recognized as the most efficient since it enabled the highest amount of transfected $RAMP2_{CFP}$ and was therefore used for future experiments.

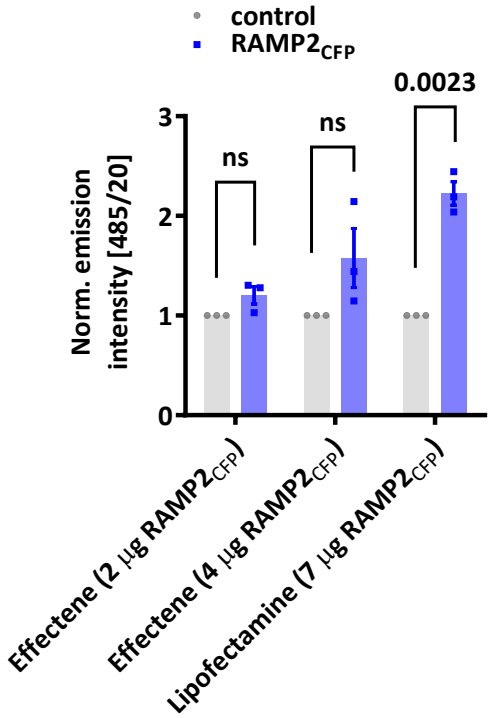

Figure 16: Comparison of different transfection methods for expression of RAMP2 protein.
HEK293 cells were transiently transfected with control or $RAMP2_{CFP}$ using different transfection reagents; Effectene with two different amounts of cDNAand Lipofectamine 3000. Indicated cDNA amounts corresponds to transfection in 10 cm plates. Fluorescence emission of CFP was visualized in a plate reader at 485 nm. Emissions of each different transfection were normalized to corresponding control groups, data from three independent experiments. The significance between experimental groups was tested with t-test, ns<0.05. The data were acquired by dr. Hannes Schihada.

Second, RT-PCR experiments were performed to compare the abundance of mRNA transcripts in the in-house cell lines. Expression profiles were visualized as inverse cycle threshold values (1/CT) to better perceive the relative comparison between the amounts. Higher 1/CT represents a more abundant transcript since it reaches the detection threshold in the earlier cycles than those with smaller 1/CT. Visualization starts at 0.025 (=1/40) to represent the latest possible cycle used and, therefore, the smallest possible 1/CT.

In some cell lines, RAMP transcripts were not detected. RAMP1,2,3 are differently coexpressed across in-house cell lines, and its amounts are in accordance with previous reports (D. L. Hay & Pioszak, 2016b). RAMPs transcripts are usually present in the CHO cells but at very low amounts, not sufficient to create functional AM, CGRP, or amylin receptor complexes (Tilakaratne *et* al., 2000; Wootten *et* al., 2013, p. 2). Here, small amount of RAMP3 was detected. COS7 cells mostly expressed no (R. J. Bailey & Hay, 2006; Bouschet et al., 2005) or very low amounts of the endogenous RAMPs and those were usually not enough to construct functional receptor complexes (Bühlmann *et* al., 1999; Tilakaratne *et* al., 2000) – cell clone of our lab detected only small amounts of RAMP1 and RAMP3. HEK293 cells according to the previous reports express RAMP1 (Bouschet *et* al., 2005), whereas HEK-TSA cells RAMP1 and RAMP2 (McLatchie *et* al., 1998). There are no reports on HEKAD cells. All examined HEK clones from the lab (HEK293, HEKAD, and HEKTSA) showed detectable amounts of RAMP2, whereas HEK293 and HEKTSA also RAMP1.

Then, it was tested if transfection of RAMP2wt could increase the amount of detected RAMP2 transcript (**Figure 17 B**) – change between endogenous and transfected transcript was in 13 cycles. With approximately 85% - 90% efficiency of duplication in one cycle (which should be separately calculated from the slope of dilution curve) speak for mRNA abundance difference of 1000-2000x. It would be good to repeat those experiments with endogenous control to correct mRNA/cDNA content variation. This variation can originate from reverse-transcription efficiency, RNA degradation or the presence of inhibitors in the RNA sample, and differences in the handling of the samples (Nemec, 2017). Therefore, we can compare reliably only samples within one cell line, where the same sample was tested with specific TaqMan ® probes for RAMP1, RAMP2, and RAMP3 (**Figure 17 A**).

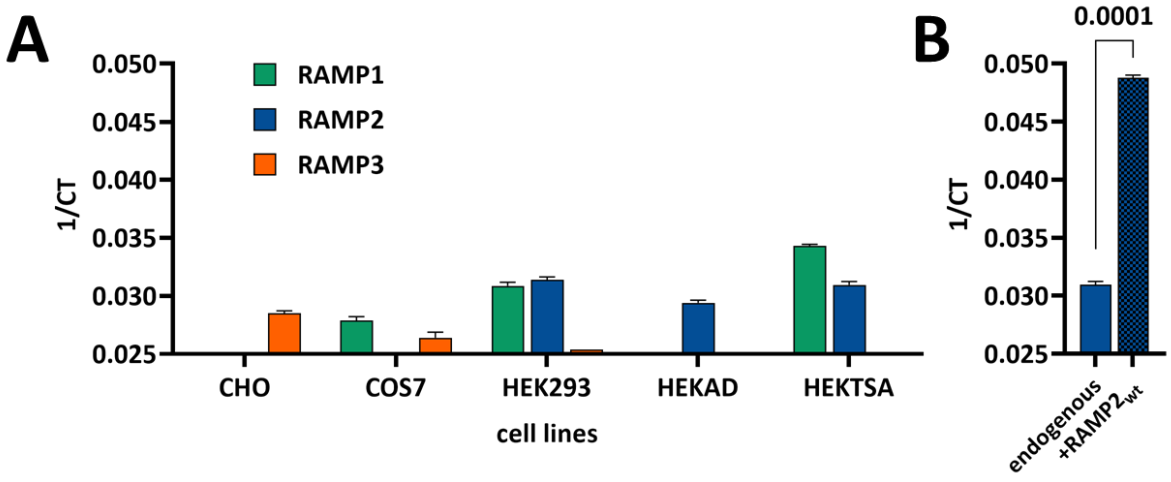

Figure 17: Expression profile of RAMPs measured by RT-PCR.
*(**A**) Endogenous expression of three RAMP isoforms in different cell lines.*
*(**B**) Impact of RAMP2wt transfection on mRNA abundance of RAMP2 transcript in HEKTSA cell line.*

Total mRNA was extracted from HEK293 cells, transfected with cDNA encoding for pcdna3 or RAMP2wt. Expression of RAMP transcripts was measured with isoform-specific TaqMan probes by RT-PCR. Inverse cycle threshold values (1/CT) values are reported for all RAMP isoforms. The data are mean ± SD of one experiment, performed in triplicates.

The current strategy to test the functionality of the reported low amounts of RAMPs in the cell lines is to characterize if the detected amount is enough to establish functional receptor complexes. For this, a prototypical receptor that interacts with all three RAMPs, CRLR, was used with Epac-S^{187} biosensor for cAMP accumulation and empty vector or RAMP123$_{wt}$. HEK293 cells were transfected accordingly and tested with increasing concentrations of cognate agonist (**Figure 18**). Endogenously present RAMP1 could form high-affinity heterooligomer CRLR/RAMP1 as shown in **Figure 18 A** with practically identic curves for control (black) and RAMP1$_{wt}$ cotransfected group (green). Interestingly, although RAMP2$_{wt}$ is present in the previously tested clone of in-house HEK293 cells, its amount wasn´t enough to construct a high-affinity complex of CRLR/RAMP2 (**Figure 18 B**). This can be seen as the two logs´ right shift of the curves when RAMP2$_{wt}$ (or RAMP3$_{wt}$) was cotransfected. As expected, since RAMP3$_{wt}$ is not present in HEK293 cells, it could not construct a functional CRLR/RAMP3 complex (**Figure 18 C**). Also here, two logs´ right shift was observed by cotransfection of RAMP3$_{wt}$.

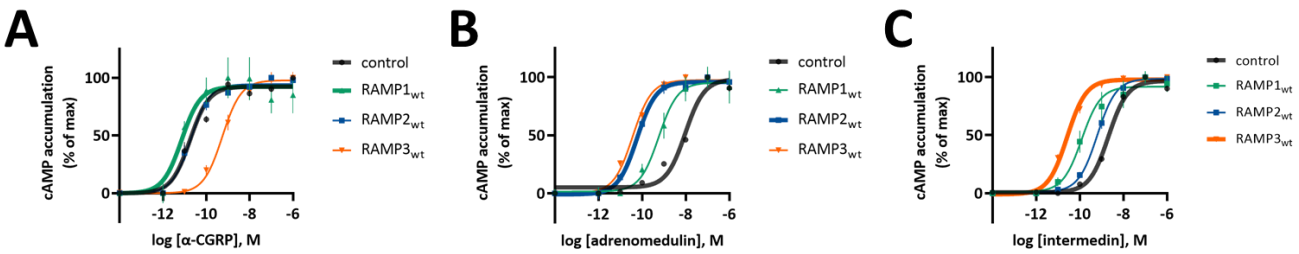

Figure 18: cAMP accumulation experiments in native and transfected HEK293 cells.
*HEK293 cells were transiently expressing CRLR$_{wt}$, cAMP-based FRET biosensor (Epac-S^{187}), and empty plasmid, RAMP1$_{wt}$, RAMP2$_{wt}$ or RAMP3$_{wt}$ in a ratio of 1:1:1. Then, cells were treated with increasing concentrations of cognate agonist for either of heterooligomers (**A**) α-CGRP for CRLR/RAMP1, (**B**) adrenomedullin for CRLR/RAMP2 and (**C**) intermedin for CRLR/RAMP3. Experiments were performed in a plate readera and the data were normalized to the final addition of 10 µM Fsk/100 µM IBMX for each corresponding group and normalized to the response of control cells (with empty plasmid). The data were fitted with three-response parameters fit and represents the mean ± SEM of three independent experiments performed in triplicates.*

In summary, in-house HEK293 cells hold a small amount of RAMP1, no RAMP3, and a detectable amount of RAMP2, which can nevertheless not present a functional CRLR/RAMP2 complex. First, efficient transfection of RAMP2 was detected via accessing CFP tag of transfected RAMP2$_{CFP}$ with measurement of fluorescence emission at the plate reader. Second, RAMP2$_{wt}$ was transfected, and the abundance of mRNA transcript was measured via RT-PCR. As later transfection showed to be overriding endogenous levels for approximately 1000x, it was supposed that cellular background does not confound performed experiments. In fact, expression levels in performed experiments mimic high expression in specific tissues in the human body (McLatchie *et* al., 1998), expecting a functional role of PTH1R-RAMP2 heterooligomer (placenta, endocrinal tissues, lung).
Hence, experimental setup was properly standardized for analysing modulation effect of RAMP2 and represents (within *ex-vivo* cell experimental context) *bona fide* image of RAMPs effects at the biochemical level.

4.1.2 Design and characterization of RAMP constructs

RAMPs have been shown to modulate several GPCRs, among others, PTH1R, but the molecular mechanism of their modulation remained poorly understood. To assemble a toolbox to study GPCR-RAMP interactions, RAMP proteins were primarily modified to obtain constructs suitable for imaging and FRET studies.

To access their localization and visualize them, RAMP proteins were tagged with different intracellular and extracellular tags on their N- or C-terminus (**Figure 19**). First, the mTurquoise2 fluorophore (Goedhart *et* al., 2012) was fused to the C-terminal of RAMP1, RAMP2, and RAMP3 (**Figure 19 A**). Second, the self-labeling SNAP-tag was fused to the C-terminal of the RAMP2 (**Figure 19 B**). Third, to investigate RAMPs at the single-molecule level, a $(GGGGS)^3$-P-HaloTag-P-$(GGGGS)^3$ module was added after Ala42, at the N-terminal portion of RAMP2 (**Figure 19 C**). Self-labeling SNAP-tag® and HaloTag® allowed maximum versatility by experiments via labeling with various SNAP-tag® and HaloTag® dyes, resulting in fluorophores emitting at different wavelengths. To further minimize the size of the tag and its potential interference with protein folding or expression, the unnatural amino acid codon TAG was inserted on the distal part of the N-terminus; after the position Leu31 or Ala42 (**Figure 19 D, E**). Finally, with combinations of N- and C-terminal insertions, UAA-$RAMP2_{ECFP}$ constructs were created (**Figure 19 E**), which were used for spatial analysis of RAMP localization. The N-terminal tags were inserted at the the unstructured (**Figure 19 F**), compared to tree highly structured helices, which play a role in intermolecular interaction with GPCRs (Ouyang *et* al., 2020). Knowing that insertion of other tags (*e.g.*, c-Myc tag) or artificial signal sequence in their N-terminal can affect their subcellular distribution in the cell, especially of RAMP2 or RAMP3 (Christopoulos *et* al., 2003), it was aimed to use RAMPs in their near-native form to ensure that modified RAMP construct would interfere minimally with examined GPCR function and avoided misinterpretation of further experiments.

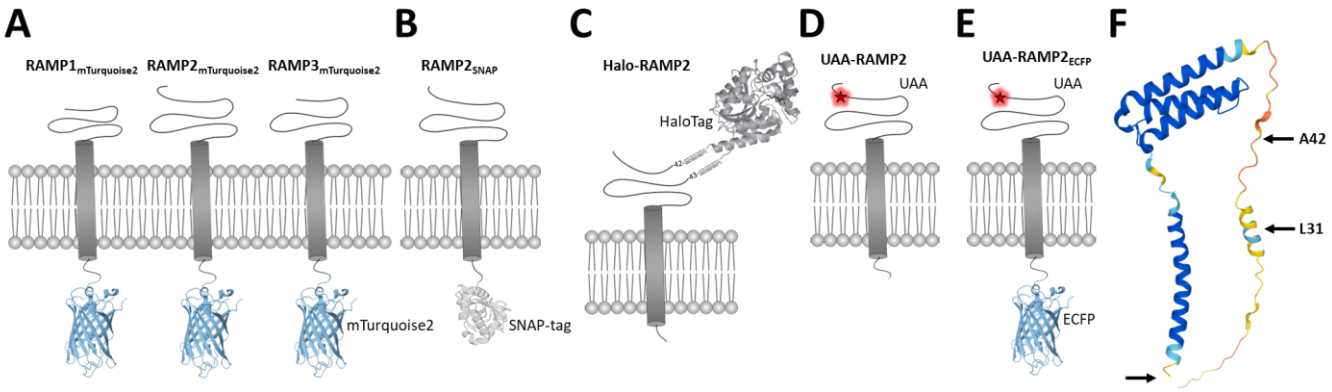

Figure 19: Tagging RAMP proteins.

(***A***) *MTurquoise2 was fused to the C-terminal of RAMP1,2,3.* (***B, C***) *RAMPs with self-labeling tags: SNAP-tag® was fused to the C-terminal of RAMP2, and HaloTag® was fused via* $(GGGGS)^3$*-P linkers after Ala42 on the N-terminal part of RAMP2.* (***D***) *RAMP2 with inserted UAA (unnatural amino acid) enables biorthogonal labeling. Two versions were created: UAA was fused after position Leu31 or Ala42.* (***E***) $RAMP2_{ECFP}$ *with inserted UAA codon after position L31 or A42.* (***F***) *RAMP2 as predicted in AlphaFold Protein Structure Database. Arrows indicate points of insertion of the UAA codon. Colour code shows per-residue confidence score (pLDDT) between 0 and 100: Very high (pLDDT > 90, blue), Very low (pLDDT < 50, orange).*

To examine RAMP2 expression at different time points and determine the best experimental conditions for future analysis, $RAMP2_{SNAP}$ was transfected into HEK293 cells (**Figure 20 A**) and imaged under a confocal microscope. Transfected cells were labeled with 1 µM SNAP-Cell® 647-SiR dye at each time point. As expected (Christopoulos *et* al., 2003), after 16 h (**Figure 20 B**)**,** RAMP2 expression was primarily detected intracellularly. Total expression of RAMP2 gradually increased after 22 h (**Figure 20 C**) and even more after 46 h (**Figure 20 D**) and at the last time point - 70 h after the transfection (**Figure 20 E**) considerable amount of RAMP2 was also detected on the cell surface. Thus far, RAMP2 was expressed mainly intracellularly and only after longer expression times reached the cell surface. Therefore, transfection times >46 hours were used for most experiments.

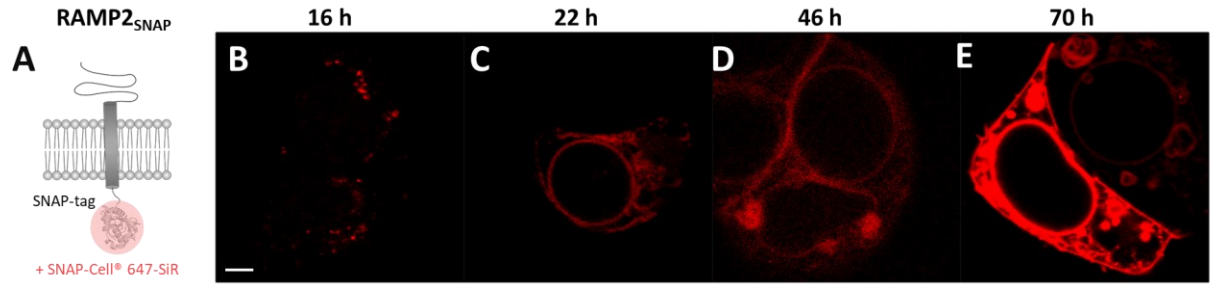

Figure 20: Visualizing RAMP2 over time.
*(**A**) Graphical depiction of $RAMP2_{SNAP}$. (**B, C, D, E**) HEK293 cells were transfected with $RAMP2_{SNAP}$, labeled with 1 µM SNAP-Cell® 647-SiR and imaged under the confocal microscope. Cells were imaged 16 h (**B**), 22 h (**C**), 46 h (**D**), and 70 h (**E**) after the transfection. Scale bar = 10 µM.*

To distinguish between intracellular and cell surface expression, constructs with intra- and extracellular tags were created; UAA-RAMP2-ECFP (**Figure 21**). UAA - unnatural amino acid codon - represents the least invasive genetic incorporation since this changes solely one residue of native genetic code and thus, minimally perturbs GPCR function (Serfling *et* al., 2019). HEK293 cells were transiently transfected with UAA-$RAMP2_{ECFP}$ (**Figure 21 A**) and tRNA/AARS plasmid.Cells were labeled with Tetrazine-Cy5 prior to imaging at the confocal microscope. Qualitatively similar expression levels of UAA31 (**Figure 21 B, C**) and UAA42-variants (**Figure 21 D, E**) were observed. Most of the RAMP was retained intracellularly with minimal expression on the cell surface. Those experiments could be further improved by using Tetrazine-Cy3 dye, which possesses a higher signal-to-noise ratio than herein used Tetrazine-Cy5 (Kowalski-Jahn *et* al., 2021).

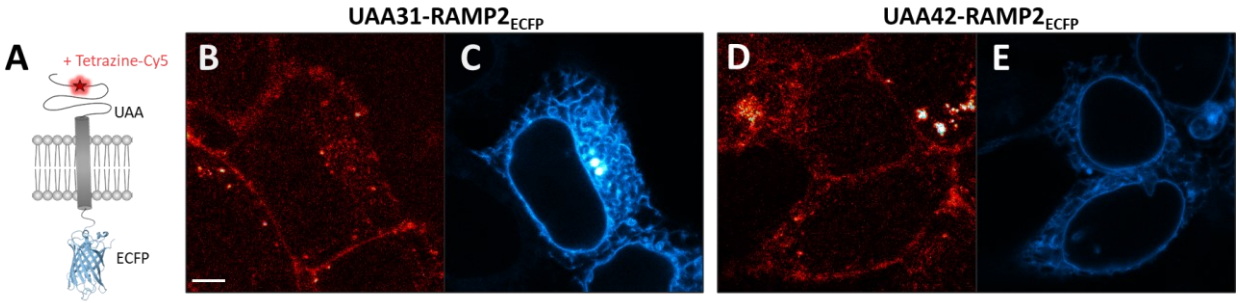

Figure 21: Visualizing RAMP2 surface and intracellular expression.

(***A***) *Graphical depiction of UAA-RAMP2ECFP. (**B-E**) HEK293 cells were transfected with UAA31-RAMP2ECFP (**B, C**) and UAA42-RAMP2ECFP (D, E), labeled with Tetrazine-Cy5, and imaged under the confocal microscope. Cy5 channel represents a cell-surface expression of RAMP2 (A, C) and ECFP channel intracellular localization (**B, D**). Scale bar = 10 µm. Cells were imaged under the confocal microscope.*

To examine RAMPs localization on the cell surface with the most accurate approach available to date, a high spatial resolution method based on total internal reflection fluorescence microscopy (TIRFM) was used. This allowed us to resolve and visualize RAMP at single-molecule precision (**Figure 22**) at the surface of intact cells. Chinese hamster ovary (CHO) cells were transiently transfected with HaloTag-RAMP2 (**Figure 22 A**) and labeled with JF 646 dye. The experiment at that resolution needed to be done at much shorter expression times of about 6 hours to achieve low expression levels so that detection and differentiation of single molecules on the cell membrane was possible (Sungkaworn *et* al., 2017; Möller *et* al., 2020b; Işbilir *et* al., 2020a). TIRFM allows to image only a very narrow evanescence field and thus can focus only on the membrane and sub-membrane compartment. From TIRF movies (single shot representation is **Figure 22 B**), it was concluded that HaloTag-RAMP2 was able to reach the cell surface and was able to diffuse. In the future, it will be convenient to exchange HaloTag® for SNAP-tag® to use benzyl guanine derivatives dyes (*e.g.*, SNAP-Surface 549) (Sungkaworn *et* al., 2017; Möller *et* al., 2020b; Işbilir *et* al., 2020a) or to synthesize HaloTag®-equivalent of this dye to achieve better efficiency and less unspecific labeling.

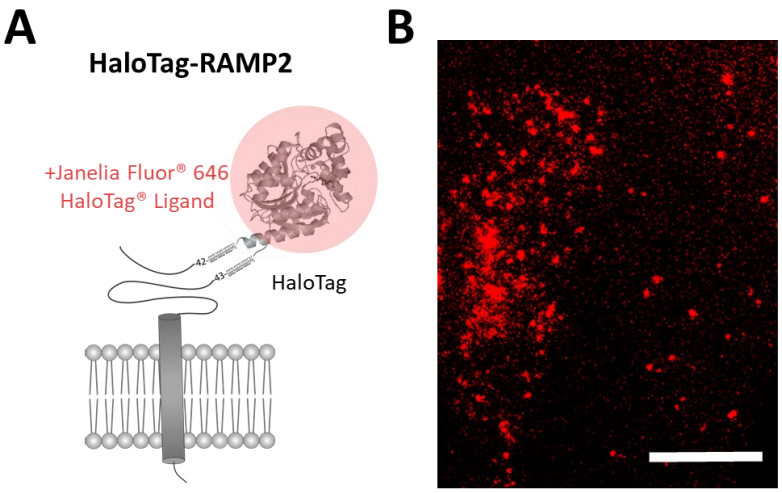

Figure 22: Visualizing RAMP2 at the single molecule level.
*(**A**) Graphical depiction of HaloTag-RAMP2. (**B**) CHO cells were transfected with HaloTag-RAMP2, labeled with 1 µM Janelia Fluor® 646 HaloTag® Ligand, and imaged with a total internal reflection microscope. Scale bar = 10 µM. The experiment was performed by dr. Jan Möller.*

This section has described different strategies used to label RAMP protein to 1) get information about its cellular localization in the absence of the interacting receptor, and 2) validate designed genetically encoded constructs, which were used for further studies. By doing so, a dominantly intracellular RAMP localization was confirmed as described previously (Christopoulos *et* al., 2003), and > 48 h post-transfection time was chosen for further experiments to achieve saturation of RAMP2 molecules on the cell surface. The portfolio of genetically encoded RAMP constructs was expanded in order to ease handling in different setups and cell types. Working materials need

to be adapted to the selected experimental techniques since each a different technique favors different approach to labeling. Here, conventional approaches of fusing fluorescent proteins with two advanced strategies are highlighted, which could help elucidate RAMP pharmacology in the future: 1) use of self-labeling SNAP-tag® and HaloTag®, enabling use with numerous dyes, and 2) incorporation of minimally intrusive unnatural amino acid codons. To note, conventional tags such as HA, FLAG, c-Myc, or similar, which could be accessible through antibody labeling, were not used due to previous reports of perturbing intracellular localization of RAMPs (Christopoulos *et* al., 2003).

Labeling dyes, probes and fluorophores can differ in ("Fluorophores, Dyes & Probes | Biocompare.com," 2022): wavelength of emission, suitability for extra- or intracellular labeling, appropriateness for labeling of proteins *in vitro* and/or *in vivo* (Juillerat *et* al., 2003; Maurel *et* al., 2008; Los *et* al., 2008; Grimm *et* al., 2017; Scholler *et* al., 2017; Grimm *et* al., 2020; Kowalski-Jahn *et* al., 2021), rightness for particular technique, for example, super-resolution microscopy (Mo *et* al., 2017; Q. Zheng *et* al., 2019), single-molecule imaging (Grimm *et* al., 2016), expansion microscopy (Sun *et* al., 2020), photoswitching (Hüll *et* al., 2018; Minoshima & Kikuchi, 2017) or labeling at the endogenous expression levels with fluorescent ligands (Vernall *et* al., 2014; Soave *et* al., 2020; Bathe-Peters *et* al., 2021) and CRISPR-ed tags (Soave *et* al., 2021; C. W. White *et* al., 2020). The suitability of labeling protocol for the specific technique is reviewed often (Chudakov *et* al., 2010; Rodriguez *et* al., 2017; Shaner *et* al., 2005; Specht *et* al., 2017; Valli *et* al., 2021; J. Zhang *et* al., 2002) and should be referred to when future research directions are designed.

4.2 Analysis of PTH1R-RAMP interaction on the cell surface

4.2.1 Colocalization analysis

Previous reports from the literature stated that PTH1R interacts with RAMP2 or with all three RAMP isoforms (Christopoulos *et* al., 2003; Lorenzen *et* al., 2019; Mackie *et* al., 2019). Eager to explore RAMPs´ role in the receptor activation process, it was set out to examine PTH1R-RAMP interaction at the cellular compartment where this process primarily occurs - on the cell surface.

Based on an established HA-PTH1R$_{wt}$ construct, a new analogous construct HA-PTH1R$_{mCitrine}$ was created (**Figure 23 A**). For this purpose, mCitrine was fused (Zacharias *et* al., 2002) after Gly497 on the C-terminus of PTH1R. In parallel, mCitrine was fused to the C-terminus of β_2AR. Other constructs were created for examining processes downstream of receptor activation: NanoLuc was fused to the C-terminus of PTH1R, CTR, and β_2AR, creating PTH1R$_{NanoLuc}$, CTR$_{NanoLuc}$, and β_2AR$_{NanoLuc}$ (**Figure 23 B**). For control constructs, mTurquoise2 and mCitrine fluorophores were targeted on their N-terminus to the membrane via a CAAX tag (mem$_{mTurquoise2}$ and mem$_{mCitrine}$) (**Figure 23 C, D**).

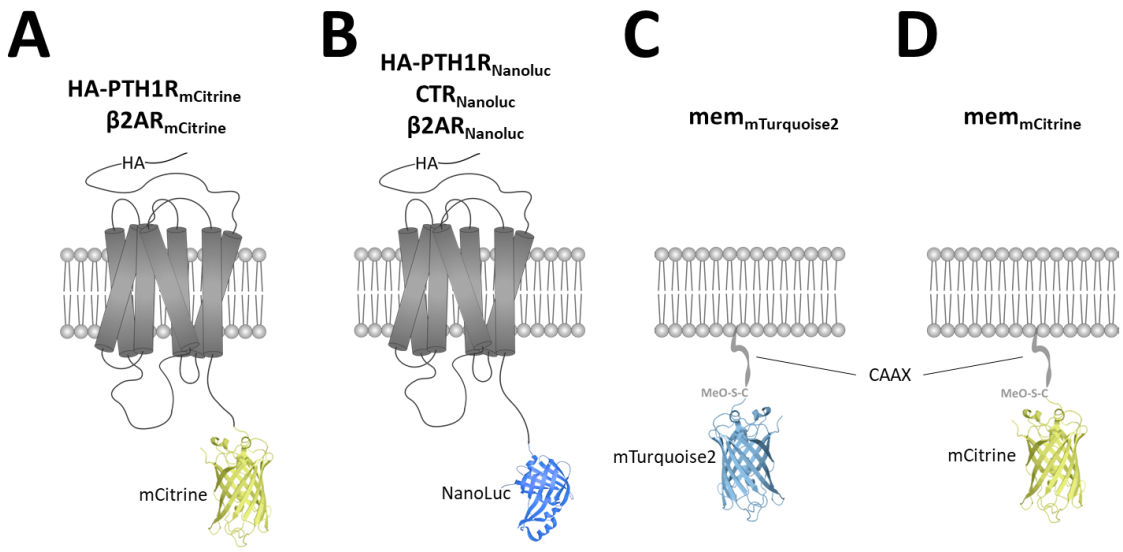

Figure 23: Tagging PTH1 receptor and control constructs.

*PTH1R was tagged at its C-terminus to construct PTH1R$_{mCitrine}$ (**A**) and PTH1R$_{NanoLuc}$ (**B**). Creating two versions: first with fluorescent mCitrine tag and second with the bioluminescent NanoLuc tag enabled its usage in various FRET- and -BRET-based assays. (**C, D**) Similarly, mCitrine and mTurquoise2 were anchored via the CAAX tag to the membrane.*

I cotransfected PTH1R$_{mCitrine}$ (**Figure 23 A**) together with RAMP1$_{mTurquoise2}$, RAMP2$_{mTurquoise2}$, or RAMP3$_{mTurquoise2}$ (**Figure 19 A**) and imaged them after 48 with a confocal microscope (**Figure 24**). Successful expression of all constructs was observed. A higher expression was measured when RAMP2$_{mTurquosie2}$ was coexpressed with PTH1R$_{mCitrine}$, which was in agreement with previous studies (Christopoulos *et* al., 2003), supposing the impact of stabilization of RAMP2 when it is in complex with the interacting receptor. Mean intensities for RAMP$_{mTurquoise2}$ channel were: 462 (**Figure 24 D**), 1607 (**Figure 24 E**) and 1302 (**Figure 24 F**) fluorescence a.u. when cells were outlined in a region of interest (ROI), and mean intensity was measured with ImageJ. Line scan analysis (**Figure 24 S, T, U**) verified colocalization of CellMask™ Deep Red Plasma membrane stain with PTH1R$_{mCitrine}$ when it was coexpressed with RAMP2$_{mTurquoise2}$ (**Figure 24 T**) or RAMP3$_{mTurquoise2}$ (**Figure 24 U**) but not RAMP1$_{mTurquoise2}$ (**Figure 24 S**). That could suggest that PTH1R and RAMP1 poorly colocalize (**Figure 24 A, D, G, M, P**). For experimental groups of PTH1R+RAMP2 (**Figure 24 B, E, H, N, Q**) and PTH1R+RAMP3 (**Figure 24 C, F, I, L, O, R**) line scan analysis revealed that they are located together on the membrane as also in other cellular compartments.

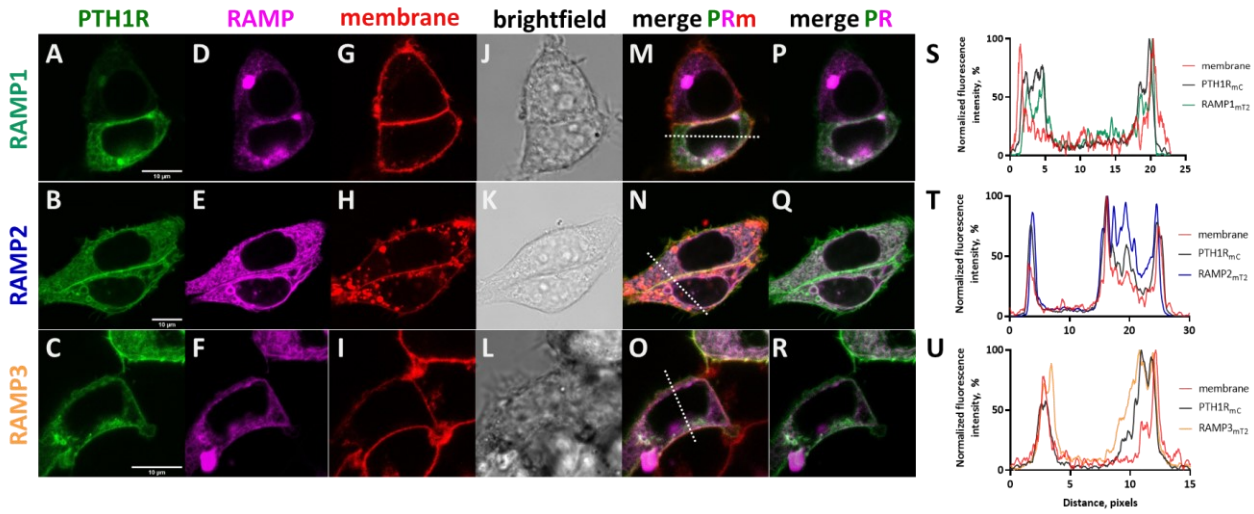

Figure 24: Colocalization analysis of PTH1R and RAMPs at the confocal microscope.

*Colocalization experiments were conducted in HEK293 cells, transiently cotransfected with a combination of PTH1R (**A-U**) and RAMP1 (**A, D, G, M, P**), RAMP2 (**B, E, H, N, Q**) or RAMP3 (**C, F, I, L, O, R**) constructs. Representative images from confocal microscope showing expression in different channels, CellMask™ Deep Red Plasma membrane stain (**G-I**), brightfield images (**J-L**), and merged images of PTH1R and RAMP with (**M-O**) or without membrane stain (**P-R**). All images were taken at the same magnification level and acquisition settings, with scale bars = 10 µM. (**S-U**) Line scans of separate channels as indicated with a dotted white line in (M-O). Absolute fluorescence values were normalized and overlayed to visualize the colocalization area (**S-U**).*

4.2.2 Acceptor photobleaching analysis

To further quantify PTH1R-RAMP2 interaction on the surface of the cells, acceptor photobleaching experiments were conducted, employing the constructs presented in **Chapter 4.1.1**.

Besides PTH1R$_{mCitirne}$, a set of control constructs was created to calculate the amount of random, nonspecific FRET, which could happen at the high expression level of the constructs and consequently cause random colocalization and collision of the fluorophores (Vilardaga *et* al., 2008). First, mCitrine was fused to the β_2-adrenergic receptor ($\beta_2AR_{mCitrine}$), as a prototypical receptor which is not interacting with RAMPs (Lenhart *et* al., 2013a; Mackie *et* al., 2019) (**Figure 23 A**). Second, mTurquoise2 and mCitrine fluorophores were targeted to the membrane via a CAAX-box, attached through their N-terminal ($mem_{mTurquoise2}$ and $mem_{mCitrine}$, respectively) (**Figure 23 C, D**).

Constructs were transiently expressed in HEK293 cells, and uniformed ROIs were selected on the cell membrane of intact cells. Acceptor photobleaching experiments were conducted, and FRET efficiencies between the protein of interest at comparable expression levels were quantified (**Figure 23 E**). The FRET efficiencies were calculated from the change in donor emission before and after photobleaching of the acceptor. Calculated FRET efficiency of cells expressing PTH1R$_{mC}$ with RAMP2$_{mT2}$ was significantly higher than for a combination of PTH1R$_{mC}$ with either RAMP1$_{mT2}$ ($p<0.001$) or RAMP3$_{mT2}$ ($p=0.02$) or for a combination of the β_2-adrenergic receptor (β_2AR_{mC}) with RAMP2$_{mT2}$ ($p<0.001$) (**Figure 25 C**). Moreover, it was also different from background FRET (**dotted line, Figure 25 C and D**), which was calculated as the mean of FRET efficiency of various control constructs; membrane tags, membrane tags with RAMP2$_{mT2,}$ and β_2-adrenergic receptor (β_2AR_{mC}) with RAMP2$_{mT2}$ (**Figure 25 D**). Summarizing the

data in **Table 16**, it was concluded that PTH1R preferentially interacts with RAMP2, only in a limited manner with RAMP3 and even less with RAMP1.

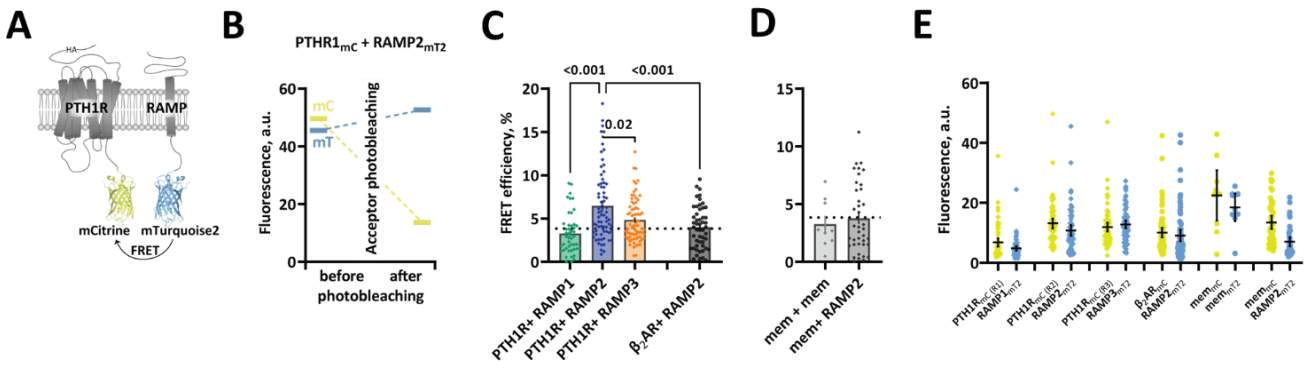

Figure 25: Intermolecular FRET reveals RAMP2 as an interaction partner of PTH1R.

(***A***) *Schematic representation of the constructs for FRET acceptor photobleaching experiments between PTH1R and RAMP2. Photobleaching experiments were conducted in HEK293 cells, transiently cotransfected with a combination of donor- and acceptor-tagged constructs. The acceptor fluorophore (mCitrine, mC) was fused to the C-terminal of the PTH1R ($PTH1R_{mC}$), to the control β2-adrenergic receptor ($β2AR_{mC}$) or targeted to the plasma membrane via a -CAAX sequence (mem_{mC}). The donor fluorophore (mTurquoise2, mT2) was fused to the C-terminal of RAMPs ($RAMP1/2/3_{mT2}$) or targeted to the plasma membrane via a -CAAX sequence (mem_{mT2}).*

(***B***) *A representative experiment showing photobleaching efficiency in cells expressing $PTH1R_{mC}$ and $RAMP2_{mT2}$. Fluorescence emissions of both donor (mC) and acceptor (mT2) were recorded before and after acceptor photobleaching.*

(***C, D***) *FRET efficiencies from photobleaching experiments were recorded with a confocal microscope. The data are expressed as % of donor emission increase after photobleaching for each experimental group. The dotted line indicates the average FRET efficiency of negative control groups (grey bars). The data are derived from at least three independent experiments and a number of cells as stated in **Table 16**: The bars represent means ± SEM. One point represent a single-cell experiments. Significance between the groups was tested by Brown-Forsythe ANOVA, followed by Dunnett's multiple comparisons test, ns: $p > 0.05$.*

(***E***) *Comparison of expression levels of tagged constructs used in intermolecular FRET photobleaching experiments. Basal fluorescence emissions of mCitrine (mC, acceptor, yellow) and mTurquoise2 (mT2, donor, cyan) before photobleaching; the experimental setting corresponds to (**A**). The data show individual values, mean ± SD of at least three independent experiments.*

	$PTH1R_{mC}$ + $RAMP1_{mT2}$	$PTH1R_{mC}$ + $RAMP2_{mT2}$	$PTH1R_{mC}$ + $RAMP3_{mT2}$	$β_2AR_{mC}$ + $RAMP2_{mT2}$	mem_{mC} + mem_{mT2}	mem_{mC} + $RAMP2_{mT2}$	Nonspecific FRET
FRET efficiency, Mean ± SEM, %	3.27 ± 0.35	6.48 ± 0.49	4.84 ± 0.30	3.99 ±0.34	3.27 ± 0.70	3.77 ± 0.48	3.84 ± 0.26
n, cells	46	70	71	51	9	39	/

Table 16: FRET efficiencies from intramolecular FRET AB experiments.

Together with the initial reports, herein described the direct quantitative assessment of the interaction on the cell surface, provides a more holistic view of the putative PTH1R-RAMP interaction.

In previous reports, PTH1R-RAMPs interaction was assessed by confocal microscopy at the single-cell level, where it was described that PTH1R expression caused increased cell-surface expression of RAMP2, but not other RAMPs. Interestingly, PTH1R expression caused also an increase in total RAMP2 levels (Christopoulos *et* al., 2003). Later studies mainly looked at the total protein-protein interactions regardless of cellular location. For example – studies with BRET assays (Lenhart *et* al., 2013a; Mackie *et* al., 2019; Harris *et* al., 2021b) or multiplexed suspension bead array (SBA) immunoassays (Lorenzen *et* al., 2019) reported that PTH1R interacts with all three RAMPs. The shortcoming of our and other studies is that they are primarily performed in overexpression conditions in conventional host cell lines (HEK293, COS7, CHO). Although it is possible to find a range of commercially-available RAMP antibodies, scientists avoid using them because of low specificity and limited selectivity to distinguish between all three RAMPs (D. L. Hay & Pioszak, 2016b). Some studies are based on the RAMP antibody recognition and further validation with common antibody tags (Lorenzen *et* al., 2019), but the results are probably overestimated, especially because Lorenzen *et* al. were overexpressing the genetically modified RAMP proteins. This could result in the false positive detection of interactors during overexpression while using low specificity and selectivity antibodies. To note, RAMP2 is 32% identical to RAMP1, and 40% identical to RAMP3, and many antibodies are made against regions, which overlap between RAMPs. Thus, it is better to avoid using antibodies and perform RT-PCR analysis of transcripts or functional assays to prove the presence of specific RAMP.

The methodology of described reports differs not only in the spatial resolution but also whether they are of qualitative (confocal microscopy) or quantitative nature. Methods as BRET, SBA, and FRET AB also provide quantification. It might indeed be possible that PTH1R interacts with all three RAMP isoforms in intracellular compartments, as shown by BRET and SBA assays. The impact of RAMP1 or RAMP3 on intracellular signaling should be further exploited with appropriate functional assays measuring the contribution of those interactions at the level of entity of interest. Especially, RAMP1 and RAMP3 impacts should be carefully controlled if experiments are performed on endogenous expression levels of RAMPs to account for potential competition between RAMPs.

4.3 Designing PTH1R conformational biosensors

4.3.1 Improving PTH1R biosensor

To obtain PTH1R conformational biosensors with improved properties such as better dynamic range and better signal to noise ratio, modification started from previous variants PTH1R-cam and $PTHR1_{Nluc/Halo618}$ (Schihada *et* al., 2018; Vilardaga *et* al., 2003a). Intramolecular GPCR FRET and BRET biosensor as those were designed with two tags, both inserted on conformational selective sites, which move during the activation process. Those insertion sites were retained from previous variants and HA tag on its N-terminal (**Figure 26**). Brighter and more photostable fluorophores were inserted; briefly, CFP-like mTurquoise2 donor was inserted in the third intracellular loop between Gly395 and Arg396 and YFP-like mCitrine acceptor was fused to the shortened C-terminus at Gly497 (**Figure 26 B**).

Emission fluorescence spectra were recorded from HEK293 cells stably expressing $PTHR_{FRET}$ (**Figure 26 C**), mCitrine, and mTurquosie2 fluorophores.

MTurquoise2-expressing cells were excited at 420 nm and emission spectrum was acquired with an emission peak at expected 474 nm (Goedhart *et* al., 2012), and similarly, mCitrine-expressing cells were excited at 516 nm, and emission spectrum acquired, peaking at 529 nm (Zacharias *et* al., 2002). $PTHR_{FRET}$ -expressing cells were excited at 420 nm, and their emission peaks were analyzed at emissions of 474 nm and 529 nm. The FRET spectrum was in correspondence with expected emission peaks and was proof of successful incorporated fluorophores. Moreover, it represented the typical FRET nature of change of intensities – decreased donor intensity at 474 nm due to transfer of energy to nearby located acceptor (3–6 nm (Sekar & Periasamy, 2003)).

$PTH1R_{FRET}$-expressing cells were visualized at the confocal microscope (**Figure 26 D**), where expression of the biosensor was expressed mainly at the cell surface and less so in other compartments of the cell.

To further advance the biosensor and validate results, a novel conformational biosensor design was explored, based on a single fluorophore, circularly permuted green fluorescent protein (cpGFP). In previous years, this protein was engineered to image fast calcium dynamics (T.-W. Chen *et* al., 2013) and was also successfully employed to detect conformational changes across various GPCRs (Patriarchi *et* al., 2018; Schihada, Kowalski-Jahn, *et* al., 2021). Positioning the cpGFP fluorophore in conformational sensitive 3rd ICL between TM5 and TM6 generated working biosensors for class A GPCRs, mostly monoaminergic receptors (F *et* al., 2018; J *et* al., 2019; Jing *et* al., 2018; Patriarchi *et* al., 2018; Wan *et* al., 2021), but also class F GPCRs (Schihada, Kowalski-Jahn, *et* al., 2021). Notably, there was no available class B GPCR cpGFP biosensor at the time of the study, and thus, I aimed to attempt if this design could be transferred to PTH1R, class B GPCRs.

The $PTH1R_{cpGFP}$ biosensor was generated by inserting a cpGFP module with linkers into the third intracellular loop (**Figure 26 E**), to the almost adequate position as was the donor insertion position in $PTH1R_{FRET}$. The biosensor was dim in the absence of ligand and showed very low initial fluorescence emission. Ligand-induced change in this type of biosensor leads to refolding of cpGFP molecule, which subsequently assembles to fully fluorescent protein, and through this, fluorescence emission increases. Addition of the agonist-induced conformational changes, coupled to assembly of cpGFP. The integrity of that change has been tested through analysis of the emission profile, where HEK293 cells were transiently transfected with $PTH1R_{cpGFP}$. Excitation at 455 nm has resulted in the expected emission spectrum peak at 530 nm (Nagai *et* al., 2001) (**Figure 26 F**). Transfected cells were visualized at the wide-

field epifluorescence microscope, where, similar to PTH1R$_{FRET}$, increased expression on the cell surface was detected besides lower expression in other compartments (**Figure 26 G**).

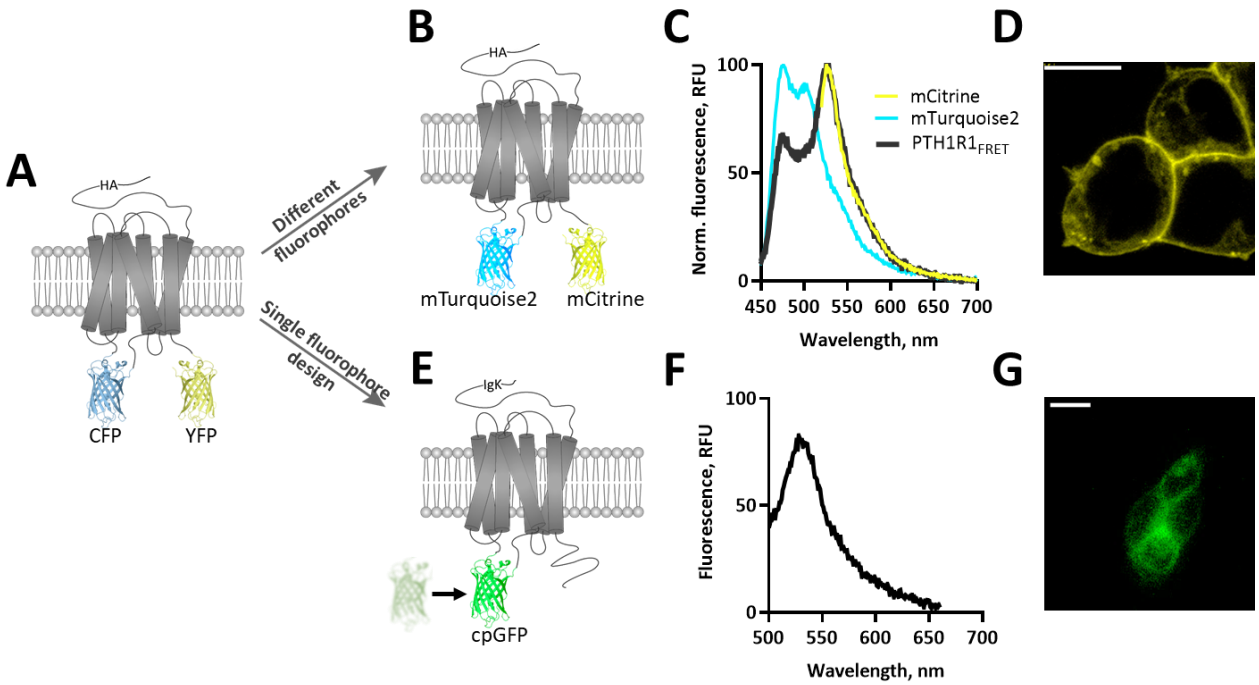

Figure 26: Improving conformational biosensor for PTH1R.

*(**A**) PTH1R receptor biosensor (PTH1Rcam) was updated with brighter and more photostable fluorophores mTurquoise2 and mCitrine to construct PTH1R$_{FRET}$ (**B**), and single fluorophore cpGFP to construct PTH1R$_{cpGFP}$ (**E**).*

*(**B**) Graphical depiction of newly made PTH1R$_{FRET}$ - mTurquoise2 was inserted in 3rd ICL, and mCitrine was fused to C-terminal.*

*(**C**) Fluorescence emission spectra of mTurquoise2 (excited at 420/20 nm) and mCitrine (excited at 516/20 nm) and FRET spectrum of PTHR1$_{FRET}$ after excitation at 420/20 nm (PTHR1$_{FRET}$) and emission intensities were recorded with a monochromator-based plate reader with 1 nm resolution from 450-700 nm.*

*(**D**) HEK293 cells, transiently expressing PTH1R$_{FRET}$. Image was taken under the confocal microscope.*

*(**E**) Graphical depiction of newly made PTH1R$_{cpGFP}$ - cpGFP module with linkers was inserted into 3rd ICL of PTH1R$_{wt}$ and IgK was fused to N-terminal of the receptor.*

*(**F**) Fluorescence emission spectrum of PTH1R$_{cpGFP}$. Cells were excited at 455 nm, and emission intensities were recorded with amonochromator-based plate reader with 1 nm resolution and 500-660 nm. PTH1R$_{cpGFP}$ spectrum was recorded 3 min after activation with 10 µM PTH.*

*(**G**) Image of HEK293 cells, transiently expressing PTH1R$_{cpGFP}$, taken on epifluorescence widefield microscope (D, G) Scale bars = 50 µm.*

4.3.2 PTH1R$_{FRET}$ biosensor at the microscope

The ability of PTH1$_{FRET}$ (**Figure 27 A**) to sense conformational changes was further explored at the wide-field epifluorescence microscope. For the fast agonist delivery, a pressurized rapid superfusion system was used to avoid the impact of agonist diffusion on the kinetics of the signal. The microfluidic device of the system connects a ligand solution-containing syringe to a small tip, which is positioned in the near vicinity of the examined cell.

Single intact cells expressing PTH1R$_{FRET}$ were excited at 420 nm, and fluorescence signals were monitored at wavelengths of both fluorophores – mCitrine as an acceptor and mTurquoise2 as a donor (**Figure 27 B**). As expected for conformational biosensors, adding the ligand, antiparallel changes in donor and acceptor intensities were detected and the FRET ratio (corrected mCitrine/mTurquoise2 emission) was calculated. Change in intensity through the activation process happened because conformational-sensitive sites moved, and therefore distance or orientation between fluorophores changed, and with this, the amount of FRET. The ratio trace of those changes was fitted with a simple monoexponential curve, which enabled calculation of time constant tau, τ. Since saturating concentrations of full agonist were used – 10 µM (**Figure 28 F**),and perfused in the near vicinity of the expressed biosensor on the cell surface, this value can be used to describe the kinetics of receptor activation. Calculations of tau confirmed previous reports defining ~ 1 s for this process (Vilardaga *et* al., 2003a). PTH1R$_{FRET}$-expressing cells switched with median tau time of 710 ms [516, 946 CI]. Plotting all calculated tau values and fitting them with a lognormal distribution enabled me to extract the mode value – the peak of this distribution, which was at 410 ms (**Figure 27 D**). To note, a slightly higher concentration (10 µM) was used in the present study as the first report on PTH1Rcam activation, where they described a mean ± SEM of τ = 3.00 ± 0.25 s (Vilardaga *et* al., 2003a). Nevertheless, in their control experiments with higher concentrations of PTH, they showed quicker kinetics ~ 1 s. Numerous control experiments which they performed excluded the possibility of intermolecular FRET between receptors dimers. Additional experiments with the antagonist PTH(7-34), which did not impact FRET, confirmed that the change from basal to stimulated state happens as a cause of agonist-induced conformational switch. Moreover, the amplitude of the agonist-induced responses was similar also in isolated membranes, supporting the notion of receptor TM switch rather than a change of the position of the fluorophores due to the receptor - G protein interaction. Moreover, experiments in **Chapter 1.4.2** confirm later since biosensor can still switch in a knock-out cell line of G proteins.

Presented biosensor design, where advanced fluorophores were used, resulted in a better dynamic range, calculated as a normalized change in FRET ratio between basal and stimulated FRET. For example, in the initial experiments before revising the fluorophore, PH1R-cam gave only ~ 5% FRET, whereas PTH1R$_{FRET}$ performed 1,5x better, as mean ± SEM of dynamic range around 7.5 ± 0.5 % was measured. In summary, the revised biosensor variant with the new fluorophores was able to increase the dynamic range when retaining the biosensor properties of the previous variants (Schihada *et* al., 2018; Vilardaga *et* al., 2003a), (**Figure 27 E**, **28 F**) and thus, showed improved usability for wide-field microscope experiments.

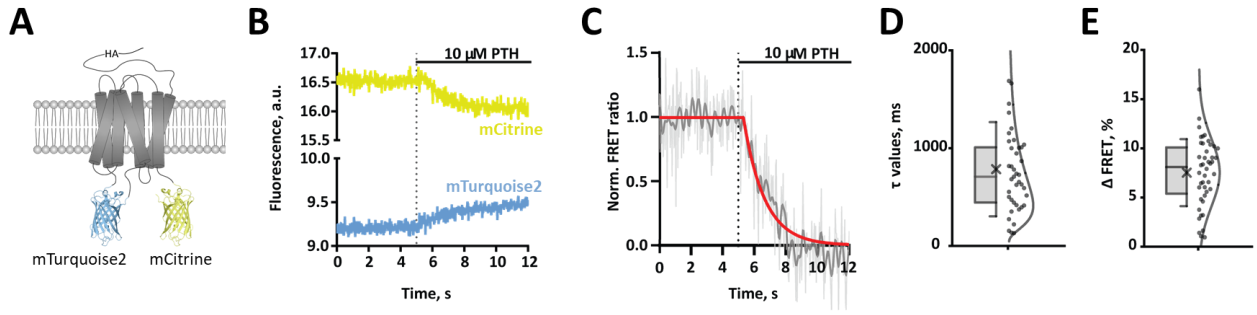

Figure 27: Characterization of the PTH1R$_{FRET}$ biosensor.

*(**A**) Graphical depiction of newly made PTH1R$_{FRET}$.*

*(**B**) Representative traces of donor (mTurquoise2, blue) and acceptor (mCitrine, yellow) fluorescence of PTH-mediated changes, recorded from single-cells, transiently expressing PTH1R$_{FRET}$ biosensor.*

*(**C**) FRET ratio traces of PTH-mediated changes in intramolecular FRET, calculated from traces as in (**A**). Traces were normalized to the baseline (set to 1) and plateau after stimulation (set to 0). Shown are FRET ratio traces raw (grey) and Fourier-lowpassed (black) with the corresponding fit (red). Traces were fitted with a monoexponential one-phase decay fit. Trace is representative of n = 41 cells acquired in five independent experiments. Horizontal lines indicate the application of 10 µM PTH with a rapid superfusion system (**A, B**).*

*(**D**) Time constants τ of PTH-induced FRET changes derived from traces as in panel B, calculated from monoexponential curve fitting. The data represents all single-cell experiments as points, fitted with a lognormal distribution. The boxplot represents mean + SD, and X represents mean. Median value and 95% confidence interval (CI) were 710 ms [516, 946 CI], n = 41 cells.*

*(**E**) Amplitude of FRET changes induced by PTH obtained from traces as in panel B. The data represents all single-cell experiments as points, fitted with a normal distribution. The boxplot represents mean ± SD, and X represents mean. Mean ± SEM, was 7.5 ± 0.5 %, n = 41 cells.*

4.3.3 PTH1R$_{FRET}$ biosensor at the plate reader

As high throughput procedures increasingly gained in importance, some of FRET and BRET conformational GPCR biosensors were adapted to be used in microtiter plates (Picard *et* al., 2018; Schihada *et* al., 2018; Schihada, 2021). This was explored for herein presented biosensor PTH1R$_{FRET}$, and it was examined if it is possible to adapt our first class B GPCR FRET biosensor to perform reliably in plate reader. Knowing that stable expression of biosensors can increase signal stability and decrease variability between the experiments (Schihada, 2021), PTH1R$_{FRET}$ was transfected in HEK293 cells and stably expressing cells were sorted with flow cytometry. Stable clones were characterized by accessing the sensor's dynamic range in a plate reader experiments and those with biggest range were cultured for future experiments (**Figure 28 A**). PTH1R$_{FRET}$-expressing cells were seeded the day before the experiment into black 96-well microtiter plates. Cells were excited at 420/50 nm, and emission was measured simultaneously at 485/20 nm and 540/25 nm as a basal signal for 5 minutes (light grey mark). Consequently, ligand solutions with multichannel pipette were added (one concentration in at least duplicates), and a further stimulated signal was recorded till full ligand occupancy state was reached and a signal was stable (dark grey mark). As on microscope, also on a plate reader-based setup, symmetrical, antiparallel increase in mTurquosie2 emission and decrease in mCitrine emission could be observed (**Figure 28 B**), typical for FRET. The FRET ratio for each well at each time point was calculated and normalized to the basal FRET of each well (**Figure 28 C**). To calculate ligand-induced FRET changes (ΔFRET (%)), basal FRET ratios (**Figure 28**, light grey mark) were averaged for each well, and

stimulated reads were normalized to that value. Subsequently, buffer wells were subtracted to get buffer normalized ΔFRET (**Figure 28 D**). This step discards ligand-independent changes which happened because of the solution addition. Such calculations were performed for each separate well, and those of the same concentration of the ligand were averaged (**Figure 28 E**), and finally, concentration-response curve was constructed (**Figure 28 F**). $PTH1_{FRET}$ biosensor achieved very good dynamic range (~8 %) with great signal/noise ratio. Also, EC_{50} value of PTH was in accordance with previously described PTH1R biosensors (Schihada *et* al., 2018; Vilardaga *et* al., 2003a).

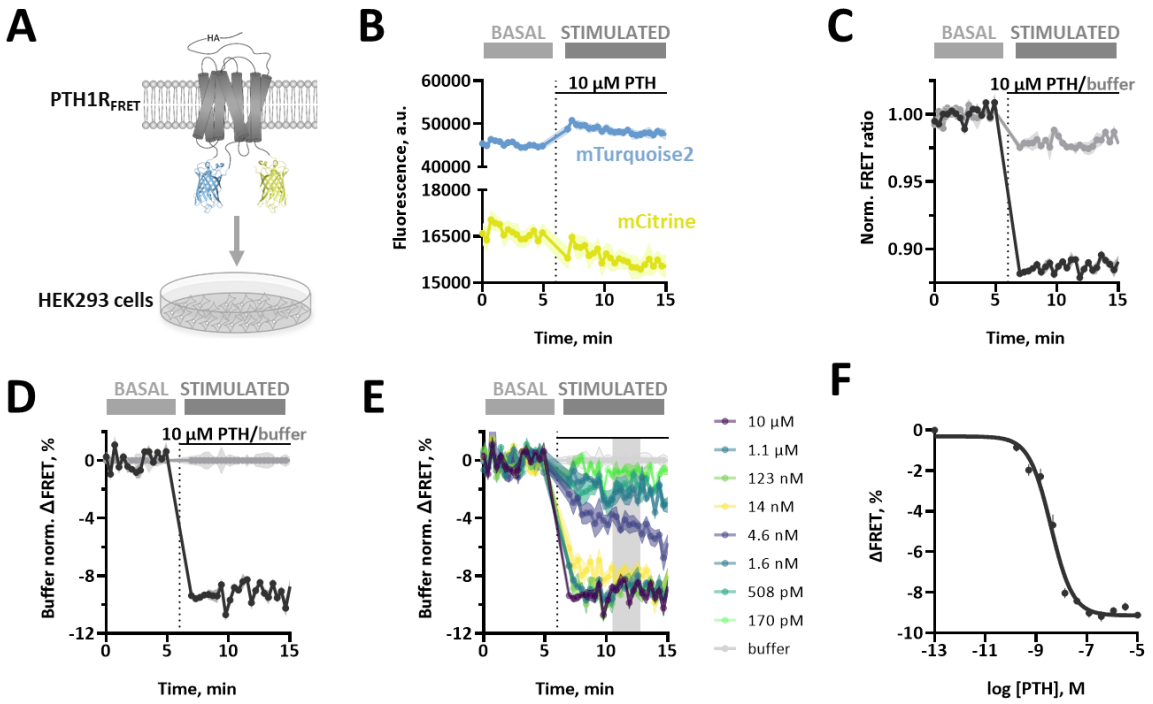

Figure 28: PTH1R$_{FRET}$ biosensor can be used for detection of conformational changes in microtiter plates.

*(**A**) PTH1R$_{FRET}$ biosensor was stably expressed in HEK293 cells.*

*(**B**) Representative traces of donor (mTurquoise2, blue) and acceptor (mCitrine, yellow) fluorescence of PTH-mediated changes, recorded in microtiter plates with a plate reader. HEK293 cells were stably expressing PTH1R$_{FRET}$ biosensor.*

*(**C**) FRET ratio traces of PTH-mediated changes in intramolecular FRET, calculated from traces as in (**B**). Traces were normalized to the baseline (set to 1). Shown are FRET ratio traces for saturating concentration of full agonist PTH (black) and buffer (grey). Horizontal lines indicate ligand/buffer addition with a multichannel pipette. The light grey rectangle and dark grey rectangle symbolize the basal and stimulated experiment window (**B - E**).*

*(**D**) ΔFRET values were normalized to buffer values at each time point.*

*(**E**) FRET ratio time curses of different concentrations of PTH. The grey area indicates saturation window, which was used to calculate stimulated FRET. ΔFRET values are expressed as percent change from the basal FRET value.*

*(**F**) Representative concentration-response curve obtained from traces in (**E**). Points were fitted with a three-response parameters fit, curve fitting resulted in pEC$_{50}$ (mean ± SEM) of PTH1R$_{FRET}$ = 8.42 ± 0.5.*

After showing that $PTH1R_{FRET}$ was able to report efficacies and potencies of the full agonist PTH, it was set out to examine if it could resemble the potencies and efficacies of other ligands targeting PTH1R receptor(Bisello *et* al., 2021). The assay in microtiter plates was performed as describes before, and cells were stimulated with nine

different ligands at saturating ligand concentrations and serial ligand dilutions to construct concentration-response curves (**Figure 29**).

Efficacy and potency of the examined ligands were reported for ligands with various pharmacological profiles (A. - agonist, AN. - antagonist, I.A. - inverse agonists) in **Table 17**. Reported values for the ligands were mostly congruent to the literature values (Bisello *et* al., 2021; Schihada, 2018). I observed a few interesting ligand effects: First, Abaloparatide, chimera between PTH(1-34) and PTHrP(1-36), well-known drug for the treatment of osteoporosis induced only partly activation and so, exhibited a profile of partial agonist. Second, surprisingly, agonist Tyr^{34} – PTH (1-34) (Jonsson *et* al., 2021) failed to induce conformational change. TIP(1-39), shown to be primarily a full agonist of PTH2R and in some assays showed antagonist activity at PTH1R (Jonsson *et* al., 2021), induced change, which could be attributed to the inverse agonists. Antagonist/inverse agonist [Leu^{11}, D-Trp^{12}]-PTHrP (7–34) acted similarily. To note, addition of fluorophores in conformational biosensor could induce different conformational state of PTH1R, and thus be sensitive to ligand-induce changes that are not to be observed with binding or downstream assays. If so, this could be tested with $PTH1R_{wt}$ and some of the biosensors for downstream activation. Such orthogonal assay could provide supplementary information of the pharmacological profile of the ligand.

Most of the ligands showed the expected pharmacological profile and potency. The biosensor was able to detect inverse agonism without previous receptor activation, what is noteworthy for potential pharmacological screens of drugs as many of the currently available and researched novel GPCR drugs block receptor activation (Hauser *et* al., 2017).

In summary, it was confirmed that the $PTH1R_{FRET}$ biosensor can accurately report the potencies and efficacies of ligands as well their pharmacological profile. The revised FRET conformational biosensor is represented as the first FRET biosensor in class B GPCR, which can accurately sense receptor activation in microtiter plates. With it, pharmacological effects of agonists as well inverse agonists were determined. Its excellent signal/noise ratio and specificity toward different classes make it a prime tool for future screening studies. In comparison to $PTHR1_{Nluc/Halo618}$ biosensor (Schihada, 2018; Schihada *et* al., 2018) requires only transfection of the plasmid in a cell line of the choice or usage of stable cell line and no additional, laborious and expensive labeling protocols.

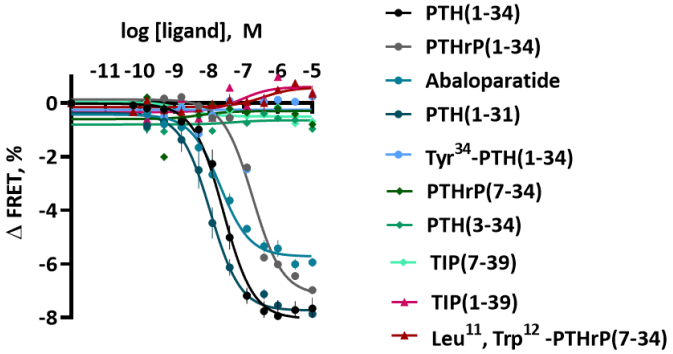

Profile	Ligand	pEC_{50}: mean ± SEM, M	Amplitude: mean ± SEM, %
A.	PTH(1-34)	7.93 ± 0.05	7.51 ± 0.19
A.	PTHrP(1-34)	6.55 ± 0.02	7.29 ± 0.05
P.A.	Abaloparatide	7.69 ± 0.08	6.15 ± 0.29
A.	PTH(1-31)	7.71 ± 0.03	7.97 ± 0.18
A.	Tyr^{34} – PTH (1-34)	ND	0.46 ± 0.14
AN.	PTHrP (7-34)	ND	0.78 ± 0.16
AN.	PTH(3-34)	ND	0.16 ± 0.54
AN.	TIP(7-39)	ND	0.55 ± 0.16
I.A.	TIP(1-39)	7.05 ± 0.44	0.97 ± 0.28
I.A.	Leu^{11}, Trp^{12} -PTHrP(7-34)	5.44 ± 0.97	0.63 ± 0.76

Figure 29: Ligand characterization with $PTH1R_{FRET}$ biosensor.
Table 17: Efficacy and potency of examined ligands.

Concentration-response curves. Points were fitted with a three-response parameters fit; curve fitting resulted in pEC_{50} and amplitude as listed in the table on the right. The action of ligands: A.-agonist, P.A.-partial agonist, AN.-antagonist, I.A.-inverse agonist. ND – not determined.

4.3.4 Creating a single fluorophore-based biosensor

To construct a $PTH1R_{cpGFP}$ biosensor, I inserted the cpGFP molecule with optimized linker module LSSLI-cpGFP-NHDQL (Patriarchi *et* al., 2018) into a similar position in the 3rd ICL as mTurquosie2 in before-mentioned $PTH1R_{FRET}$ biosensor (**Figure 30 A**). Amino acids 389-399 of $PTH1R_{wt}$ were removed and the insertion was made between Lys388 and Arg400. In comparison, the previous $PTH1R_{FRET}$ biosensor carries mTurquoise2 between Gly395 and Arg396. Knowing that "kinky" basic amino acids in combination with the serines increased maximal coupling of activation-induced conformational changes to cpGFP fluorescence, I cut out part of the 3rd ICL to optimize the insertion site (Patriarchi *et* al., 2018).

In cpGFP biosensor design, activation through agonist-induced conformational changes leads to the structural rearrangement of the dim cpGFP molecule to the fully fluorescent protein, and fluorescence emission increases (**Figure 30 A, B**). Stimulation of cells, transiently expressing $PTH1R_{cpGFP}$ biosensor with saturating concentrations of PTH induced increase in fluorescence emission of cpGFP, which was interpreted as activation of PTH1R. That process occurred with a similar speed as activation of $PTH1R_{FRET}$ – for the $PTH1R_{cpGFP}$ activation process, tau ~950 ms was calculated (**Figure 30 B, C**), and for $PTH1R_{FRET}$ ~710 ms (**Figure 27 D**). The amplitude of the signal was the highest of currently established PTH1R biosensors, reaching 15.3 ± 1.1 % (**Figure 30 D**). Cells transiently expressing $PTH1R_{cpGFP}$ were measured in the microtiter plates after being treated with increasing concentrations of ligand to quantify PTH potency (**Figure 30 E**). The potency for the representative experiment was in the nanomolar range (pEC_{50} = 8.61).

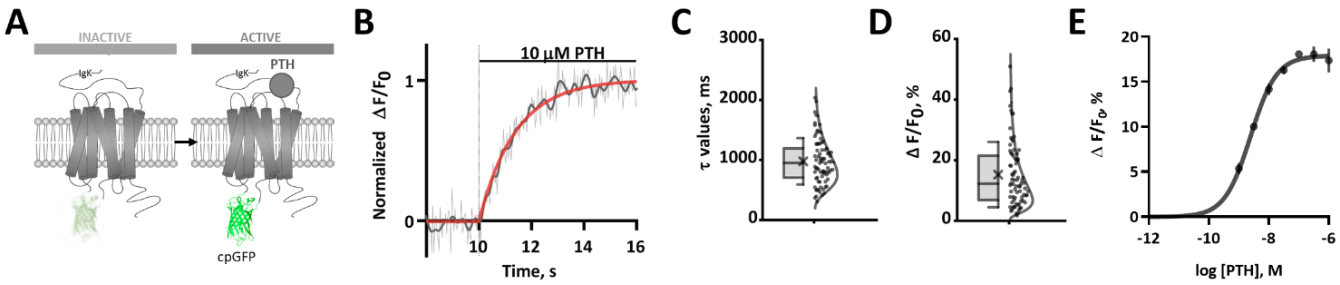

Figure 30: Characterization of PTH1RcpGFP biosensor.

*(**A**) Graphical depiction of newly made $PTH1R_{cpGFP}$.*

*(**B**) Representative fluorescence traces of PTH-mediated changes in $\Delta F/F_0$ recorded in a microscopic FRET setup in single HEK293 cells transiently expressing PTH1RcpGFP. Horizontal lines indicate the application of 10 µM PTH with a rapid superfusion system.*

*(**C**) Kinetic activation constant τ of PTH-induced ΔF/F0 changes derived from traces as in panel (**B**), calculated from monoexponential curve fitting. The data represents all single-cell experiments as points, fitted with a lognormal distribution. The boxplot represents median, box interquartile range (IQR), whiskers are SD, and X represents mean. Median value and 95% confidence interval (CI) were $PTH1R_{cpGFP}$ = 950 ms [817, 1057 CI], n = 78 cells.*

*(**D**) Amplitude of the ΔF/F0 signals induced by PTH. The boxplot represents median, box interquartile range (IQR), whiskers are SD, X represents mean. The mean ± SEM in % of the ΔF/F0 amplitudes from all cells examined was 15.3 ± 1.1 %, n = 78 cells.*

*(**E**) Representative concentration-response curve obtained from plate-reader experiments with PTH1R$_{cpGFP}$. Points were fitted with a three-response parameters fit, curve fitting resulted in pEC$_{50}$ (mean ± SEM) of: 8.61 ± 0.07.*

4.3.5 Comparison of newly created biosensors properties

Summarized biosensor properties in **Figure 31** and **Table 18** provide an overview of the newly made biosensors compared to the old FRET variant PTH1Rcam (Vilardaga *et* al., 2003a).

First, time constant tau (**Figure 31 A**) was compared, and it was in the expected range for both newly made biosensors– around 1 s. There was a modest difference in activation kinetics between PTH1R$_{FRET}$ and PTH1R$_{cpGFP}$. Mentioned decrease in activation speed could be due to; 1) different biosensor design and/or 2) cut out amino acids in TM5,6, which could make conformational transition different of the previously described biosensors. Reports from the GPCR (Patriarchi *et* al., 2018; Ravotto *et* al., 2022) or the calcium field (Kostyuk *et* al., 2019), where cpGFP biosensors are longer in use, describe many aspects where slight changes in biosensor design – single mutations - impacted amplitudes, kinetics or affinity of the biosensors.

Second, amplitudes (**Figure 31 B**) were compared, and the initial aim to improve the dynamic range of old biosensor were successfully fulfilled. As expected, the change of the fluorophores in PTH1R$_{cam}$ yielded a PTH1R$_{FRET}$ biosensor with enhanced properties. The amplitude was increased 1,6-fold for PTH1R$_{FRET}$: from 5% of PTH1Rcam to 8% of PTH1R$_{FRET,}$ and 3-fold for PTH1R$_{cpGFP}$: from 5% of PTH1Rcam to 15% of PTH1R$_{cpGFP}$. A higher dynamic range enabled biosensor´s use in microtiter format, what significantly added to scalability, high throughput-ability, and reproducibility of the experiments. Used combination of mTurquoise2 and mCitrine was selected rationally based on recent characterization of fluorophore-impacted biosensors efficiencies, which reported higher FRET efficiency when selected fluorophores were used (Klarenbeek *et* al., 2015; Thomas, 2019).

As third, PTH1R biosensors potencies were compared (**Figure 31 C**), which demonstrated that as old and newly created constructs report wild-type potency (Bisello *et* al., 2021), comparable with previous biosensor variants (Vilardaga *et* al., 2003a; Schihada *et* al., 2018) and thus, reliably reported pharmacology of PTH1R.

In summary, the design of the two new types of PTH1R biosensors, PTH1R$_{FRET}$ and PTH1R$_{cpGFP,}$ and their successive characterization yielded two variants with improved properties and an enlarged toolset available for evaluating the activity of this, clinically important GPCR.

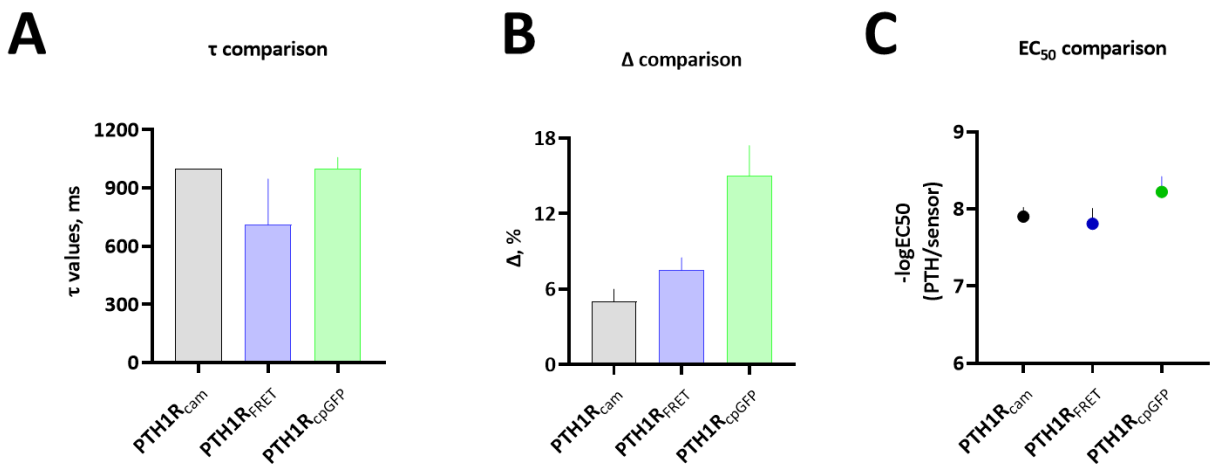

Figure 31: Comparison of three different PTH1R biosensors.

*(**A**) Comparison of the time constant tau for three different PTH1R biosensors. The data shows a single value for PTH1Rcam (1000 ms) and mean ± SEM in ms for $PTH1R_{FRET}$ (710 ms) and $PTH1R_{cpGFP}$ (950 ms).*

*(**B**) Comparison of the dynamic range. The data shows mean ± SEM ΔFRET (for PTH1Rcam and $PTH1R_{FRET}$) and ΔF/F0 (for $PTH1R_{cpGFP}$) in %.*

*(**C**) Potency comparison. The data shows log EC_{50} values of PTH, M of different biosensors.*

Sensor design	Fluorophores	τ, ms	Amplitude, %	pEC_{50}, M	Applicability	Source
$PTH1R_{cam}$	CFP, YFP	~ 1000*	~ 5*	7.9	Microscope	(Vilardaga, 2003)
$PTH1R_{FRET}$	mTurquoise2, mCitrine	710	8	8.0-8.4	Microscope, plate reader	This work
$PTH1R_{cpGFP}$	cpGFP	950	15	8.2-8.6	Microscope, plate reader	This work

Table 18: PTH1R biosensor properties: design, kinetics, amplitudes, potencies, and applicability.

4.3.6 Signaling capacity of newly created biosensors

The biosensors $PTH1R_{FRET}$ and $PTH1R_{cpGFP}$ reliably reported the activation of various PTH1R ligands with different pharmacological profiles. Next, it was aimed to further characterize their capability of coupling to their cognate G proteins and stimulation downstream signaling cascades.

The cell surface expression of newly made biosensors was not separately quantified, as previous studies showed that surface expression of PTH1R BRET biosensor $PTH1R_{Nluc/Halo618}$ was not significantly altered, compared to $PTH1R_{wt}$ (Schihada, 2018). Those findings suggested that intracellular fusions don´t affect cell surface expression significantly (even for bigger HaloTag insertion in the 3rd ICL), and thus, my study focused on examining their potency and efficacy.

The PTH1R primarily couples to different G proteins. Gs stimulates adenylyl cyclases (AC) and consequently raises intracellular cAMP levels. Through another coupler, Gq, stimulates PLC, which leads to the accumulation of inositol

monophosphate (IP1). To quantify PTH1R biosensors-mediated downstream changes, HTRF technology from Cisbio was used, where the amount of accumulated metabolites – cAMP and IP1 was quantified.

This approach represents a competitive immunoassay, where native cAMP or IP1 produced by cells compete with d2-labeled cAMP/IP1 (acceptor) for binding to anti-cAMP/IP1-Cryptate (donor). FRET is thus inversely proportional to the concentration of IP1/cAMP in the standard or sample. In the state of only a few native cAMP/IP1 molecules, there will be more FRET as the d2-labeled acceptor transfers the maximum amount of FRET to the anti-Cryptate donor. When the concentration of native metabolite increases, they outcompete d2-labeled metabolite, and the amount of FRET will decrease.

HEK293 cells with $PTH1R_{wt}$ or PTH1R biosensors were transfected, and the accumulation of metabolites with the corresponding kit was monitored after the selected stimulation time according to the manufacturer´s protocol. Results were plotted inversely (**Figure 32**), representing the amount of cAMP/IP1 accumulation relative to the accumulation caused by $PTH1R_{wt}$. Upon stimulation with serial dilutions of the endogenous agonist, PTH came to the full ($PTH1R_{wt}$) or partial accumulation of cAMP ($PTH1R_{FRET}$**,** $PTH1R_{cpGFP}$) (**Figure 32 A**) – potencies of $PTH1R_{FRET}$-mediated cAMP accumulation were right-shifted by two logs, resulting in pEC_{50} values of pEC_{50} ~ 9.12, comparing to pEC_{50} ~ 11.23 of $PTH1R_{wt}$ (**Table 19**). $PTH1R_{cpGFP}$ induced cAMP accumulation only at the highest concentration – 10 µM PTH.

These data suggest that biosensors can couple to cognate G proteins and induce G protein activation and cAMP accumulation. Nevertheless, a fusion of fluorescent proteins reduces biosensors potency to activate endogenous Gs proteins (right-shift of the EC_{50}) in $PTH1R_{FRE.}$ It allows only partial activation when high concentrations of PTH were used to stimulate $PTH1R_{cpGFP}$ (**Figure 32 A**). Later is in line with previous reports of cpGFP GPCR biosensors (Patriarchi *et* al., 2018), where similar constructs failed to couple with Gs proteins and induce intracellular cAMP accumulation.

Similarly, $PTH1R_{FRET}$- and $PTH1R_{cpGFP}$-mediated IP1 accumulation quantification showed that both biosensors can only partially couple to Gq and induce limited downstream signaling (**Figure 32 B**). It is evident that comes to a certain levela of preactivation of Gq-dependent IP1 accumulation with $PTH1R_{FRET}$ and $PTH1R_{cpGFP}$ as different basal level as in $PTH1R_{wt}$ were observed. These data indicate that the attachment of fluorophores induced steric conflicts and through that, conformation that enabled increased Gq-dependent IP1 accumulation in the agonist-free state (increased of the basal IP1 accumulation ratio). Herein, a fusion of fluorescent proteins reduced biosensor´s capacity for the intracellular IP1 accumulation.

Saturating concentration with the PTH induced similar cAMP accumulation in the $PTH1R_{wt}$- and $PTH1R_{FRET}$-expressing cells. However, the right-shifted EC_{50} values displayed reduced potency. This might be due to the design of the biosensor – mCitrine was fused to the truncated PTH1R C-terminal, lacking terminal 96 amino acids Pro498 – Met593. In the recent PTH1R structures (Ehrenmann *et* al., 2018; L.-H. Zhao *et* al., 2019), that part is not resolved well or is absent, thus is hard to predict if that receptor part is really needed for successful signal transduction. Additionally, also truncated versions of PTH1R can still partially recruit β-arrestin2, suggesting that signal transduction could be successfully initiated also without the last AA of C-terminal (Zindel *et* al., 2016). Moreover, in the $PTH1R_{cpGFP}$ biosensor, this part is not truncated, but the coupling and connected signal transduction resulted in only partial efficacy – as for cAMP and IP1 accumulation. A possible scenario is that bulky intracellular tags sterically hinder coupling to G proteins, and consequently, the intracellular cavity cannot accommodate G proteins, which would enable complete signal transduction.

Similar right shifts in inducing downstream effects were also shown for the earlier PTH1R biosensors (Vilardaga *et* al., 2003a; Schihada *et* al., 2018; Schihada, 2018).

In summary, new PTH1R biosensors preserved the functionality of transmitting extracellular stimulation and provoking G protein-dependent cAMP and IP1 accumulation, albeit not to the full extent. This presumably happens due to bulky intracellular tags that cause reduced efficacy and potency compared to $PTH1R_{wt}$.

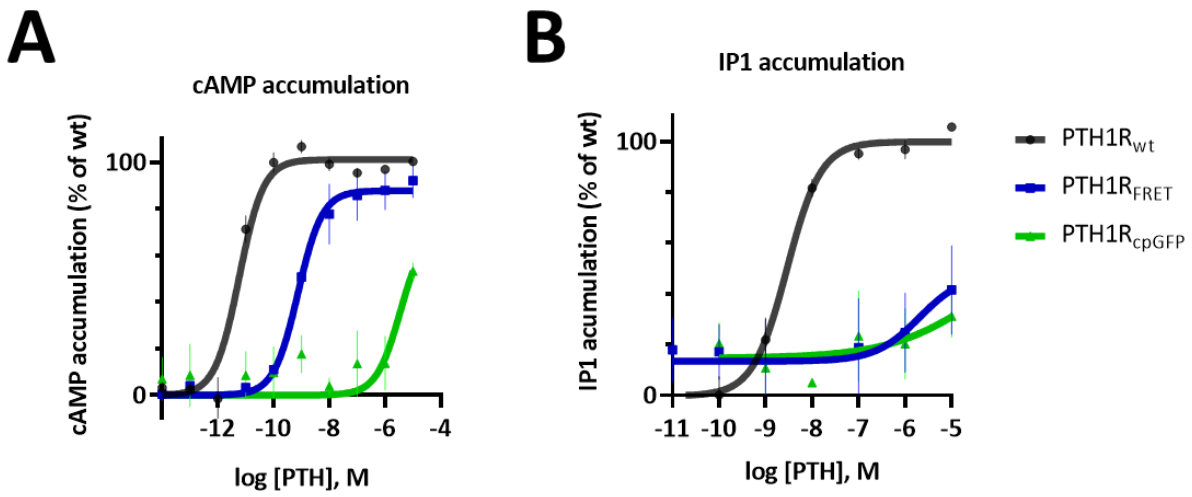

Figure 32: Signaling capacity of $PTH1R_{wt}$ and newly made biosensors.

*Normalized concentration–response curves for cAMP (**A**) or IP1 (**B**) accumulation measured in HEK293 cells expressing $PTH1R_{wt}$ or $PTH1R_{FRET}$ or $PTH1R_{cpGFP}$ biosensor. Measurements were performed with the HTRF kit: Gs HiRange (**A**) and IP1 (**B**). The data are shown as mean + SEM of two independent experiments performed in duplicates. For further statistics and results, see **Table 19**.*

		$PTH1R_{wt}$	$PTH1R_{FRET}$	$PTH1R_{cpGFP}$
cAMP	**pEC_{50}, mean ± SEM, M**	11.23 ± 0.10	9.12 ± 0.17	5.45 ± 0.56
	Amplitude, mean ± SEM, %, M	101.20 ± 2.46	87.79 ± 4.64	/
		$PTH1R_{wt}$	**$PTH1R_{FRET}$**	**$PTH1R_{cpGFP}$**
IP1	**pEC_{50}, mean ± SEM, M**	8.54 ± 0.10	5.69 ± 3.62	4.46 ± 41.53
	Amplitude, mean ± SEM, %, M	100.10 ± 3.93	34.57 ± 98.73	/

Table 19: Values for efficiencies and potencies from Figure 32.

4.4 RAMP2 impact on PTH1R conformations

RAMP proteins are considered capable of allosterically modulating conformation of the CRLR, the prototypical receptor, interacting with all three RAMPs (Liang, Belousoff, Fletcher, *et* al., 2020c). Remarkably, CRLR, with RAMP1,2,3 created three distinct receptor phenotypes. Each exhibited slightly different motions of ECD, which were coordinated with G protein dynamics, as reported by cryo-EM micrographs and molecular simulations studies. This proposed that RAMP can modify receptor conformation in a very delicate way. Nevertheless, there was no study that would investigate if RAMPs can modulate receptor dynamics or kinetics. Moreover, there was no data about RAMPs´ effects on PTH1R, although literature suggested they form (patho-)physiologically oligomer (Kadmiel *et* al., 2017). To fill that knowledge gap and inspect RAMPs´ impact on the PTH1R conformations, an experiment with the before-mentioned $PTH1R_{FRET}$ biosensor (**Figure 26**) and $RAMP2_{SNAP}$ (**Figure 19 B**) was designed. In the FRET AB experiment (**Figure 25)**, interaction between PTH1R and RAMPs showed the highest FRET efficiency for the PTH1R-RAMP2 pair. Because of this preferential interaction, this pair was used for first experiments.

In the initial experiment, I evaluated which concentration of SNAP ligand should be used to achieve total labeling efficiency of SNAP-tagged RAMP2. HEK293 cells were transfected with $RAMP2_{SNAP,}$ and labeled with increasing concentrations of permeable fluorescent dye SNAP-Cell SiR-647. Labeling efficiency was evaluated in a plate reader format by accessing emission intensities at 681 nm (**Figure 33**). The recommended 1 µM of SNAP-Cell® SiR-647 showed very similar labeling efficiency (95.44 ± 5.37%) as the highest concentration used and was thus used for the subsequent experiments. It was essential to establish total labeling efficiency to titrate and measure RAMP2 expression in the following experiment.

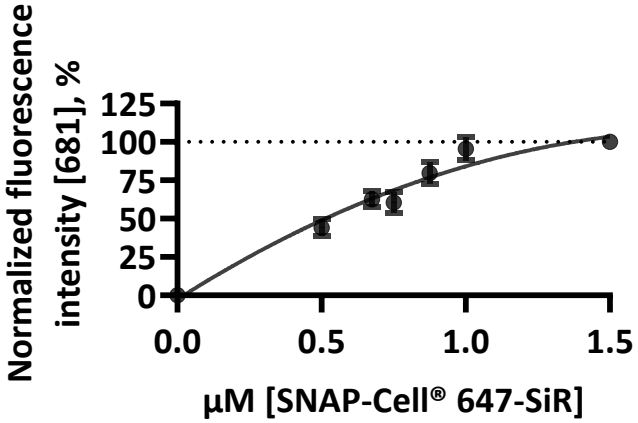

Figure 33: Labeling efficiency of $RAMP2_{SNAP}$ after labelling with SNAP-Cell® 647-SiR.
Labeling efficiencies were determined by assessing % of labeling at HEK293 cells, transfected with $RAMP2_{SNAP}$ and labeled with different concentrations of SNAP-Cell® 647-SiR. The data were fitted with a total binding model.
1 µM concentration of SNAP-Cell® 647-SiR was chosen for the subsequent experiments (labeling efficiency 95.44 ± 5.37%).

To inspect RAMP2 impact on PTH1R conformation, I transfected HEK293 cells with the $PTH1R_{FRET}$ biosensor, with or without $RAMP2_{SNAP}$ (**Figure 34**)**.** To quantify the expression of RAMP2 in those experiments, titration analysis was performed via measuring the emission of SNAP-Cell® SiR-647 as a function of RAMP2 expression. With this, it was evaluated which should be the correct transfection ratio for further experiments.

With the increased amount of $RAMP2_{SNAP}$ transfected, significantly elevated expression of labeled $RAMP2_{SNAP}$ was measured (**Figure 34**), and transfection by up to 2 µg of $RAMP2_{SNAP}$ cDNA (corresponding to a 1:2 PTH1R:RAMP2 transfection ratio) did not alter $PTH1R_{FRET}$ expression. Transfection ratio $PTH1R_{FRET}$:$RAMP2_{SNAP}$ = 1:1 was used for all consecutive experiments (**Figure 34 A, B**).

HEK293 cells were transfected with $PTH1R_{FRET}$ in the presence of mock control, $RAMP2_{wt}$ or $RAMP2_{SNAP}$ (**Figure 34 C**) and measured FRET ratio between the acceptor and donor fluorophore in the basal state. The amount of FRET and consequently, the FRET ratio depends on the inter-fluorophore distance and relative orientation (Förster, 1948). It was hypothesized that structural changes caused by RAMP2 already in a preactivated state, induce different distance and/or relative orientation, which was indeed detected as different FRET ratios in experimental groups where RAMP2 was coexpressed (**Figure 34 C**). Next, cells were stimulated with serial dilutions of PTH and measured time courses of PTH-dependent FRET changes in microtiter plates. Significantly smaller amplitude was detected when $RAMP2_{SNAP}$ was coexpressed with the $PTH1R_{FRET}$ biosensor (**Figure 34 E**) and this was true for the majority of tested concentrations of PTH (**Figure 34 F**). The potency of PTH was similar for both examined experimental groups and, likewise, when $RAMP2_{wt}$ or $RAMP2_{SNAP}$ were used (**Figure 34 C**).

To investigate RAMP2 impact on the basal and stimulated conformation of $PTH1R_{FRET}$ biosensor, photobleaching was performed at the single-cell resolution at the confocal microscope (**Figure 34 G-I**). The advantage of specific experiments was that it could precisely select cells, which coexpressed $PTH1R_{FRET}$ and labeled $RAMP2_{SNAP}$. This is different and more specific than only looking at the average signal, characteristic of ensemble methods of the cell population (**Figure 34 B-F**). Photobleaching experiments were executed, as described in **Figure 34**, measuring in this context intramolecular FRET between the fluorophores in conformational biosensor. Recovery of donor emission after photobleaching of the acceptor (FRET efficiency) was measured, and this was reduced in the presence of $RAMP2_{wt,}$ as also $RAMP2_{SNAP}$ (**Figure 34 G, Table 20**). After stimulation with saturating concentration of PTH, further reduced FRET efficiency was observed, as expected by activation of PTH1R and movement of the fluorophores apart in the conformational biosensor. Notably, a similar pattern was observed - in experimental groups with RAMP2, FRET efficiency was significantly smaller (**Figure 34 H, Table 20**)**.** Remarkably, there was no difference in the ability to modulate PTH1R between $RAMP2_{wt}$ and $RAMP2_{SNAP}$ experimental group, confirming that the addition of the SNAP-tag ® did not compromise RAMP2 functionality and that conformation change originates from RAMP2 itself.

To note, RAMP2 decreased FRET efficiency more in the basal that in the PTH-stimulated state (**Figure 32 G, H, Table 20**). FRET efficiency change was smaller in groups with RAMP2 (**Figure 32 I, Table 20**), suggesting that activation with or without RAMP2 is a different process. It could also mean that RAMP2 causes specific structural changes, priming intermediate state or leading to pre-activation of PTH1R.

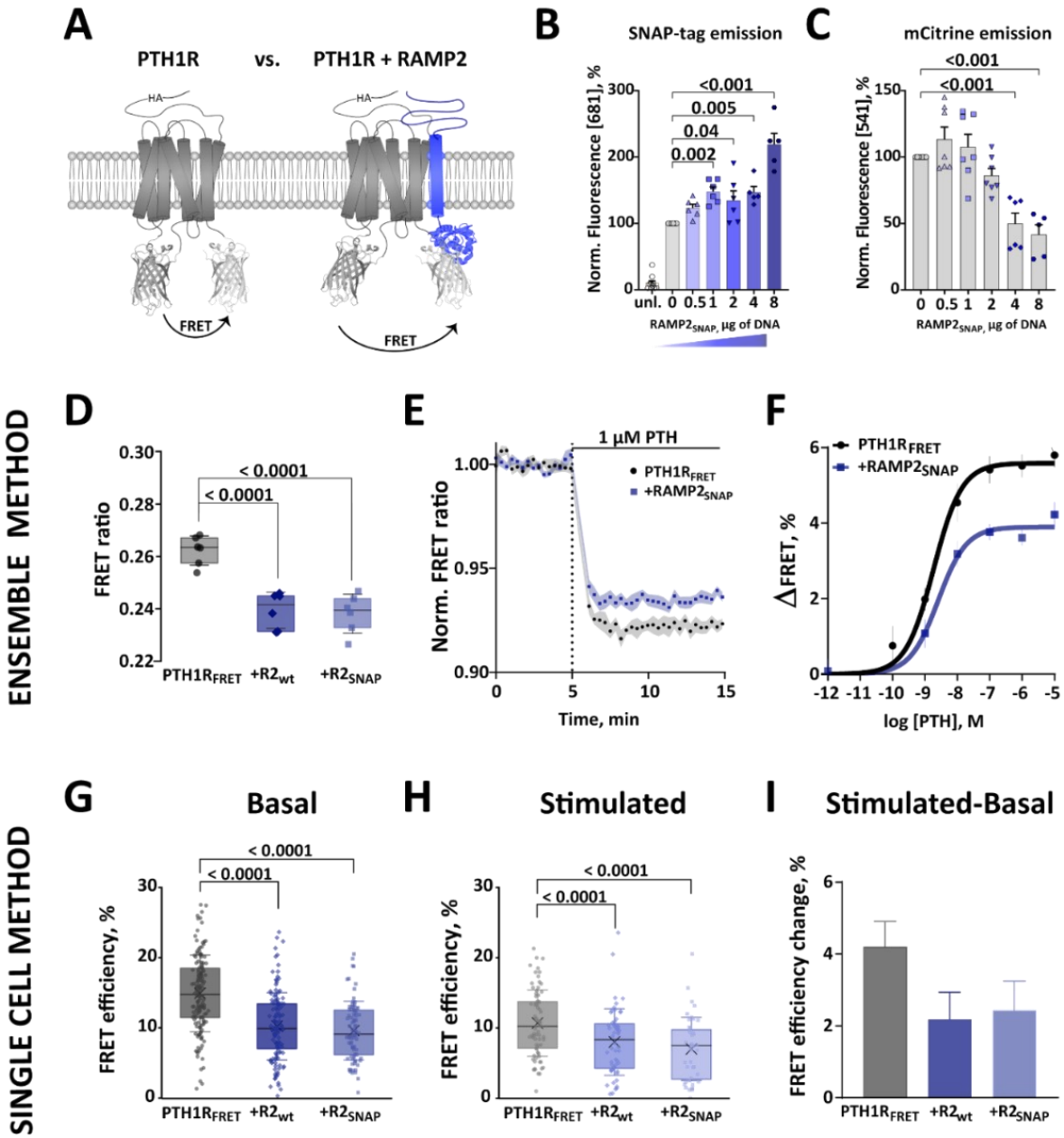

Figure 34: RAMP2 modulates PTH1R basal and PTH-stimulated conformations.

*(**A**) Schematic representation of intramolecular $PTH1R_{FRET}$ biosensor with and without $RAMP2_{SNAP}$. To control RAMP2 expression, its C-terminally fused SNAP-tag was labeled with 1 µM SNAP-Cell SiR-647.*

*(**B - C**) HEK293 cells were transfected with the $PTH1R_{FRET}$ biosensor plus different amounts of cDNA coding for $RAMP2_{SNAP}$. Emissions of SNAP-tag labeled with the 1 µM SNAP-Cell® SiR-647 (**B**) and mCitrine (**C**) were measured in a plate reader. The bars represent means ± SEM, points are means of the duplicates of individual wells from three (**B**) and five (**C**) independent experiments. Significance between the groups was tested with one-way ANOVA followed by Dunnett's multiple comparisons test; ns: $p > 0.05$.*

*(**D**) Basal FRET ratios recorded in a plate reader from HEK293 cells transiently expressing $PTH1R_{FRET}$ alone (black) or together with $RAMP2_{wt}$ (dark blue) or $RAMP2_{SNAP}$ (light blue).*

*(**E**) Average time course of PTH-induced FRET changes recorded in a plate reader from cells as in (**D**). The data are an average of five independent experiments normalized to the initial FRET value (set to 1).*

*(**F**) Concentration-response curves obtained from traces as in (**B**). ΔFRET values are expressed as percent change from the initial FRET value. PEC_{50} values (means ± SEM) were calculated from curve fitting.*

*FRET efficiencies of basal (**G**) and 100 µM PTH-stimulated (**H**) HEK293 cells transiently expressing $PTH1R_{FRET}$ (black) alone or together with $RAMP2_{wt}$ (dark blue) or $RAMP2_{SNAP}$ (light blue). The data are from six (basal) and three (stimulated) independent experiments. Data show values from individual cells; boxes represent the first and third interquartile range (IQR), and whiskers indicate SD. Significance between the groups was tested with one-way ANOVA followed by Dunnett's multiple comparisons test, ns: $p > 0.05$.*

*(**I**) FRET efficiency changes calculated from (**G**) and (**H**), represented as percent change ± SEM. For further statistics and results, see **Table 20**.*

		$PTH1R_{FRET}$	$+RAMP2_{wt}$	$+RAMP2_{SNAP}$
BASAL	**FRET efficiency, mean ± SEM, %**	14.92 ± 0.44	10.23 ± 0.42	9.61 ± 0.46
	N, cells (exp.days)	153 (6)	130 (6)	82 (6)
STIMULATED PTH (1-34)	**FRET efficiency, mean ± SEM, %**	10.71 ± 0.55	8.02 ± 0.63	7.02 ± 0.68
	N, cells (exp.days)	73 (3)	56 (3)	44 (3)
STIMULATED-BASAL	**FRET efficiency, mean ± SEM, %**	4.20 ± 0.70	2.18 ± 0.76	2.59 ± 0.82

Table 20: FRET efficiencies from intermolecular FRET AB experiments.

$PTH1R_{FRET}$ biosensor expression across the groups in photobleaching experiments was comparable (**Figure 35 A**), as also photobleaching (**Figure 35 B**). Plotting FRET efficiency as a function of acceptor intensity resulted in a hyperbolic curve by fitting one-site specific binding (**Figure 35 C**) and confirmed that FRET was specific (Vilardaga *et* al., 2008; Meral *et* al., 2018; Işbilir *et* al., 2020a).

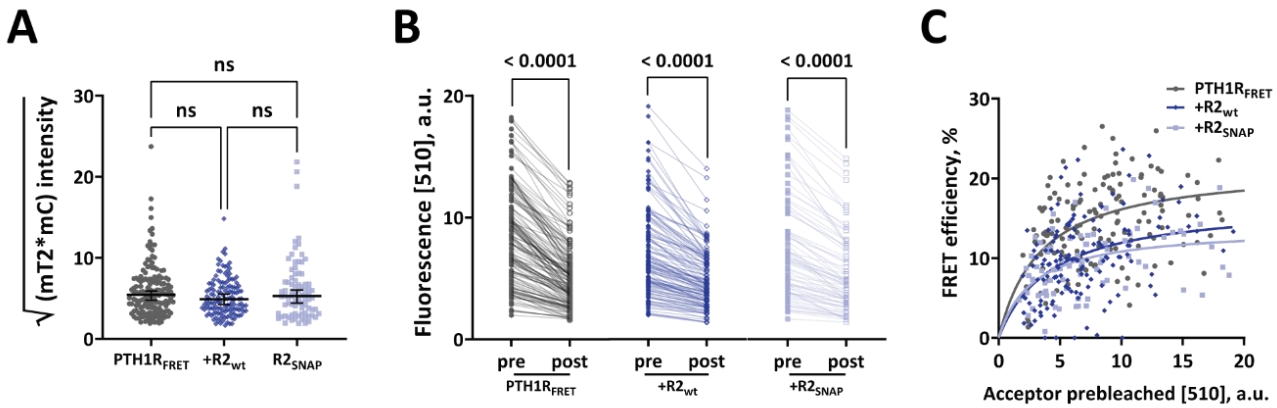

Figure 35: Comparison of expression levels of fluorophores and photobleaching experiments with $PTH1R_{FRET}$ expressed in intact HEK293 cells.

*(**A**) Basal fluorescence emission of mCitrine (mC, acceptor) and mTurquoise2 (mT2, donor) were measured in a confocal microscope before photobleaching of HEK293 cells expressing the indicated constructs. The square root of the product of mT2 and mC normalizes for different expression levels of fluorophores to compare biosensor expression between experimental*

groups. The data show median emission + 95 % CI from all cells examined from four independent experiments. Each data point represents a single cell. Significance between experimental groups was determined by Kruskal-Wallis nonparametric test with Dunn´s post-hoc test.

*(**B**) Fluorescence emissions before (pre) and after (post) photobleaching show comparable extents of photobleaching in the different experimental groups. Median photobleaching was PTH1R$_{FRET}$ = 39.9 %, RAMP2$_{wt}$ = 31.7 % and RAMP2$_{SNAP}$ = 28.5 %. Significance between pre and post emission was tested with Wilcoxon paired test, ns > 0.05.*

*(**C**) FRET efficiencies of PTH1R$_{FRET}$ in the absence or presence of RAMP2$_{wt}$ or RAMP2$_{SNAP}$ were calculated as described in **Figure 25**. The data are plotted as a function of the acceptor´s emission before photobleaching. The curves were fitted with a one site-specific binding fit. Each data point represents a single cell. The data are from three independent experiments, for cell number see **Table 20**.*

To rule out whether the expression of RAMP2 could impact the surface or total expression of the PTH1R$_{FRET}$ biosensor and those differences would cause reduced FRET ratio and FRET efficiency, expression levels of PTH1R$_{FRET}$ were measured in all experimental groups. Surface expression was controlled through HA-tag, positioned in the N-terminus of PTH1R$_{FRET}$ (**Figure 36 A**), and total expression by measuring direct excitation of mC in PTH1R$_{FRET}$ (**Figure 36 B**). Emission of PTH1R$_{FRET}$ was constant in all experimental groups, reassuring that coexpression of RAMP2$_{wt}$ or RAMP2$_{SNAP}$ was not modulating the surface or total expression of PTH1R$_{FRET.}$ Analogous, also total expression of PTH1R$_{cpGFP}$ was not impacted by coexpression of RAMP2$_{SNAP}$ (**Figure 36 D**). RAMP impact on the concentration-response curve of both novel biosensors PTH1R$_{FRET}$ and PTH1R$_{cpGFP}$ was quantified (**Figure 36 C, E, Table 21**). A slight right shift of the curves was observed when RAMP2 was coexpressed – similar to previously described decreased potency impact on BRET PTH1R biosensor (Schihada, 2018). Furthermore, in both biosensors, and with both forms of RAMP2 (RAMP2$_{wt}$ and RAMP2$_{SNAP}$), smaller amplitude when RAMP2 was present was detected (**Figure 36 C**)**.** This was true for stable cell line (**Figure 36 C**), and transiently transfected HEK293 cells (**Figure 36 E**). **Table 21** summarizes the potencies and efficiencies of both PTH1R biosensor variants with RAMP2$_{wt}$ and RAMP2$_{SNAP}$.

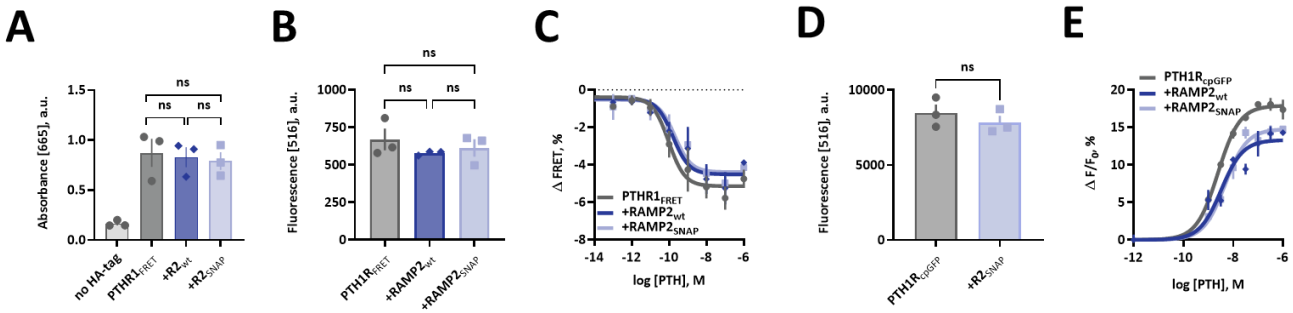

Figure 36: Surface and total expression of PTH1R$_{FRET}$ biosensor are not modulated by RAMP2$_{SNAP}$ overexpression.

*(**A, B**) HEK293 cells transiently expressing the PTH1R$_{FRET}$ biosensor were cotransfected with an empty control vector, RAMP2$_{wt}$ or RAMP2$_{SNAP}$. (**A**) Comparison of cell surface expression levels of PTH1R$_{FRET}$ visualized by detecting the anti-HA tag epitope fused to its N-terminus and quantified by ELISA (absorbance at 665 nm). (**B**) Comparison of total expression levels of PTH1R$_{FRET}$ visualized by recording fluorescence of mCitrine in the same cells as in panel (**A**) The bars show means ± SEM of three independent experiments done in quadruplicates. Significance between the groups was tested with one-way ANOVA; ns: p > 0.05.*

*(**C**) Concentration-response curve for stimulation of PTH1R$_{FRET}$ with increasing concentrations of PTH. The data show the mean ± SEM of three independent experiments performed in quadruplicate. The curve was fitted with a three-parameters concentration-response curve fit. For further statistics and results, see **Table 21**.*

*(**D**) Comparison of total expression levels of $PTH1R_{cpGFP}$ visualized by recording fluorescence of cpGFP in a plate reader. Significance between the groups was tested with a t-test; ns: $p > 0.05$. The bars represent means ± SEM, and points are means of the quadruplicates from three independent experiments.*
*(**E**) Concentration-response curve for stimulation of $PTH1R_{cpGFP}$ with increasing concentrations of PTH. The data show the mean ± SEM of three independent experiments performed in quadruplicate. The curve was fitted with a three-parameters concentration-response curve fit. For further statistics and results, see **Table 21**.*

	$PTH1R_{FRET}$	$+RAMP2_{wt}$	$+RAMP2_{SNAP}$
pEC_{50}, mean ± SEM, M	10.02 ± 0.21	9.80 ± 0.27	9.69 ± 0.26
Amplitude, mean + SEM, %	4.76 ± 0.45	4.04 ± 0.50	3.87 ± 0.42
	$PTH1R_{cpGFP}$	$+RAMP2_{wt}$	$+RAMP2_{SNAP}$
pEC_{50}, mean ± SEM, M	8.61 ± 0.07	8.48 ± 0.13	8.32 ± 0.07
Amplitude, mean + SEM, %	17.89 ± 0.49	13.31 ± 0.72	14.76 ± 0.44

Table 21: Potency and amplitude of PTH1R biosensors in the presence of RAMP2.

4.5 RAMP1 and RAMP3 impact on PTH1R conformations

Although previous experiments showed only poor interaction of RAMP1 and RAMP3 with PTH1R (**Figure 25**), I tested if those interactions were functional and could impact ligand-stimulated $PTH1R_{FRET}$ activation.
For this reason, a stable cell line of the $PTH1R_{FRET}$ biosensor was cotransfected with an empty plasmid or one of the $RAMP_{SNAP}$ proteins. RAMP expression was controlled via its SNAP-tag in each experimental group (**Figure 37**). While transfection of $RAMP1_{SNAP}$ and $RAMP2_{SNAP}$ resulted in similar expression level of RAMP isoforms, $RAMP3_{SNAP}$ seemed to be expressed approximately 2-3 times better. By the same expression level of the biosensor (**Figure 37 A**), neither $RAMP1_{SNAP}$ nor $RAMP3_{SNAP}$ exhibited significant modulation of the amplitude of the $PTH1R_{FRET}$ activation, induced by saturating concentration of PTH, PTHrP, or Abaloparatide (**Figure 37 A, B, C**). In the same experimental setup, $RAMP2_{SNAP}$ impacted PTH- and Abaloparatide-stimulated amplitude significantly ($p<0.01$) and showed a slight but not significant trend to decrease PTHrP-induced activation of $PTH1R_{FRET}$. Latter suggests an agonist-specific effect of RAMP2 on PTH1R modulation. A decrease of the amplitude is to expect with all agonists of PTH1R since it appears that RAMP2 can modulate already basal conformations (**Figure 34 G**). On the other hand, ligand- and RAMP-specific effects on GPCRs are generally accepted and endorsed by many studies (D. L. Hay *et* al., 2016; D. L. Hay & Pioszak, 2016b; Klein *et* al., 2016; J Gingell *et* al., 2016b; Harris *et* al., 2021b; Shao *et* al., 2021; A. J. Clark *et* al., 2021). Thus, it might be possible that the PTH1R-RAMP2 complex favors activation by PTH (and Abaloparatide) and less so by PTHrP. One possible explanation is the cocreation of different GPCR-RAMP complexes, where RAMP allosteric alters GPCR conformation (J Gingell *et* al., 2016b; Garelja *et* al., 2020; Liang, Belousoff, Fletcher, *et* al., 2020c) and differentiates between pharmacological preferences for certain ligands.

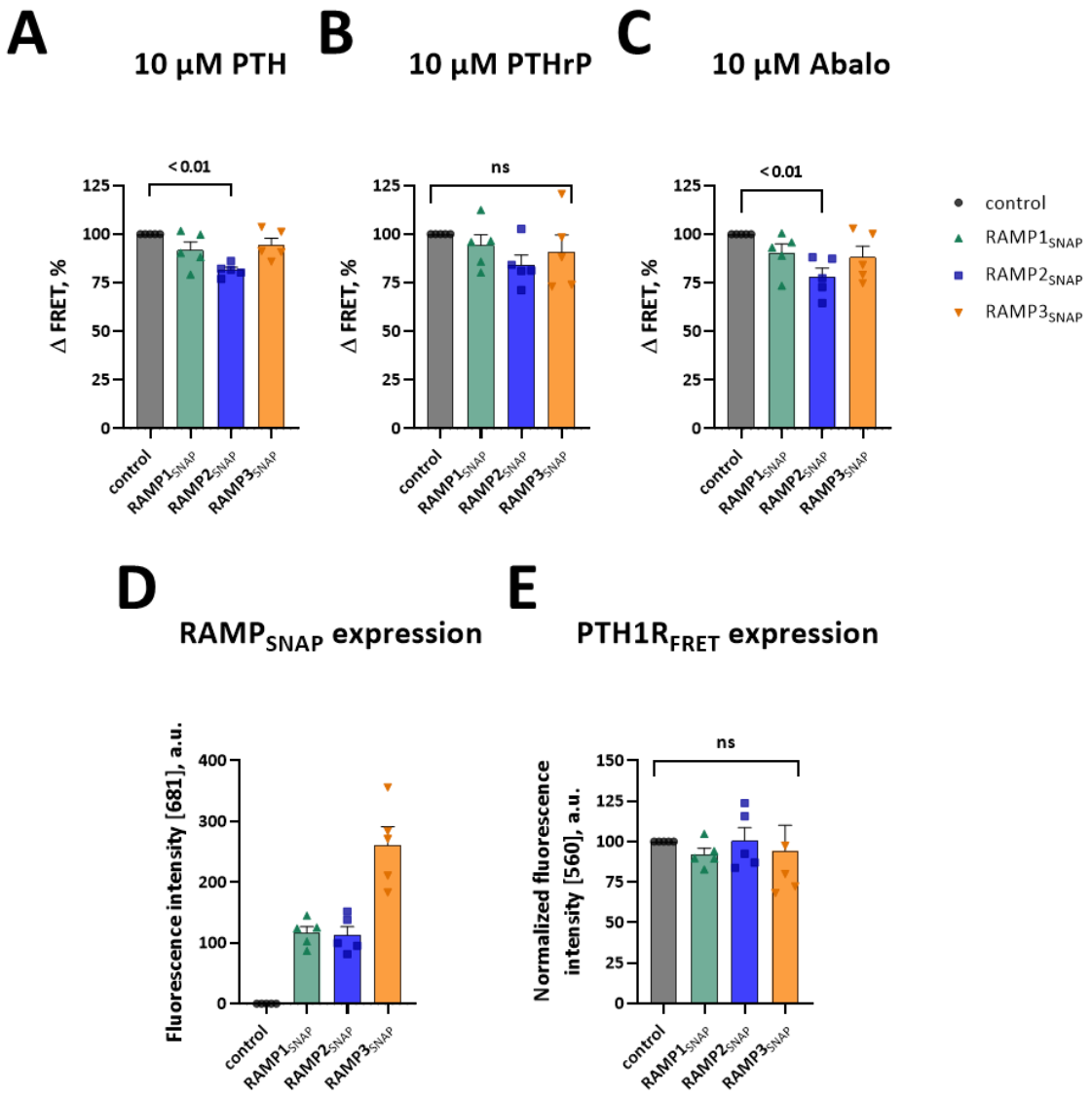

Figure 37: Effects of SNAP-labeled RAMP isoforms on the amplitude of PTH1R$_{FRET}$ signals evoked by PTH and PTHrP.
HEK293 cells stably expressing PTH1R$_{FRET}$ biosensor were transfected with one of the three RAMP$_{SNAP}$ isoforms.
*(**A, B, C**) Amplitudes of FRET changes in PTH1R$_{FRET}$ induced by PTH (**A**), PTHrP (**B**), and Abaloparatide (**C**). The bars represent means ± SEM of the FRET amplitudes from five independent experiments performed in quadruplicates.*
*(**D**) Emissions RAMP$_{SNAP}$, accessed via SNAP-tag, labeled with the 1 µM SNAP-Cell SiR-647.*
*(**E**) Emissions of mCitrine in PTH1R$_{FRET}$ were measured to assess the equal expression of the PTH1R$_{FRET}$ biosensor in all experimental groups. The bars represent means ± SEM, points are means of 16-plicates of individual wells from five independent experiments. Significance between the groups was tested with one-way ANOVA, followed by Dunnett's multiple comparisons tests; ns: p > 0.05.*

4.6 RAMP2 impact on receptor activation kinetics

Inspired to access RAMP2 impact on the activation kinetics of PTH1R, characteristic experiments were designed, to measure changes in subsecond activation of receptors. For those experiments, intact cells expressing biosensors were recorded with wide-field microscope. A rapid superfusion system was used, which was able to deliver ligand in the near the cell surface and eliminate the diffusion time of the agonist. Stable cell line of $PTH1R_{FRET}$ biosensor was used, in the presence or absence of $RAMP2_{SNAP}$ (**Figure 38 A**). Assuring coexpression of both constructs in examined cells, cells were labeled with cell-permeable SNAP-tag® ligand SNAP-Cell® SiR-647 and prior to experiments, selected cells coexpressing both constructs. Intact cells were stimulated with a saturating concentration of endogenous ligand, and time courses of the PTH1R activation process were recorded. As expected, and seen in earlier experiments with $PTH1R_{FRET}$ biosensor, stimulation resulted in decreased FRET ratio, and antiparallel changes of donor and acceptor emission channels reported that it went for specific FRET (**Figure 35 B**). Calculating the activation time constant tau (τ) in the presence and absence of RAMP2 resulted in intriguing results. Tau, calculated from time curves as in **Figure 38 C**, fitted with a monoexponential one-phase decay function, was reduced from a median time of 710 ms to 330 ms in the experimental group where RAMP was present (**Figure 38 B, C, Table 9**). By plotting all calculated tau values, significant shift of activation kinetics with RAMP2 was observed. Values were fitted with a lognormal distribution, which allowed to calculate mode – the peak of the distribution, located at 410 ms and 50 ms, for $PTH1R_{FRET}$ and $+RAMP2_{SNAP}$ group, respectively (**Figure 38 C, Table 22**). From the one-phase decay fit, the amplitude of the signal was derived, which was significantly decreased in the experimental group with RAMP2, similarly as in microtiter plate and photobleaching experiments. The amplitude of the signal was about two times smaller (**Figure 38 D, Figure 3.16**) when $PTH1R_{FRET}$ (~7.5 %) was coexpressed with $RAMP2_{SNAP}$ (~3.8 %).

Previously described control experiments (**Figure 36**) confirmed this reduction is not due to the different expression levels of the biosensor when coexpressed with RAMP2, as both the cells´ surface expression and total expression $PTH1R_{FRET}$ were similar in the presence or absence of $RAMP2_{SNAP}$ as also $RAMP2_{wt}$.

Equipped with the novel $PTH1R_{cpGFP}$ biosensor, able to sense PTH activation with similar potency and kinetics yet superior dynamic range (**Figure 30**), it was aimed to set out the experiment, to validate RAMP2 impact on PTH1R activation.

We transiently coexpressed $PTH1R_{cpGFP}$ with mock plasmid or $RAMP2_{SNAP}$ (**Figure 38 E**) and monitored coexpression of both constructs in examined cells as previously described. Perfusing cells with the same, saturating 10 µM PTH induced an expected increase in fluorescence (**Figure 38 F**), from which activation time constant tau and the signal amplitude were calculated. In line with the results for the $PTH1R_{FRET}$ sensor, RAMP2 decreased tau ~two fold, from a median 950 ms to 390 ms. In addition, the distribution variable mode was decreased from 760 ms to 190 ms in the presence of RAMP2 (**Figure 38 G**). Moreover, RAMP2 also decreased the amplitude ($\Delta F/F0$) of the signal, which was decreased from 15.3 % to 9.1 % (**Figure 38 H**), reassuring that RAMP2 impact can also be endorsed with novel $PTH1R_{cpGFP}$ biosensor. Due to the superior amplitudes and easier handling with $PTH1R_{cpGFP}$, those experiments were performed with another endogenous ligand PTHrP, known to exert somewhat different PTH1R activation (Ferrandon *et* al., 2009; Vilardaga *et* al., 2012). A slight decrease was observed, yet no significant amplitude reduction (from 17.6 % to 13.6 %) in the presence of RAMP2 (**Figure 38 K**). This was anyhow expected as previously detected RAMP2 reduces basal ratios as well as the amount of FRET (**Figure 34 D, G**) and would so probably

decrease the amplitude of every ligand-induced signal. PTHrP-induced activation time were in accordance with previous descriptions. Strikingly, activation constant was very similar for both experimental groups, yet in line with previously reported values for PTHrP (Ferrandon *et* al., 2009). Ferrandon *et* al. described a tau value of 1600 ms, whereas our results suggest that PTHrP-induced PTH1R activation takes a median time of 1960 ms, in the presence of RAMP2 1910 ms (**Figure 38 J**). It seems that structural changes induced by RAMP2 are very subtle and that this modulation is agonist-specific, adding another level of complexity to the PTH1R-RAMP2 signaling model. This might be due to the structural reshaping of PTH1R by RAMPs. This is further discussed in **Chapter 4.9**.

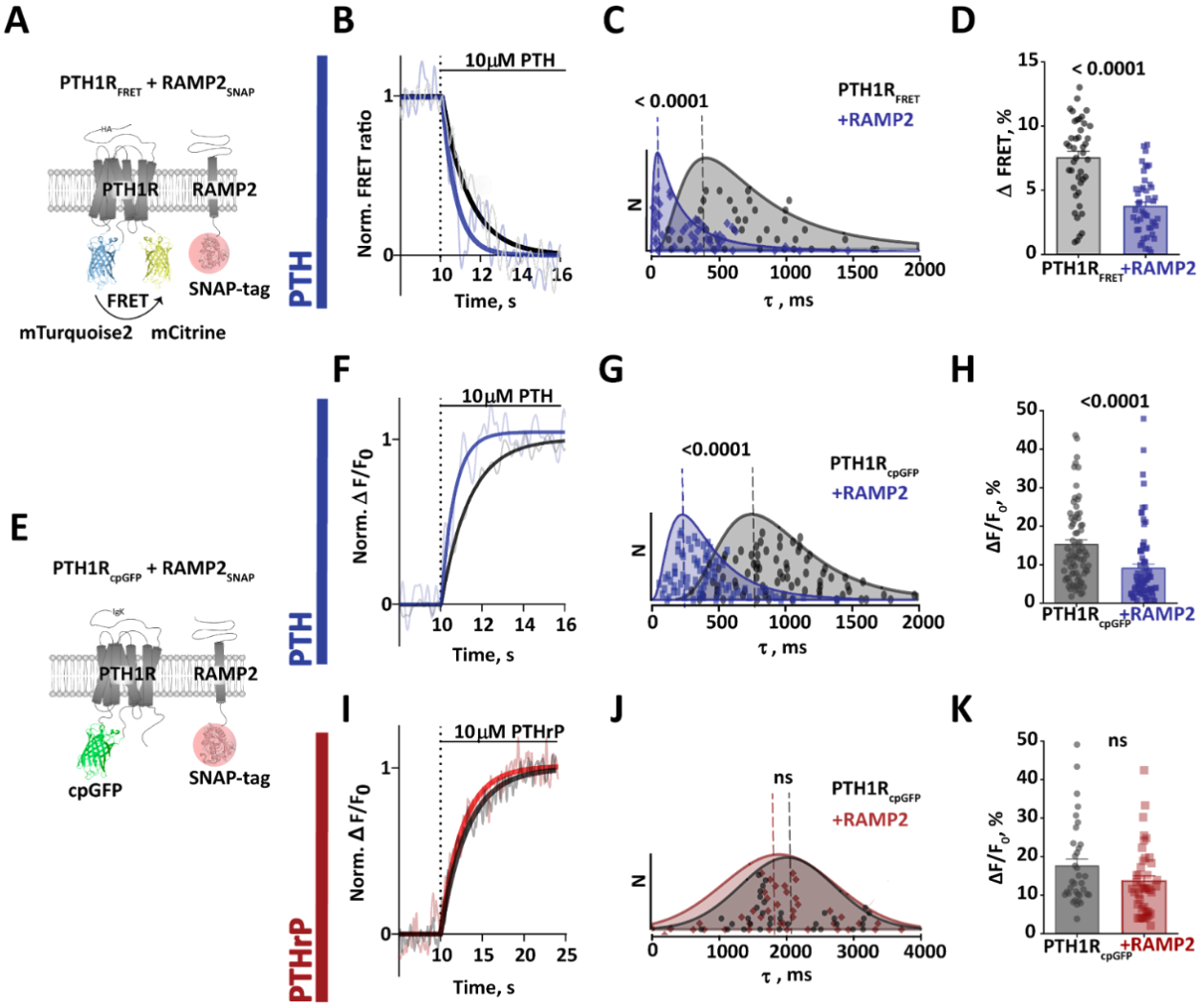

Figure 38: Modulatory effects of RAMP2$_{SNAP}$ coexpression on PTH1R$_{FRET}$ and PTH1R$_{cpGFP}$ biosensor activation.

*(**A**) Schematic representation of intramolecular PTH1R$_{FRET}$ biosensor. To control RAMP2 expression, its C-terminally fused SNAP-tag® was labeled with 1 µM SNAP-Cell® SiR-647 (red circle).*

*(**B**) Representative ratio traces of PTH-mediated FRET changes in single HEK293 cells stably expressing PTH1R$_{FRET}$ and in the presence of transiently coexpressed RAMP2$_{SNAP}$, recorded in a microscopic FRET setup. To analye only cells that expressed both, cells were labeled with 1 µM SNAP-Cell SiR-647, and regions of interest were selected where PTH1R$_{FRET}$ and RAMP2$_{SNAP}$ were coexpressed. Horizontal lines indicate the application of 10 µM PTH with a rapid superfusion system. Traces were normalized to the baseline (set to 1) and plateau after stimulation (set to 0). Shown are FRET ratio traces raw (grey and light blue) and Fourier-*

lowpassed (black, dark blue). Traces are representative of n = 41 cells (PTH1R$_{FRET}$) and n = 46 cells (+RAMP2$_{SNAP}$), acquired in five independent experiments.

*(**C**) Time constants τ of PTH-induced FRET changes derived from traces as in panel (**B**), calculated from monoexponential curve fitting. The data were fitted with a lognormal distribution, and the dashed line indicates the mode, global maximum of the distribution. The median value and 95% confidence interval (CI) are stated in the **Table 22**. A Mann-Whitney test was used to assess a significant difference between the groups (p < 0.001).*

*(**D**) Amplitude of FRET changes induced by PTH obtained from traces as in panel (**B**). The bars represent means ± SEM, % of the FRET amplitudes from all examined cells. A t-test was used to assess a significant difference between the groups (p < 0.001).*

*(**E**) Schematic representation of the cpGFP-based biosensor to monitor PTH1R activity in single-cell experiments. Receptor activation upon agonist stimulation was monitored by recording fluorescence at 516 nm.*

*(**F, I**) Representative fluorescence traces of PTH (**F**) and PTHrP (**I**) mediated changes in ΔF/F0 recorded in a microscopic FRET setup in single HEK293 cells transiently expressing PTH1RcpGFP alone or with RAMP2$_{SNAP}$, labeled with 1 µM SNAP-Cell SiR-647. Horizontal lines indicate the application of 10 µM PTH or PTHrP with a rapid superfusion system. The data shown are in panel B.*

*(**G, J**) Time constants τ of PTH-induced and PTHrP-induced activation derived from traces as in panels F and I. The data were analyzed as described in panel C. Dashed line indicates the mode, global maximum of the distribution. Median value and 95% CI for PTH are stated in **Table 22**. A Mann-Whitney test was used to assess a significant difference between the groups (p < 0.001).*

*(**H, K**) Effects of RAMP2 on the amplitude of the ΔF/F0 signals induced by PTH (**F**) and PTHrP (**H**). The bars represent means ± SEM in % of the ΔF/F0 amplitudes from all cells examined. A t-test was used to assess a significant difference between the groups (p < 0.001).*

		PTH1R$_{FRET}$	+RAMP2$_{SNAP}$
	Mode τ, ms	410	50
PTH	**Median τ [95% CI], ms**	710 [516, 946]	330 [144, 416]
	Amplitude, mean ± SEM, %	7.5 ± 0.5	3.8 ± 0.3
	N, cells (experimental days)	41 (5)	46 (5)
		PTH1R$_{cpGFP}$	**+RAMP2$_{SNAP}$**
	Mode τ, ms	760	190
PTH	**Median τ [95% CI], ms**	950 [817, 1057]	400 [322, 448]
	Amplitude, mean ± SEM, %	15.3 ± 1.1	9.1 ± 1.1
	N, cells (experimental days)	78	77
PTHrP	**Median τ [95% CI], ms**	1960 [1770, 2660]	1910 [1670, 2100]
	Amplitude, mean ± SEM, %	17.5 ± 1.8	13.6 ± 1.4
	N, cells (experimental days)	38	41

Table 22: Kinetic values from the data in Figure 3.20.

To further characterize RAMP2-induced changes in the PTH1R activation, tau values and amplitudes were evaluated through additional statistical analysis.

First, for each cell, the amplitude value was correlated with its respective tau value to confirm that there is no dependence between tau and amplitude at the saturating concentration of PTH used, thus at the full activation (**Figure 39**). The data were plotted and two variables were analyzed: slope and intercepts with y-axis. The slope was not different in both cases, indicating that ΔFRET is independent of tau values. This suggests that it goes for the

similar process which is happening on different amplitude level. In addition, the intercept with y-axis indicates that the activation process with RAMP happens on smaller amplitude level. This is statistically different for both examined biosensors (**Figure 39 A, B, Table 23**).

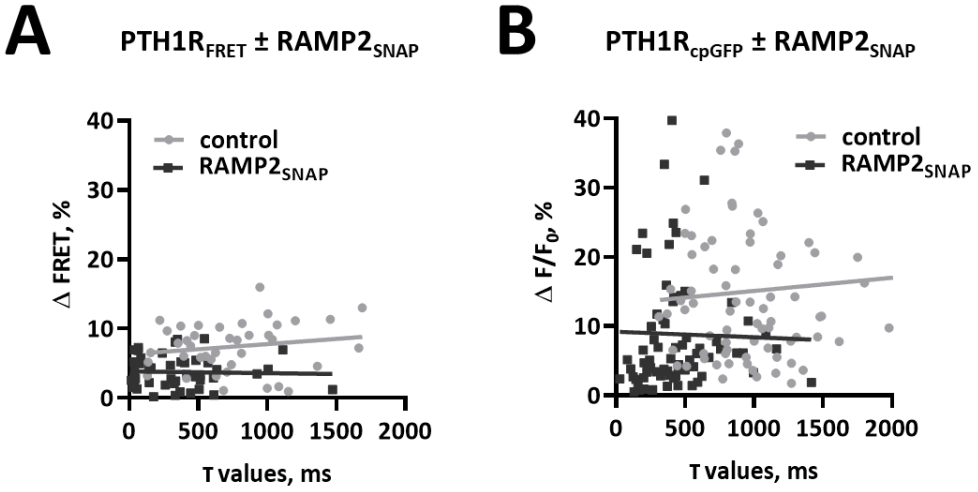

Figure 39: Correlation between tau values and amplitude of the PTH1R activation.

*(**A, B**) Ligand-induced ΔFRET or ΔF/F0 responses are independent of T values. Shown are FRET or ΔF/F0 responses induced by the saturating concentration of PTH. HEK293 cells were expressing PTH1R$_{FRET}$ (**A**) or PTH1R$_{cpGFP}$ (**B**), in the presence or absence of RAMP2$_{SNAP}$. Values for slopes and Y-intercepts are in **Table 23**.*

The data were fitted with a simple linear regression and tested for differences in slopes and intercepts.

	PTH1R$_{FRET}$	+RAMP2$_{SNAP}$	p
Slope	0.0015	-0.00024	p=0.692
Y-Intercept	6.30	3.83	p<0.0001
	PTH1R$_{cpGFP}$	**+RAMP2$_{SNAP}$**	**p**
Slope	0.0019	-0.00080	p=0.6133
Y-Intercept	13.19	9.20	p=0.009

Table 23: Calculated parameters from the data in Figure 3.21.

Second, it was examined if RAMP modulation is titratable and finally, saturable phenomenon, reflecting that RAMP modulation is conditioned at certain expression levels of RAMP proteins in the human body. The amount of RAMP2 modulation was titrated via different amounts of transfected RAMP2$_{SNAP}$ cDNA in a stable cell line of PTH1R$_{FRET}$. This led to different expression levels of RAMP2$_{SNAP}$ (**Figure 34 B**), which corresponded to different amplitude of the PTH-stimulated PTH1R activation (**Figure 40 A, B**).

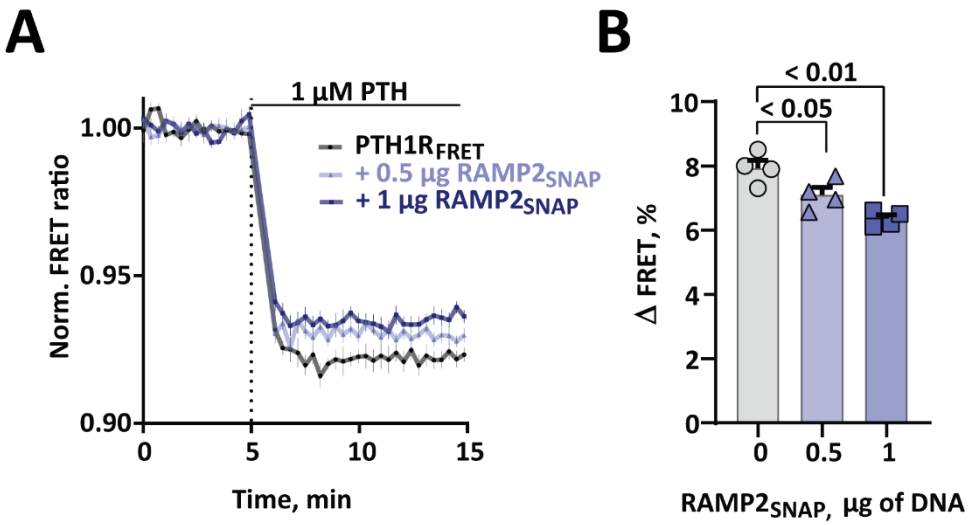

Figure 40: Effects of RAMP2 expression levels on the modulation of PTH1R$_{FRET}$ activation dynamics.

*(**A**) HEK293 cells were transfected with the PTH1R$_{FRET}$ biosensor plus two different amounts of cDNA coding for RAMP2$_{SNAP}$. The amplitudes of FRET changes induced by 10 µM PTH were measured in a plate reader. The bars represent means ± SEM, % of the FRET amplitudes from five independent experiments.*

*(**B**) Amplitudes of FRET changes induced by 1 µM PTH in the experiment shown in **Figure 34 B**. The bars represent means ± SEM, from five independent experiments. Statistical differences were tested by one-way ANOVA.*

Then, single-cell experiments of PTH-stimulated PTH1R$_{cpGFP}$ activation with coexpressed RAMP2$_{SNAP}$ were analyzed for cell-to-cell variability. Although equal amounts of cDNA encoding PTH1R$_{cpGFP}$ and RAMP2$_{SNAP}$ were used for those experiments, the expression of proteins varied from cell to cell. To evaluate if this variability can provide some insights into the level of RAMP2 modulation on PTH1R kinetics, ROIs (from which tau values were derived) were inspected for the RAMP2$_{SNAP}$ expression (via fluorescence emission of its labeled SNAP-tag®), and PTH1R$_{cpGFP}$ expression (via emission of cpGFP). As next, the time constant t for each ROI was plotted as a function of RAMP2$_{SNAP}$ expression (**Figure 41 A**) or PTH1R$_{cpGFP}$ expression (**Figure 41 B**). Time constant τ was not dependent on the expression level of PTH1RcpGFP (**Figure 41 B**), whereas increasing RAMP2$_{SNAP}$ expression lowered τ values. Values from the control group were plotted as mean ± SEM (black point), and a three-parameters logistic function was used to fit the data. Consequent fit displayed decreasing nature of PTH-induced PTH1R activation (τ) by increasing the expression level of RAMP2$_{SNAP}$. This trend advocates in favor of the assumption that RAMP2 modulation depends on the expression level – likely, when the amount of RAMP2 molecules is enough to "ramp" all PTH1R, the kinetics of the activation process decreases till 378 ms (bottom of the fit). This is in accordance with median kinetic values which were calculated for the +RAMP2$_{SNAP}$ group by single-cell kinetic experiments (**Table 22**).

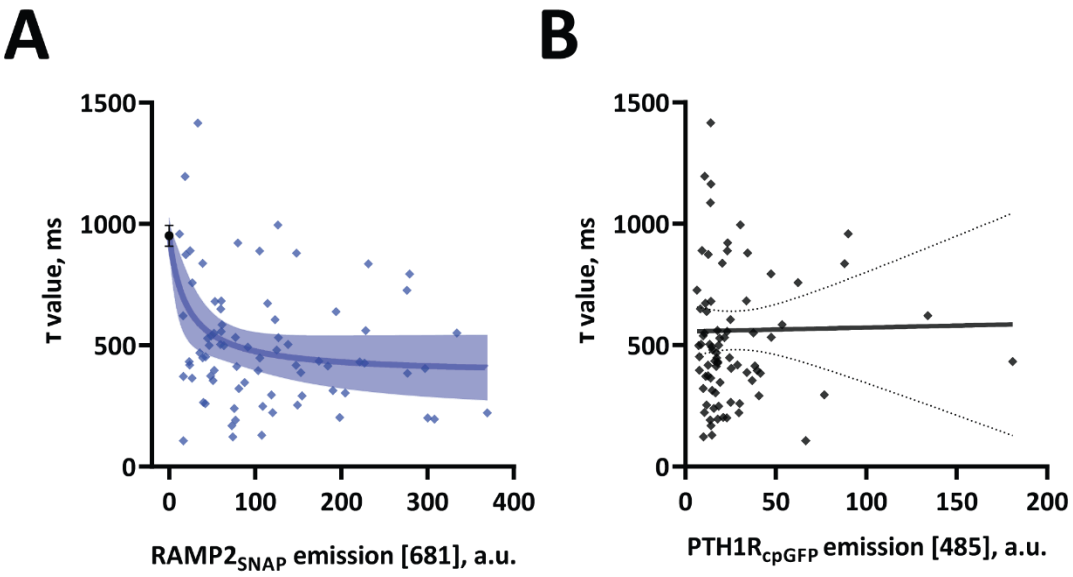

Figure 41: Effects of RAMP2 expression levels on the modulation of $PTH1R_{cpGFP}$ activation kinetics.

(A) *Time constant τ of PTH-induced PTH1R activation in single HEK293 cells transiently expressing $PTH1R_{cpGFP}$ alone (black) or with $RAMP2_{SNAP}$. The data from **Figure 38 G** were analyzed for the time constant τ as a function of $RAMP2_{SNAP}$ expression, quantified by labeling with 1 µM SNAP-Cell SiR-647. The data were fitted with a three-parameters logistic function and shown is fit ± 95% confidence intervals. Bottom ± 95 % CI = 378 [202, 554], top ± 95 % CI = 952 [878, 1024], IC_{50} = 20.36 [0, 49.58].*

(B) *Time constant τ of PTH-induced PTH1R activation in single HEK293 cells does not depend on $PTH1R_{cpGFP}$ emission. The data were fitted with a simple linear regression fit.*

In summary, these data indicate that expression of RAMP2 modulates the PTH1R activation process in a titratable manner; higher expression of RAMP2 decreases the amplitude of PTH1R activation more as well activation process happens faster. For the context of the human body, this would suggest two things: 1) that modulation could depend on the expression level of RAMPs, and 2) that this process can be saturated, presumably when all GPCRs bind their interacting partner.

4.7 RAMP2 effect on G protein-dependent signaling

4.7.1 RAMP2 effect on G protein activation

Ligand stimulation of its cognate receptors triggers activation of the GPCR, and the next step in the signal transduction cascade is the interaction of the receptor with G proteins. PTH1R couples primary to Gs and Gq family of heterotrimeric proteins, in certain conditions also to G12/13 and Gi (Abou-Samra *et* al., 1992; Miyauchi *et* al., 1990; Singh *et* al., 2005b; Bisello *et* al., 2021; Avet *et* al., 2022; Hauser *et* al., 2022). To investigate G protein activation, a set of BRET-based G protein biosensors was employed (Schihada, Shekhani, *et* al., 2021) (**Figure 42, Table 24**). In these biosensors, intermolecular BRET changes when subunits of trimeric G protein dissociate: Gα subunit with fused luminescent donor NanoLuc moves apart from Gβγ with fused fluorescent acceptor cpVenus. HEK293 cells were transfected with the tricistronic plasmid, encoding for three proteins; Gα-NanoLuc, Gβ and Gγ-cpVenus, together with $PTH1R_{wt}$, with or without $RAMP2_{wt}$ - **Figure 42 A** shows schematics of the experimental setup. Next, cells were stimulated with serial dilutions of PTH and PTHrP, and time courses of ligand-dependent BRET changes in microtiter plates were measured. Gs (**Figure 42 B - E**), Gq (**Figure 42 F - I**), Gi3 (**Figure 42 J - M**) and G13 (**Figure 42 N - Q**) protein activations were quantified with cognate biosensors and concentration-response curves for PTH (**Figure 42 C, G, K, O**) and PThrP (**Figure 42 E, I, M, Q**) were constructed. Both ligands successfully induced concentration-dependent G protein activation of all biosensors in the expected range of EC_{50} values (**Figure 42 R, S, Table 26**)**.** PTH1R primary couples to Gs; this was reflected in highest efficacy for activation of this G protein, followed by Gq, G13, and lastly, Gi3. The summary of calculated efficacy values is represented in the spider plots (**Figure 42 R, S**) and **Table 24.**The data are following previously reported values (Bisello *et* al., 2021; Sato *et* al., 2021), moreover, it extends the knowledge of the field – never before were PTH, and PTHrP-induced G protein activation analyzed in its entirety with all interacting G proteins.

Then, RAMP2 effects on G protein activation were analyzed, and remarkably, in the presence of RAMP2, PTH evoked a higher efficacy of Gi3 activation ($p < 0.001$), and small, albeit not significant trend was visible for PTHrP (**Figure 42 N - Q**). Another exciting change was a slightly increased amplitude of Gs activation for both PThrP ($p < 0.05$) and PTH (**Figure 42 B - E**). Later changes were reviewed in detail - looking at the most relevant first 10 minutes of PTH-induced Gs and Gi3 activation process (**Figure 43 A, B**)**.** Upon high concentration of PTH, RAMP2-coexpressing cells induced a clear overshot of Gs activation (**Figure 43 A**)**,** which was faster and happened with a ~20% higher amplitude. Similar was visible for Gi3 activation, although here at smaller concentrations – for example, at the 10 nM PTH came to quicker signal saturation when RAMP2 was coexpressed (**Figure 43 B**).

We hypothesized that this overshot of signaling comes either from 1) the different starting position of G proteins when coexpressed with RAMP2 or/and 2) because the preceding process – receptor activation happens faster (as described in **Chapter 4.6**.

To test the first hypothesis, basal ratios of trimeric G proteins were analyzed without stimulation. Analysis was undertaken with the $BRET_0$ method, which accounts for various cofounding factors which could prevent reliable results of G protein analysis between two groups. For example, some of those factors are technical (varying expression levels of the biosensor or the cell amount in experimental groups) and some biological (interaction partners of G proteins such as RGS, GTPase activating proteins could have impact on sensitivity of G protein activation) (Schihada, Shekhani, *et* al., 2021; Y. Wang & Townsend, 2012). In this approach, emission intensities of the donor as a function of BRET ratio for corresponding wells were plotted for both experimental groups. By linear

interpolation fit, the Y-intercept of each group were determined, which were assigned to be the $BRET_0$ value (Schihada, Shekhani, *et* al., 2021). $BRET_0$ before stimulation was analyzed for all before mentioned G proteins, in the presence and absence of $RAMP2_{wt}$ (**Figure 44**)**.** In none of the groups, statistical differences between $BRET_0$ in the presence or absence of $RAMP2_{wt}$ were detected. Thus, it was concluded that RAMP2 does not induce constitute activity nor exert direct modulation effects on G proteins. At least not within limits of detection of the currently used method. In summary, the overshoot, observed with Gs and Gi3 activation in the presence of $RAMP2_{wt}$ was probably due to accelerated receptor activation, which precedes G protein activation.

Described experiments suggesting differential coupling in the presence of RAMPs are not isolated case. There are much evidence that RAMPs can act as signaling switch and this was reported for some other interacting GPCRs (Christopoulos *et* al., 2003); classical interactor CRLR (Bühlmann *et* al., 1999; Garelja *et* al., 2020; A. J. Clark *et* al., 2021), CTR (Morfis *et* al., 2008), GIPR (Harris *et* al., 2021b), glucagon receptors (Shao *et* al., 2021), VPAC2 and CRF1 (Wootten *et* al., 2013). It was suggested that the short, although important, C-terminus of RAMPs might be responsible for some of the observed effects (Udawela *et* al., 2006, 2008), besides recently described motions of receptors ECD, which are governing receptor and G protein dynamics (Josephs *et* al., 2021a; Liang, Belousoff, Fletcher, *et* al., 2020c), and collectively help to stabilize receptor.

		PTH				PTHrP			
		control	$RAMP2_{wt}$	p	n	control	$RAMP2_{wt}$	p	n
G_s	pEC_{50}, M	8.88 ± 0.39	8.71 ± 0.36	ns	4	8.12 ± 0.18	8.12 ± 0.18	ns	4
	E_{max}, %	2.78 ± 0.43	3.28 ± 0.45	ns		2.04 ± 0.27	2.62 ± 0.27	< 0.05	
	$BRET_0$	0.24 ± 0.02	0.24 ± 0.02	ns					
G_q	pEC_{50}, M	7.84 ± 0.19	7.72 ± 0.20	ns	3	8.16 ± 0.25	8.13 ± 0.22	ns	3
	E_{max}, %	26.02 ± 2.38	25.63 ± 2.35	ns		20.20 ± 2.29	21.98 ± 2.21	ns	
	$BRET_0$	0.21 ± 0.05	0.23 ± 0.06	ns					
G_{13}	pEC_{50}, M	7.76 ± 0.24	8.15 ± 0.25	ns	4	8.14 ± 0.18	7.77 ± 0.25	ns	4
	E_{max}, %	8.84 ± 0.90	8.47 ± 0.90	ns		9.48 ± 0.74	9.72 ± 1.01	ns	
	$BRET_0$	0.25 ± 0.05	0.31 ± 0.05	ns					
G_{i3}	pEC_{50}, M	7.06 ± 0.33	8.35 ± 0.44	< 0.05	4	7.49 ± 0.68	7.93 ± 0.41	ns	4
	E_{max}, %	4.43 ± 0.68	4.16 ± 0.73	ns		2.98 ± 0.82	3.29 ± 0.58	ns	
	$BRET_0$	0.31 ± 0.04	0.34 ± 0.03	ns					

Table 24: Potency and efficiency for PTH- and PTHrP-induced G protein activation.

Potency (pEC_{50}, M) and efficiency (E_{max}, %) values were obtained from a plate reader experiment as shown in ***Figure 42****. The data are mean ± SEM of n independent experiments. Extra-sum-of-squares test was used to assess the difference between the curves, ns > 0.05. Part of the data was acquired by dr. Hannes Schihada.*

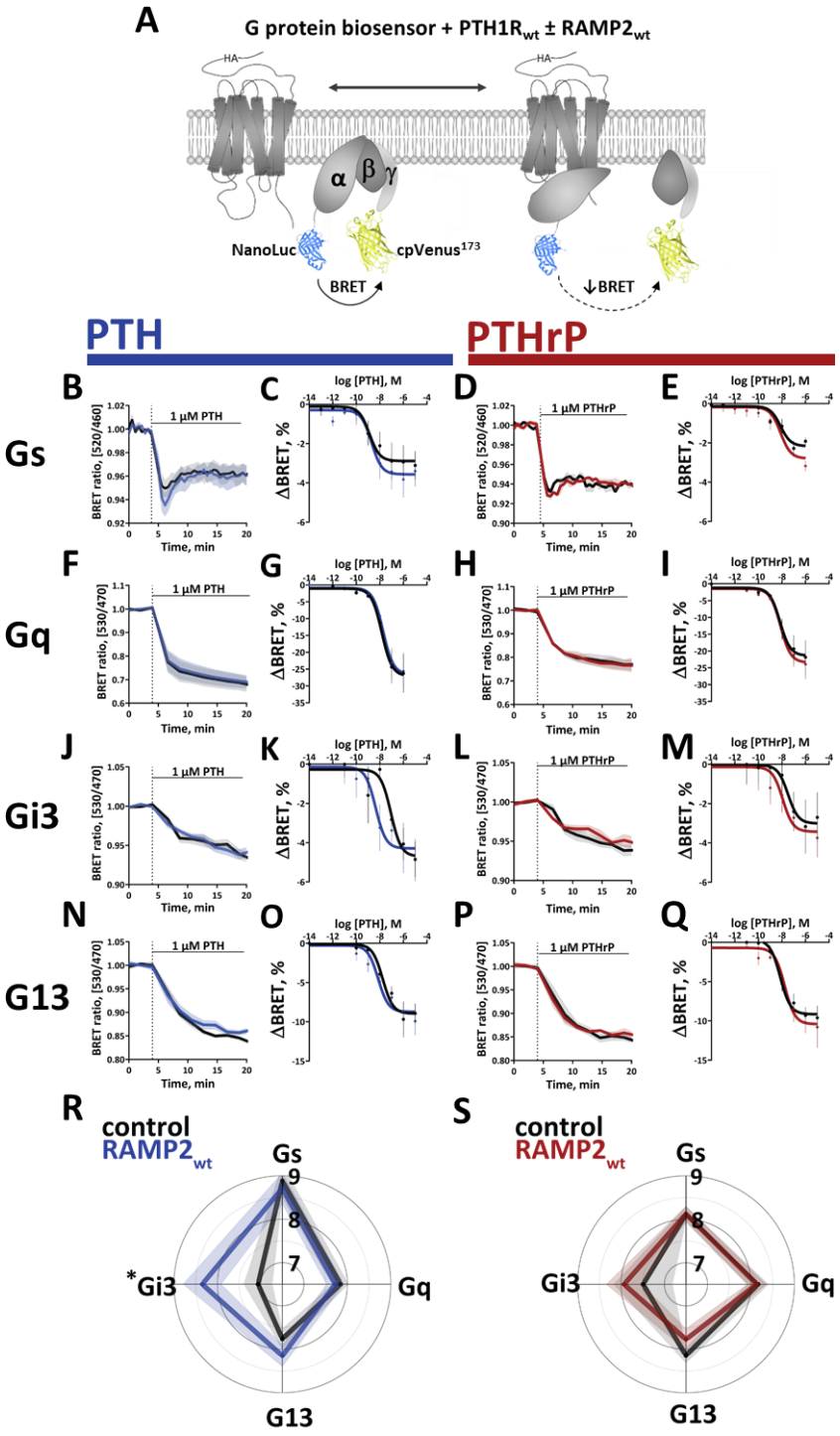

Figure 42: RAMP2 effects on PTH-stimulated G protein activation.

(***A***) *Graphical depiction of the construct used in the study: NanoLuc was fused to Gα, and cpVenus173 was fused to Gγ. HEK293 cells were transiently transfected with cDNA encoding for G biosensor tricistronic plasmid along with PTH1R$_{wt}$ with (red, blue points and traces), or without RAMP2$_{wt}$ (black points and traces).*

*(**B-Q**) HEK293 cells transiently transfected with cDNA encoding for BRET biosensors of G_s (**A -E**), G_q (**F -I**), G_{i3} (**J - M**), G_{13} (**N - Q**), along with PTH1R$_{wt}$ (blue, red), or without RAMP2$_{wt}$ (black).*

BRET signals were recorded in a plate reader from cells stimulated with PTH (black, blue) or PTHrP (black, red). Shown are time courses of agonist stimulation and corresponding concentration-response curves, fitted with a three-parameters concentration-response curve fit. The data are mean ± SEM of at least three independent experiments performed in duplicates or more. For further statistics and results, see ***Table 24****.*

*(**R, S**) "Spider plots" show mean ± SEM pEC_{50} (M) values calculated from the concentration-response curves. Parts of the data was acquired by dr. Hannes Schihada.*

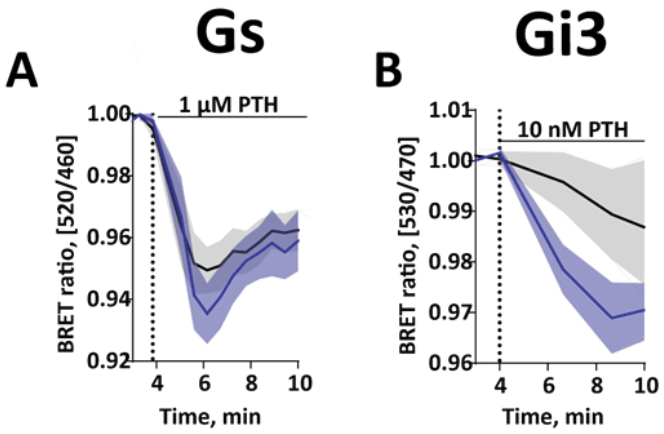

Figure 43: RAMP2 effects on PTH-stimulated G protein activation.

*(**A, B**) HEK293 cells transiently transfected with cDNA encoding for BRET biosensors of G proteins: Gs (**A**) and Gi3 (**B**) along with $PTH1R_{wt}$, with (blue curve) or without $RAMP2_{wt}$ (black curve).*

BRET signals were recorded in a plate reader from cells stimulated with indicated concentrations of PTH. Shown are time courses of agonist stimulation. The data are mean ± SEM of three independent experiments performed in duplicates or more. For further statistics and concentration-response curves, see ***Table 24****. Part of the data was acquired by dr. Hannes Schihada.*

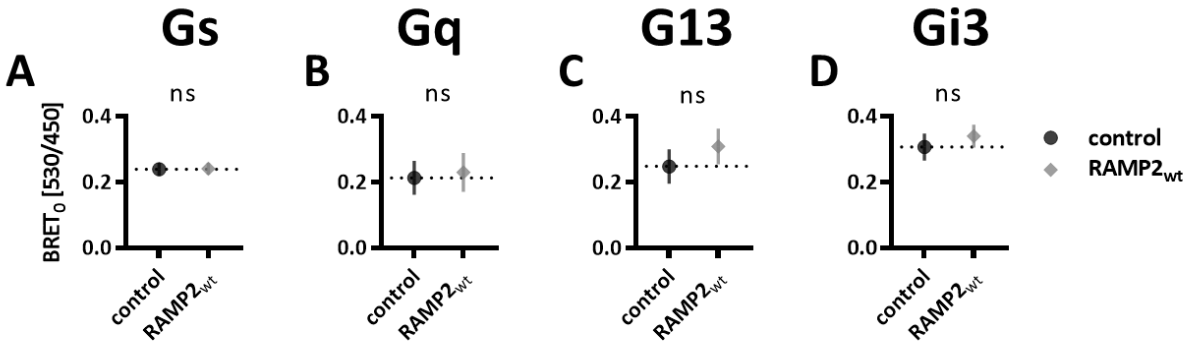

Figure 44: RAMP2 does not have an effect on the basal ratio of G protein activation.

*(**A - D**) HEK293 cells were transiently transfected with cDNA encoding for BRET biosensors for Gs (A), Gq (B), G13 (C), Gi3 (D), along with $PTH1R_{wt}$, with (grey) or without $RAMP2_{wt}$ (black).*

BRET signals were recorded in a plate reader before stimulation with ligands. $BRET_0$ was calculated according to the described method. Shown is the $BRET_0$-corrected ratio ($G\gamma$-mVenus/Gα-NanoLuc). The data are mean ± SEM of at least three independent experiments performed in duplicates or more. For further statistics see ***Table 24****. A t-test was used to assess a significant difference between the groups (ns; $p > 0.05$). The data were acquired by dr. Hannes Schihada.*

4.7.2 RAMP2 effect on G protein-dependent downstream effectors

Observations of the accelerated PTH1R receptor activation in the presence of RAMP2 were translated to the overshoot of G protein activation at Gs and Gi3 proteins. To test if faster G protein activation consequently leads to the faster cAMP accumulation and show that enhancement in speed can be translated even further, to the downstream effectors, cAMP accumulation with Epac (cAMP effector protein biosensor) was measured. Therefore, the advanced version of the initial FRET-based Epac1-camps biosensor (Nikolaev *et* al., 2004) - Epac-S^{H187} biosensor (Klarenbeek *et* al., 2015) was employed, which reports on the conformational change when cAMP binds to Epac (exchange protein directly activated by cAMP) (**Figure 45 A**).

First, changes in cAMP accumulation at the FRET microscope were measured using the same setup and settings as earlier for PTH1R receptor activation. HEK293 cells were transfected with Epac-S^{H187} biosensor, $PTH1R_{wt}$, with or without $RAMP2_{wt}$ and perfused with saturating (**Figure 45 F**) concentration of PTH (**Figure 45 A**). Stimulation resulted in complete cAMP accumulation for both experimental groups, and there was no observed difference in the amplitudes (**Figure 45 D**). Interestingly, when activation constant τwas calculated, ~two times increase in speed of cAMP accumulation in RAMP2-expressing cells was observed (**Figure 45 C**). Those results were in agreement with quicker activation kinetics of the $PTH1R_{FRET}$ biosensor. The median time constant tau was statistically different ($p<0.0001$); 49 s for the control group and 28 s in the presence of $RAMP2_{wt}$ (**Table 25**).

Next, experiments in microtiter plates to calculate the efficacy and potency of cAMP accumulation in the presence and absence of $RAMP2_{wt}$ were performed. Such measurements are less laborious, more reproducible, and advantageous for the construction of concentration-response curves for different conditions or ligands compared to the experiments at the microscope.

HEK293 cells were transfected in the same manner as mentioned in the previous paragraph and agonist-stimulated cAMP accumulation was measured. Interestingly, the time course of stimulation with PTH showed similar overshoot in signal (**Figure 45 E**) as recorded with the preceding process, Gs a protein activation (**Figure 42 A**)**.** Also, subsequent cAMP accumulation happened with overshot, which, however, after normalization to the saturating 10 µM FSk + 100 µM IBMX resulted in the same calculated amplitude. There was no detected difference from a concentration-response curve, moreover, it looked that ±$RAMP2_{wt}$ groups induced a similar amount of potency as also efficacy (**Figure 45 F, Table 25**)**.** Notably, when cAMP accumulation experiments with another ligand, PTHrP were performed, there was no before-mentioned observed overshoot in the signal. This observation was in agreement with no overshoot at PThrP-stimulated G protein activation level. There was no difference between concentration-response curves in any parameters calculated (**Figure 45, Table 25**)**.** The observation that PTH induces overshot and PThrP not (**Figure 45 E, G**) points further research to the different conformations to which those ligands favorably bind (Vilardaga *et* al., 2012) as well spatial precision of PTH1R signaling – PTH can signal from membrane and endosomes, whereas PThrP only from the membrane. This may suggest that RAMP2 could modulate PTH-stimulated endosomal cAMP accumulation, an observation that was described for CGRP receptor (Yarwood *et* al., 2017). Since RAMPs are *per se* expressed in thecell interior, this might functionally explain their localization and provide physiological diversification of receptor roles – this was seen for CGRP mediating pain transmission and could help to understand various biological outcomes of PTH1R signaling. It is already known that spatial bias at PTH1R specifies the amount of circulating vitamin D and Ca^{2+}, and bone constitution in mice (A. D. White *et* al., 2021). To understand potential RAMP contribution better, tethered cAMP biosensors (DiPilato *et* al.,

2004; Wachten *et* al., 2010) or other strategies (Gidon *et* al., 2016) could be used to measure either membrane or endosomal fraction of cAMP-dependent signaling. Some other downstream cascades, for example, potential contribution of ERK signaling, is described in **Chapter 4.8.3**.

In summary, differential activation of both endogenous ligands, PTH and PThrP, is transduced downstream till cAMP accumulation level. A measured increase in kinetics of PTH-stimulated cAMP accumulation was specifically seen as overshoot on Gs activation as well cAMP accumulation level. However, there were no differences for PThrP. That finding adds another layer of complexity to thealready differential signal transduction and associated biology of those two ligands.

Control experiments of the biosensor Epac-S^{H187} emission levels in microtiter plates showed that both experimental groups were expressed to the same extent (**Figure 46 A**)**.** The total dynamic range of the biosensor remained equal (**Figure 46 B**). Later was controlled with the addition of 10 µM Fsk + 100 µM IBMX, positive control, used for normalization. Fsk induces direct activation of cAMP accumulation, and IBMX acts as nonspecific inhibitor of phosphodiesterase (PDE), hence prevents that PDE would degrade available cAMP molecules in the cytosol compromising measured responses. Furthermore, such positive control ensured that equal dynamic range of cAMP accumulation was used for both groups. The amplitudes for single-cell experiments are plotted in **Figure 45 D,** and amplitudes for microtiter plates, in **Figure 45 B,** respectively.

The last control was of basal ratios, which could indicate that $RAMP2_{wt}$ induced a certain amount of de/preactivation of Gs-depending signaling, and thus, detection of smaller basal ratios would be possible. A comparison of basal ratios prior to the stimulation showed that this was not the case (**Figure 46 C**).

		PTH				PTHrP			
		control	$RAMP2_{wt}$	p	n	control	$RAMP2_{wt}$	p	n
Ensemble	pEC_{50}, M	11.57 ± 0.05	11.60 ± 0.06	ns	4	11.12 ± 0.14	11.08 ± 0.19	ns	4
	E_{max}, %	100.00 ± 2.46	99.18 ± 2.86	ns		100.00 ± 8.60	97.40 ± 11.03	ns	
	$FRET_0$	1.13 ± 0.09	1.15 ± 0.002	ns					
Single-cell	Median τ [95% CI], ms	49 [45, 62]	28 [23, 35]	<0.0001					
	Δ FRET, %	75.8 ± 4.1	79.3 ± 2.1	ns					
	N, cells	14	16						

Table 25: Potency and efficiency for PTH- and PTHrP-induced cAMP accumulation.
The results are from the single-cell method, recorded at FRET microscope, and ensemble method in microtiter plates.

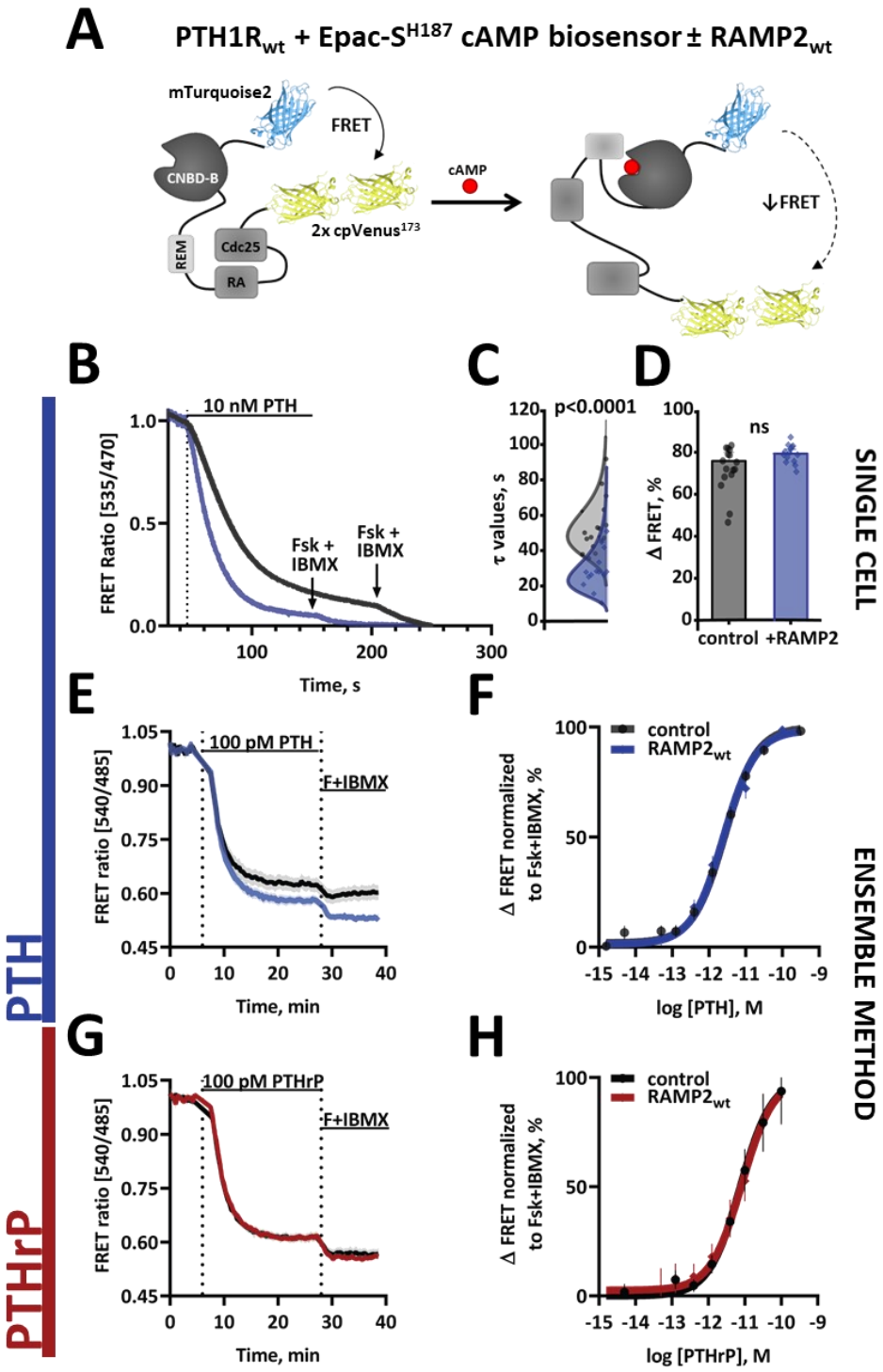

Figure 45: RAMP2 effects on PTH-stimulated cAMP accumulation.

*(**A**) HEK293 cells transiently transfected with cDNA encoding for the cAMP-based FRET biosensor (Epac-S^{187} cAMP biosensor), along with PTH1R$_{wt}$, with or without RAMP2$_{wt}$.*

*(**B**) Shown are representative ratio traces of PTH-mediated FRET changes in single HEK293 cells recorded in a microscopic FRET setup. Horizontal lines indicate the application of 10 nM PTH with a rapid superfusion system. The arrow indicates the addition of 10 µM Fsk/100 µM IBMX after signal saturation. Traces were normalized to the baseline (set to 1) and plateau after stimulation*

with Fsk/IBMX (set to 0). Traces are representative of n = 16 cells (control) and n = 14 cells (+RAMP2$_{wt}$), acquired in two independent experiments.

*(**C**) Time constants τ of PTH-induced FRET changes derived from traces as in panel C, calculated from monoexponential curve fitting. The data were fitted with a lognormal distribution. Median value and 95% confidence interval (CI) were: PTH1R$_{FRET}$ = 49 s [45, 62 CI], n = 14 cells; RAMP2$_{SNAP}$ = 28 s [23, 35 CI], n = 14 cells. A Mann-Whitney test was used to assess a significant difference between the groups (p < 0.001).*

*(**D**) Effects of RAMP2 on the amplitude of the FRET signals induced by PTH. The bars represent means ± SEM in % of the ΔFRET amplitudes from all cells examined: Epac-S^{187} +PTH1R$_{wt}$ = 75.8 ± 4.1 % (n = 16 cells); Epac-S^{187} +PTH1$_{wt}$ +RAMP2$_{wt}$ = 79.3 ± 2.1 %, (n = 14 cells). A t-test was used to assess a significant difference between the groups (ns, p > 0.05).*

*(**E-H**) HEK293 cells are transiently transfected with cDNA encoding for the cAMP-based FRET biosensor (Epac-S^{187}), along with PTH1R$_{wt}$, with or without RAMP2$_{wt}$. FRET signals were recorded in a plate reader from cells stimulated with PTH (black, blue) or PTHrP (black, red). Shown are time courses of agonist stimulation and corresponding concentration-response curves, fitted with a three-parameters concentration-response curve fit. The data are mean ± SEM of at least three independent experiments performed in quadruplicates or more. For further statistics and results, see **Table 25**.*

*(**U, V**) "Spider plots" show mean ± SEM of the pEC$_{50}$ (M) values calculated from the concentration-response curves.*

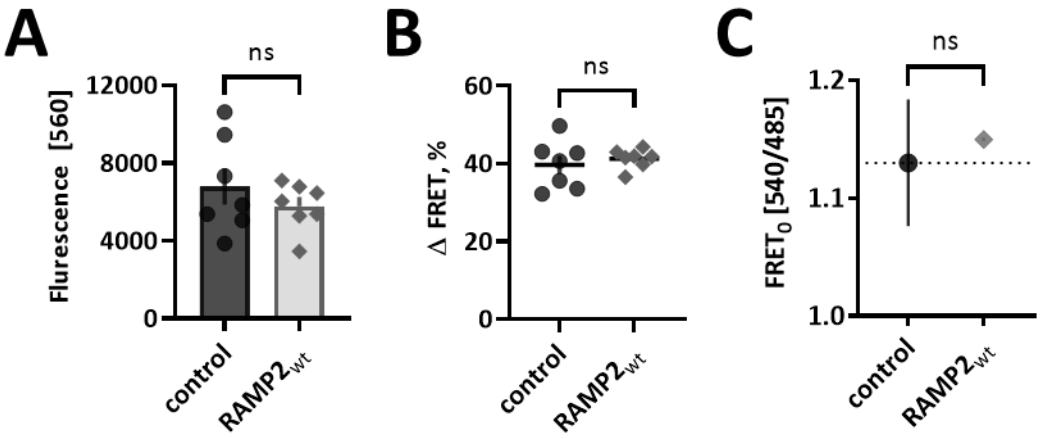

Figure 46: Controls for cAMP accumulation assay.

The data were obtained from plate reader experiments with HEK293 cells transiently expressing cAMP-based FRET biosensor (Epac-S187 cAMP biosensor), along with PTH1R$_{wt}$, with or without RAMP2$_{wt}$. The data are from four independent experiments done in quadruplicates and represent means ± SEM. A t-test was used to assess significance between the groups, ns > 0.05.

*(**A**) Comparison of emission of a cAMP biosensor used in the assay in the absence (black) and presence of RAMP2$_{wt}$ (grey) after excitation at 510 nm. The mean was calculated from 48 wells in a single 96-well plate.*

*(**B**) Comparison of ΔFRET responses in % after the full stimulation with 10 µM Fsk/100 µM IBMX.*

*(**C**) Comparison of basal ratios before stimulation.*

Next, the orthogonal assay was used to access possible differences in the accumulated amount of downstream effectors in the presence of RAMP2$_{wt}$. Two assays, for cAMP and IP1 accumulation, based on HTRF technology (described in **Chapter 4.3.6**) were employed, which measure changes, downstream of Gs and Gq proteins, respectively. HEK293 cells were transfected with PTH1R$_{wt}$, with or without RAMP2$_{wt}$ and incubated in the presence of agonist PTH for requisite time (30 minutes for cAMP and 1,5 hours for IP1) and lysed thereafter. Comparing potency for those assays showed there is a slight right-shift (p=0.0014) for PTH-stimulated cAMP accumulation

when $RAMP2_{wt}$ was coexpressed with $PTH1R_{wt}$ (**Figure 47 A, Table 26**). There was no difference in PTH-stimulated IP1 accumulation (**Figure 47 B, Table 26**), concurring measurements of preceding Gq activation (**Figure 42 F, G**).

In comparison to previously used assays, offers HTRF detection industry-suitable, no-wash technology, which is with the less laborious procedure, robustness, and superior sensitivity used in industry. Time-resolved detection of ratio emission omits possible interferences of solutions, and the final signal is proportional to the extent of analyte formation. Sensitive and robust measurement offer the possibility of miniaturization of the assay (can be used in 384- and 1536-well). Therefore, this technology signifies for primary and secondary screening phases in the drug discovery campaigns.

Downside of this detection method is the required lysis of the cells after stimulation as currently available donors aren´t cell-permeable. Such technology unfortunately cannot report on real-time signaling in the intact cells. On the other hand, FRET and BRET assays enable monitoring real-time signaling in intact cells but are harder to employ in such miniaturized formats – however, some successful reports are encouraging this will eventually change (Schihada, 2018, 2021; Schihada *et* al., 2018).

In summary, this chapter demonstrates, that HTRF assays verified results demonstrated with BRET and FRET-based methods previously. After a holistic examination of PTH1R-succeeded G protein cascade, it can be concluded that $RAMP2_{wt}$ does not significantly changes sensitivity of this signaling branch, but it can induce quicker transduction of the signal.

It remains to be seen how these differences translate to the gene expression profiles and finally, functional effects.

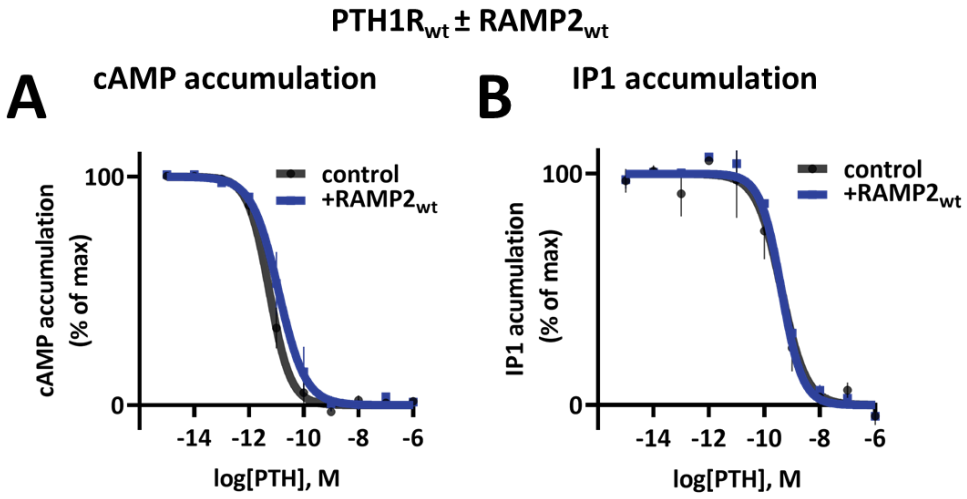

Figure 47: PTH-stimulated cAMP and IP1 accumulation.

*Normalized concentration–response curves for cAMP (**A**) or IP1 (**B**) accumulation measured in HEK293 cells expressing $PTH1R_{wt}$ with or without $RAMP2_{wt}$. Measurements were performed with the HTRF kit: Gs HiRange (**A**) and IP1 (**B**). The data are shown as mean + SEM of two independent experiments performed in duplicates.*

	PTH				
		control	$RAMP2_{wt}$	p	n
cAMP	pEC_{50}, M	11.26 ± 0.05	10.92 0.08	0.0014	2
IP1	pEC_{50}, M	9.50 ± 0.12	9.28 ± 0.06	ns	2

Table 26: Potency for PTH-induced cAMP and IP1 accumulation.

4.8 RAMP2 effect on non-G protein-dependent signaling

Besides G protein-dependent cascade, signaling of GPCR is further regulated by phosphorylation of G protein-coupled receptor kinases (GRKs) (Benovic *et* al., 1987b, 1989), a process which leads to the binding of β-arrestins (Lohse *et* al., 1990), and initiates receptor internalization and likely, also β-arrestin-dependent signaling (Shenoy *et* al., 2006). β-arrestin-dependent signaling joins the MAPK/ERK pathway, which is also regulated via G proteins. The cascade transfers signals from the exterior towards DNA in the nucleus of the cell, where they regulate the activation of various transcription factors. The following chapter discusses steps of the non-G protein-dependent signaling cascade, which were analyzed by corresponding FRET and BRET biosensors.

In recent years, structural and signaling studies added more details to both signaling cascades downstream of GPCRs and revealed that the conformational fingerprint of non-G protein dependent one may be different from the G protein-dependent one (Benovic *et* al., 1987b, 1989; Gurevich & Gurevich, 2019). Structural requirements for one either way were also exploited for PTH1R, and two different ligands are known to exert either G protein: [Trp1]PTHrp-(1–36) (Bisello *et* al., 2002; Gesty-Palmer *et* al., 2006) or β-arrestin bias: (D-Trp12,Tyr34)-PTH(7–34) (Gesty-Palmer *et* al., 2006, 2009). More importantly, there is an ongoing discussion in the field (Grundmann *et* al., 2018; Rajagopal, Kim, *et* al., 2010; Rajagopal, Rajagopal, *et* al., 2010; Shenoy *et* al., 2006) if professed biased ligands truly exist. Those ligands are converging declared functional selectivity; prefer to activate one signaling branch over other, and are of considerable therapeutic interest (Whalen *et* al., 2011). First such "biased drug" oliceridine was recently approved by FDA (Mullard, 2020).

4.8.1 RAMP2 effect on GRK2 recruitment

GRKs regulate the first phase of desensitization of GPCRS by phosphorylating serine and threonine residues in intracellular parts of GPCRs (Chaturvedi *et* al., 2020; Q. Chen *et* al., 2021), mostly in ICL3 and C-terminus. GRKs and their phosphorylation pattern (Liggett, 2011; Mayer *et* al., 2019; Nobles *et* al., 2011; Staus *et* al., 2018), often referred to as phosphorylation barcode, is considered to specify β-arrestin2 binding. Exploring seven isoforms of GRKs and their involvement in phosphorylation patterns was recently further enabled by the knockout cell lines of GRKs, characterized by Drube *et* al. (Drube *et* al., 2022a) and Kawakami *et* al. (Kawakami *et* al., 2022).

To examine whether $RAMP2_{wt}$ could modulate distinct phosphorylation patterns in the PTH1R, recruitment of GRK to PTH1R was quantified in the presence or absence of $RAMP2_{wt}$. Since it has been shown that GRK2 phosphorylates PTH1R with the highest efficacy (preceding GRK3 and GRK5) (Dicker *et* al., 1999), GRK2 isoform was cloned to $GRK2_{YFP}$ and used with $PTH1R_{NanoLuc}$ (**Figure 48**). The resulting BRET assay reported an increase in BRET when GRK2 was recruited to the activated PTH1R receptor. BRET signals after the full ligand occupancy were measured at the time of the maximal responses (**Figure 48 B, D**). Time courses with the saturating concentration of agonist did not show a change in efficacy between experimental groups – this was the case for PTH (**Figure 48 B - C**) as well for PTHrP (**Figure 48 D - E**). The amount of GRK2 recruitment was concentration-dependent, and, slightly

higher potencies ($p<0.05$) were detected when RAMP2 was coexpressed (**Figure 48 C, Table 27**). For PTHrP, no differences in potency or efficacy of GRK2 recruitment (**Figure 48 D – E, Table 27**) were observed.

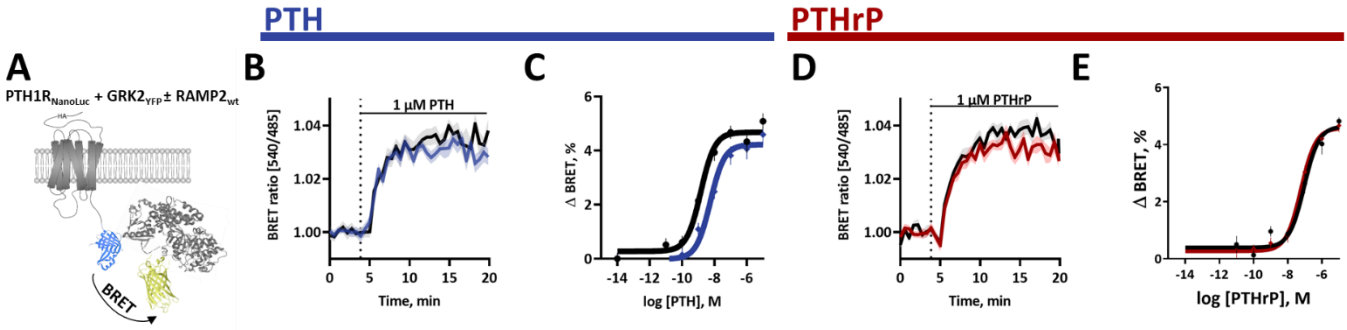

Figure 48: RAMP2 effects on GRK2 recruitment.

*(**A**) Graphical depiction of the construct used in the study: NanoLuc was fused to the C-terminus of PTH1R, and YFP to the N-terminus of GRK2.*

*(**B-E**) HEK293 cells were transiently transfected with cDNA encoding for β-arrestin2$_{mVenus}$ along with PTH1R$_{NanoLuc}$ with (colour points and traces) or without RAMP2$_{wt}$ (black points and traces).*

*BRET signals were recorded in a plate reader from cells stimulated with PTH (**B, C,** black, blue) or PTHrP (**D, E,** black, red). Shown are time courses of agonist stimulation (B, D) and corresponding concentration-response curves (C, E), fitted with a three-parameters concentration-response curve fit. The data are mean ± SEM of three independent experiments performed in quadruplicates. For further statistics and results, see **Table 27**.*

		PTH				PTHrP			
		control	RAMP2$_{wt}$	p	n	control	RAMP2$_{wt}$	p	n
GRK2 r.	pEC$_{50}$, M	8.84 ± 0.13	8.25 ± 0.14	< 0.05	3	7.04 ± 0.12	7.23 ± 0.11	ns	3
	E$_{max}$, %	4.40 ± 0.23	4.23 ± 0.25	ns		4.25 ± 0.24	4.32 ± 0.20	ns	
	BRET$_0$	0.76 ± 0.01	0.70 ± 0.02	0.0012					

Table 27: The potency and efficiency for PTH- and PTHrP-induced GRK2 recruitment.

*Potency (pEC$_{50}$, M) and efficiency (E$_{max}$, %) values were obtained from plate reader experiments, as shown in **Figure 48**. The data are mean ± SEM of n independent experiments. Extra-sum-of-squares test was used to assess the difference between the curves, ns > 0.05. A t-test was used to assess significance between the groups, ns > 0.05.*

Control experiments quantified similar expression for both proteins by assessing the emission of their coupled fluorophore (YFP in GRK2$_{YFP}$) (**Figure 49 A),** and bioluminescent enzyme (NanoLuc in PTH1R$_{NanoLuc}$) (**Figure 49 B).** Next, also basal ratios were compared to test if RAMP2$_{wt}$ induced ligand-independent GRK2 recruitment, and thus, it would be possible to detect higher basal ratios in the presence of RAMP2$_{wt}$. Interestingly, it appeared that the basal ratio was smaller in the presence of RAMP2$_{wt}$ (**Figure 49 C**). That could indicate a different amount of BRET between examined proteins – such difference could be due to different orientations between the fluorophores or different distances between them. A possible explanation is that the PTH1R$_{NanoLuc}$ is in da ifferent conformation when coexpresed with RAMP2, which causes different amount of BRET between donor and acceptor (**Figure 49 C**). Nevertheless, a different starting position does not impact GRK2 recruitment (**Figure 48, Table 27**). NanoLuc was fused after final Met593 of PTH1R C-terminus, which enables accessibility to all phosphorylation sites (curated in

such a way that most important clusters are intact in the construct; Ser489–Ser495 and Ser501–Thr506 (Zindel *et* al., 2016)). Interestingly, a recent studies suggest that C-terminal sites previously marked as critical are not of such importance, which was confirmed by phosphorylation deficient mutant of C-terminus which still yielded successful β-arrestin recruitment. The study by White *et* al. (A. D. White *et* al., 2021) also proposes that although there is a different amount of β-arrestin recruitment when cells are stimulated with different ligands, this is not seen as phosphorylation pattern of PTH1R. Thus, the proposed phosphorylation might not be directly translated into β-arrestin recruitment - this is widely researched and believed for some receptors (Latorraca *et* al., 2020; Liggett, 2011; Mayer *et* al., 2019; Nobles *et* al., 2011; Staus *et* al., 2018).

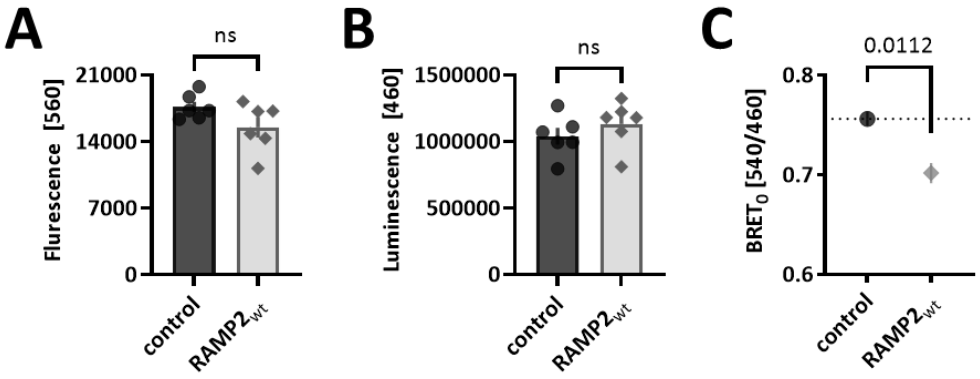

Figure 49: Controls for GRK2 recruitment.

The data were obtained from plate reader experiments with HEK293 cells transiently $GRK2_{YFP}$ along with $PTH1R_{NanoLuc}$ with or without $RAMP2_{wt}$. A t-test was used to assess significance between the groups, ns > 0.05.

*(**A**) Comparison of emission of $GRK2_{YFP}$ in absence (black) and presence of $RAMP2_{wt}$ (grey) after excitation of YFP at 510 nm. Mean was calculated from 48 wells in a single 96-well plate.*

*(**B**) Comparison of emission of $PTH1R_{NanoLuc}$ in absence (black) and presence of $RAMP2_{wt}$ (grey) after incubation with substrate furimazine. Mean was calculated from 48 wells in a single 96-well plate.*

*(**C**) Comparison of basal ratios before stimulation. The data are from four independent experiments done in quadruplicates and represent means ± SEM.*

4.8.2 RAMP2 effect on β-arrestin2 recruitment

To further explore what impact $RAMP2_{wt}$ has on PTH1R downstream signals, β-arrestin2 recruitment was monitored. BRET assays were employed, in which β-arrestin2 was tagged with mVenus (**Figure 50 A**) and used besides the previously described $PTH1R_{NanoLuc}$ construct, as in experiments of GRK2 recruitment.

In this series of experiments, HEK293 cells were transfected with $PTH1R_{NanoLuc,}$ $\beta\text{-arrestin2}_{mVenus}$ with or without $RAMP2_{wt}$ (**Figure 350**). Cells in microtiter plates were stimulated with endogenous agonists PTH (**Figure 50 B, G**) and PTHrP (**Figure 50 C, H**)**.** Remarkably, a profound increase in the amplitude of BRET recruitment in the presence of $RAMP2_{wt}$ was detected for both ligands. This was true for all concentrations observed and was concentration-dependent. As previous results showed rather ligand-specific effects in RAMP2 modulation of receptor activation and G protein activation, here, RAMP2 modulation had an effect on recruitment, surprisingly, on both ligands, PTH and PTHrP. Encouraged by those findings, different PTH1R agonists were examined; a shorter version of PTH(1-34):

PTH(1-31) (**Figure 50 D, I**); chimera between PTH and PThrP; Abaloparatide (Miller *et* al., 2016; Tella *et* al., n.d.; Varela *et* al., 2017) (**Figure 50 E, J**) and lastly, only 14 aa long peptide agonist of PTH1R; DPCAJ-1951 (Carter *et* al., 2007) (**Figure 50 F, K**). Higher BRET signals were quantified with all tested ligands in the presence of $RAMP2_{wt}$ (**Figure 50, Table 28**). Besides general RAMP2-induced increase, was this effect ligand-dependent which suggests that RAMP2 as also ligands affected recruited amount of β-arrestin2 to PTH1R.

Control experiments did not show differences in expression levels of the constructs (**Figure 52 A, B**). However, surprisingly, basal ratios, quantified with $BRET_0$ method (Schihada, Shekhani, *et* al., 2021) (described in **Chapter 4.7.1**) in the absence of receptor stimulation, were found to be significantly higher in RAMP2 group (**Figure 52 C, Table 28**)**.** This might suggest that RAMP2 could induce a higher inherent affinity of β-arrestin2 towards PTH1R, also in the absence of ligand. Previously it was described that the agonist-stimulated PTH1R was still able to recruit β-arrestin2 in GRK knockout cell lines (Drube *et* al., 2022a) – RAMP could further increase affinity and, thus, basal ratio.

The feasible explanation is that RAMP2 allosterically modifies PTH1R conformation and the newly created conformation accommodates more β-arrestin2. Many studies from the literature show that PTH1R indeed possesses such allosteric point, which can modify amount of β-arrestin recruitment. For example, in Clark *et* al. (L. J. Clark *et* al., 2020b), group described PTH with modified aa His9. Newly-made peptide after ligand-binding interacts with the TM core of the receptor and ECL2 residues (**Figure 74**), creating a unique receptor conformation. This engagement is further translated toward conformational change in PTHR IL3, abolishing interactions with β-arrestin's finger loop. Another study by Sarkar *et* al. (Sarkar *et* al., 2019) describes that their monoclonal antibody directed towards the PTH1R α1 helix of the ECD is able to abolish β-arrestin recruitment after PTH-induced receptor activation. Despite the total inhibition of β-arrestin2 recruitment, Gs-dependent signaling still functions and thus creates bias in signal transduction.

On the other hand, ECL2 of the receptor is a hotspot of GPCR-RAMPs interaction. RAMPs are located between TM3,4,5 and help to stabilize receptor at their ECL2 (Liang *et* al., 2018; Liang, Belousoff, Fletcher, *et* al., 2020c). Mutation of the linker region, which connects RAMPs TM with its extracellular helices is contacting receptors ECL2 (**Figure 73**). Modifications of this region of RAMP were shown to dictate receptor phenotype (Liang, Belousoff, Fletcher, *et* al., 2020c).

Chapter 5.3.5 discusses the importance of ECL2 for GPCR-RAMP interaction and emphasizes possible implications for the β-arrestin recruitment.

Available literature offers many examples of the RAMP-interacting GPCRs, which suggest that RAMP´s modulation of β-arrestin2 binging might have broader implications as previously appreciated. For instance, Cegla *et* al. (Cegla *et* al., 2017) found that RAMP2 abolished β-arrestin2 recruitment at the GCGR, and a subsequent study by McGlone *et* al. (McGlone *et* al., 2021) revealed that this is due to RAMP2´s effects to promote internalization and increased activation of Gαs proteins at endosomes. They observed apparent decrease in the β-arrestin2 recruitment with no difference in recruitment of mini-Gαs, -Gαi, and -Gαq proteins. Thus, RAMP2 at GCGR was able to induce biased responses. Further study with GIPR receptor by Harris *et* al. (Harris *et* al., 2021b) described increased β-arrestin2 recruitment for GIPR´s primary interactor RAMP3.

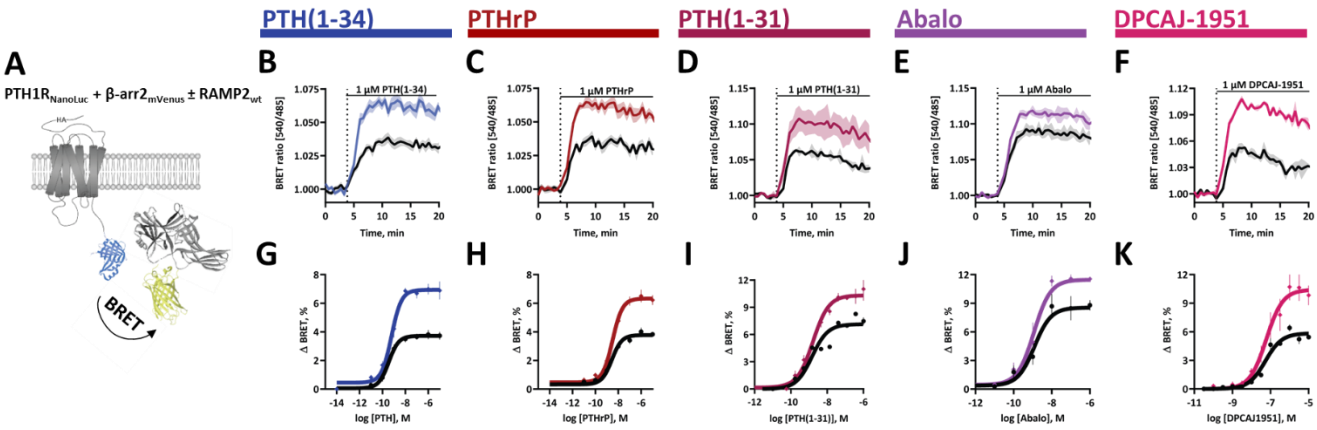

Figure 50: RAMP2 effects on ß-arrestin2 recruitment to PTH1R.

*(**A**) Graphical depiction of the construct used in the study: NanoLuc was fused to the C-terminus of PTH1R, and mVenus to the N-terminus of ß-arrestin2. HEK293 cells were transiently transfected with cDNA encoding for ß-arrestin2$_{mVenus}$ along with PTH1R$_{NanoLuc}$ with (colour points and traces) or without RAMP2$_{wt}$ (black points and traces).*

*(**B - F**) Averaged time courses of ligand stimulation with 1 µM PTH(1-34), (**B**) PTHrP (**C**), PTH(1-31) (**D**), Abaloparatide (**E**), DPCAJ-1951(**F**), and corresponding concentration-response curves (**G – K**), fitted with a three-parameters concentration-response curve fit. The data are mean ± SEM of at least two independent experiments performed in duplicates or more. For further statistics and results, see **Table 28**. BRET signals were recorded in a plate reader.*

With the motivation of observed RAMP effects on PTH1R, other GPCRs were examined. First, β-arrestin2 recruitment was analyzed at another interacting class B GPCR, CTR (**Figure 51**). A set of similar constructs as described before was utilized – receptor was tagged with NanoLuc at its C-terminus and mVenus was fused to β-arrestin2. β-arrestin2 recruitment was quantified upon stimulation with human calcitonin (hCT) (**Figure 51**) and salmon CT (sCT) (**Figure 51**)**.** There was no change in the potency, but there was a slight, albeit significant increase in β-arrestin recruitment when RAMP2 was coexpressed (**Table 28**). Control experiments showed that (**Figure 52 D, E**) expression of constructs in both experimental groups didn't differ, and basal ratio did not show the change (**Figure 52 F**), as for example before for PTH1R. This suggests that there might be a trend of RAMP promoting β-arrestin recruitment at their interacting GPCRs, however, it is receptor-, and, as shown before, ligand-dependent.

In addition, negative control of β2AR was employed as a prototypical receptor known not to interact with RAMPs. As anticipated, no RAMP2-modulated changes were observed – nor in potency or efficacy. Furthermore, control experiments showed that expression of the constructs used in the study were not different and this was true for various expression levels (**Figure 52 G – I**). This excluded possibility that observed changes would be due to RAMPs´ modulation of β-arrestin2 confirmation or binding rather than modulation of their interacting GPCRS.

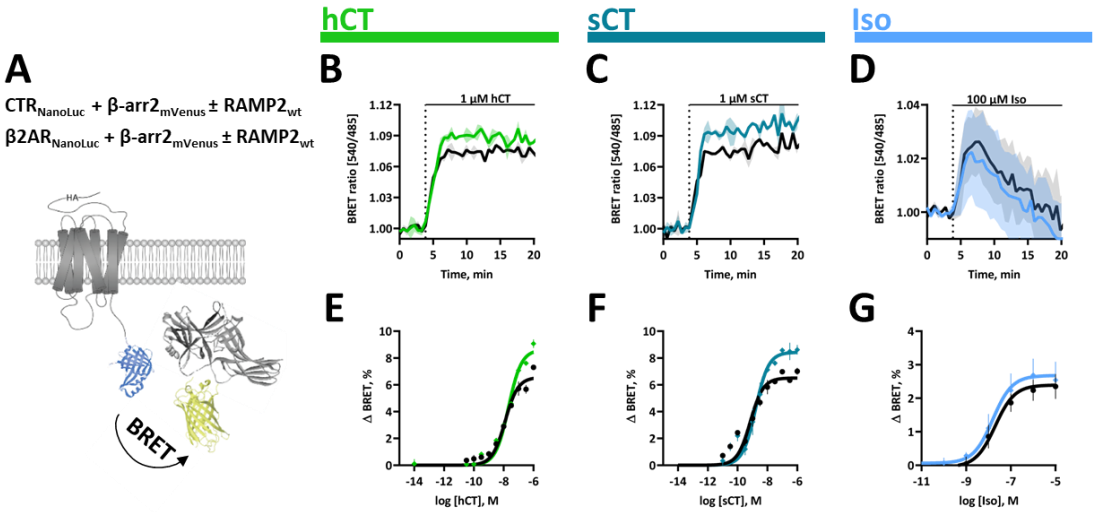

Figure 51: RAMP2 effects on ß-arrestin recruitment to other GPCRs.

(***A***) *Graphical depiction of the construct used in the study: NanoLuc was fused to the C-terminus of CTR and ß2AR, respectively, and mVenus to the N-terminus of ß-arrestin2. HEK293 cells were transiently transfected with cDNA encoding for: ß-arrestin2$_{mVenus}$ along with PTH1R$_{NanoLuc}$ with (colour points and traces) or without RAMP2$_{wt}$ (black points and traces).* (***B - F***) *Averaged time courses of agonist stimulation and corresponding concentration-response curves* (***G – K***)*, fitted with a three-parameters concentration-response curve fit. The data are mean ± SEM of at least two independent experiments performed in duplicates or more. For further statistics and results, see* ***Table 28****. BRET signals were recorded in a plate reader .*

receptor	ligand		pEC$_{50}$, M	E$_{max}$, %	n	BRET$_0$
PTH1R	PTH(1-34)	control	9.45 ± 0.14	3.66 ± 0.21		0.75 ± 0.02
		RAMP2$_{wt}$	9.21 ± 0.12	6.48 ± 0.32	3	0.85 ± 0.02
		p	ns	< 0.05		0.0060
	PTHrP	control	8.56 ± 0.12	3.45 ± 0.16		
		RAMP2$_{wt}$	8.45 ± 0.09	5.85 ± 0.21	3	
		p	ns	< 0.05		
	PTH(1-31)	control	8.56 ± 0.12	3.45 ± 0.16		
		RAMP2$_{wt}$	8.45 ± 0.09	5.85 ± 0.21	2	
		p	ns	< 0.05		
	Abalo	control	8.56 ± 0.12	3.45 ± 0.16		
		RAMP2$_{wt}$	8.45 ± 0.09	5.85 ± 0.21	2	
		p	ns	< 0.05		
	DPCAJ-1951	control	8.56 ± 0.12	3.45 ± 0.16		
		RAMP2$_{wt}$	8.45 ± 0.09	5.85 ± 0.21	2	
		p	ns	< 0.05		
CTR	hCT	control	7.90 ± 0.08	6.56 ± 0.23		0.75 ± 0.04
		RAMP2$_{wt}$	7.68 ± 0.06	8.62 ± 0.26	2	0.73 ± 0.01
		p	ns	<0.0001		ns
	sCT	control	9.15 ± 0.11	6.51 ± 0.09		
		RAMP2$_{wt}$	8.79 ± 0.26	8.43 ± 0.30	2	
		p	ns	<0.0001		
β2AR	Iso	control	7.58 ± 0.13	2.43 ± 0.10		0.83 ± 0.01
		RAMP2$_{wt}$	7.81 ± 0.15	2.72 ± 0.13	4	0.82 ± 0.01
		p	ns	ns		ns

Table 28: Potency and efficiency for ligand-induced ß-arrestin2 recruitment.

Potency (pEC$_{50}$, M) and efficiency (E$_{max}$, %) values were obtained from plate reader experiments in ***Figure 50, 51****. The data are mean ± SEM of n independent experiments. Extra-sum-of-squares test was used to assess the difference between the curves, ns > 0.05.*

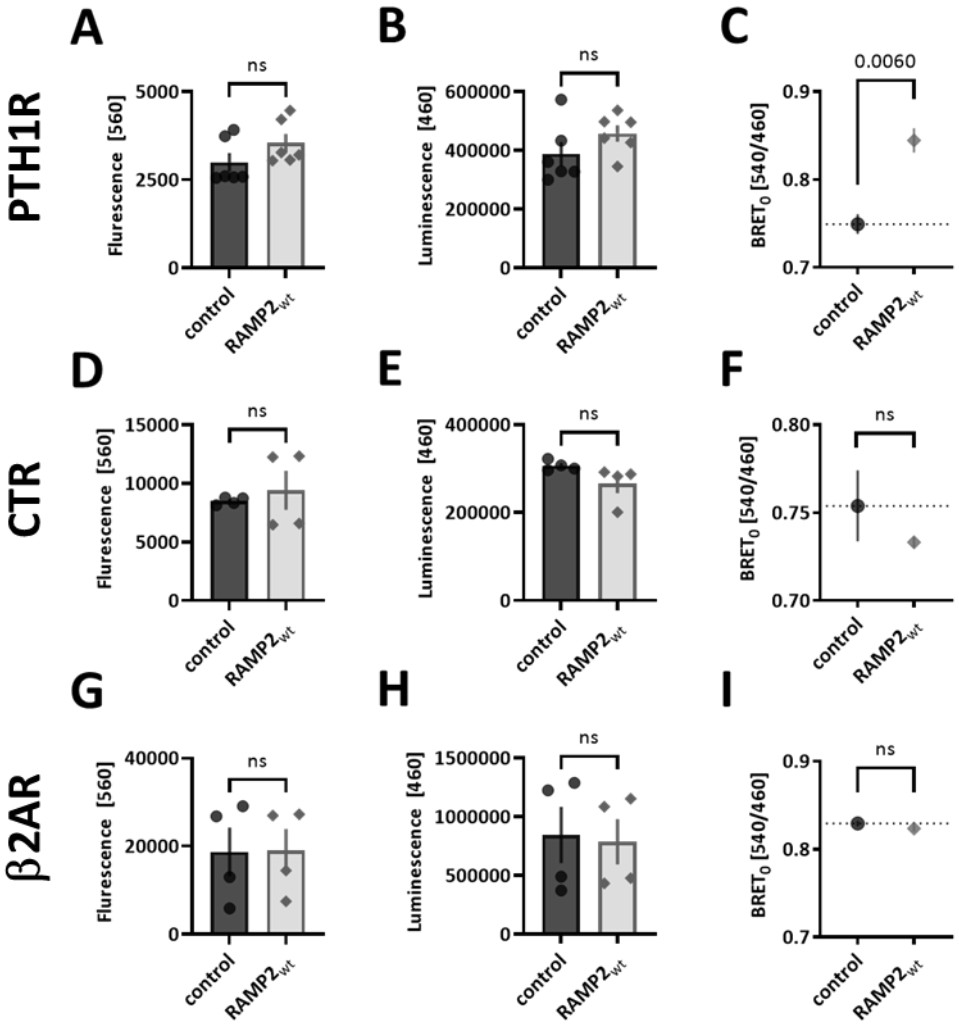

Figure 52: Controls for β-arrestin2 recruitment assays.

The data were obtained from plate reader experiments with HEK293 cells transiently β-arrestin2$_{mVenus}$ along with PTH1R$_{NanoLuc}$ with or without RAMP2$_{wt}$. A t-test was used to assess the significance between the groups, ns > 0.05.

*(**A**) Comparison of emission of β-arrestin2$_{mVenus}$ in the absence (black) and presence of RAMP2$_{wt}$ (grey) after excitation of mVenus at 510 nm. The mean was calculated from 48 wells in a single 96-well plate.*

*(**B**) Comparison of emission of PTH1R$_{NanoLuc}$ in absence (black) and presence of RAMP2$_{wt}$ (grey) after incubation with substrate furimazine. The mean was calculated from 48 wells in a single 96-well plate.*

*(**C**) Comparison of basal ratios before stimulation. The data are from four independent experiments done in quadruplicates and represent means ± SEM.*

4.8.3 RAMP2 effect on ERK phosphorylation

Motivated to see if changes observed in previous cascade steps translate to the ERK1/2 pathway, the FRET-based EKAR (extracellular signal-regulated kinase activity reporter) biosensor (Harvey *et* al., 2008) was employed to observe ERK activity. This biosensor was designed using a conformational sensitive substrate from Cdc25C (Cell

Division Cycle 25C phosphatase) containing the consensus ERK target sequence (Gonzalez *et* al., 1991), and the proline-directed WW phospho-binding domain (Lu *et* al., 1999). ERK activity induces phosphorylation of the substrate sequence, and thus, substrate and phospho-binding domain rearrangea leading to an increase in FRET between the attached fluorophores. Since the WW domain is primarily localized in the cell nucleus, the initial version of the sensor, $EKAR_{nucl}$, residues there. The addition of a C-terminal nuclear export sequence (**Figure 3.41 A**) creates a cytoplasmic version of the biosensor ($EKAR_{cyto}$) (Harvey *et* al., 2008).

Effects on PTH and PTHrP-induced activation of ERK1/2 pathway were measured with both biosensor variants (**Figure 53 A, Table 29**) in HEK293 cells, transiently transfected with one of EKAR biosensor, $PTH1R_{wt}$, with or without $RAMP2_{wt}$.

Effects on PTH and PTHrP-induced activation of ERK1/2 pathway were measured with both biosensor variants (**Figure 53 B – E, Table 29**) in HEK293 cells, transiently transfected with one of the EKAR biosensors, $PTH1R_{wt}$, with or without $RAMP2_{wt}$.

Cells were stimulated with increasing concentrations of agonists and recorded FRET changes in microtiter plates. First, changes with the $EKAR_{cyto}$ biosensor were quantified, where the concentration-dependent difference in amplitudes and efficiencies of RAMP2-induced ERK phosphorylation was observed. Those changes were statistically higher for both agonists – PTH (**Figure 53 B**) and PTHrP (**Figure 53 C**). Contrary, when $EKAR_{nucl}$ was used, neither PTH-, nor PTHrP-stimulation showed differences between the experimental groups (**Figure 53 F – I**).

In summary, it is indisputable that the presence of RAMP2 causes specific alterations of PTH1R signaling in cell interior and is very possible that initial interaction of PTH1R-RAMP2 and conformational rearrangement already at the level of receptor activation dictate observed changes. To explore a structural fingerprint of differential signaling patterns, structural homology modeling was employed and described in **Chapter 4.9**.

		PTH				PTHrP			
		control	$RAMP2_{wt}$	p	n	control	$RAMP2_{wt}$	p	n
ERK cyto.	pEC_{50}, M	9.43 ± 0.37	9.12 ± 0.37	ns	3	7.86 ± 0.86	7.53 ± 0.43	ns	3
	E_{max}, %	2.23 ± 0.29	4.53 ± 0.63	0.0078		1.75 ± 0.56	4.28 ± 0.69	0.00143	
	$FRET_0$	1.09 ± 0.10	0.65 ± 0.05	0.0020					
ERK nucl.	pEC_{50}, M	10.21 ± 0.24	9.34 ± 0.39	ns	3	9.92 ± 0.40	9.12 ± 0.49	ns	3
	E_{max}, %	5.95 ± 0.76	5.39 ± 1.00	ns		6.02 ± 0.82	5.42 ± 0.78	ns	
	$FRET_0$	0.84 ± 0.04	0.85 ± 0.004	ns					

Table 29: Potency and efficiency for PTH- and PTHrP-induced ERK phosphorylation.

*The potency (pEC_{50}, M) and efficiency (E_{max}, %) values were obtained from plate reader experiments in **Figure 53**. The data are mean ± SEM of n independent experiments. Extra-sum-of-squares test was used to assess the difference between the curves, and a t-test was used to determine the significance between the groups, ns > 0.05.*

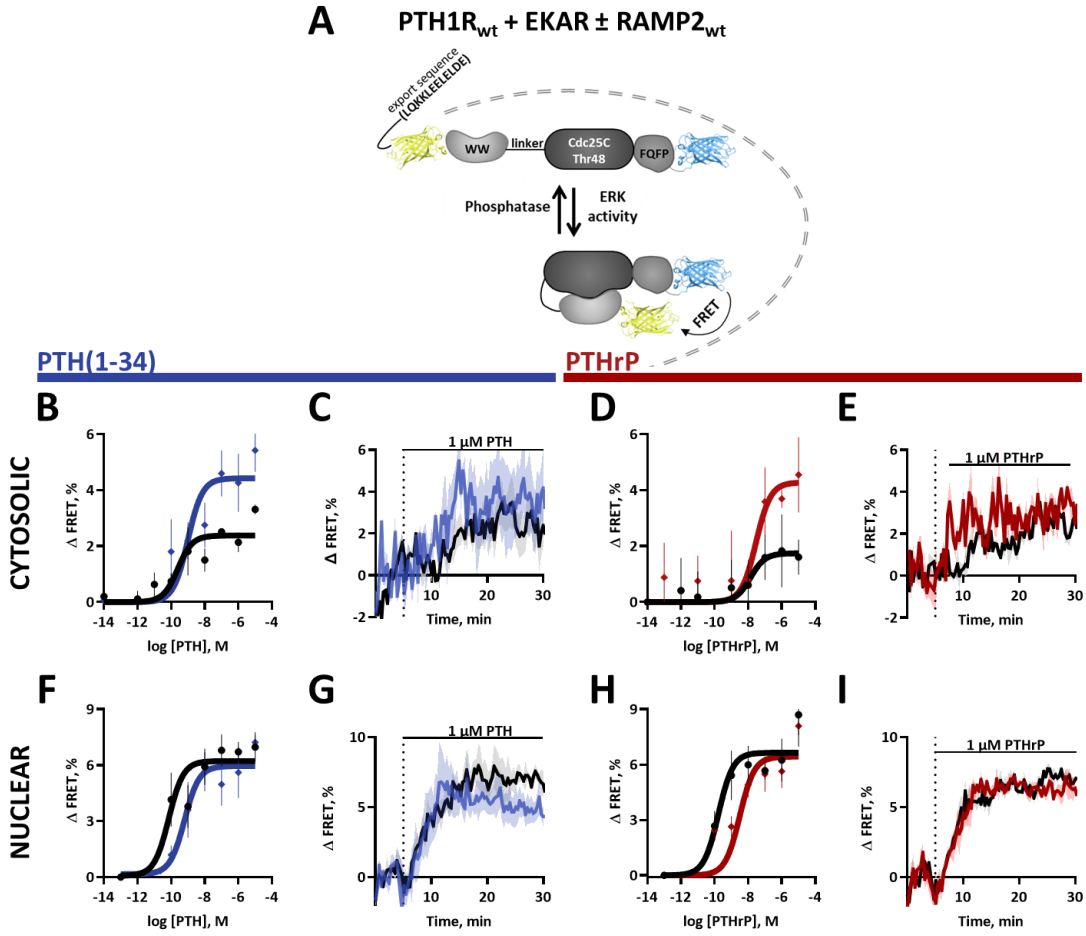

Figure 53: RAMP2 effects on PTH- and PTHrP-induced ERK phosphorylation in nucleus and cytosol.

(A) *Graphical depiction of EKAR construct:* YFP *was fused to the C-terminus of Phospho-binding domain WW and CFP to the ERK docking domain. Upon ERK phosphorylation comes to a conformational change, and FRET increases.*

*(**B - E**) HEK293 cells were transiently transfected with cDNA encoding for nuclear EKAR biosensor along with PTH1R$_{wt}$ with (red, blue points and traces) or without RAMP2$_{wt}$ (black points and traces).*

*(**F - I**) HEK293 cells were transiently transfected with cDNA encoding for nuclear EKAR biosensor along with PTH1R$_{wt}$ with (red, blue points and traces) or without RAMP2$_{wt}$ (black points and traces). The data are normalized to the expression of cytosolic EKAR sensor.*

*Concentration-response curves (**B, D, F, E**) were fitted with a three-parameters curve fit, and the bottom was constrained to 0. The data are mean ± SEM of three independent experiments performed in quadruplicates. For further statistics and results, see **Table 29**. BRET signals were recorded in a plate reader.*

The expression of cytosolic (**Figure 54 A**) and nuclear biosensor (**Figure 54 D**) were controlled through direct excitation of YFP – in the case of cytosolic biosensor, different, ~ 35% smaller expression of the biosensor was observed, which could compromise signal readout, and therefore, amplitudes were normalized to the direct expression of the cytosolic biosensor in each separate group (**Figure 54 B – C).** The sensitivities of both experimental groups to Epidermal growth factor (EGF) were tested as a positive control (**Figure 54 B, E**), and they did not differ between the groups. Lastly, basal ratios were compared to check if RAMP2$_{wt}$ could induce ligand-

independent ERK phosphorylation (**Figure 3. C, F, Table 29**). Interestingly, a comparison of the $FRET_0$ value (basal ratios) of the cytosolic biosensor in both experimental groups suggested that this pathway is somewhat slightly deactivated in the presence of $RAMP2_{wt}$ (**Figure 52**). Therefore, it could be that higher amplitudes of $EKAR_{cyto}$ after stimulation are result of compensation of downregulated pathway (**Table 29**).

Studies of PTH1R-mediated ERK activation (Gesty-Palmer *et* al., 2006) report two peaks of ERK activity after receptor stimulation, where the first contributes to the Gs-related increase, and the second, to the sustained ERK activation. Tohgo *et* al. (Tohgo *et* al., 2003) attributed the first wave of ERK activation to the G protein-dependent pathway and the second one, to the β-arrestin-dependent ERK1/2 pathway. Comparing those studies with the results from **Figure 53** it could be predicted that RAMP2 modulates the second pool of PTH1R-dependent ERK activation and, thus, reshapes receptor signaling towards β-arrestin.

Exploration beyond the used assay would help understand how $RAMP2_{wt}$ shapes the activity of the ERK1/2 pathway of both signaling pools, and further, how it regulates gene transcription. Orthogonal assays used in other studies relied on either protein quantification with Western Blot (Gesty-Palmer *et* al., 2006) or commercially available kits (Harris *et* al., 2021b) and thus, measured the accumulated amount of phosphorylated ERK. In contrast, currently employed assay enables detection of ERK activity in intact cells in real-time. Latter approach is better as it does not represent only a snapshot in very noisy signal transduction pathway, which is influenced by numerous factors. However, signal-to-noise ratio could be still optimized for better performance. Therefore, it should be aimed to explore ERK activity also with other available biosensors in intact cells (Xu *et* al., 2013; de la Cova *et* al., 2017; Q. Zhang *et* al., 2018; Mehta *et* al., 2018; Chavez-Abiega *et* al., 2022). Moreover, it would be worth pursuing a follow-up study with selective PTH analogs, [Trp1]PTHrp-(1–36) for selectively activating Gs/PKA-mediated ERK1/2 activation and [d-Trp12,Tyr34]PTH-(7–34) for G protein-independent/β-arrestin-dependent ERK1/2 activation.

Structural studies from the Sexton lab suggest that different effects on ERK and cAMP efficacy seen for sCT and hCT at CTR originate from different conformational dynamics states for those signaling pathways (dal Maso *et* al., 2019; Furness *et* al., 2016).

Regarding to RAMPs modulation of ERK1/2 pathway, Harris *et* al. detected an increase in amount of ERK phosphorylation when GIPR was coexpressed with RAMP3 (Harris *et* al., 2021b). This was preceded by increased β-arrestin2 recruitment, what mirrors experimental findings from **Chapter 4.8.2** and **Chapter 4.8.3**. Yarwood *et* al. (Yarwood *et* al., 2017) found that the endosomal fraction of CGRP-stimualted CRLR-RAMP1 signaling axis contributes to pain transmission. Similarly, as seen in White *et* al. (A. D. White *et* al., 2021) for PTH1R, both groups attribute important physiological signals to the endosomal fraction. They show that compartmentalized signal transduction matters in cellular perception of signals.

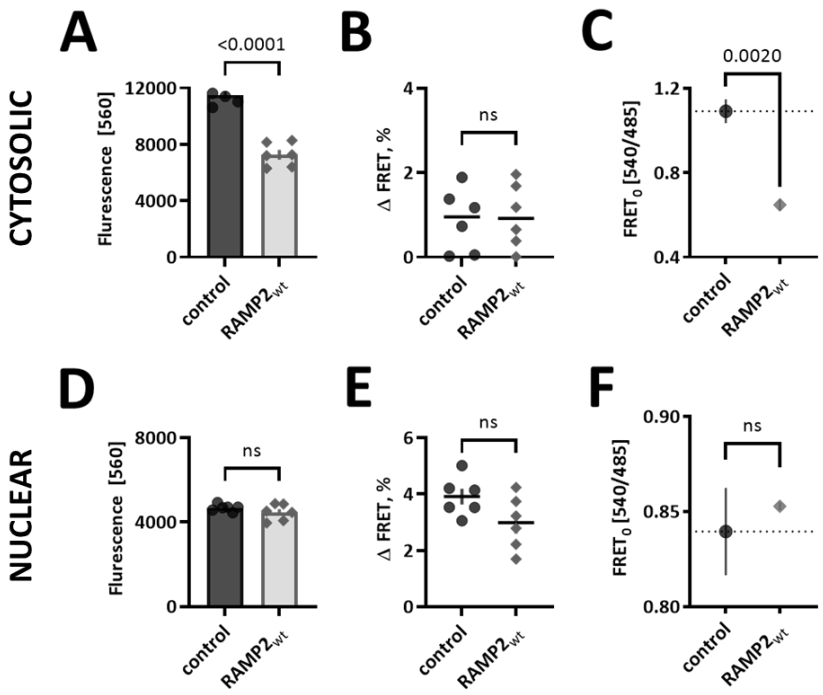

Figure 54: Controls for ERK phosphorylation assays.

The data were obtained from plate reader experiments with HEK293 cells transiently expressing EKAR biosensors (ERKcyto, ERKnucl biosensor), along with $PTH1R_{wt}$, with or without $RAMP2_{wt}$. The data are from four independent experiments done in quadruplicates and represent means ± SEM. A t-test was used to assess significance between the groups, ns > 0.05.

*(**A, D**) Comparison of emission of ERK biosensor used in the assay in the absence (black) and presence of $RAMP2_{wt}$ (grey) after excitation at 510 nm. The mean was calculated from 48 wells in a single 96-well plate.*

*(**B**) Comparison of ΔFRET responses in % after the complete stimulation with 10 µg/µL EGF.*

*(**C**) Comparison of basal ratios before stimulation.*

4.9 Structural basis of PTH1R-RAMP2 interaction

In recent years, the GPCR field observed fireworks in structural studies. Hence, the structural basis of PTH1R (Ehrenmann *et* al., 2018; L.-H. Zhao *et* al., 2019) was exploited along with other GPCRs (Hauser *et* al., 2021; Kooistra, Munk, *et* al., 2021). On the other hand, the first structures of full-length RAMPs with their interacting GPCRs shed light on their modulation character (Garelja *et* al., 2020; Josephs *et* al., 2021b; Liang *et* al., 2018; Liang, Belousoff, Fletcher, *et* al., 2020c). Structurally, RAMPs consist of a single transmembrane domain, located between TM3,4,5 of the receptor and make contact with receptors ECL2. There are no direct contacts with the ligands, although it is clear that RAMPs can reshape the binding interface to accommodate peptides with different affinities (Garelja *et* al., 2020; Josephs *et* al., 2021b; Liang, Belousoff, Fletcher, *et* al., 2020c). Structural studies comparing receptor states with and without RAMPs recently enlarged our structural and mechanistic understanding about GPCR – RAMP association (Cao *et* al., 2022). However, PTH1R and RAMP2 have not yet been crystallized together, and their complex was not determined structurally. To explore the structural fingerprint of the examined interaction partners, AlphaFold (Jumper *et* al., 2021; Tunyasuvunakool *et* al., 2021; Varadi *et* al., 2022) was used besides structural homology modeling.

4.9.1 Structural prediction with AlphaFold

Since AlphaFold can also predict multimers (Evans *et* al., 2021), it was aimed to probe the form of predicted PTH-PTH1R-RAMP2 complexes. First, structures for PTH1R, PTH, PTHrP, and RAMP2 were downloaded from AlphaFold Protein Structure Database (https://alphafold.ebi.ac.uk/) (**Figure 55**) and visualized separately to get an initial impression of their monomeric structural appearance of used proteins.

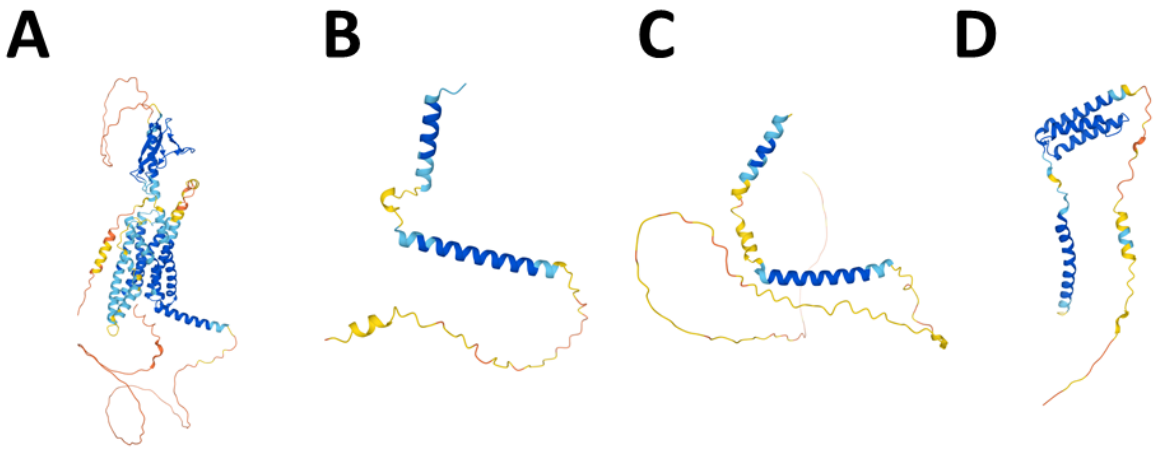

Figure 55: Predicted structures from AlphaFold Protein Structure Database.
Following proteins as predicted in AlphaFold Protein Structure Database; PTH1R (A), PTH (B), PTHrP (C), and RAMP2 (D). The structure was folded by AlphaFold v2.1.0 using the monomer model and sequences in ***Table 30****.*
Colour code shows per-residue confidence score (pLDDT) between 0 and 100; very high (pLDDT > 90, blue), very low (pLDDT < 50, orange).

Sequences for PTH, PThrP, PTH1R, and RAMP2 (**Table 30**) were then copied to the Jupyter Colab notebook of AlphaFold v2.1.0 (https://colab.research.google.com/github/deepmind/alphafold/blob/main/notebooks/AlphaFold.ipynb), and a multimer model was used to fold the complex. The resulting model structures (**Figure 56**) were then visualized in PyMOL and recolored into distinct chains in the predicted multimer complex of proteins; PTH/PTH1R/RAMP2 multimer complex (**Figure 56 A**) and PTHrP/PTH1R/RAMP2 multimer complex (**Figure 56 A**). Both complexes resulted in a very similar structure of PTH1R and relative position of RAMP2 TM towards receptor TM5 and TM6, which is slightly different from the currently proposed location more towards TM3-4-5 of CRLR receptors. Interestingly, the position of ECD of RAMP2 in the PTH/PTH1R/RAMP2 complex is similar to the one expected from previous structures and does not interfere specifically with the PTH. On the other hand, in the complex with PTHrP, RAMP2 ECD seemed substantially more bent, oddly positioning three helixes at an angle of 90°C towards the receptor ECD. The position of the N-terminus is according to the previously described PTH1R structure (L.-H. Zhao *et* al., 2019), and PThrP is bent in the binding pocket, as suggested by the initial PTHrP structure (Weidler *et* al., 1999) and prediction from AlphaFold Protein Structure Database (**Figure 56**). Our collaborators Gunnar Kleinau and Patrick Scheerer (Charité - Universitätsmedizin Berlin) further curated models to get additional insights into the structural prediction – their results are presented in the next chapter.

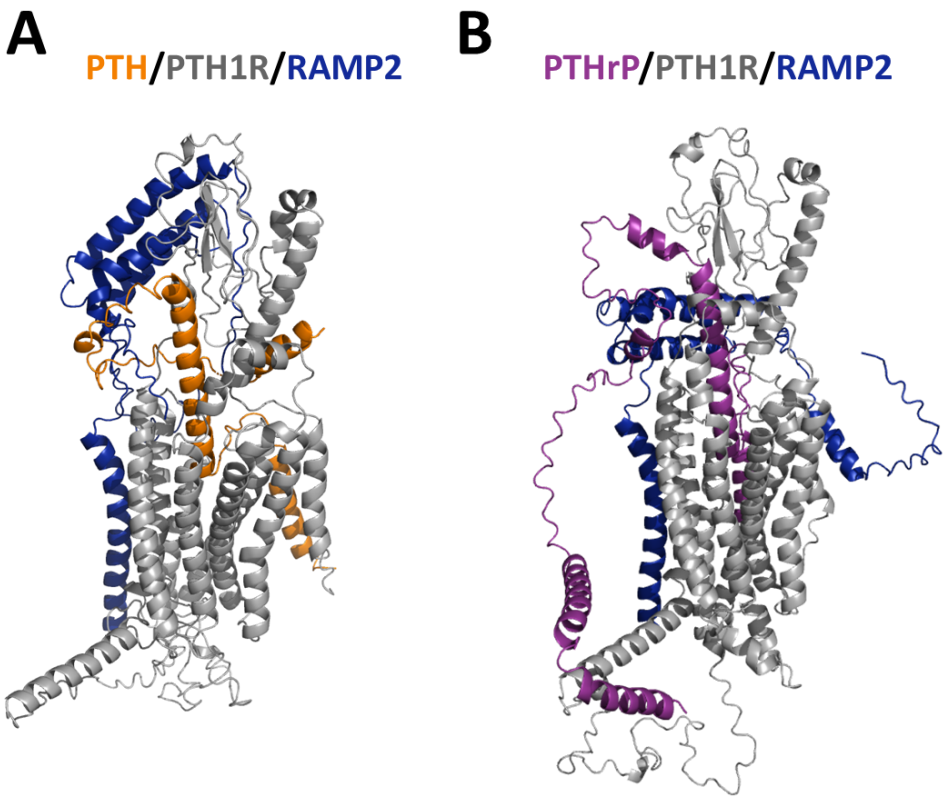

Figure 56: A predicted complex of PTH-PTH1R-RAMP2 and PTHrP-PTH1R-RAMP2.
RAMP2 is depicted in blue, PTH1R in grey, PTH in orange, and PTHrP in purple. The structure was folded by AlphaFold v2.1.0 using sequences in ***Table 30*** *with a multimer model. Structures were visualized in PyMOL.*
*(**A**) PTH/PTH1R/RAMP2 multimer complex.*
*(**B**) PTHrP/PTH1R/RAMP2 multimer complex.*

hPTH	MIPAKDMAKVMIVMLAICFLTKSDGKSVKKRSVSEIQLMHNLGKHLNSMERVEWLRKKLQDVHNFVALGAPLAP RDAGSQRPRKKEDNVLVESHEKSLGEADKADVNVLTKAKSQ
hPTHrP	MQRRLVQQWSVAVFLLSYAVPSCGRSVEGLSRRLKRAVSEHQLLHDKGKSIQDLRRRFFLHHLIAEIHTAEIRATSE VSPNSKPSPNTKNHPVRFGSDDEGRYLTQETNKVETYKEQPLKTPGKKKKGKPGKRKEQEKKKRRTRSAWLDSGV TGSGLEGDHLSDTSTTSLELDSRRH
hPTH1R	MGTARIAPGLALLLCCPVLSSAYALVDADDVMTKEEQIFLLHRAQAQCEKRLKEVLQRPASIMESDKGWTSASTSG KPRKDKASGKLYPESEEDKEAPTGSRYRGRPCLPEWDHILCWPLGAPGEVVAVPCPDYIYDFNHKGHAYRRCDRN GSWELVPGHNRTWANYSECVKFLTNETREREVFDRLGMIYTVGYSVSLASLTVAVLILAYFRRLHCTRNYIHMHLFL SFMLRAVSIFVK DAVLYSGATLDEAERLTEEELRAIAQAPPPPATAAAGYAGCRVAVTFFLYFLATNYYWILVEGLYLHSLIFMAFFSEKK YLWGFTVFGWGLPAVFVAVWVSVRATLANTGCWDLSSGNKKWIIQVPILASIVLNFILFINIVRVLATKLRETNAGR CDTRQQYRKLLKSTLVLMPLFGVHYIVFMATPYTEVSGTLWQVQMHYEMLFNSFQGFFVAIIYCFCNGEVQAEIKK SWSRWTLALDFKRKARSGSSSYSYGPMVSHTSVTNVGPRVGLGLPLSPRLLPTATTNGHPQLPGHAKPGTPALETL ETTPPAMAAPKDDGFLNGSCSGLDEEASGPERPPALLQEEWETVM
hRAMP2	MASLRVERAGGPRLPRTRVGRPAALRLLLLLGAVLNPHEALAQPLPTTGTPGSEGGTVKNYETAVQFCWNHYKDQ MDPIEKDWCDWAMISRPYSTLRDCLEHFAELFDLGFPNPLAERIIFETHQIHFANCSLVQPTFSDPPEDVLLAMIIAP ICLIPFLITLVVWRSKDSEAQA

Table 30: Sequences used for AlphaFold folding.

4.9.2 Structural homology modeling

Modeling of PTH1R in a complex with PTH and RAMP2 was performed by collaborators Gunnar Kleinau and Patrick Scheerer (Charité - Universitätsmedizin Berlin). First, the structure of PTH1R with long-acting PTH (LA-PTH) and Gs based on a cryo-EM structure was determined (L.-H. Zhao *et* al., 2019). Second, RAMP binding to the PTH1R complex was mirrored from the RAMP1-CRLR (Liang *et* al., 2018) complex since this contained more structural information than the available RAMP2-CRLR (Liang, Belousoff, Fletcher, *et* al., 2020c) structure.

There were a few details to consider while building the model:

1. Although the PTH1R and CRLR are similar in the receptor-ECD sequences and their structural folding, this is not true for highly divergent ligands that are distinct in secondary structure and orientation to the receptor´s ECD. While CGRP (Josephs *et* al., 2021b; Liang *et* al., 2018) or adrenomedullin (Liang, Belousoff, Fletcher, *et* al., 2020c) are described as kinked helix, LA-PTH has a linear structure. This might be due to an artificially constructed sequence of LA-PTH ligand (Shimizu *et* al., 2016), which enabled structural studies. On the other hand, native PTH (and PThrP) are, as similar peptidic ligands, kinked. Predicted AlphaFold structures (**Figure 56**) and NMR structures (Austermann *et* al., 1995; Weidler *et* al., 1999, p. 1) support this premise.
2. The CGRP ligand's N-terminus is different from LA-PTH at the transmembrane receptor part, having a specific orientation of the CRLR-ECD and the length of extracellular loop 2 (EL2). This causes CGRP to be shifted towards TM1 and TM2 of the CRLR compared to the LA-PTH orientation in the PTH1R.

3. Comparing CGRP and PTH1R aa sequences indicated that crucial aas between the receptor ECD and RAMP2 RCD are also present in the N-terminal extracellular PTH1R sequence. That aa are Q45 and E54 in PTH1R (similar to Q54 in CRLR). This strongly suggested that RAMP2 ECD could also bind to the PTH1R ECD in a mode comparable to that observed for the CRLR-ECD/RAMP1 complex. Moreover, R162 in ECD was identified as the main aa involved in binding LA-PTH to PTH1R and CGRP to CRLR and is corresponding and identical to both receptors. This suggests a certain level of conservation in the ligand-binding mode.
4. Lastly, there is a clear distinction between aas, which contribute to either ligand or RAMP1 binding in CGRP/CR/RAMP1, later being present in PTH1R-ECD.

Thus, it was proposed that binding of the RAMP2 to the PTH1R-ECD could be feasible in a similar manner as observed for the CGRP/CR/RAMP1 complex. Proceeding from these premises, RAMP2 was structurally mapped to the active structure of the LA-PTH/PTH1R/Gs complex in two different ways.

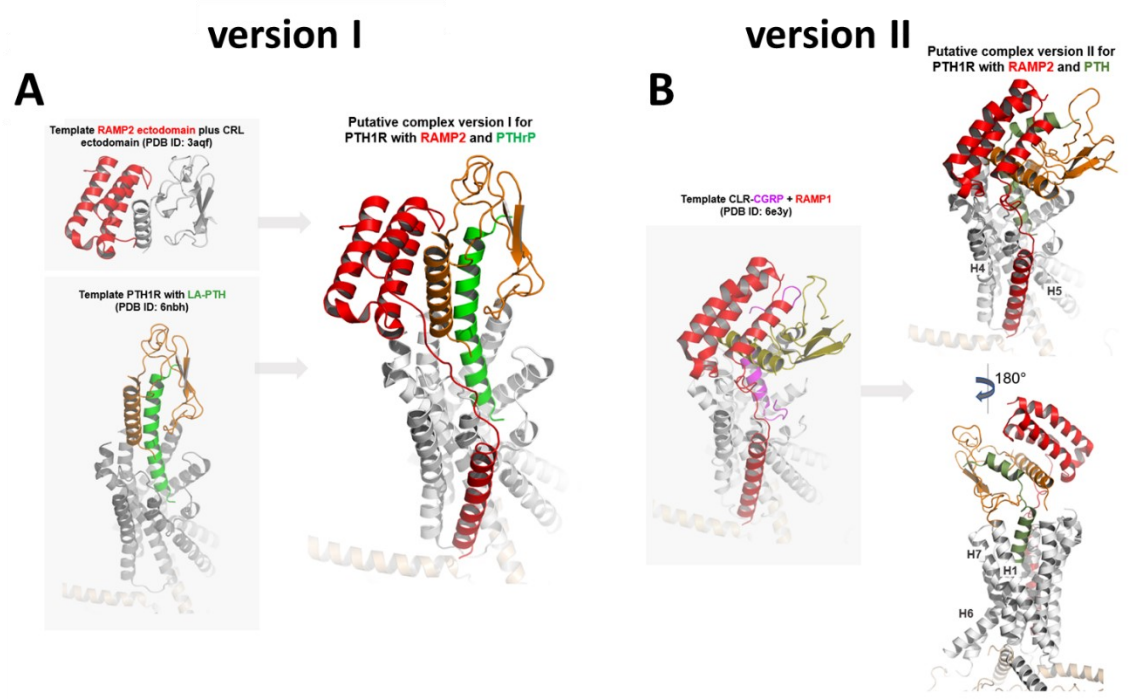

Figure 57: Modeled ligand/PTH1R/RAMP2/Gs complexes.

As indicated in the figure, structural templates were starting material to model putative ligand/PTH1R/RAMP2/Gs-complexes, resulting in two versions of possible arrangements. RAMP2 is depicted in red, PTH in green, and PTH1R in light grey.
(***A***) *In version I, the RAMP2 ECD is oriented toward the PTH1R. Still, the principle receptor ECD is adjusted according to the determined LA-PTH/PTH1R/Gs complex* (L.-H. Zhao *et* al., 2019)*, whereby the ligand forms a regular straight helix.*
(***B***) *In version II, CGRP/CRLR/RAMP1/Gs complex (Josephs et al., 2021b) was a structural template used to adjust the complex components relative to each other; the PTH1R ECD bound with RAMP2 ECD is differently oriented toward the TMD. In addition, the ligand (PTH) has a modified secondary structure in the central part compared to LA-PTH in the determined version I complex* (***A***).

The first version I (**Figure 57 A**) was constructed with RAMP2-ECD, bound to the PTH1R-ECD similar to the CGRP/CR/RAMP1 (Liang *et* al., 2018) complex, while the previously predicted PTH1R/LA-PTH structure stayed unaffected. The RAMP1 sequence was exchanged by the RAMP2 sequence, and the linker was connected to the

RAMP2 ECD already merged into the initial LA-PTH/PTH1R /RAMP2 model. The LA-PTH sequence was replaced by the PTH or the PTHrP sequences, resulting in two versions of the PTH1R/RAMP2/Gs complex with both ligands, PTH and PTHrP (shown is the version with PThrP).

The second version II (**Figure 57 B**) was produced with CGRP/CR/RAMP1 (Liang *et* al., 2018) complex as a template. The part of the PTH1R ECD with the LA-PTH C-terminus (L.-H. Zhao *et* al., 2019) (amino acids 22-34) part was superpositioned in the CGRP/CR/RAMP1 complex. RAMP1 was inserted from this complex into the PTH1R model and, after that, substituted with the RAMP2 sequence. Lastly, the extracellular C-terminus and the bound N-terminus of LA-PTH were connected. The ligand sequence was replaced by the PTH or the PTHrP sequences (shown is the version with PThrP).

Finally, version II (**Figure 57 B**) was identified as more suitable for predicting actual interaction positions. Besides a few predicted sites for PTH1R/RAMP2 interaction, it was observed that RAMP2 reshaped receptor conformation in the way that PTH1R ECD and TMD were making novel contacts. In this version, receptor ECD interacted with the EL3, possibly with EL1. Few new receptor ECD-ligand contacts were possible: K13 of PTH contacted D133 of the PTH1R. RAMP2 interacted extracellularly with the EL2 of the receptor but also intracellularly with the IL2, low part of receptor TM 3 and 4, a region associated with G protein binding (Ntt, N-terminal tail; Ctt, C-terminal tail).

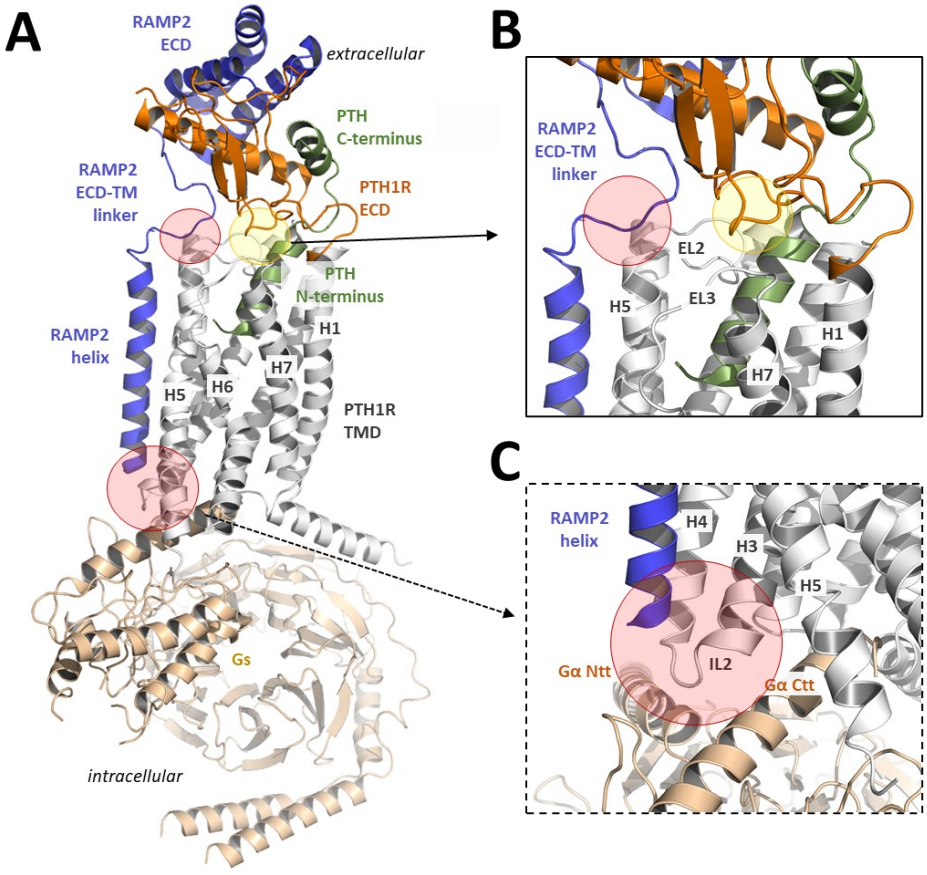

Figure 58: Putative RAMP2 binding mode in a PTH1R-PTH-Gs complex model.

(A) *A homology model of PTH/PTH1R/Gs/RAMP2 suggests several specific contacts between the components of this complex. RAMP2 is depicted in blue, PTH1R TMD in light grey, PTH1R ECD in orange, PTH in green, and Gs in beige.*

(B) *RAMP2 shall interact extracellularly with the EL2 of the receptor (**B**), but also intracellularly with the IL2 and adjacent transitions to receptor helices 3 and 4 (**C**) (red circles), a region that is associated with G protein binding (Ntt, N-terminal tail; Ctt, C-terminal tail). New intramolecular contacts from the PTH1R ECD to the TMD (yellow circle) are not present in the recent PTH1R structure **(L.-H. Zhao et al., 2019)** (PDB ID: 6NBH). In this version, the receptor ECD would interact directly with the EL3 and potentially with EL1. Moreover, several new receptor ECD-ligand contacts are possible, such as between K13 of PTH and D133 of PTH1R. Modeling was performed by dr. Gunnar Kleinau and dr. Patrick Sheerer (Charite - Universitätsmedizin Berlin).*

Interestingly, comparing both generated models, it is an apparent difference in the location of RAMP2 in the PTH1R structure: AlpaFold model yielded structure, where helix 8 is almost contacting RAMP2, which was not observed in structure homology versions. This was true for both complexes, either with PTH or PTHrP. It must be noted that AlphaFold model does not contain Gs protein and could therefore differ in specific structural insights. On the other hand, due to its nature, AlphaFold predicted the model from the accumulated structural knowledge available at that very moment can thus provide a probably more integrated view of the possible conformation of PTH1R with RAMP2. AlphaFold data is not curated by the structural specialist, and there was some skepticism about its ability to generate complexes. As of now, algorithms for AlphaFold-Multimer are constantly updated, and believed that accuracy of the prediction will only increase (Evans *et* al., 2022).

Present structural information suggests that RAMPs are in firm contact with interacting GPCRs – there are placed between TM3-5, contacting TM5 and adjacent ECL2 and the intracellular side of the receptors at TM3 and 4 (Booe *et* al., 2020; Josephs *et* al., 2021; Liang *et* al., 2018, 2020; Cao *et* al., 2022). Mentioned contacts are located near structural regions involved in the GPCR activation process.

Model variant II suggests that RAMP2 binding alters the structure of PTH1R to induce novel intramolecular interactions between ECD and TMD of the receptor, besides new contacts between ligand and receptor TMD. In comparison to the known PTH1R structure (L.-H. Zhao *et* al., 2019), model variant II differs in the ECD-TMD location of the receptor and ligand PTH. Ligand is in the kinked conformation, similar to CGRP or adrenomedullin in GPCR/RAMPs structures (Booe *et* al., 2020; Josephs *et* al., 2021b; Liang *et* al., 2018; Liang, Belousoff, Fletcher, *et* al., 2020c). Such PTH structure was already proposed by NMR studies (Austermann *et* al., 1995) and varies to the straight helix of LA-PTH in the PTH1R structure (L.-H. Zhao *et* al., 2019). RAMP2-linker interacts with receptor ECL2 and receptors ECD further contacts EL3, a bridge between TM6 and TM7, regions specifically dictating receptor activation, Gs activation, and β-arrestin binding. Thus, it is reasonable to conclude that RAMP2 binding induces novel receptor conformation. The mentioned change could be the origin of the observed acceleration of activation speed (**Chapter 4.6**) or differential binding of effector proteins (**Chapter 4.7, 4.8**). Model version II hints at how possible pre-activation or unique conformation of PTH1R might occur. Novel intra- and intermolecular contacts described above could cause pre-activation or stabilization of a unique conformation of the receptor. RAMPs stabilize the receptor structure in the case of calcitonin-like receptors (Garelja *et* al., 2020; Josephs *et* al., 2021b; Liang *et* al., 2018; Liang, Belousoff, Fletcher, *et* al., 2020c), which is feasible also for PTH1R. This unique conformation could stabilize some of the many conformational states, which would preferentially attract a particular downstream signaling partner over another. RAMP2-helix contacts IL2 and the adjacent junctions to TM3 and TM4 in the intracellular part of PTH1R – part, which governs G protein binding; thus, it might affect constitutive receptor activation. The short but functionally crucial, the intracellular part of RAMP is likewise known to control G protein activation (Udawela *et* al., 2006).

Regarding differential ligand effects observed in previous chapters, it needs to be noted that so far, there is no available full-length structure of PTHrP with PTH1R, which could help get a holistic view of the structure-activity-relation differences between PTH and PTHrP. The crystal structure of the ECD of PTH1R with PTHrP (Pioszak *et* al., 2009) is informative and suggests that PTHrP binds to the same ECD part of the receptor. In contrast to the straight PTH helix, the PTHrP is slightly bent and has unwound C-terminal. Aa L41 and I115 of receptor ECD are slightly shifted to accommodate PTHrP binding. The model version I (**Figure 57 A**) nicely grasped curved PThrP, which does not induce significant structural changes – and agrees with the hypothesis of relatively negligible effect observed in activation kinetics of PThrP on PTH1R/RAMP2 (**Chapter 4.6**). PThrP and PTH sequences are "only" 32% identical and are known to prefer different PTH1R conformations (Cheloha *et* al., 2015b), which translates to divergent functional and biological effects operated through PTH1R (Cheloha *et* al., 2015b). RAMP2 modulation could prompt another level of complexity for the roles of two endogenous ligands, PTH and PTHrP, which act through a single receptor.

In summary, these results establish a molecular model for a better understanding of how RAMP2 might shape the structural architecture of PTH1R with PTH and/or PTHrP. Moreover, those structural models could provide a template for designing specific therapeutics targeting PTH1R/RAMP2 complex.

4.10 Beyond PTH1R conformational biosensor

In this chapter, I am outlining two sets of the data, where I explored the ability of the newly created $PTH1R_{FRET}$ biosensor to report different conformations. First, the mutation was introduced to the biosensor, which induced constitutively active biosensor form $PTH1R_{FRET}$ H223R. Second, the conformational switch of $PTH1R_{FRET}$ was investigated in the absence of G proteins.

4.10.1 Switch of mutated receptor $PTH1R_{FRET}$ H223R

$PTH1R_{FRET}$ biosensor was able to detect differences in conformation induced by RAMP2, and it was of further interest to understand if introducing single point mutation would still preserve the functionality of the biosensor and ability to report conformational changes. Therefore, the conformationally sensitive site was mutated (**Figure 59 A**) – H223R, previously reported being the cause of constitutively active receptor phenotype, inducing ligand-independent activity (Schipani *et* al., 1995; Parfitt *et* al., 1996; Schipani *et* al., 1997). This position is beside two others: T410P and I458R (Schipani *et* al., 1999), activating mutation related to Jansen's Metaphyseal Chondrodysplasia (JMC), a rare disease associated with increased calcium concentration in our blood as a consequence of overactive PTH1R receptor. Notably, patients with JMC see a reduced or low normal concentrations of endogenously expressed and circulating PTH and PTHrP (Kruse & Schütz, 1993). However, those two hormones can still bind to the receptor with smaller efficacy and in the case of PTHrP also smaller potency. Loss of PTHrP-related role on PTH1R is prominently seen in JMC (Schipani *et* al., 1995). For instance, patients suffer from abnormal formation of endochondral bone. Currently incurable disease is still lacking adequate therapeutics, and a biosensor with mutation could help to identify and characterize prospective treatment for JMC. Therefore, mutated biosensor $PTH1R_{FRET}$ H223R was designed and characterized.

First, the biosensor was examined in FRET AB experiments (**Figure 59 B**). I could detect smaller FRET efficiency; from previously 15.06 % for the $PTH1R_{FRET}$ biosensor, mutation induced statistically significant fall to 12.83 %. This is in line with the proposed mutation´s effect toward active-like conformation. Previous studies showed that all three-mutation led to the difference in ICL3 conformation, a place which is sensitive for activation on one side and on another – where fluorophores in biosensor are attached. Mutation-imposed conformational change has presumably induced reposition or reorientation, and thus, distance and/or orientation between fluorophore changed. This was detected as smaller FRET efficiency.

Next, it was investigated if mutation exerted an effect on ligand-induced activation of the mutated biosensor. PTH- and PTHrP-stimulated FRET responses were measured in microtiter plates (**Figure 59 C, D, Table 31**). As expected, the amplitude of those responses was smaller for the cells expressing mutated biosensor. Not only PTH but also PTHrP stimulation led to the ~two times concentration-dependent decrease in the amplitude of the mutated biosensor $PTH1R_{FRET}$ H223R. Interestingly, PTH-induced responses were of similar, slightly left-shifted potency, whereas PTHrP-induced major right-shift for more than one log unit. First, this suggested that H223R mutation-imposed conformational dynamics represent different interface for their interacting ligands and highlight another level of complexity which might be seen in patients with JMC. It might be that observed left-shifted potency happens because of easier activation of H223R mutant (FRET AB data suggest that is a receptor in the basal state in more active-like conformation). Second, different potencies and efficacies for both ligands indicate that there might be ligand-specific conformations of $PTH1R_{FRET}$ H233R. Finally, it could be that mutation induces an almost

fully active PTHrP-induced state (and thus very little further activation is seen with this agonist), while being only partially active in the direction of the PTH-induced state.

Ligand-specific conformations of PTH1R for PTH and PTHrP were characterized previously (Hoare *et* al., 2001; Dean *et* al., 2006, 2008). R0 conformation is stable in the presence of GTPγS and is bound preferentially by PTH. Another conformation named RG, is sensitive to GTPγS addition and is bound preferentially by PTHrP. H233R mutation could change the natural preference of the PTH1R receptor toward those conformations.

Older control experiments showed that poorer surface expression of $PTH1R_{FRET}$ H223R is not a cause for the change in the amplitude since the mutated receptor showed only a slightly (~15%) reduced level of cell surface expression (Schihada, Shekhani, *et* al., 2021). This is not surprising for the constitutive active receptors, as internalization represents protection from the enhanced signaling. Nevertheless, two times reduction in the amplitude (**Figure 59 C, D, Table 31**) presumably does not arise only from the cell surface change and likely represents the ability of the $PTH1R_{FRET}$ H223R biosensor to pick up different, more active-like conformation.

This data argue that biosensor can report 1) mutation-induced conformation, and 2) different ligand-specific conformations.

Hence, I add the new tool to the panel of biosensors, which could be useful in design of novel therapeutics for JMC. Recently described negative allosteric modulator of PTH1R, Pitt12 (Sutkeviciute *et* al., 2021), is an example of a guide compound, which might be used for drug discovery of future compounds against that, currently incurable disease.

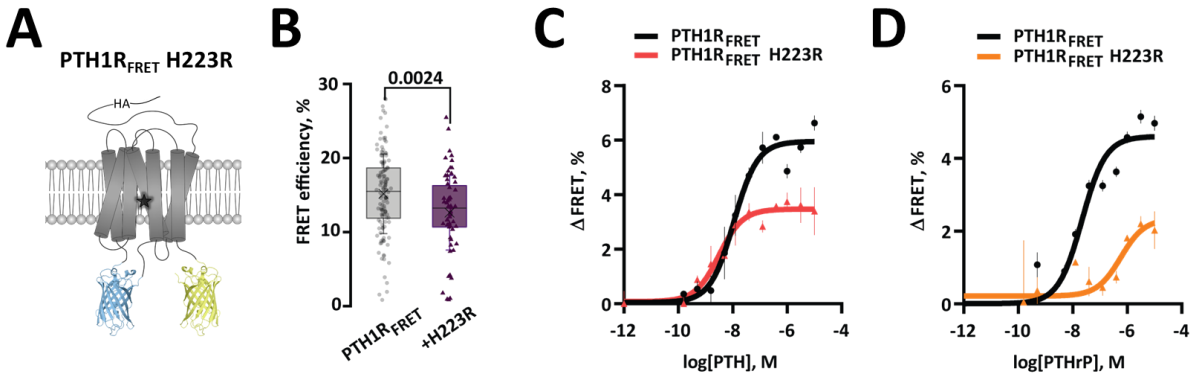

Figure 59: $PTH1R_{FRET}$ biosensor reports mutant-induced conformational change.

*(**A**) Schematic representation of intramolecular $PTH1R_{FRET}$ biosensor with constitutive activity causing H223R mutation. (**B**) FRET efficiencies from photobleaching experiments recorded with a confocal microscope. The data are expressed as % of a donor emission increase after photobleaching for each experimental group. A t-test was used to assess a significant difference between the groups ($p < 0.001$).*

*(**C, D**) The data were fitted with three response parameters fit to construct concentration-response curves. ΔFRET values are expressed as percent change from the initial FRET value. For further statistics and results, see **Table 31**.*

		$PTH1R_{FRET}$	$PTH1R_{FRET}$ H223R
BASAL	FRET efficiency, mean ± SEM, %	15.06 ± 0.45	12.83 ± 0.62
	N, cells (experimental days)	149 (6)	60 (2)
PTH	pEC_{50}, M	7.96 ± 0.12	8.51 ± 0.19
	Amplitude, %	5.91 ± 0.34	3.40 ± 0.33
	N, experimental days	2	2
PTHrP	pEC_{50}, M	7.66 ± 0.16	6.24 ± 0.42
	Amplitude, %, M	4.60 ± 0.33	2.12 ± 0.52
	N, experimental days	2	2

Table 31: Descriptive statistics for Figure 59.

4.10.2 $PTH1R_{FRET}$ switch in absence of G proteins

Although are GPCRs characterized by common structural architecture, they differ between the classes in key "microswitches" which control the receptor activation process (**Chapter 1.1.2**) (Hauser *et* al., 2021; Hilger *et* al., 2020; Kooistra *et* al., 2021) as well the final conformation of TM6 in the active state. The dynamic of receptor activation was widely described in the past, mostly employing crystallography, cryo-EM, NMR and single-molecule fluorescence techniques (Deupi & Kobilka, 2007; Dror *et* al., 2011; Manglik & Kruse, 2017; Rasmussen *et* al., 2007). It was believed that class A and class B GPCRs share common activation characteristics. In contrast, a recent analyses of a large amount of structural data are now discovering that the key switches between classes A and B differ and dictate different process (Hauser *et* al., 2021; Hilger *et* al., 2020; Kooistra *et* al., 2021). For example, fluorescence and double electron-electron resonance studies from Hilger *et* al. suggest that switching in GCGR, class B GPCRs requires a higher energy barrier and its TM6 fully moves only when G protein engages with the receptor.

To test the hypothesis if class B GPCRs truly require the presence of G proteins for TM6 to switch in active confromation, a ΔG protein knock-out cell line was employed. $PTH1R_{FRET}$ biosensor was used to monitor ligand-induced receptor activation in the presence or absence of heterotrimeric G proteins. Stimulation of cells expressing $PTH1R_{FRET}$ biosensor with increasing concentrations of PTH resulted in decreased FRET ratio in both experimental groups (**Figure 60 A**). The amplitudes of FRET responses were concentration-dependent (**Figure 60 B**) and slightly, but not significantly smaller in the presence of G proteins. Moreover, the affinity of the responses was somewhat higher when G proteins were cotransfected, as expected for imitating the scenario of high-affinity binding (Wehbi *et* al., 2013).

In summary, the switch of PTH1R also happened in the absence of G proteins, which was against initial hypothesis of Hilger *et* al. – or it might be specifically the case for PTH1R and not for GCGR. The difference in the amplitude could mean that it still comes to "kink" for a certain population of the receptors; however, in the presence of G

proteins, the majority of the population makes a move towards fully active conformation. It could also mean that the receptor switches anyway, but its conformations are still switching, and G proteins help to stabilize the final state. The molecular basis of this state, previously noted as high affinity state, was recently described by Warne *et* al. (Warne *et* al., 2019). Group described a smaller orthosteric binding pocket, shorter hydrogen bonds, and up to 30% of increase in atomic contacts between ligand and receptor – an increased number of connections makes sticks ligand better to the receptor. Such tighter bonds would stabilize the final state of TM6, which would mean that a higher population of receptors stays in it. Moreover, for glucagon receptor it was observed that TM6 sustained in the active state even after Gs detachment. This might be one of the reasons for prolonged, persistent cAMP signaling, described for certain class B receptor (Ferrandon *et* al., 2009; Dror *et* al., 2011; Thomsen *et* al., 2016; Manglik & Kruse, 2017).

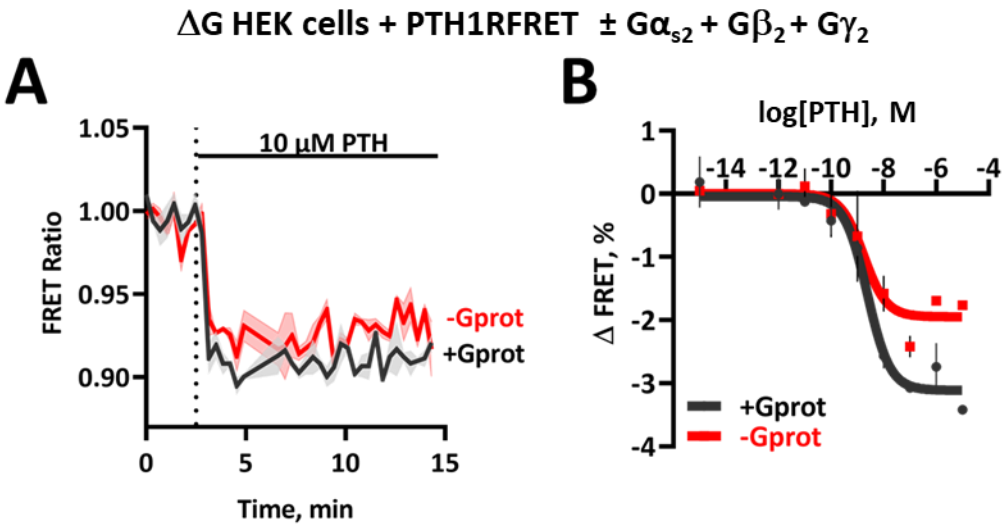

Figure 60: PTH1R$_{FRET}$ is able to switch in the absence of G proteins.

*(**A**) Average time course of PTH-induced FRET changes recorded in plate reader from ΔG protein HEK cells transiently expressing PTH1R$_{FRET}$ (black) alone or together with trimeric G proteins ($G_{\alpha s2}$ + $G_{\beta 2}$ + $G_{\delta 2}$) (red). The data are an average of two independent experiments normalized to the initial FRET value (set to 1).*

*(**B**) Concentration-response curves obtained from traces as in (**A**). ΔFRET values are expressed as percent change from the initial FRET value. Curve fitting gave pEC$_{50}$ values (mean ± SEM, M) of: PTH1R$_{FRET}$ = 8.62 ± 0.15 and PTH1R$_{FRET}$ + G proteins = 8.76 ± 0.29. Top of the curve (mean ± SEM, %): PTH1R$_{FRET}$ = 3.11 ± 0.14 and PTH1R$_{FRET}$ + G proteins = 1.95 ± 0.17. The top of the curve is statistical different (p<0.0001). The difference was tested with extra sum-of square F test.*

4.11 Multiplexed detection of PTH1R signaling

To probe if it is possible to detect real-time PTH1R signaling wave of GPCR as well intracellular effector, two parameters imaging setup was established. For this experiment, the $PTH1R_{cpGFP}$ biosensor was coexpressed with R-Flinc A, a red single-fluorophore-based biosensor, capable of detecting cAMP signaling with low affinity (Kd = 0.3 µM) and excellent dynamic range (Ohta *et* al., 2018). **Figure 61** shows two single fluorophore-based biosensors which allowed multi-channel/function imaging of the PTH1R signaling cascade. HEK293 cells were grown at 32°C (Harada *et* al., 2017) and imaged at the wide-field microscope, using GFP/RFP emission filter to simultaneously detect the intensities of both observed channels in intact cells. Imaging successfully detected PTH1R signaling wave, originating at the cell surface with activation of $PTH1R_{cpGFP}$ and thereafter leading to cAMP accumulation, observed by R-Flinc A biosensor (**Figure 61 D**). cAMP accumulation started with a ~10 s delay after stimulation, which is expected (Vilardaga *et* al., 2012), and accounted for the time of G protein activation, dissociation from the receptor, and following activation of adenylyl cyclases. The addition of saturating concentrations of 10 µM Fsk + 100 µM IBMX caused saturation of the signal.

Although the concentration (1 µM PTH) used in those experiments should produce saturating amounts of cAMP (**Figure 45**), it lacks full signal, probably due to the reduced signaling capacity of $PTH1R_{cpGFP}$ (**Figure 32 A**). Therefore, it might be useful to cotransfect $PTH1R_{wt}$ in such experiments and enhance signal-to-noise to detect the accurate kinetic and full signal detection. The experimental setup is still in its infancy and could get a few practical upgrades.

In summary, it is feasible to access the PTH-stimulated signaling cascade using the multiplexed imaging with $PTH1R_{cpGFP}$ and R-Flinc A. Furthermore, since detection is made with GFP/RFP filters, which are often present in microscopic laboratories, such an approach can be generally used and help to pave the way for the ultimate elucidation of GPCR cascade dynamics.

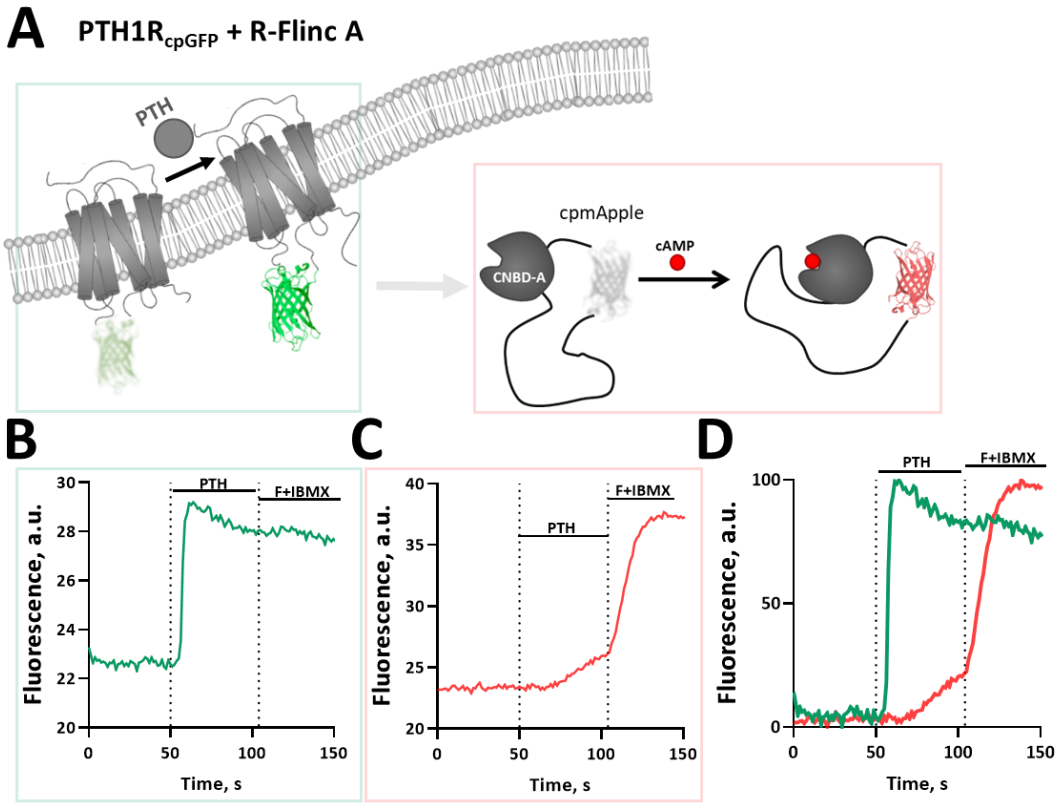

Figure 61: Multiplexing of PTH1R$_{cpGFP}$ and R-Flinc A biosensor for simultaneous detection of PTH-stimulate signaling pathway.

*(**A**) HEK293 were cotransfected with PTH1R$_{cpGFP}$ and R-Flinc A, single fluorophore biosensor for detection of cAMP accumulation. Schematics represent activation of signaling cascade which starts with activation of receptor in the presence of PTH and continues in cell interior (with few intermediate steps) till binding of cAMP into the cAMP-binding motif of PKA regulatory subunit Iα (CNBD-A), which is fused to cpmApple fluorophore.*

*(**B**) Representative fluorescence time courses of PTH-mediated changes, recorded in a microscopic FRET setup in single HEK293 cells transiently coexpressing PTH1Rcp$_{GFP}$ and R-Flinc A. Horizontal lines indicate application of 1 µM PTH and 10 µM Forsokolin/100 µM IBMX with a rapid superfusion system. Fluorescence was simultaneously recorded at (**B**) and (**C**) using GFP/RFP emission filter.*

*(**D**) Time courses from (B) and (C) were normalized to 0 and 100 and represent two-parameters real-time transduction of the signal from receptor activation to cAMP accumulation. The data are representative for n = 9 cells from two independent experimental days.*

4.12 Expanding repertoire of conformational biosensors for class B GPCRs

To probe the transferability of recently described FRET and BRET conformational biosensors for class A GPCRs (Schihada, 2018; Schihada *et* al., 2018, 2020), and enlarge the toolbox of available conformational biosensors for class B GPCRs, physiology-relevant secretin-like CTR, CRLR, and PTH2R were selected as the new test receptors. FRET and BRET versions of them were generated, following the previously described biosensor design:

1) FRET biosensors were based on $PTH1R_{FRET}$ design: in 3rd ICL mTurquoise2 was inserted, and mCitrine was fused to the C-terminus;
2) BRET biosensors were based on $PTH1R_{Nlc/Halo}$ design: in 3rd ICL HaloTag® was inserted, and NanoLuc was added to the truncated C-terminus.

Since none of the stated receptors had available biosensor precedent, were available receptor sequences aligned with earlier successfully designed biosensors, and similar insertion places in 3rd ICL and on the C-terminus were selected. Selected insertion sites are stated in **Table 32**. For PTH2R two BRET variants a and b were created, of which variant a showed improved performance in this same insertion site was used for transferring design to $PTH2R_{FRET}$ biosensor.

FRET variants	Acceptor: mCitrine	Donor: mTurquosie2	BRET variant	Acceptor: HaloTag	Donor: NanoLuc
Position	C-terminal	3rd ICL	**Position**	3rd ICL	C-terminal
$PTH1R_{FRET}$	After Gly497	Gly395-Arg396	**$PTH1R_{Nluc/HaloTag}$** (Schihada et al., 2018)	After Gly497	Gly395-Arg396
$PTH2R_{FRET}$	After Val451	Val350-Gly351	**$PTH2Ra_{BRET}$** **$PTH2Rb_{BRET}$**	After Val451	a: Val350-Gly351 b: His348-Asn349
$CRLR_{FRET}$	After Thr422	Ser328-Asn329	**$CRLR_{BRET}$**	After Thr422	Ser328-Asn329
CTR_{FRET}	After Ala429	Ser335-His336	**CTR_{BRET}**	After Ala429	Ser335-His336

Table 32: Insertion sites for donors and acceptors in FRET and BRET biosensors.

4.12.1 Generation of the PTH2R, CRLR and CTR FRET biosensors

PTH2R, CRLR, and CTR FRET biosensors were transiently transfected into HEK293 cells and visualized by fluorescence microscopy. All biosensors achieved excellent transfection efficiency when used in HEK293 cells (**Figure 62**).

Cells expressing biosensors were seeded for the experiments in microtiter plates, and first emission spectra were acquired. Cells were excited at 420/20 nm, and emission spectra were generated, which peaked at expected 474 nm and 529 nm (**Figure 63**), similar to the described for $PTH1R_{FRET}$ biosensor in **Chapter 4.3.1** (also mTurquoise2- and mCitrine-based sensor). This confirms the successful incorporation of fluorophores, which are presumably located at the FRET distance of 3-6 nm (Zacharias *et* al., 2002) and, thus, the generation of FRET-able biosensors for PTH2R, CRLR, and CTR.

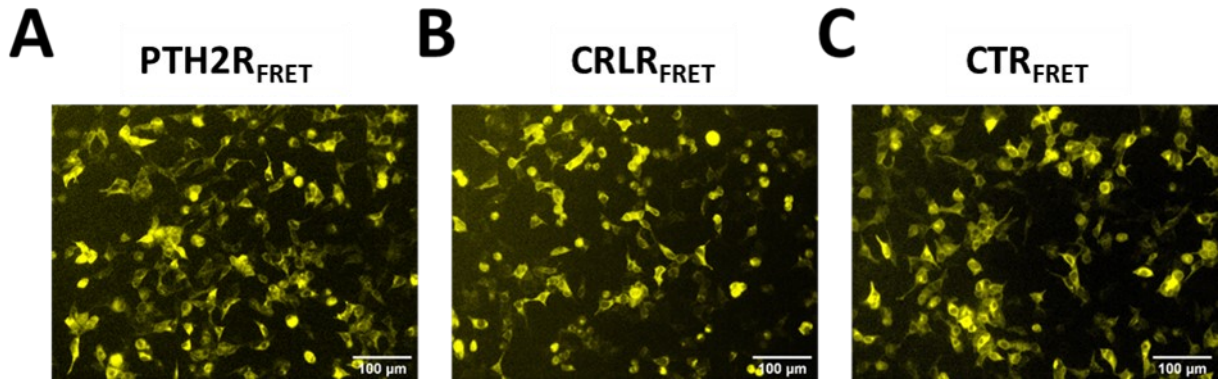

Figure 62: Expression of FRET biosensors in HEK293 cells.
*Fluorescence photo of HEK293 cells, transiently expressing (**A**) PTH2R$_{FRET}$, (**B**) CRLR$_{FRET}$, and (**C**) CTR$_{FRET}$. Scale bar = 100 µm.*

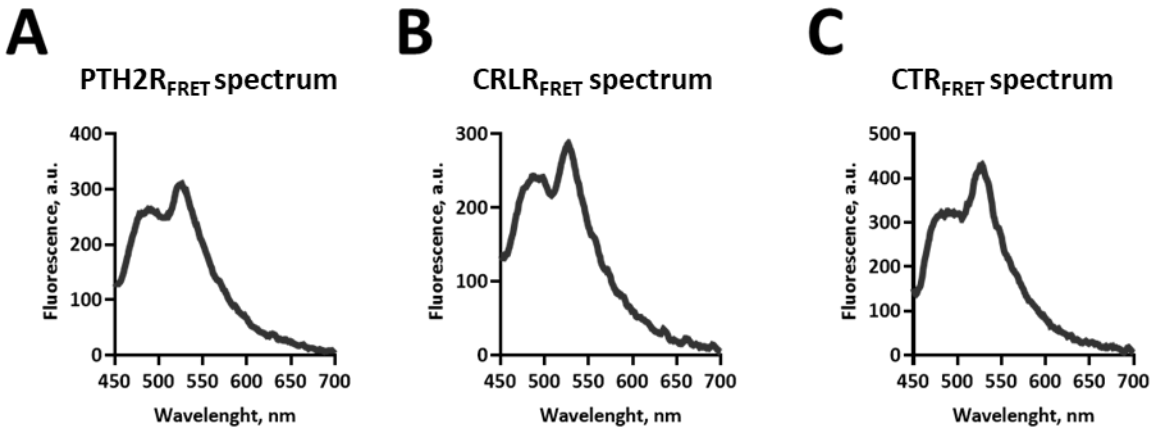

Figure 63: Spectra of FRET biosensors in HEK293 cells.
*Fluorescence emission spectra of HEK293 cells, transiently expressing (**A**) PTH2R$_{FRET}$, (**B**) CRLR$_{FRET}$, and (**C**) CTR$_{FRET}$.*
Cells were excited at 420/20 nm, and emission intensities were recorded with a monochromator-based plate reader with 1 nm resolution from 450-700 nm.

Second, ΔFRET responses were measured with serial dilutions of their cognate endogenous agonist. All biosensors exhibited concentration-dependent responses, which could be monitored in microtiter plates. Surprisingly, PTH2R$_{FRET}$ (**Figure 64 A**) induced higher amplitudes at smaller concentrations, which could be an indication of unspecific FRET changes upon ligand-induced activation. The nature of that signal remains to be elucidated. Ligand stimulation of the CRLR$_{FRET}$ biosensor (**Figure 64 B**) induced a modest amplitude change; 1.54 ± 0.60 %, which was concentration-dependent and in accordance with expected potency of α-CGRP at this receptor (Hay *et* al., 2021). Stimulation of CT$_{FRET}$ with h-CT caused a maximal amplitude of 3.22 ± 0.61 % (**Figure 64 C**). Stimulated responses were concentration dependent and resulted in ~two logs higher potency value as expected for h-CT at CTR$_{wt}$ (D. Hay *et* al., 2021). It could be predicted that the insertion of fluorescent tags caused a conformational destabilization of

the receptor. Through that, rearrangement of the binding pocket is feasible, which could result in a change in the potency of the tested ligand.
In summary, the creation of novel FRET biosensors yielded at least two novel successful reporters that might be further developed for studies of receptor activation of CTR and CRLR receptors.

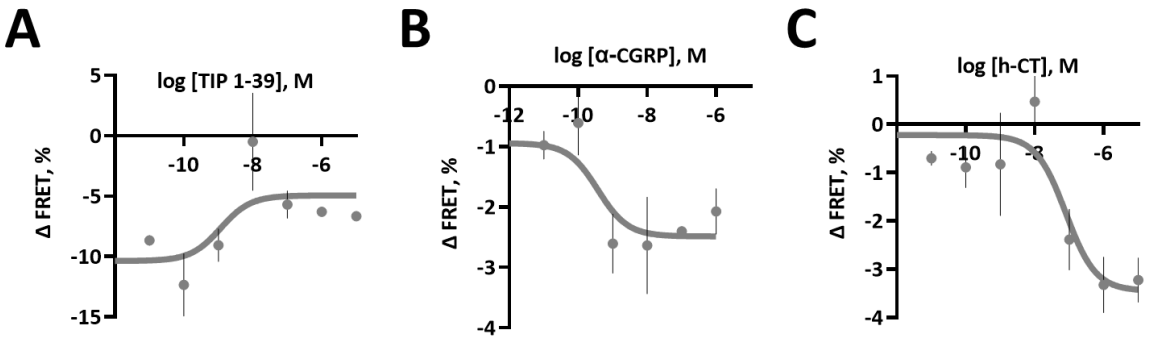

Figure 64: Concentration-response curves of FRET biosensors in HEK293 cells.
*HEK293 cells, transiently expressing (**A**) $PTH2R_{FRET}$, (**B**) $CRLR_{FRET}$, and (**C**) CTR_{FRET} were seeded in black 96-well plates, and ΔFRET responses were measured after stimulation with serial dilutions of their cognate agonists.*
Representative concentration-response curves for TIP (1-39) stimulation at $PTH2_{RFRET}$ (A), α-CGRP stimulation at $CRLR_{FRET}$ (B), and h-CT stimulation at CTR_{FRET} (C). Points were fitted with a three-parameters fit, curve fitting resulted in pEC_{50} (mean ± SEM) of two independent transfections: $PTH2R_{FRET}$ = 8.94 ± 0.87, $CRLR_{FRET}$ = 9.43 ± 0.43, CTR_{FRET} = 7.10 ± 0.41.

4.12.2 Generation of the PTH2R BRET biosensor

For the generation of the PTH2R BRET biosensors, the insertion sites for donor and acceptor were selected as described in **Chapter 4.3.1.** Briefly, the two BRET biosensor variants were constructed by inserting donor NanoLuc to the 3rd ICL either between Val350-Gly351 (variant a) or His348-Asn349 (variant b) (**Table 32**). BRET acceptor HaloTag was inserted after Val451. HEK293 cells were transfected with both biosensor variants, and spectra in basal state were recorded (**Figure 65 B**). Spectra of furimazine-treated NanoLuc resulted in an expected emission maximum at 450 nm, and when cells were labeled additionally with HaloTag® NanoBRET™618 Ligand, additional acceptor emission peak at 620 nm and decreased donor peak were measured. That indicated evident energy transfer (**Figure 65 B**) between fluorophores in both biosensor variants. Variant a resulted in a higher amount of energy transfer between activated NanoLuc and labeled HaloTag, and since it was performing better, it was selected for further experiments. When HEK293 cells were visualized under the microscope and labeled HaloTag with cell-permeant TMR ligand, successful $PTH2Ra_{BRET}$ expression in the cells could be observed (**Figure 65 C**). Subsequently, a stable cell line of the $PTH2Ra_{BRET}$ was created and used for experiments in microtiter plates. Stimulation of these cells with serial dilutions of the endogenous PTH2R agonist Tuberoinfundibular peptide (TIP) provoked a ligand-specific, concentration-dependent decrease in BRET ratio and consequently ΔBRET (**Figure 65 D, E**), as in similar GPCR biosensors (Vilardaga *et* al., 2003a; Schihada *et* al., 2018). Moreover, PTH, noted as full agonist of PTH2R induced similar but slower and partial decrease in BRET – different efficacy of this ligand was detected. So it might be that PTH actually exerts partial agonistic properties on PTH2R. In the recent cryo-EM structure of PTH2R, Wang *et* al. described the mechanism of specificity difference between TIP and PTH on PTH2R.

The critical residue of the interacting peptide makes decisive hydrophobic interactions with the PTH2R receptor core. Hydrophobic interaction with the aromatic Phe10P of TIP39 is stronger than the interactions with the smaller hydrophobic side chains of corresponding residues at PTH (Met8P), which could contribute to the different pharmacological profile of those two ligands (X. Wang *et* al., 2021).

To rule out any unspecific BRET changes, different peptide ligand CXCL12 was tested on PTH2Ra_{BRET} biosensor, and confirmed no significant change in BRET, when PTH2R_{BRET}-expressing cells were stimulated with the mentioned ligand. In fact, caused change was superimposed to another control – stimulation with buffer (**Figure 65 D**). From time courses at different concentrations of ligands, concentration-response curves were constructed, and EC_{50} values were calculated, indicating reduced potency of PTH2R biosensor (**Figure 65 E**) compared to currently available values of affinity from ratio ligand biding experiments (Bisello *et* al., 2021). Nevertheless, since PTH2Ra_{BRET} biosensors showed successful expression, satisfying amount of BRET energy transfer, and concentration-dependence by stimulation with agonist, it was evaluated as a successful example of a transferability of BRET conformational biosensors design to a new receptor. Reporting on different efficacies and potencies of two agonists, could be further used to explore pharmacological characteristics of this understudied receptor. This PTH2R biosensor seems to be better suitable for such studies than in the earlier chapter described FRET version of the biosensor.

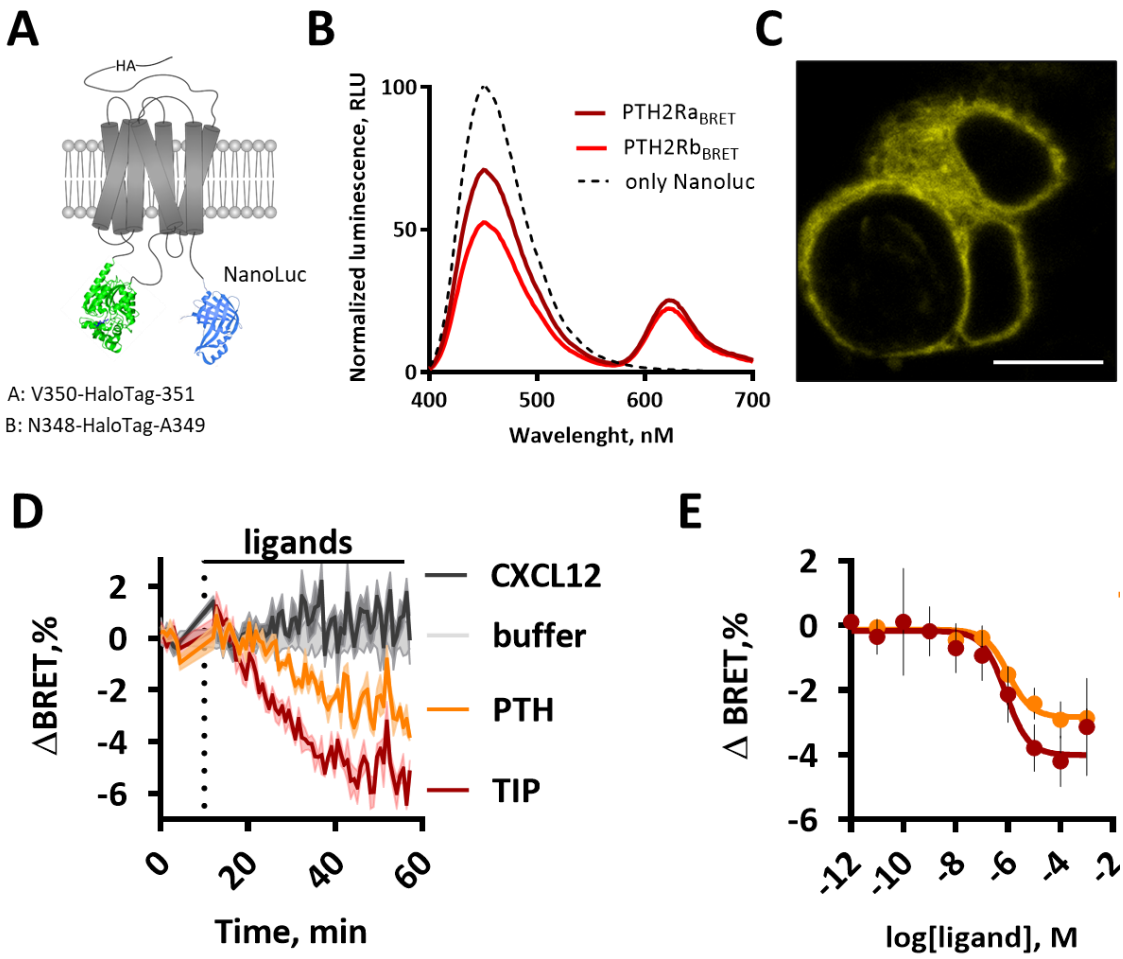

Figure 65: Design and characterization of conformational biosensor for PTH2R - PTH2R$_{BRET}$.

*(**A**) PTH2R receptor biosensor (PTH2RBRET) was created based on PTH1R$_{Nluc/Halo618}$. HaloTag unit was inserted into two different sites of the 3rd ICL, and NanoLuc was fused to its C-terminal. As a result, two variants, A and B, were created.*

*(**B**) Luminescence emission spectra of two biosensor variants and biosensor, labeled only with donor.*

*(**C**) Confocal photo of corresponding biosensors variant PTH2Ra$_{BRET}$, transiently expressed in HEK293 cells. HaloTag was labeled with intracellular HaloTag ® ligand TMR. Scale bar = 50 µm.*

*(**D**) Time courses of PTH2Ra$_{BRET}$ transfected cells with the following ligands: 1 µM CXCL12, 100 µM PTH(1-34), 10 µM TIP(1-39).*

*(**E**) Concentration curses from traces as in (**D**). Curves were fitted with a three-parameters fit, which resulted in pEC$_{50}$ ± SEM (M) values: PTH: 6.10 ± 0.38 and TIP: 6.00 ± 0.19.*

4.13 Exploring novel GPCR-RAMP interactions

Since the initial identification of the first GPCR-RAMP interaction in 1997 (McLatchie *et* al., 1998) and the expansion of further interaction partners to nearly all class B1 receptors in early 2000, have current years experienced a additional wave of novel RAMP interactors. Recently, Caron (Lenhart et al., 2013b; Mackie et al., 2019), Ladds (Mackie et al., 2019; Harris et al., 2021b; S. Bailey et al., 2019; Weston et al., 2015), Sakmar (Barbash et al., 2017, 2019; Lorenzen et al., 2019), and other groups (Wootten et al., 2013; Shao et al., 2021; McGlone et al., 2021; Meyrath et al., 2021) expanded the list of interacting GPCRs beyond class B by using a multiplexed suspension bead array (SBA), BRET saturation methods, or functional assays. In parallel, bioinformatics-based studies (Benítez-Páez & Cárdenas-Brito, 2008; Topaz *et* al., 2017; Barbash *et* al., 2017, 2019) evaluating genomic- and expression-based observations established the global role of RAMPs in GPCR interactome. As part of this, bioinformatics tools were generated to explore GPCR-RAMP interactions, for example, a database (Topaz *et* al., 2017) available at http://rampdb.biology.gatech.edu/.

Inspired by the many recent reports of novel GPCR-RAMP interactions and the universal role of RAMPs in GPCRs´ signaling, and on the other side, having available tools at hand to interrogate PPI interaction, it was set to evaluate available bioinformatics data (Barbash *et* al., 2017), and prepare a method to test further GPCRs for the interaction with RAMPs.

A supplementary dataset (Barbash *et* al., 2017) was downloaded. First, class B of GPCRs was evaluated and visualized (**Figure 66**) to compare proteins on three entities - % of shared species, phylogenetic correlation coefficient, and coexpression correlation coefficient. The generated heat maps represent a quantified measure of each comparing entity (**Figure 66 A-C**).

The first entity of comparison, % of shared species, reflects the number of orthologous genes across the species and presents the most general estimate of coevolution as it shows the direction of a gene pair to coevolve. A higher coefficient should indicate higher interaction, relying on the prediction that interacting proteins would coexist in genomes of more species (Pazos *et* al., 2005). **Figure 66 A** shows % of shared species across class B GPCRs, and by first observation, it can be seen that VIPR1 and VIPR2 receptors don´t share orthologues across many species, whereas, for example, PTH1R and RAMP3 as well GHRHR and RAMP1, 3 do. Interestingly, stimulation of PTH1R was shown to induce higher expression of RAMP3 (Phelps *et* al., 2005), although its main interactor is not RAMP3 but RAMP2 (Christopoulos *et* al., 2003) (this work). Interestingly, also reverse trend can be observed – the main interactor of GIPR is RAMP3 (Harris *et* al., 2021b). However, shared species show a higher % of orthologues for RAMP2.

The phylogenetic correlation coefficient indicates if pairs of analyzed proteins have coevolved and have spread through generations together (Pazos *et* al., 2005). This suggests shared functions that were important for the organism. Besides shared function, those proteins would also have related phylogenetic changes – mutation and alteration would be happening simultaneously because of evolution pressure to evolve together. Surprisingly, comparing phylogenetic correlation coefficients, VIPR1 and RAMPs indicate to be important interaction partners – also confirmed in the past studies (Christopoulos *et* al., 2003; Wootten *et* al., 2013).

Another important observed feature of this analysis is that RAMP1 and RAMP3 have related, higher correlation coefficients with interacting GPCRs, unlike RAMP2, which mainly shows smaller coefficients. Although not to such

an extent, a similar trend is visible for % of shared species (**Figure 66 A**). This observation might be explained by its sequence and structural similarity - RAMP1 and RAMP3 are more similar than RAMP2 and, consequently, interact with a matching set of proteins. It might also give a thought that although they went through a very similar evolution procedure, both might not be needed – it could be that RAMP1 -3 are redundant, and one could execute the job for another. This seems to be different for the remaining isoform of the family - RAMP2, which was shown to play a crucial role in embryonal development, as its knockout in mice causes the death of an embryo (Kadmiel *et* al., 2011a, 2012; Kechele *et* al., 2016). CALCRL (CRLR) (McLatchie *et* al., 1998), cadherin EGF LAG seven-pass G-type receptor 1 (CELSR1), and secretin receptor (SCTR) (Shao *et* al., 2021) show equivalent phylogenetic correlation coefficients with all three RAMPs. CELSR1 interaction with RAMPs was still not explored, although it plays a vital role in embryonic development, similar to RAMPs (Kadmiel *et* al., 2011a, 2011b, 2012). Considering the essentiality of all three RAMPs with CALCRL (CRLR) to construct functional CGRP, AM1, and AM2 receptors, it could be assumed that CELSR1 and SCTR would also form important heterooligomers.

It must be noted that both mentioned entities of comparison account for proteins being direct or indirect interaction partners – there might also be part of the more extensive protein complex executing specific functions.

The third entity of comparison, the coexpression correlation coefficient (**Figure 66 C**), represents the measure of coexpression networks (Butte *et* al., 2000), relevant since coexpressed genes constitute the same pathway, protein complex, or are under the shared transcriptional regulatory program, which accounts for functional connection. The coexpression correlation coefficient suggests that RAMP2 and RAMP3 are coexpressed with proteins at a similar level (**Figure 66 C**), distinct from RAMP1-interacting proteins. The highest coefficient was detected for obligate interactor CALCRL and previously mentioned CELSR1. A very high coefficient was also shown for VIPR2 with RAMP1; interestingly, some studies did not identify the interaction between those two partners (Lorenzen *et* al., 2019).

Barbash *et* al. (Barbash *et* al., 2017) analyzed coexpression patterns throughout the whole GPCR-RAMP interactome. They were compared to random coexpressed proteins (this negative control was shown to be around 0) and receptor−ligand and receptor complex gene pairs (positive controls around correlation coefficient 0.3). The heat map in **Figure 66 C** shows that class B GPCRs reach coefficients of 0.5. Also, global analysis (Barbash *et* al., 2017) revealed that GPCR−RAMP pairs showed a higher correlation coefficient than expected by chance, positioned between mentioned positive and negative controls.

Evaluating class B GPCR with all three analyses shows that neither of the used parameters can unambiguously predict the interaction between GPCRs and RAMPs. For some protein pairs, bioinformatics parameters contradict experimentally-argumented studies from the literature as described before. Once more is shown that dry-lab bioinformatics needs wet-lab experiments to confirm their hypothesis. Nevertheless, a holistic analysis review can provide valuable clues to identify potential partners but should not be used as an isolated methodology to give claims on functional interactors.

Similarly, class C GPCRs were also analyzed for their potential interactions with RAMP1, RAMP2, and RAMP3 (**Figure 67**). In this class, CaSR (Bouschet *et* al., 2005) was the only GPCR known so far to interact with RAMPs. Evaluating heat maps, CaSR seems to be expressed in many shared species with RAMP3 and less so with RAMP1 and RAMP2 (**Figure 67 A**). All three RAMP isoforms are highly phylogenetically connected (**Figure 67 B**), but it seems that they are not abundantly coexpressed together, rated by the coexpression correlation coefficient (**Figure 67 C**). Also, in class C, specific patterns are observed: 1) Phylogenetic correlation coefficient is higher and akin for RAMP1 and

RAMP3-potential interactors, and 2) coexpression correlation coefficients are more alike for RAMP2 and RAMP3 interactors. First would suggest that RAMP1 and RAMP3 coevolved with similar GPCRs but differently from RAMP2, which was also the conclusion from the Barbash *et* al. global analysis of GPCR-RAMP interactome (Barbash *et* al., 2017). The second could suggest that the coexpression network includes either RAMP1 or RAMP2 and RAMP3.

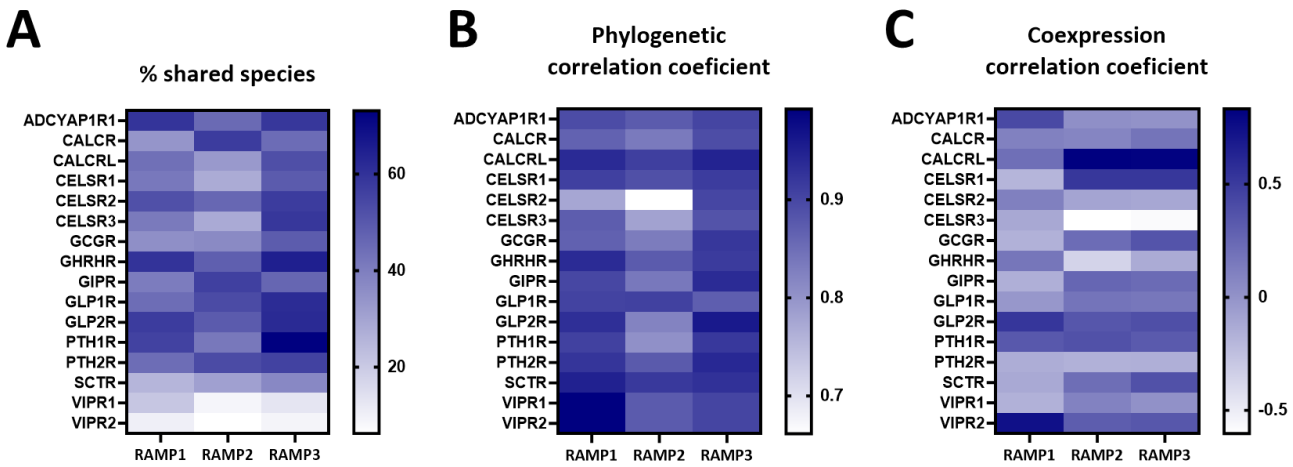

Figure 66: Evaluation of potential RAMP interactors between class B GPCRs.

(***A – C***) *Heat maps of the class B GPCRs for % of shared species* (***A***)*, coexpression analysis, phylogenetic correlation coefficient* (***B***)*, coexpression correlation coefficient* (***C***)*. Cell range from blue (max rank in each category) to white (minimal rank). Receptor gene symbols as reported in GPCRDB.*

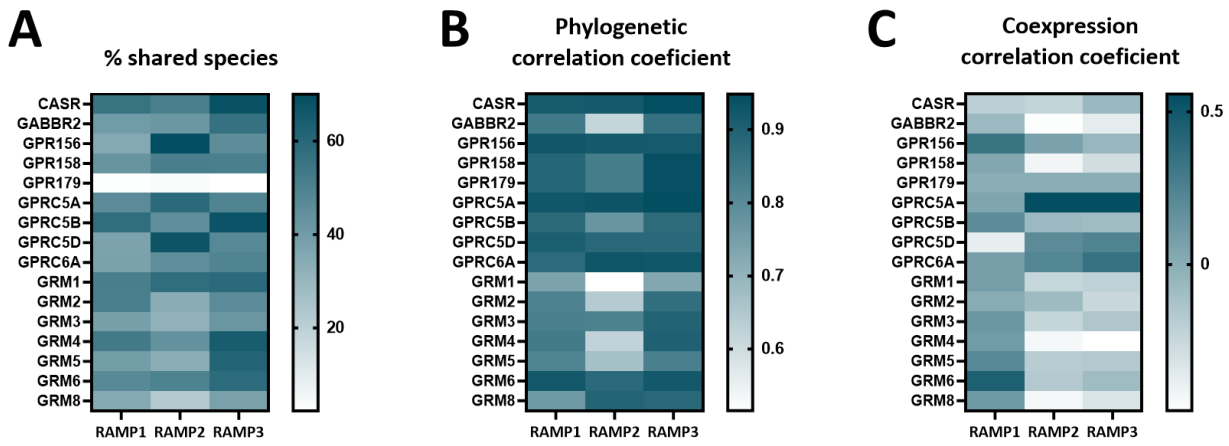

Figure 67: Evaluation of potential RAMP interactors between class C GPCRs.

(***A – C***) *Heat maps of the class C GPCRs for % of shared species* (***A***)*, coexpression analysis, phylogenetic correlation coefficient* (***B***)*, coexpression correlation coefficient* (***C***)*. Cell range from teal (max rank in each category) to white (minimal rank). Receptors are rearranged in alphabetic order. Receptor gene symbols as reported in GPCRDB.*

The current understanding of RAMPs-GPCRs modulation suggests that pairs of proteins need to be expressed together for a functional modulation to happen. They are probably physically connected (at least transiently) and also propose structural studies (Garelja *et* al., 2020; Liang *et* al., 2018; Liang, Belousoff, Fletcher, *et* al., 2020c).
Accounting for this knowledge, it was set to explore further potential GPCRs in class A, F, and Taste receptors assessing only the coexpression correlation coefficient. This analysis will still return GPCR as a potential interactor for allosteric modulation or indirect interactions (*e.g.*, if pairs are part of the more extensive complex as for example receptor signalosomes (Nguyen *et* al., 2019; Sutkeviciute & Vilardaga, 2020)).
The selected coexpression correlation coefficient was analyzed and visualized for all provided GPCRs from the supplementary data set (Barbash *et* al., 2017). GPCR−RAMP pairs were eliminated, where all RAMPs that showed a correlation coefficient equal to or less than zero were eliminated before the analysis and visualization.
Again, the previously described trend is visible across analyzed and visualized protein pairs, indicating that RAMP2 and RAMP3 coexpressed with similar GPCRs, differently from RAMP1. This is true throughout all studied classes. For example, HTR1F is highly coexpressed with RAMP2 and RAMP3 and HTR1E with RAMP1. In addition, subtypes of the same receptor are often coexpressed with either RAMP2 and RAMP3 or RAMP1.

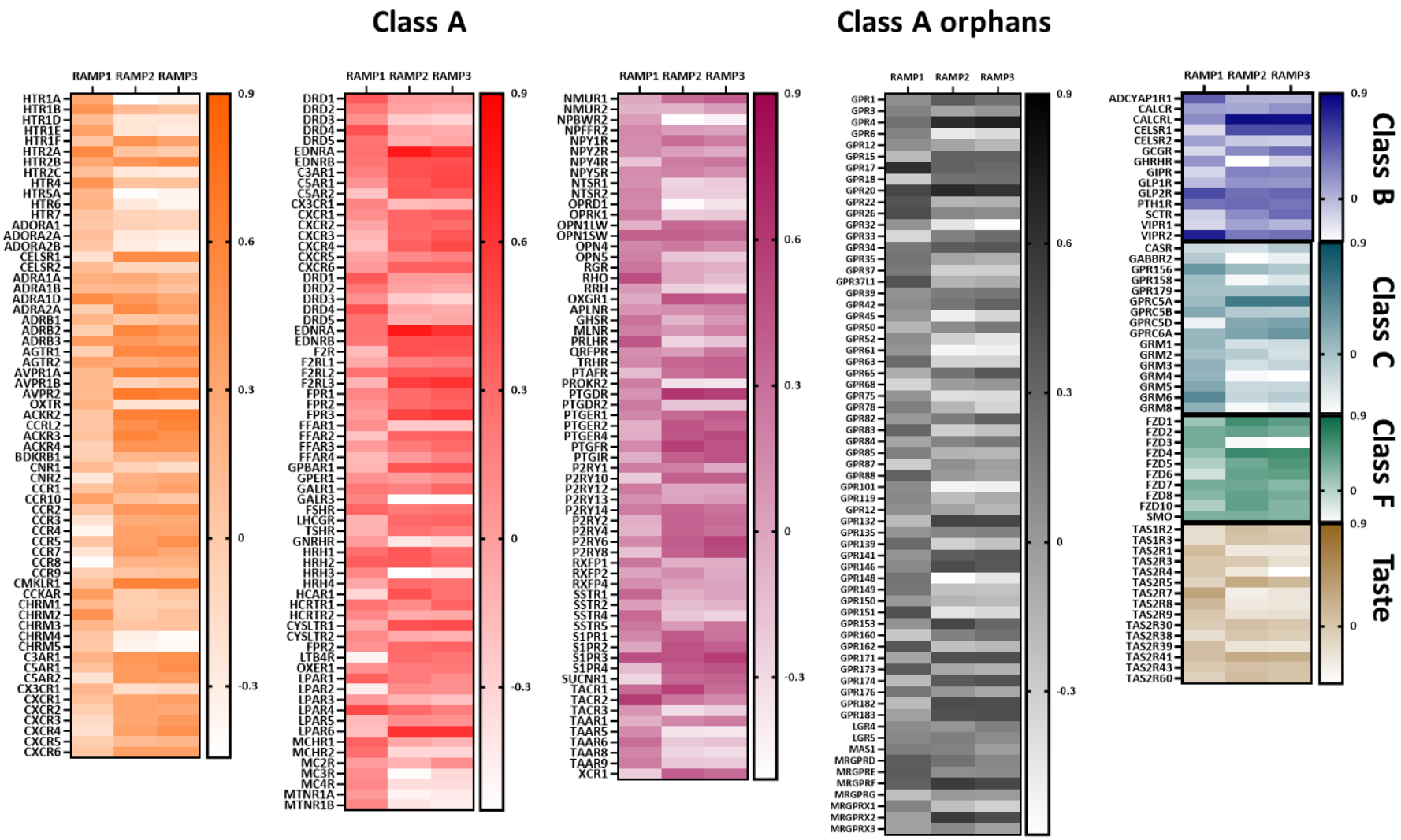

Figure 68: Evaluation of potential RAMP interactors between GPCRs through coexpression correlation coefficient.

Heat maps of the ranked values for % of shared species for different classes of GPCRs. Cell ranges from full saturation (max rank in each category) to white (minimal rank). Receptor gene symbols as reported in GPCRDB.

As noted, this can provide a valuable clue; however, additional analysis to evaluate the functionality of those interactions is needed. Therefore, it was aimed to scale up the previously described method (**Chapter 4.2.2**) to detect PPI interactions – FRET AB. Experiments, which are traditionally performed on fluorescent wide-field or confocal microscopes, provide reliable assessment for potential PPI.

First, it was set out to evaluate possible interaction with in-house available GPCRs, which might interact with RAMPs. First, the mGluR1 receptor, a member of class C GPCRs, was used in combination with one of the RAMP isoforms. **Figure 69 A** shows the schematics of the experiment conducted with the wide-field microscope. Emission intensities of donor and acceptor were collected before and after 3 min of photobleaching of the acceptor fluorophore. More than 70% bleaching of the acceptor fluorophore was achieved during this procedure, and donor intensity subsequently increased (**Figure 69 A**). A combination of $mGluR1_{CFP}$ with EYFP-tagged RAMPs was tested (**Figure 69 B**) as well reverse combination of $mGluR1_{EYFP}$ with CFP-tagged RAMPs (**Figure 69 C**). Both experimental combinations yielded FRET efficiencies between 16 and 25%. As a control receptor, β2AR was used in similar setup combinations as mGluR1. FRET efficiencies for those combinations were between 2 and 16% (**Figure 69 D, E**). Although experiments with mGluR1-RAMPs resulted in higher FRET efficiencies than those with β2AR-RAMPs, testing efficiencies between **Figure 69 B** and **Figure 69 D** didn´t significant differ. Moreover, the results of this analysis might be confounded since no identical donor fluorophore was used with GPCR. Besides this, more experiments and experiments with positive control should be performed to give a reliable claim about a potential interacting partner of RAMPs. The downside of those experiments is that they are expensive and time-consuming and thus, enable only a limited amount of the potentially tested pairs in one go.

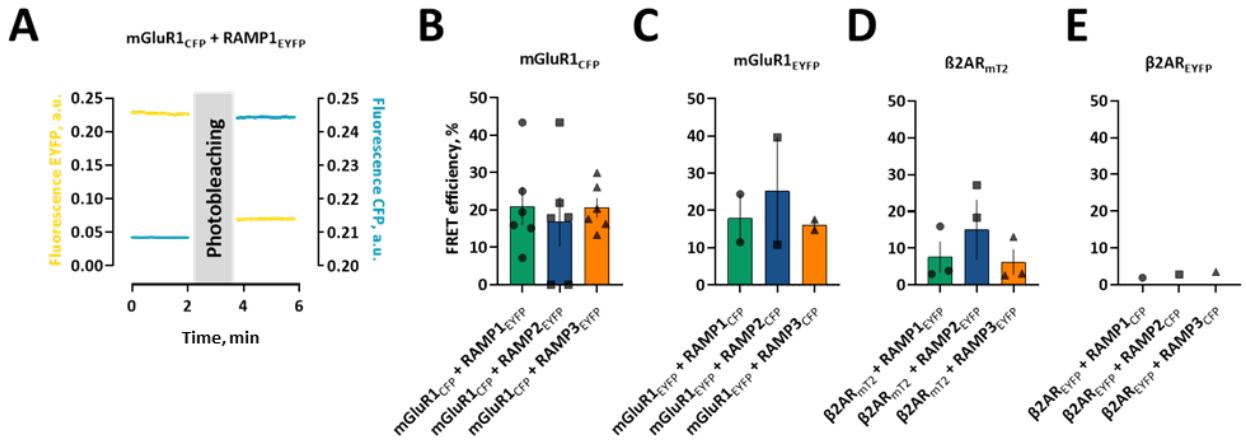

Figure 69: Preliminary FRET acceptor photobleaching experiments for interaction between mGluR1 and RAMPs.

Photobleaching experiments were conducted in HEK293 cells, transiently cotransfected with a combination of donor- and acceptor-tagged constructs. The acceptor (EYFP) and donor fluorophores (CFP, mT2) were fused to the C-terminal of the mGluR1 ($mGluR1_{CFP}$, $mGluR1_{EYFP}$), to the control β2-adrenergic receptor ($β2AR_{mT2}$, $β2AR_{EYFP}$), and the C-terminal of RAMPs ($RAMP1/2/3_{EYFP}$, $RAMP1/2/3_{CFP}$).

*(**A**) A representative experiment showed the fluorescence emission change before and after photobleaching in cells expressing $mGluR1_{CFP}$ and $RAMP1_{EYFP}$.*

*(**B - D**) FRET efficiencies from photobleaching experiments were recorded with a wide-field microscope. The data are expressed as % of donor emission increase after photobleaching for each experimental group. The bars indicate means + SEM. One point represents one experimental day.*

To overcome laborious and low throughput single-cell measurement, an updated experimental set-up was envisioned where it would be possible to test for PPI in the high throughput screening (HTS) format (**Figure 70**). Selected combinations of protein of interest (**Figure 70 A**) would need to be transfected and seeded into the microtiter plates (**Figure 70 B**). Still, the use of the plate reader (**Figure 70 D**) to measure fluorescence intensity before and after the bleaching (**Figure 70 C**) would facilitate a greater number of examined combinations of proteins.

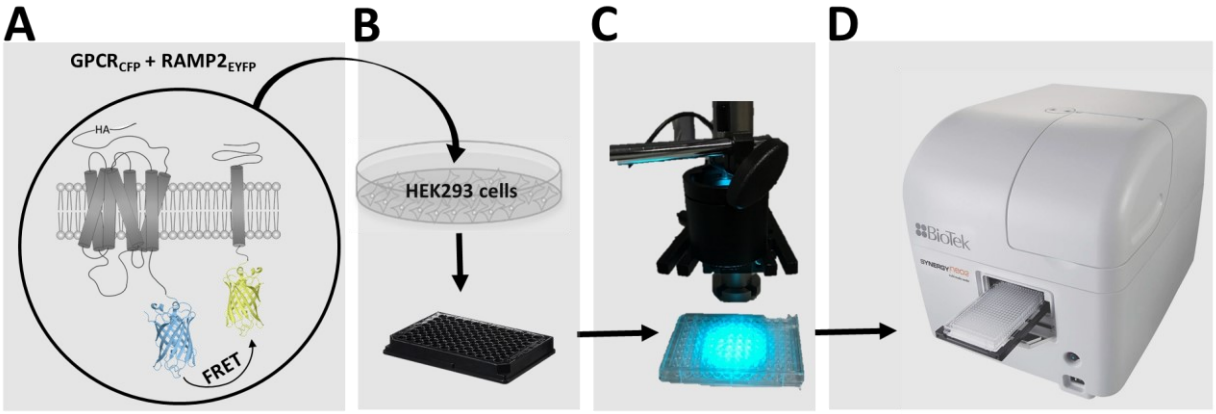

Figure 70: Experimental plan for HTS FRET-AB setup for detecting novel PPI.

*(**A**) Schematic representation of the constructs for FRET acceptor photobleaching experiments between GPCRs and RAMPs. Photobleaching experiments were conducted in HEK293 cells, transiently cotransfected with a combination of donor- and acceptor-tagged constructs. The donor fluorophore (CFP) was fused to the C-terminal of the GPCRs. The acceptor fluorophore (EYFP) was fused to the C-terminal of RAMPs (RAMP1/2/3$_{EYFP}$).*

*(**B**) HEK293 cells were transfected and seeded into black 96-well microtiter plates one day before the experiment.*

*(**C**) In all experiments, pE4000 (CoolLED Ltd., UK) diode system was used for photobleaching acceptor (EYFP). A 500 nm and 525 nm diodes were used, which were coupled to the collimator (COP-1A, Thorlabs GmbH, Germany) through a liquid light guide. The collimator with an aspheric condenser lens (Ø50 mm, f=40 mm, NA=0.60, ARC: 350-700 nm) provided sufficiently even illumination of nine wells with cells on a microtiter plate.*

*(**D**) Fluorescence emission was measured with a plate reader before and after the photobleaching process.*

Dr. Eugene Grushevskyi participated in the experimental design.

The hypothesis that differences in fluorescence emission due to photobleaching are possible to access also in microtiter format was tested with the protocol mentioned above and selection of proteins, all being fused to CFP and EYFP fluorophores. First, the α2A-CFP-EYFP biosensor (Vilardaga *et* al., 2003a), a well-characterized intramolecular biosensor, was used as a positive control. Second, muscarinic acetylcholine receptor M2 (M2$_{EYFP}$) together with mGluR1$_{CFP}$ was employed as negative control accounting for nonspecific interactions, which could happen because of random colocalization of the fluorophores. Lastly, mGluR1$_{CFP}$ was coexpressed with one of three RAMPs; RAMP1-3$_{EYFP}$. **Figure 71 A** shows an exemplary experiment and changes in emissions before and after the photobleaching process. The efficiency of the photobleached acceptor was smaller than in the single-cell microscopic experiments; nevertheless, it was possible to observe donor increase, which reached around 5 % for the visualized exemplary experiment (**Figure 71 A**).

FRET efficiencies for donor increase of positive control were around 7 %, negative control around 1 %, and values for RAMPs proteins with mGluR1 were about 3% (**Figure 71 B**). Those results suggest that mGluR1 might interact with RAMP proteins. Nevertheless, because of the infancy of the used method, orthogonal assays would be required to confirm those results.

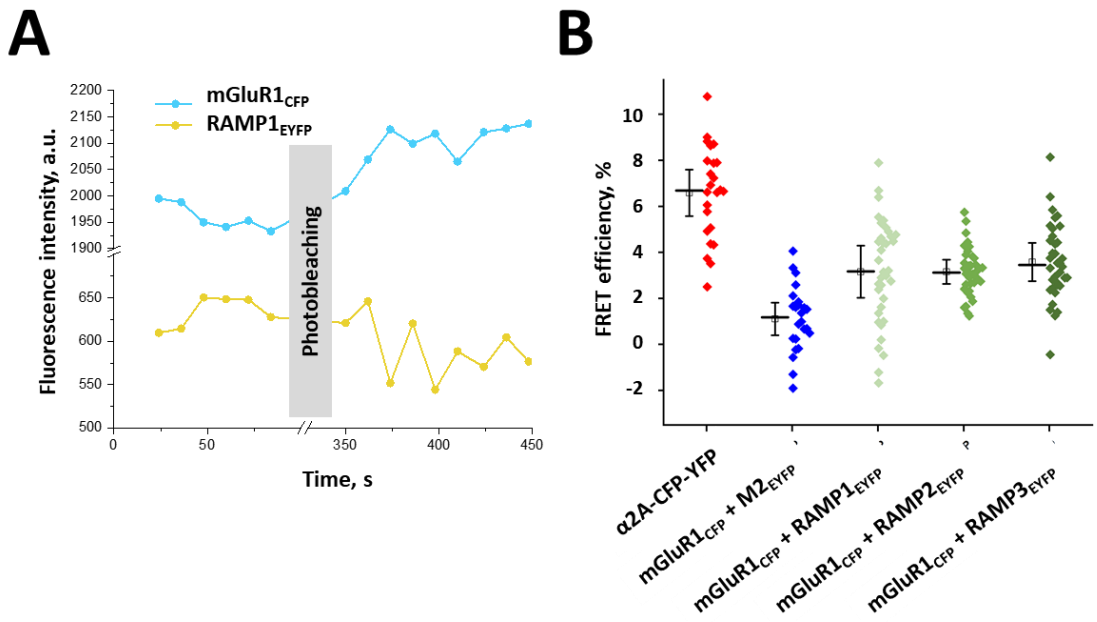

Figure 71: FRET-AB microplate reader-based set-up for detecting novel PPI.

*(**A**) A representative experiment showed the fluorescence emission change before and after photobleaching in cells expressing $GPCR_{CFP}$ and $RAMP_{EYFP}$.*

*(**B**) FRET efficiencies from photobleaching experiments recorded with a plate reader. The data are expressed as % of donor emission increase after photobleaching for each experimental group. The data shows mean ± SEM with data points representing wells from two independent experiments.*

The envisioned method would be further equipped with more biological and technical controls. For example, when investigating GPCRs-RAMP interaction, it would be helpful to include described interactors and their cognate controls when used for other PPI proteins.

Moreover, it would be meaningful to control for 1) amount of bleaching between groups, and 2) the expression level of the fluorophores, and thus introduce a similar controlling procedure as was used in **Chapter 4.2.2**.

Further improvements of the setup and a step closer to the endogenous-like expression levels would be to CRISPR fluorescently tagged RAMP into the cell of interest and examine the interaction at the more native-like level.

The scalable method could be broadly employed to discover novel PPI, allowing for quicker data collection than conventionally used single-cell-based methods. Moreover, data output from a plate reader is effortlessly connected to automatic data processing software, enabling more efficient detection of novel PPI.

4.14 CONCLUSION

This work represents one of the first studies examining the impact of accessory proteins on the GPCR activation process. First, I report on the engineering of novel tools to study the interactions between proteins and their modulation effect (**Chapter 4.1**). Second, I use those tools to follow the signaling cascade from the activation process toward downstream effectors to elucidate the impact of intermolecular interactions between PTH1R and RAMPs (**Chapters 4.2, 4.4. - 4.8**).

The first chapters demonstrate how the FRET and BRET conformational biosensor can be broadly used to study the activation dynamics of physiologically and therapeutically important class B GPCRs (**Chapters 4.3, 4.11, 4.13, 4.14**) and engineered RAMPs, visualizing the proteins using different setups and attaining distinct levels of precision (**Chapter 4.1**). It further establishes unique experimental designs to study specific RAMP modulation mechanisms. This is broadly examined and discussed to prove that RAMPs have modulatory roles in activation dynamics from the biophysical (**Chapter 4.4, 4.5**) and structural perspective (**Chapter 4.10**).

The novel concept that RAMPs modulate receptor kinetics is a significant addition to the current understanding of the roles that RAMPs play. The demonstration that these effects are ligand-specific suggests that modulation is very delicately orchestrated and adds another level of complexity to established concepts of GPCR pharmacology. Assessing downstream levels of PTH1R-RAMP2 heterooligomer, I proved that interaction is highly relevant. I could observe a few unique alterations in the signaling cascade; ligand-specific change of Gi3 potency (**Chapter 4.7**), and increased β-arrestin2 recruitment, which is further translated to differences in cytosolic EKAR signaling (**Chapter 4.8**). This divergence of signaling cascade after interaction of RAMP2 provides clues that such signaling modes could exist in particular cells or tissues.

The specific modulation of β-arrestin-dependent PTH1R signaling is has been shown to increase bone mass, suggesting that the examined heterooligomer constitutes a plausible therapeutic target. The fact that RAMPs are forming tissue-dependent heterooligomers with their interacting partners advocates that it could be possible to create very specific drug designs, avoiding adverse effects.

The broader implications of GPCR-RAMP interactions are explored in **Chapter 4.14,** where bioinformatic GPCR-RAMP datasets are used to look for potential novel interactors and pave the way for future experiments. In that chapter I propose a new, HTS method to study PPI interactions to validate those predictions.

In summary, I establish novel tools and experimental setups to precisely study the way GPCR activities are modulated by accessory proteins. We prototype our approach on the therapeutically important PTH1R-RAMP2 heterooligomer and inaugurate a novel role for RAMPs, as functionally important modulators of GPCR activation dynamics.

5 OUTLOOK

This work illustrates that accessory proteins have a significant modulating impact on receptor activation and downstream signaling and provides an example of how GPCR signaling can be modulated in highly specific way. I discuss the experimental results directly in connection with the findings in the Results chapter. Here I outline selected inspiring insights and significant findings from my studies.

5.1 Revised PTH1R biosensors and their potential in the drug discovery

To precisely examine the modulation effect of RAMPs on receptor activation, it was required to establish a FRET-based biosensor with better quality of signal-to-noise ratio as previously available. Therefore, two new biosensors were created, which proved to be valuable tools for looking at the activation process with a microscope and a plate reader. Expanding their usability to plate readers made work less laborious and smoothened data collection. Moreover, it provided an important tool to study the modulational effect on PTH1R conformation, which was our main scope, and potential novel ligands against therapeutically important receptors. PTH1R is an essential target for osteoporosis and hyper- and hypoparathyroidism, a prospective target for Eiken syndrome, Jansen's metaphyseal chondrodysplasia, and humoral hypercalcemia during cancer (Cheloha *et* al., 2015a). The current repertoire of registered drugs targeting PTH1R receptor (Teriparatide, Abaloparatide and their Biosimilars (*Drugs@FDA*, n.d.; EMA, 2022)) will likely expand, and currently available biosensors could help to speed up drug discovery by providing a tool to test potential ligands. Especially in the Eiken syndrome and Jansen's metaphyseal chondrodysplasia, where inverse agonists against PTH1R constitute receptor phenotype are lacking, ligands could be screened with the $PTH1R_{FRET}$ H223R biosensor, which was able to report constitutive activity.

Additionally, employing those sensors together with modulators as Ca^{2+} ions or accessory proteins can fine-tune ligand pharmacology further and help to understand in which context they work best. It could be plausible to construct a specific antibody targeting heterooligomers of PTH1R-RAMP2, similarly to the already approved erenumab, which targets CRLR-RAMP1 (Dolgin, 2018). Another strategy would be to deliver drugs together with Ca2+ ions, potentiating agonistic effects and achieving synergistic mode or even super agonism (A. D. White *et* al., 2019). Agonists with chelators could decrease activation by depletion of Ca2+ ions, allosteric modulators of PTH1R activation. Bioconjugates of chelators with peptides had a significant diagnostic and therapeutical impact in the cancer field (Jackson *et* al., 2020); therefore, it would be pragmatic to rethink if hypercalcemia during cancer could be treated in that way. All mentioned targeting strategies could be tested with the use of PTH1R biosensors.

Thus, revised PTH1R biosensors represent a valuable tool for drug discovery of novel ligands and could be broadly employed in the future studies in the academic or industrial context.

5.2 Different approaches to measure the kinetics

For a holistic understanding of signaling dynamics, high temporal and spatial resolution methods are required. The appropriate techniques need to be used to derive the parameters required to describe the signaling profiles of specific molecules. For this purpose, two more general experimental setups on how to collect pharmacology-

relevant data are represented in this work. At first, cells responses are recorded in ensemble acquisition mode (at the plate reader) and second from the single-cells (at the microscope).

Ensemble methods are performed in microtiter plates, which convey a less laborious way to collect a larger amount of data and are usually connected to more automated forms of data analysis. The downside is that currently, available plate readers cannot measure single-cell responses and thus, report on cell-to-cell variability. Nevertheless, machines that combine a microscopic acquisitions and a plate reader setups are entering the market – for example, Cytation series from Agilent or Spark® Cyto from Tecan, and CellInsight from Thermo Fisher. Those can significantly increase the number of analyzed cells per experiment but cannot precisely measure kinetic parameters. Microscopic investigations can thus, give us supreme precision and, with 43x objective, track real-time changes of 5-6 HEK293 single-cells and deliver more precise kinetic parameters. Microscopic setup is equipped with automated perfusion system (as OctaFlow II (*OctaFlow II – Automated Perfusion System – NPI Electronic*, n.d.)) which can deliver ligands in the near vicinity of the cell membrane with expressed receptors (< 100 µm) and by incorporated solenoid valves, which switch within 1-2 ms, enables rapid solution delivery in less than 10 ms.

FRET biosensors were the most precise way to measure kinetics parameters for a substantial period of time. In the last years, the time needed for the ligand delivery was overcome with the elegant use of an uncaging experimental setup (Grushevskyi *et* al., 2019), where photolabile inactive caged ligand derivative is already positioned in the near vicinity of the binding pocket. Subsequently, a UV laser pulse is applied to break the cage, rapidly release the ligand, and consequently the ligand immediately activate the receptor. Another way to measure precise activation kinetic is by using photoswitchable ligands, where one of the *cis-trans* isomers is able to activate the receptor and another would not. Mentioned photo-pharmacological strategies are already available (Broichhagen *et* al., 2015; P. Donthamsetti, Konrad, *et* al., 2021; P. C. Donthamsetti *et* al., 2019; P. Donthamsetti, Winter, *et* al., 2021; Morstein *et* al., 2022), and there are experimental optical setup developed, that are able to photoswitch and measure activation with high temporal precision in living cells.

5.3 GPCR-RAMP interaction

5.3.1 Stabilization of functionally different conformations by RAMPs

Interpreting the data in the context of energy landscapes, field, widely employed to explore a conformational variety of GPCRs can provide a link between the structure and function of GPCRs (Deupi & Kobilka, 2010; Dong *et* al., 2016; Alhadeff *et* al., 2018; Fleetwood *et* al., 2020). It is generally accepted that GPCRs use their structural plasticity for existing in multiple conformations and alternate between them. Specific ligand stabilize some of the active conformations and through that dictate particular pathways (Kenakin, 2002). Different ligands, lipids, or molecular interacting partners (*e.g.,* G proteins, GRKs, arrestins) (Sengupta & Chattopadhyay, 2015; Damian *et* al., 2021) can shift preference for activation for particular pathways via inducing a higher probability of certain conformation. This dynamic structural ensemble is most evident when describing ligand-specific conformations that transduce extracellular stimuli to different intracellular cascades. For a pleiotropic receptor, such as PTH1R, different interactors could induce active-state conformations favoring specific downstream patterns. Regarding the presented work, it is believed that RAMP proteins possess the power to shift the functional selectivity of PTH1R signaling. To illustrate this, **Figure 72** shows different conformations of PTH1R and corresponding thermodynamic energy profiles. The first section presents receptor biosensor in their inactive state (R), ligand-free state. When the

agonist is added, the binding energy of the agonists shifts the equilibrium to the ligand-activated state (R*), portrayed in the third section. The results section of this thesis shows and argues that RAMP2 can induce a novel, partially pre-activated state; it could also be a (meta)stable intermediate state, which is different from R or R* and is energetically closer to the ligand-activated state. This state allows a quicker activation process with faster kinetics and smaller amplitude as described with $PTH1R_{FRET}$ and $PTH1R_{cpGFP}$ biosensor. RAMP2-induced confirmation was not recognized as active by G proteins biosensors or GRKs (unaltered basal ratio). It, however, changed the basal ratio of the PTH1R - β-arrestin BRET experiment. The existence of β-arrestin-primed high-affinity conformation was described for some class A and B GPCRs (Jorgensen *et* al., 2005; Sanni *et* al., 2010). Different ligand-induced GPCR conformation can be recognized by β-arrestin even in the absence of receptor phosphorylation (Shukla *et* al., 2008) and exert functionally specific conformations in β-arrestin structure. It might be that β-arrestin can sense and functionally specify ligand-induced conformations and RAMP-induced conformation. This phenomenon is described in **Chapter 4.8** where it was shown that RAMP coexpression led to an enhanced amount of β-arrestin recruitment – finding, also described for some other GPCR-RAMP complexes (Harris *et* al., 2021b; Shao *et* al., 2021; Pearce *et* al., 2022). This indicates that distinct receptor conformations induced and stabilized by RAMP can promote specific and functionally important divergence in signaling.

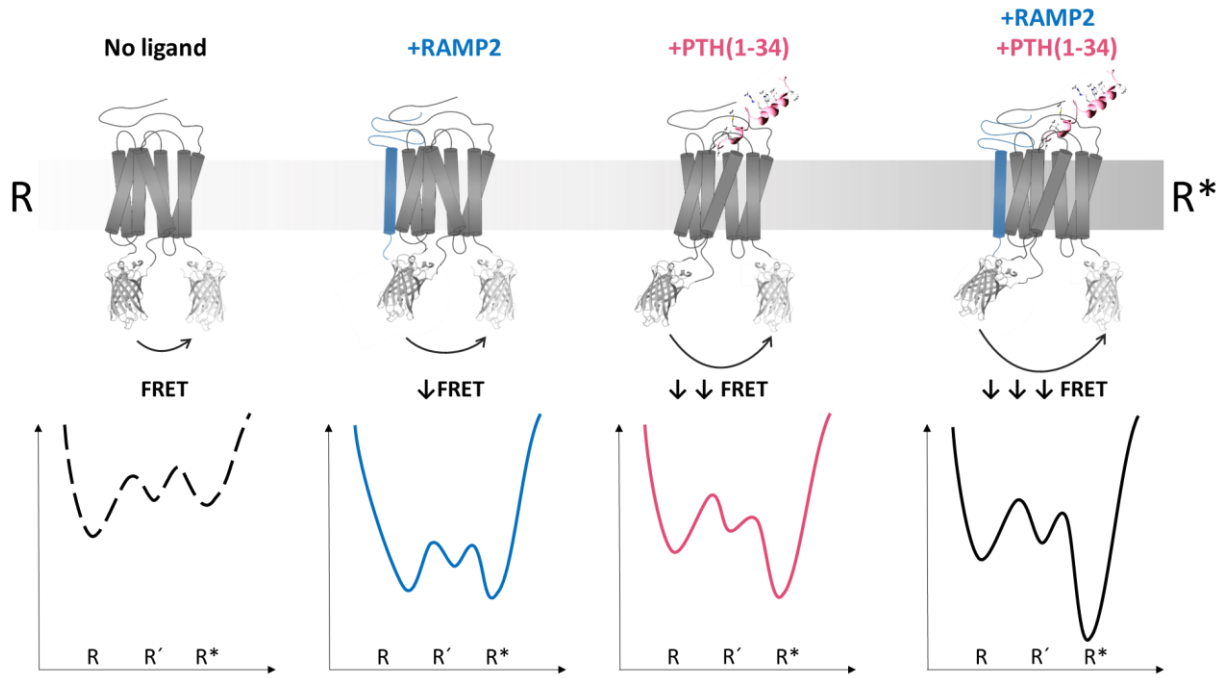

Figure 72: Activation model of PTH1R-RAMP interpreted in the energy landscape.

Moreover, it would be exciting to evaluate if stabilization of GPCR conformation by RAMP is a permanent or transient event, already initial studies which suggested that receptor dimers are "born" together in ER and travel to the membrane were recently outmoded by refined methodology (Calebiro *et* al., 2013; Möller *et* al., 2020a; Işbilir *et* al., 2020b, 2021; Ferré *et* al., 2014), and similar predictions were proposed for RAMPs (McLatchie *et* al., 1998; Klein *et* al., 2016). To tackle this question, FRET studies that require single-molecule precision and multiplexing are needed (Sungkaworn *et* al., 2017; Möller *et* al., 2020a; Işbilir *et* al., 2020a). This work initiated a few constructs (**Chapter 4.1.2**) which will be helpful in such studies.

In summary, to expand knowledge of the proposed RAMP-stabilized conformational landscape, different structural and biophysical methods need to be employed as double electron-electron resonance (DEER) analysis, single-molecule FRET experiments, NMR studies, Hydroxyl radical footprinting mass spectrometry (HRFMS) and hydrogen-deuterium exchange mass spectrometry (HDX-MS) (Deupi & Kobilka, 2010; Gregorio *et* al., 2017; Gusach *et* al., 2020).

It was extensively described for CRLR receptors that RAMP changed their structural dynamics and cocreated different receptor profiles (Liang, Belousoff, Fletcher, *et* al., 2020a; Josephs *et* al., 2021b; Liang *et* al., 2018; J Gingell *et* al., 2016b), and it is to believe that (at least RAMP2) can recreate one of the unique PTH1R conformations with relevant functional outcomes.

5.3.2 Modulation of ligand-binding by RAMPs

Is RAMP able to dictate to the GPCR which ligand should preferentially bind? Indeed, studies suggest that RAMPs help to allosterically reshape binding pocket and dictate preference for binding between amylin and calcitonin at their cognate receptors (Cao *et* al., 2022). Those observations are highly relevant for human physiology; since there are many circulating ligands present, RAMPs could help the GPCR to decide which one to bind.

Reviewers raised the need to experimentally demonstrate this by using conformational biosensors during the revision of our article (Nemec *et* al., 2021). Reviewer 2 suggested to tackle this question with simultaneous perfusion of two endogenous PTH1R ligands – PTH and PTHrP. This experiment would probably not result in wanted observation, since I would probably observe mixture of PTH- and PTHrP-stimulated responses.

Most of the RAMPs interacting partners are peptide receptors – very high-affinity substances. They are all binding to the same position; therefore, it would be more beneficial to observe this in the context of binding – part of the signal transduction, which was not analyzed in our experiments. A binding experiment setup in the presence and absence of RAMPs could help to answer this question.

Different ligands have been shown to regulate and further fine-tune GPCR-RAMP pharmacology. Therefore, it is to the aspect that RAMP with GPCR can recreate or reshape binding pocket and slightly switch preference for ligands.

5.3.3 Which GPCR to "ramp"?

Another exciting question is what happens in the cell where are many interacting GPCRs and a limited number of RAMPs: does some of GPCR possesses a higher affinity to bind RAMPs than others, or is it solely coexpression driver, which dictates the likelihood of GPCR-RAMP complexation? When we have all three RAMPs and the interacting GPCR, which complexation happens initially?

In one way, it is to expect that obligate GPCR partners as CRL would have an initial higher affinity to bind RAMP than non-obligate interactors such as CTR or PTH1R. However, some GPCRs, such as CRL, can interact with all three RAMPs. So which event is most likely?

Recent CRISPR studies reveal that each of the CRL-RAMP phenotypes is needed for human cardiovascular cells since it displays differential phenotypes (A. J. Clark *et* al., 2021). To uncover preferences for engagement between GPCRs and RAMPs, one should approach multiplexing methods and label GPCRs and RAMPs with different colors to look at intermolecular dynamics of the changes. Such experiments should be done with single molecule FRET to achieve appropriate precision. Then, receptors should be stimulated with different ligands to reveal if interaction can be

modulated and if it is transient or stable over time. Laboratory of dr. Graham Ladds (University of Cambridge) recently initiated such studies.

Also, it is known that likelihood of oligomerization increases with the higher expression level of proteins and that this is relevant in certain pathophysiological situations (Işbilir *et* al., 2020b). That would suggest that the rate-limiting step for the interaction of GPCR and RAMP originates from the protein expression. If this were regulated via gene expression, the cell would be able to modulate the number of RAMP proteins synthesized to interact with GPCRs to exert specific function. Thus, the cell somehow dictates how many RAMPs are present, what they do, and with which receptor they interact with.

Interestingly, it was shown that increased stimulation of the PTH-stimulated cAMP cascade could increase RAMP3 mRNA synthesis (Phelps *et* al., 2005). Moreover, RAMP2 and RAMP3 transcripts are enriched in failing rat cardiomyocytes, associated with increased adrenomedullin responsiveness (Øie *et* al., 2005). Is this a mechanism to make the receptor more potent and increase its efficacy? It is feasible that RAMP helps sustain a higher degree of signaling in examples of drug-tolerant acute myeloid leukemia (AML) cells (Larrue *et* al., 2021), where its cascade controls relapse of AML. Instead, this intensification speaks for noxious effects; thus, therapeutic designs should aim to inhibit this overreactive cascade. Since RAMPs-interacting receptors critically orchestrate cellular signaling, it should be sought to develop precise targeting strategies. First, targeting only receptors or only RAMP is not viable since both play essential roles in signaling. Instead, it could be aimed to break oligomers by targeting specific GPCR-RAMP interfaces and avoiding complexation in certain tissues. Certain nanobodies were shown to possess the ability to break GPCR dimers by spherical hindrance and, thus, inhibit downstream cascades (Işbilir *et* al., 2020b).

Intriguingly, suppose we align the expression profile of RAMP2 with energy-consuming organs or (patho-)physiological scenarios. In that case, the brain, heart, placenta, or cancer are each significant consumers of energy, and also those where the role of RAMP2 is well established (Øie *et* al., 2005; Ichikawa-Shindo *et* al., 2008, p. 2; Igarashi *et* al., 2014, p. 2; Kadmiel *et* al., 2017; Larrue *et* al., 2021). It could be expected that the RAMP-involving cascade might be connected with ATP synthesis or some other mechanism that feeds the cells.

In summary, many unresolved questions in the GPCR-RAMP pharmacology remain to be investigated henceforth.

5.3.4 Importance of (novel) GPCR-RAMP interactions

Recent years saw significant expansion of the GPCR repertoire with which RAMPs are interacting - as of now counting, around 40 described interactors. The current repertoire of interactors could be structurally analyzed to recognize and develop a structural basis for GPCR-RAMP interaction, which could be translated into a system to decode new potential receptor partners. Such structural debugging could help with deorphanization of specific receptors, which is still a neglected but very relevant field, since 29% of non-olfactory GPCRs keep being orphans (Tang *et* al., 2012). The orphan GPCR, which might be an obligate RAMP partner, would fail to induce signaling in the deorphanization screenings since it lacks part of the complex, which constructs functional receptor phenotype – a story most known for rudimentary RAMP partner CRLR (McLatchie *et* al., 1998).

Moreover, exploring structural fingerprints will help better understand “druggable GPCR pocket,” which should be revised to GPCR-RAMP pocket. Such a pocket constitutes a more specific drug target and could represent tissue-dependent therapy. This drug design strategy was successfully probed with the first-ever antibody against GPCRs, erenumab (Dolgin, 2018), a monoclonal antibody against CRLR-RAMP1 complex, approved for migraine therapy.

Moreover, a few small molecule ligands such as Rimegepant or Ubrogepant targeting CRLR-RAMP1 complex. Analogous targeting strategies will be of undeniable relevance in drug designs of the future.

Regarding the broader functional importance of RAMP modulation on expanding the repertoire of GPCRs, it is to envision that RAMPs will be part of experimental designs in preclinical studies for GPCR drugs. Moreover, cell and tissue-dependent effects will be more closely monitored, which could ultimately help to understand some adverse effects and construct very specific therapeutics.

High expression of CRLR-RAMP2 was shown to be the driver of relapses of AML malignancy (Larrue *et* al., 2021; Vázquez *et* al., 2021), thus, this oligomer would not only represent potential drug target but also prognostic marker for the acute myeloid leukemia.

Ultimately, discovering new GPCR-RAMP pairs generates many opportunities for drug discovery and disease prognosis. Deorphanization of GPCRs, the creation of specific drug targets, and prognostic markers are some of the areas which would enormously benefit from accumulating knowledge of novel interactions.

5.3.5 Conservation of GPCR-RAMP oligomerization and modulation across class B GPCRs

Just five years ago, there were only 11 interacting GPCRs described to interact with RAMPs (Klein *et* al., 2016), all except GPER and CaSR being members of class B GPCRs. Recent exploration of novel interaction showed that RAMP interactome is wider than previously appreciated and broadened described RAMP interactors to almost all members of class B. Therefore, it could be that exist specific structural fingerprint dictating the interaction and, even more interestingly, mode of modulation. Initial structural studies identified that structural conservation of residues is important to interact with RAMP (Liang *et* al., 2018). In currently available structures (Booe *et* al., 2015; Liang *et* al., 2018; Garelja *et* al., 2020; Liang *et* al., 2020; Josephs *et* al., 2021; Cao *et* al., 2022), this region compromises TM3, TM4, and TM5 of the receptor and ECL2, which is an especially interesting structural motif. An extensive mutagenesis study of the linker region of RAMP, performed by Liang *et* al. showed that this part is crucial in shaping peptide selectivity and efficacy. This part is described as an allosteric hotspot in PTH1R (L. J. Clark *et* al., 2020a), which impacts β-arrestin2 recruitment after stimulation with a specific ligand. The Ser355 and Gly357 of PTH1R are part of more extensive region (aa 348-356), which according to our structural models in **Chapter 4.9** contacts RAMP. **Figure 73** shows ECL2 residue conservation across some class B GPCRs; CW+ at the position .50, .51, and .52. It is interesting that RAMP modulation of GIP and glucagon modulated β-arrestin recruitment (Cegla *et* al., 2017; Harris *et* al., 2021b; Pearce *et* al., 2022), similar to the experiments in **Chapter 4.8.**

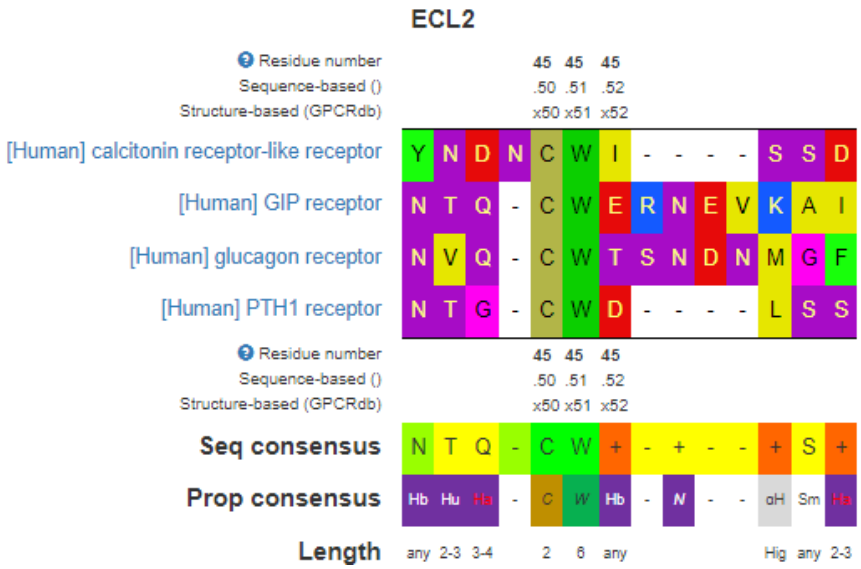

Figure 73: Conservation of ECL2 residue between some class B GPCRs.

Sequence alignment of class B GPCRs residues .50, .51, and .52 and adjacent ones from GPCRdb show a high conservation degree. Sequence alignment was created with GPCRDB.

The second interesting structural motif in PTH1R, presumably essential for RAMP modulation, could be part of "kink 5", which is also highly conserved across class B GPCRs (**Figure 74**). It goes for inward kink in the cytosolic extension of TM5 (residues V382$^{5.58}$–T392$^{5.68}$), where PTH1R and GIPR have polar aa, whereas in GCGR nonpolar aa on position 5.63. The nature of those structural motifs could be investigated with the mutational screenings. Information about the decisive aa would add to the knowledge of the activation mechanism of class B GPCRs.

	CTR	CALCRL	CRF_1R	CRF_2R	GHRHR	GIPR	GLP-1R	GLP-2R	GCGR	SCTR	PTH1R	PTH2R	PAC_1R	$VPAC_1R$	$VPAC_2R$
5.58	V320	V313	V291	V287	I304	L318	I328	L362	V326	L317	V382	V337	I328	I316	I303
5.59	R321	R314	R292	R288	R305	G319	C329	K363	Q327	R318	R383	R338	V329	R317	R304
5.60	V322	V315	I293	I289	I306	I320	I330	L364	L328	I319	V384	V339	I330	I318	I305
5.61	L323	L316	L294	L290	L307	L321	V331	L365	L329	L320	L385	L340	L331	L319	L306
5.62	V324	I317	M295	M291	V308	L322	V332	I366	V330	M321	A386	A341	V332	L320	L307
5.63	T325	T318	T296	T292	R309	S323	S333	S367	A331	R322	T387	T342	Q333	Q321	Q308
5.64	K326	K319	K297	K293	K310	K324	K334	K368	K332	K323	K388	K343	K334	K322	K309
5.65	M327	L320	L298	L294	L311	L325	L335	L369	L333	L324	L389	I344	L335	L323	L310

Residue Property: Nonpolar | Polar | Basic | Glycine | Cysteine

Figure 74: Amino acids position of kink five residues among class B GPCRs.

Sequence alignment of class B GPCRs residues 5.58 – 5.65 (Numbering after Wooten) from GPCRDB shows a high conservation degree among class B GPCRs. Colors represent the chemical properties of the residues. Reprinted with permission 5295681171628 from Springer Nature: Nature Chemical Biology, Allosteric interactions in the parathyroid hormone GPCR–arrestin complex formation, Clark et al., Copyright © 2020, Springer Nature (2018).

6 SUMMARY

The G protein-coupled receptors (GPCRs) constitute the largest and pharmacologically most important family of cell surface receptors, which supervise many (patho-)physiological processes in the human body. GPCRs transfer extracellular signals to the cell interior during the receptor activation process, where extracellular stimulation initiates conformational rearrangements of the receptor core and enables binding of intracellular binding partners – G proteins, G protein-coupled receptor kinase, and β-arrestins. Thus, this is a critical process in signal transduction that can be modulated by some of the endogenous molecules, including ions, lipids, or other proteins, and impacts downstream signaling cascades. GPCRs are forming tissue-dependent oligomers with their interacting partners, receptor activity-modifying proteins (RAMPs), ubiquitously expressed membrane proteins. They are known to modulate ligand-binding, G protein coupling, downstream signaling, trafficking, and recycling of some GPCRs.

Yet, only limited research was conducted on their role in the most critical signal transduction process – receptor activation.

Using the physiologically and therapeutically important parathyroid hormone 1 receptor (PTH1R), a class B GPCR, modulation effects of RAMPs on the receptor activation process and its consequences for downstream signaling were analyzed. Therefore, different optical biosensors to measure the activation of PTH1R and its signaling cascade were developed and employed in various setups to construct a holistic view of PTH1R-RAMP interaction and its functional outcomes.

Interaction between PTH1R and RAMPs proved to be most prominent for RAMP2 and RAMP2 showed specific allosteric modulation on PTH1R conformation, in both basal and ligand-activated states. A unique RAMP2-induced pre-activated (or meta-stable) state enabled faster receptor activation in a ligand-specific manner. Furthermore, RAMP2 affected G protein and non-G protein signaling. It modulated PTH-mediated Gi3 signaling sensitivity and kinetics of cAMP accumulation. Additionally, RAMP2 elevated the amount of β-arrestin2 recruitment to PTH1R and increased the amount of cytosolic ERK, which was distinctive from nuclear ERK phosphorylation. In order to suggest a molecular mechanism for presented findings, several structural models were developed and analyzed.

This work provides evidence that RAMP modulates GPCR activation with functional consequences on cellular signaling. This should be interpreted in the context of cell-specific coexpression patterns and could lead the design of advanced therapeutics. Since GPCRs coordinate an array of cell functions and have always been significant drug targets, the knowledge presented here adds to the universal understanding of molecular mechanisms which orchestrate the human body.

7 ZUSAMMENFASSUNG

G Protein-gekoppelte Rezeptoren (GPCRs) bilden die größte und pharmakologisch wichtigste Familie von Zelloberflächenrezeptoren, die zahlreiche (patho-)physiologische Prozesse im menschlichen Körper steuern. GPCRs übertragen während des Rezeptoraktivierungsprozesses extrazelluläre Signale in das Zellinnere, wo durch die extrazelluläre Stimulation Konformationsänderungen des Rezeptorkerns auslöst und die Bindung intrazellulärer Bindungspartner – G Proteine, G Protein-gekoppelte Rezeptorkinase und Arrestine - ermöglicht. Es handelt sich also um einen kritischen Prozess in der Signaltransduktion, der durch einige endogene Moleküle wie Ionen, Lipide oder andere Proteine moduliert werden kann und Auswirkungen auf nachgeschaltete Signalkaskaden hat.

GPCRs bilden gewebeabhängige Oligomere mit ihren interagierenden Partnern, Rezeptor-Aktivitäts-modifizierende Proteinen (RAMPs), ubiquitär exprimierten Membranproteinen. Bekannt ist, dass sie die Ligandenbindung, die G-Protein-Kopplung, die nachgeschaltete Signalisierung, das Trafficking und das Recycling einiger GPCRs modulieren. Ihre Rolle im kritischsten Prozess der Signaltransduktion - der Rezeptoraktivierung - wurde jedoch nur begrenzt erforscht.

Anhand des physiologisch und therapeutisch wichtigen Parathormon-Rezeptors (PTH1R), einem GPCR der Klasse B, wurden die Modulationseffekte von RAMPs auf den Prozess der Rezeptoraktivierung und ihre Folgen für die nachgeschaltete Signalübertragung analysiert. Hierzu wurden verschiedene optische Biosensoren zur Messung der Aktivierung des PTH1R und seiner Signalkaskade entwickelt und in verschiedenen Versuchsanordnungen eingesetzt, mit dem Ziel einen holistischen Blick auf die Interaktion zwischen PTH1R und RAMPs und ihre funktionellen Auswirkungen zu erhalten.

Die Interaktion zwischen PTH1R und RAMPs erwies sich als besonders ausgeprägt für RAMP2, und RAMP2 zeigte eine spezifische allosterische Modulation der PTH1R-Konformation, sowohl im basalen als auch im Liganden-aktivierten Zustand. Ein einzigartiger voraktivierter oder (meta-stabiler) Zustand ermöglichte eine schnellere Rezeptoraktivierung auf Liganden-spezifische Weise. Außerdem beeinflusste RAMP2 die G Protein- und Nicht-G Protein-vermittelte Signalübertragung indem es die PTH-vermittelte Gi3-Signalempfindlichkeit und die Kinetik der cAMP-Akkumulation modulierte. Weiterhin erhöhte RAMP2 die Menge der β-Arrestin2-Rekrutierung an PTH1R auf Liganden-spezifische Weise. Dies könnte mit einer erhöhten zytosolischen ERK-Menge zusammenhängen, die hat sich von der nukleären ERK-Phosphorylierung unterscheidet. Um einen molekularen Mechanismus für die vorgestellten Ergebnisse vorzuschlagen, wurden mehrere strukturelle Modelle entwickelt und analysiert.

Diese Arbeit liefert den Beweis, dass RAMP die GPCR-Aktivierung mit funktionellen Auswirkungen auf die zelluläre Signalübertragung reguliert. Die Ergebnisse sollten im Zusammenhang mit zellspezifischen Koexpressionsmustern interpretiert werden und können zur Entwicklung von fortschrittlichen Therapeutika positiv beitragen. Da GPCRs praktisch alle Zellfunktionen koordinieren und seit jeher wichtigen Angriffspunkten für Medikamente sind, tragen die vorgestellten Erkenntnisse zum universellen Verständnis der molekularen Mechanismen bei, die den menschlichen Körper orchestrieren.

8 REFERENCES

Abou-Samra, A. B., Jüppner, H., Force, T., Freeman, M. W., Kong, X. F., Schipani, E., Urena, P., Richards, J., Bonventre, J. V., & Potts, J. T. (1992). Expression cloning of a common receptor for parathyroid hormone and parathyroid hormone-related peptide from rat osteoblast-like cells: A single receptor stimulates intracellular accumulation of both cAMP and inositol trisphosphates and increases intracellular free calcium. *Proceedings of the National Academy of Sciences*, *89*(7), 2732–2736. https://doi.org/10.1073/pnas.89.7.2732

Alexander, S. P., Davenport, A. P., Kelly, E., Marrion, N., Peters, J. A., Benson, H. E., Faccenda, E., Pawson, A. J., Sharman, J. L., Southan, C., & Davies, J. A. (2015). The Concise Guide to PHARMACOLOGY 2015/16: G protein-coupled receptors. *British Journal of Pharmacology*, *172*(24), 5744–5869. https://doi.org/10.1111/bph.13348

Alhadeff, R., Vorobyov, I., Yoon, H. W., & Warshel, A. (2018). Exploring the free-energy landscape of GPCR activation. *Proceedings of the National Academy of Sciences*, *115*(41), 10327–10332. https://doi.org/10.1073/pnas.1810316115

Alvarez-Curto, E., Inoue, A., Jenkins, L., Raihan, S. Z., Prihandoko, R., Tobin, A. B., & Milligan, G. (2016). Targeted Elimination of G Proteins and Arrestins Defines Their Specific Contributions to Both Intensity and Duration of G Protein-coupled Receptor Signaling*. *Journal of Biological Chemistry*, *291*(53), 27147–27159. https://doi.org/10.1074/jbc.M116.754887

Andreassen, K. V., Hjuler, S. T., Furness, S. G., Sexton, P. M., Christopoulos, A., Nosjean, O., Karsdal, M. A., & Henriksen, K. (2014). Prolonged Calcitonin Receptor Signaling by Salmon, but Not Human Calcitonin, Reveals Ligand Bias. *PLOS ONE*, *9*(3), e92042. https://doi.org/10.1371/journal.pone.0092042

Apostolakou, A. E., Baltoumas, F. A., Stravopodis, D. J., & Iconomidou, V. A. (2020). Extended Human G-Protein Coupled Receptor Network: Cell-Type-Specific Analysis of G-Protein Coupled Receptor Signaling Pathways. *Journal of Proteome Research*, *19*(1), 511–524. https://doi.org/10.1021/acs.jproteome.9b00754

Arimont, M., van der Woude, M., Leurs, R., Vischer, H. F., de Graaf, C., & Nijmeijer, S. (2019). Identification of Key Structural Motifs Involved in 7 Transmembrane Signaling of Adhesion GPCRs. *ACS Pharmacology & Translational Science*, *2*(2), 101–113. https://doi.org/10.1021/acsptsci.8b00051

Attramadal, H., Arriza, J. L., Aoki, C., Dawson, T. M., Codina, J., Kwatra, M. M., Snyder, S. H., Caron, M. G., & Lefkowitz, R. J. (1992). Beta-arrestin2, a novel member of the arrestin/beta-arrestin gene family. *Journal of Biological Chemistry*, *267*(25), 17882–17890. https://doi.org/10.1016/S0021-9258(19)37125-X

Attwood, T. K., & Findlay, J. B. C. (1994). Fingerprinting G-protein-coupled receptors. *Protein Engineering, Design and Selection*, *7*(2), 195–203. https://doi.org/10.1093/protein/7.2.195

Austermann, S., Adermann, K., Walter, S., Schmid, F.-X., Jaenicke, R., Forssmann, W.-G., Marx, U. C., Bayer, P., Ejchart, A., Sticht, H., & Rösch, P. (1995). Structure of Human Parathyroid Hormone 1–37 in Solution (∗). *Journal of Biological Chemistry*, *270*(25), 15194–15202. https://doi.org/10.1074/jbc.270.25.15194

Avet, C., Mancini, A., Breton, B., Le Gouill, C., Hauser, A. S., Normand, C., Kobayashi, H., Gross, F., Hogue, M., Lukasheva, V., St-Onge, S., Carrier, M., Héroux, M., Morissette, S., Fauman, E. B., Fortin, J.-P., Schann, S., Leroy, X., Gloriam, D. E., & Bouvier, M. (2022). Effector membrane translocation biosensors reveal G protein and βarrestin coupling profiles of 100 therapeutically relevant GPCRs. *ELife*, *11*, e74101. https://doi.org/10.7554/eLife.74101

Azzi, M., Charest, P. G., Angers, S., Rousseau, G., Kohout, T., Bouvier, M., & Piñeyro, G. (2003). β-Arrestin-mediated activation of MAPK by inverse agonists reveals distinct active conformations for G protein-coupled

receptors. *Proceedings of the National Academy of Sciences*, *100*(20), 11406–11411. https://doi.org/10.1073/pnas.1936664100

Bailey, R. J., & Hay, D. L. (2006). Pharmacology of the human CGRP1 receptor in Cos 7 cells. *Peptides*, *27*(6), 1367–1375. https://doi.org/10.1016/j.peptides.2005.11.014

Bailey, S., Harris, M., Barkan, K., Winfield, I., Harper, M. T., Simms, J., Ladds, G., Wheatley, M., & Poyner, D. (2019). Interactions between RAMP2 and CRF receptors: The effect of receptor subtypes, splice variants and cell context. *Biochimica et Biophysica Acta (BBA) - Biomembranes*, *1861*(5), 997–1003. https://doi.org/10.1016/j.bbamem.2019.02.008

Baker, J. G., Hall, I. P., & Hill, S. J. (2003). Agonist and Inverse Agonist Actions of β-Blockers at the Human β2-Adrenoceptor Provide Evidence for Agonist-Directed Signaling. *Molecular Pharmacology*, *64*(6), 1357–1369. https://doi.org/10.1124/mol.64.6.1357

Barbash, S., Lorenzen, E., Persson, T., Huber, T., & Sakmar, T. P. (2017). GPCRs globally coevolved with receptor activity-modifying proteins, RAMPs. *Proceedings of the National Academy of Sciences*, *114*(45), 12015–12020. https://doi.org/10.1073/pnas.1713074114

Barbash, S., Persson, T., Lorenzen, E., Kazmi, M. A., Huber, T., & Sakmar, T. P. (2019). Detection of Concordance between Transcriptional Levels of GPCRs and Receptor-Activity-Modifying Proteins. *IScience*, *11*, 366–374. https://doi.org/10.1016/j.isci.2018.12.024

Barros-Álvarez, X., Nwokonko, R. M., Vizurraga, A., Matzov, D., He, F., Papasergi-Scott, M. M., Robertson, M. J., Panova, O., Yardeni, E. H., Seven, A. B., Kwarcinski, F. E., Su, H., Peroto, M. C., Meyerowitz, J. G., Shalev-Benami, M., Tall, G. G., & Skiniotis, G. (2022). The tethered peptide activation mechanism of adhesion GPCRs. *Nature*, 1–6. https://doi.org/10.1038/s41586-022-04575-7

Bathe-Peters, M., Gmach, P., Boltz, H.-H., Einsiedel, J., Gotthardt, M., Hübner, H., Gmeiner, P., Lohse, M. J., & Annibale, P. (2021). Visualization of β-adrenergic receptor dynamics and differential localization in cardiomyocytes. *Proceedings of the National Academy of Sciences*, *118*(23). https://doi.org/10.1073/pnas.2101119118

Benítez-Páez, A., & Cárdenas-Brito, S. (2008). Dissection of Functional Residues in Receptor Activity-Modifying Proteins through Phylogenetic and Statistical Analyses. *Evolutionary Bioinformatics*, *4*, EBO.S705. https://doi.org/10.4137/EBO.S705

Benovic, J. L., DeBlasi, A., Stone, W. C., Caron, M. G., & Lefkowitz, R. J. (1989). Beta-Adrenergic Receptor Kinase: Primary Structure Delineates a Multigene Family. *Science*, *246*(4927), 235.

Benovic, J. L., Kühn, H., Weyand, I., Codina, J., Caron, M. G., & Lefkowitz, R. J. (1987a). Functional desensitization of the isolated beta-adrenergic receptor by the beta-adrenergic receptor kinase: Potential role of an analog of the retinal protein arrestin (48-kDa protein). *Proceedings of the National Academy of Sciences*, *84*(24), 8879–8882. https://doi.org/10.1073/pnas.84.24.8879

Benovic, J. L., Kühn, H., Weyand, I., Codina, J., Caron, M. G., & Lefkowitz, R. J. (1987b). Functional desensitization of the isolated beta-adrenergic receptor by the beta-adrenergic receptor kinase: Potential role of an analog of the retinal protein arrestin (48-kDa protein). *Proceedings of the National Academy of Sciences*, *84*(24), 8879–8882. https://doi.org/10.1073/pnas.84.24.8879

Bianchi, E. N., & Ferrari, S. L. (2009). β-ARRESTIN2 REGULATES PARATHYROID HORMONE EFFECTS ON A P38 MAPK AND NFκB GENE EXPRESSION NETWORK IN OSTEOBLASTS. *Bone*, *45*(4), 716–725. https://doi.org/10.1016/j.bone.2009.06.020

Bisello, A., Chorev, M., Friedman, P. A., Gardella, T., Hills, R., Jueppner, H., Martin, T. J., Nissenson, R. A., John Thomas Potts, Jr., Silve, C., Usdin, T. B., & Vilardaga, J.-P. (2021). *Parathyroid hormone receptors (version 2021.2) in the IUPHAR/BPS Guide to Pharmacology Database*. https://doi.org/10.2218/gtopdb/F53/2021.2

Bisello, A., Chorev, M., Rosenblatt, M., Monticelli, L., Mierke, D. F., & Ferrari, S. L. (2002). Selective Ligand-induced Stabilization of Active and Desensitized Parathyroid Hormone Type 1 Receptor Conformations*. *Journal of Biological Chemistry*, *277*(41), 38524–38530. https://doi.org/10.1074/jbc.M202544200

Bokoch, G. M., Katada, T., Northup, J. K., Ui, M., & Gilman, A. G. (1984). Purification and properties of the inhibitory guanine nucleotide-binding regulatory component of adenylate cyclase. *Journal of Biological Chemistry*, *259*(6), 3560–3567. https://doi.org/10.1016/S0021-9258(17)43131-0

Bomberger, J. M., Parameswaran, N., Hall, C. S., Aiyar, N., & Spielman, W. S. (2005). Novel Function for Receptor Activity-modifying Proteins (RAMPs) in Post-endocytic Receptor Trafficking*. *Journal of Biological Chemistry*, *280*(10), 9297–9307. https://doi.org/10.1074/jbc.M413786200

Bomberger, J. M., Spielman, W. S., Hall, C. S., Weinman, E. J., & Parameswaran, N. (2005). Receptor Activity-modifying Protein (RAMP) Isoform-specific Regulation of Adrenomedullin Receptor Trafficking by NHERF-1 *. *Journal of Biological Chemistry*, *280*(25), 23926–23935. https://doi.org/10.1074/jbc.M501751200

Booe, J. M., Walker, C. S., Barwell, J., Kuteyi, G., Simms, J., Jamaluddin, M. A., Warner, M. L., Bill, R. M., Harris, P. W., Brimble, M. A., Poyner, D. R., Hay, D. L., & Pioszak, A. A. (2015). Structural Basis for Receptor Activity-Modifying Protein-Dependent Selective Peptide Recognition by a G Protein-Coupled Receptor. *Molecular Cell*, *58*(6), 1040–1052. https://doi.org/10.1016/j.molcel.2015.04.018

Booe, J. M., Warner, M. L., & Pioszak, A. A. (2020). Picomolar Affinity Antagonist and Sustained Signaling Agonist Peptide Ligands for the Adrenomedullin and Calcitonin Gene-Related Peptide Receptors. *ACS Pharmacology & Translational Science*, *3*(4), 759–772. https://doi.org/10.1021/acsptsci.0c00031

Börner, S., Schwede, F., Schlipp, A., Berisha, F., Calebiro, D., Lohse, M. J., & Nikolaev, V. O. (2011). FRET measurements of intracellular cAMP concentrations and cAMP analog permeability in intact cells. *Nature Protocols*, *6*(4), 427–438. https://doi.org/10.1038/nprot.2010.198

Bouschet, T., Martin, S., & Henley, J. M. (2005). Receptor-activity-modifying proteins are required for forward trafficking of the calcium-sensing receptor to the plasma membrane. *Journal of Cell Science*, *118*(20), 4709–4720. https://doi.org/10.1242/jcs.02598

Bouxsein, M. L., Pierroz, D. D., Glatt, V., Goddard, D. S., Cavat, F., Rizzoli, R., & Ferrari, S. L. (2005). β-Arrestin2 Regulates the Differential Response of Cortical and Trabecular Bone to Intermittent PTH in Female Mice. *Journal of Bone and Mineral Research*, *20*(4), 635–643. https://doi.org/10.1359/JBMR.041204

Brain, S. D., Williams, T. J., Tippins, J. R., Morris, H. R., & MacIntyre, I. (1985). Calcitonin gene-related peptide is a potent vasodilator. *Nature*, *313*(5997), 54–56. https://doi.org/10.1038/313054a0

Broichhagen, J., Damijonaitis, A., Levitz, J., Sokol, K. R., Leippe, P., Konrad, D., Isacoff, E. Y., & Trauner, D. (2015). Orthogonal Optical Control of a G Protein-Coupled Receptor with a SNAP-Tethered Photochromic Ligand. *ACS Central Science*, *1*(7), 383–393. https://doi.org/10.1021/acscentsci.5b00260

Bühlmann, N., Leuthäuser, K., Muff, R., Fischer, J. A., & Born, W. (1999). A Receptor Activity Modifying Protein (RAMP)2-Dependent Adrenomedullin Receptor Is a Calcitonin Gene-Related Peptide Receptor when Coexpressed with Human RAMP1*. *Endocrinology*, *140*(6), 2883–2890. https://doi.org/10.1210/endo.140.6.6783

Butte, A. J., Tamayo, P., Slonim, D., Golub, T. R., & Kohane, I. S. (2000). Discovering functional relationships between RNA expression and chemotherapeutic susceptibility using relevance networks. *Proceedings of the National Academy of Sciences*, *97*(22), 12182–12186. https://doi.org/10.1073/pnas.220392197

Calebiro, D., Nikolaev, V. O., Gagliani, M. C., Filippis, T. de, Dees, C., Tacchetti, C., Persani, L., & Lohse, M. J. (2009). Persistent cAMP-Signals Triggered by Internalized G-Protein–Coupled Receptors. *PLOS Biology*, *7*(8), e1000172. https://doi.org/10.1371/journal.pbio.1000172

Calebiro, D., Rieken, F., Wagner, J., Sungkaworn, T., Zabel, U., Borzi, A., Cocucci, E., Zürn, A., & Lohse, M. J. (2013). Single-molecule analysis of fluorescently labeled G-protein–coupled receptors reveals complexes with

distinct dynamics and organization. *Proceedings of the National Academy of Sciences*, *110*(2), 743–748. https://doi.org/10.1073/pnas.1205798110

Cao, J., Belousoff, M. J., Liang, Y.-L., Johnson, R. M., Josephs, T. M., Fletcher, M. M., Christopoulos, A., Hay, D. L., Danev, R., Wootten, D., & Sexton, P. M. (2022). A structural basis for amylin receptor phenotype. *Science*, *375*(6587), eabm9609. https://doi.org/10.1126/science.abm9609

Carter, P. H., Liu, R.-Q., Foster, W. R., Tamasi, J. A., Tebben, A. J., Favata, M., Staal, A., Cvijic, M. E., French, M. H., Dell, V., Apanovitch, D., Lei, M., Zhao, Q., Cunningham, M., Decicco, C. P., Trzaskos, J. M., & Feyen, J. H. M. (2007). Discovery of a small molecule antagonist of the parathyroid hormone receptor by using an N-terminal parathyroid hormone peptide probe. *Proceedings of the National Academy of Sciences*, *104*(16), 6846–6851. https://doi.org/10.1073/pnas.0605125104

Carter, P. H., Shimizu, M., Luck, M. D., & Gardella, T. J. (1999). The Hydrophobic Residues Phenylalanine 184 and Leucine 187 in the Type-1 Parathyroid Hormone (PTH) Receptor Functionally Interact with the Amino-terminal Portion of PTH-(1–34)*. *Journal of Biological Chemistry*, *274*(45), 31955–31960. https://doi.org/10.1074/jbc.274.45.31955

Cassel, D., & Selinger, Z. (1976). Catecholamine-stimulated GTPase activity in turkey erythrocyte membranes. *Biochimica et Biophysica Acta (BBA) - Enzymology*, *452*(2), 538–551. https://doi.org/10.1016/0005-2744(76)90206-0

Castro, M., Nikolaev, V. O., Palm, D., Lohse, M. J., & Vilardaga, J.-P. (2005). Turn-on switch in parathyroid hormone receptor by a two-step parathyroid hormone binding mechanism. *Proceedings of the National Academy of Sciences of the United States of America*, *102*(44), 16084–16089. https://doi.org/10.1073/pnas.0503942102

Cegla, J., Jones, B. J., Gardiner, J. V., Hodson, D. J., Marjot, T., McGlone, E. R., Tan, T. M., & Bloom, S. R. (2017). RAMP2 Influences Glucagon Receptor Pharmacology via Trafficking and Signaling. *Endocrinology*, *158*(8), 2680–2693. https://doi.org/10.1210/en.2016-1755

Chang, W., Tu, C.-L., Jean-Alphonse, F. G., Herberger, A., Cheng, Z., Hwong, J., Ho, H., Li, A., Wang, D., Liu, H., White, A. D., Suh, I., Shen, W., Duh, Q.-Y., Khanafshar, E., Shoback, D. M., Xiao, K., & Vilardaga, J.-P. (2020). PTH hypersecretion triggered by a GABA B1 and Ca 2+ -sensing receptor heterocomplex in hyperparathyroidism. *Nature Metabolism*, 1–13. https://doi.org/10.1038/s42255-020-0175-z

Chaturvedi, M., Maharana, J., & Shukla, A. K. (2020). Terminating G-Protein Coupling: Structural Snapshots of GPCR-β-Arrestin Complexes. *Cell*, *180*(6), 1041–1043. https://doi.org/10.1016/j.cell.2020.02.047

Chavez-Abiega, S., Grönloh, M. L. B., Gadella, T. W. J., Bruggeman, F. J., & Goedhart, J. (2022). Single cell imaging of ERK and Akt activation dynamics and heterogeneity induced by G protein-coupled receptors. *Journal of Cell Science*, jcs.259685. https://doi.org/10.1242/jcs.259685

Cheloha, R. W., Gellman, S. H., Vilardaga, J.-P., & Gardella, T. J. (2015a). PTH receptor-1 signalling—Mechanistic insights and therapeutic prospects. *Nature Reviews Endocrinology*, *11*(12), nrendo.2015.139. https://doi.org/10.1038/nrendo.2015.139

Cheloha, R. W., Gellman, S. H., Vilardaga, J.-P., & Gardella, T. J. (2015b). PTH receptor-1 signalling—Mechanistic insights and therapeutic prospects. *Nature Reviews Endocrinology*, *11*(12), 712–724. https://doi.org/10.1038/nrendo.2015.139

Chen, Q., Plasencia, M., Li, Z., Mukherjee, S., Patra, D., Chen, C.-L., Klose, T., Yao, X.-Q., Kossiakoff, A. A., Chang, L., Andrews, P. C., & Tesmer, J. J. G. (2021). Structures of rhodopsin in complex with G-protein-coupled receptor kinase 1. *Nature*, *595*(7868), 600–605. https://doi.org/10.1038/s41586-021-03721-x

Chen, T.-W., Wardill, T. J., Sun, Y., Pulver, S. R., Renninger, S. L., Baohan, A., Schreiter, E. R., Kerr, R. A., Orger, M. B., Jayaraman, V., Looger, L. L., Svoboda, K., & Kim, D. S. (2013). Ultrasensitive fluorescent proteins for imaging neuronal activity. *Nature*, *499*(7458), 295–300. https://doi.org/10.1038/nature12354

Christopoulos, A., Christopoulos, G., Morfis, M., Udawela, M., Laburthe, M., Couvineau, A., Kuwasako, K., Tilakaratne, N., & Sexton, P. M. (2003). Novel Receptor Partners and Function of Receptor Activity-modifying Proteins. *Journal of Biological Chemistry*, *278*(5), 3293–3297. https://doi.org/10.1074/jbc.C200629200

Chudakov, D. M., Matz, M. V., Lukyanov, S., & Lukyanov, K. A. (2010). Fluorescent Proteins and Their Applications in Imaging Living Cells and Tissues. *Https://Doi.Org/10.1152/Physrev.00038.2009*. https://doi.org/10.1152/physrev.00038.2009

Clark, A. J., Mullooly, N., Safitri, D., Harris, M., de Vries, T., MaassenVanDenBrink, A., Poyner, D. R., Gianni, D., Wigglesworth, M., & Ladds, G. (2021). CGRP, adrenomedullin and adrenomedullin 2 display endogenous GPCR agonist bias in primary human cardiovascular cells. *Communications Biology*, *4*(1), 1–12. https://doi.org/10.1038/s42003-021-02293-w

Clark, L. J., Krieger, J., White, A. D., Bondarenko, V., Lei, S., Fang, F., Lee, J. Y., Doruker, P., Böttke, T., Jean-Alphonse, F., Tang, P., Gardella, T. J., Xiao, K., Sutkeviciute, I., Coin, I., Bahar, I., & Vilardaga, J.-P. (2020a). Allosteric interactions in the parathyroid hormone GPCR–arrestin complex formation. *Nature Chemical Biology*, *16*(10), 1096–1104. https://doi.org/10.1038/s41589-020-0567-0

Clark, L. J., Krieger, J., White, A. D., Bondarenko, V., Lei, S., Fang, F., Lee, J. Y., Doruker, P., Böttke, T., Jean-Alphonse, F., Tang, P., Gardella, T. J., Xiao, K., Sutkeviciute, I., Coin, I., Bahar, I., & Vilardaga, J.-P. (2020b). Allosteric interactions in the parathyroid hormone GPCR–arrestin complex formation. *Nature Chemical Biology*, *16*(10), 1096–1104. https://doi.org/10.1038/s41589-020-0567-0

Codina, J., Hildebrandt, J. D., Sekura, R. D., Birnbaumer, M., Bryan, J., Manclark, C. R., Iyengar, R., & Birnbaumer, L. (1984). Ns and Ni, the stimulatory and inhibitory regulatory components of adenylyl cyclases. Purification of the human erythrocyte proteins without the use of activating regulatory ligands. *Journal of Biological Chemistry*, *259*(9), 5871–5886. https://doi.org/10.1016/S0021-9258(18)91097-5

Cong, Z., Liang, Y.-L., Zhou, Q., Darbalaei, S., Zhao, F., Feng, W., Zhao, L., Xu, H. E., Yang, D., & Wang, M.-W. (2022). Structural perspective of class B1 GPCR signaling. *Trends in Pharmacological Sciences*. https://doi.org/10.1016/j.tips.2022.01.002

Craft, C. M., Whitmore, D. H., & Wiechmann, A. F. (1994). Cone arrestin identified by targeting expression of a functional family. *Journal of Biological Chemistry*, *269*(6), 4613–4619. https://doi.org/10.1016/S0021-9258(17)41820-5

dal Maso, E., Glukhova, A., Zhu, Y., Garcia-Nafria, J., Tate, C. G., Atanasio, S., Reynolds, C. A., Ramírez-Aportela, E., Carazo, J.-M., Hick, C. A., Furness, S. G. B., Hay, D. L., Liang, Y.-L., Miller, L. J., Christopoulos, A., Wang, M.-W., Wootten, D., & Sexton, P. M. (2019). The Molecular Control of Calcitonin Receptor Signaling. *ACS Pharmacology & Translational Science*, *2*(1), 31–51. https://doi.org/10.1021/acsptsci.8b00056

Damian, M., Louet, M., Gomes, A. A. S., M'Kadmi, C., Denoyelle, S., Cantel, S., Mary, S., Bisch, P. M., Fehrentz, J.-A., Catoire, L. J., Floquet, N., & Banères, J.-L. (2021). Allosteric modulation of ghrelin receptor signaling by lipids. *Nature Communications*, *12*(1), 3938. https://doi.org/10.1038/s41467-021-23756-y

de la Cova, C., Townley, R., Regot, S., & Greenwald, I. (2017). A Real-Time Biosensor for ERK Activity Reveals Signaling Dynamics during C. elegans Cell Fate Specification. *Developmental Cell*, *42*(5), 542-553.e4. https://doi.org/10.1016/j.devcel.2017.07.014

Dean, T., Linglart, A., Mahon, M. J., Bastepe, M., Jüppner, H., Potts, J. T., Jr., & Gardella, T. J. (2006). Mechanisms of Ligand Binding to the Parathyroid Hormone (PTH)/PTH-Related Protein Receptor: Selectivity of a Modified PTH(1–15) Radioligand for GαS-Coupled Receptor Conformations. *Molecular Endocrinology*, *20*(4), 931–943. https://doi.org/10.1210/me.2005-0349

Dean, T., Vilardaga, J.-P., Potts, J. T., & Gardella, T. J. (2008). Altered Selectivity of Parathyroid Hormone (PTH) and PTH-Related Protein (PTHrP) for Distinct Conformations of the PTH/PTHrP Receptor. *Molecular Endocrinology*, *22*(1), 156–166. https://doi.org/10.1210/me.2007-0274

Deganutti, G., Liang, Y.-L., Zhang, X., Khoshouei, M., Clydesdale, L., Belousoff, M. J., Venugopal, H., Truong, T. T., Glukhova, A., Keller, A. N., Gregory, K. J., Leach, K., Christopoulos, A., Danev, R., Reynolds, C. A., Zhao, P., Sexton, P. M., & Wootten, D. (2022). Dynamics of GLP-1R peptide agonist engagement are correlated with kinetics of G protein activation. *Nature Communications*, *13*(1), 92. https://doi.org/10.1038/s41467-021-27760-0

Deupi, X., & Kobilka, B. (2007). Activation of G Protein–Coupled Receptors. In *Advances in Protein Chemistry* (Vol. 74, pp. 137–166). Academic Press. https://doi.org/10.1016/S0065-3233(07)74004-4

Deupi, X., & Kobilka, B. K. (2010). Energy landscapes as a tool to integrate GPCR structure, dynamics and function. *Physiology (Bethesda, Md.)*, *25*(5), 293–303. https://doi.org/10.1152/physiol.00002.2010

Dicker, F., Quitterer, U., Winstel, R., Honold, K., & Lohse, M. J. (1999). Phosphorylation-independent inhibition of parathyroid hormone receptor signaling by G protein-coupled receptor kinases. *Proceedings of the National Academy of Sciences*, *96*(10), 5476–5481. https://doi.org/10.1073/pnas.96.10.5476

DiPilato, L. M., Cheng, X., & Zhang, J. (2004). Fluorescent indicators of cAMP and Epac activation reveal differential dynamics of cAMP signaling within discrete subcellular compartments. *Proceedings of the National Academy of Sciences*, *101*(47), 16513–16518. https://doi.org/10.1073/pnas.0405973101

Dolgin, E. (2018). First GPCR-directed antibody passes approval milestone. *Nature Reviews Drug Discovery*, *17*(7), 457–459. https://doi.org/10.1038/nrd.2018.103

Dong, S. S., Goddard, W. A., & Abrol, R. (2016). Conformational and Thermodynamic Landscape of GPCR Activation from Theory and Computation. *Biophysical Journal*, *110*(12), 2618–2629. https://doi.org/10.1016/j.bpj.2016.04.028

Donthamsetti, P. C., Broichhagen, J., Vyklicky, V., Stanley, C., Fu, Z., Visel, M., Levitz, J. L., Javitch, J. A., Trauner, D., & Isacoff, E. Y. (2019). Genetically Targeted Optical Control of an Endogenous G Protein-Coupled Receptor. *Journal of the American Chemical Society*, *141*(29), 11522–11530. https://doi.org/10.1021/jacs.9b02895

Donthamsetti, P., Konrad, D. B., Hetzler, B., Fu, Z., Trauner, D., & Isacoff, E. Y. (2021). Selective Photoswitchable Allosteric Agonist of a G Protein-Coupled Receptor. *Journal of the American Chemical Society*, *143*(24), 8951–8956. https://doi.org/10.1021/jacs.1c02586

Donthamsetti, P., Winter, N., Hoagland, A., Stanley, C., Visel, M., Lammel, S., Trauner, D., & Isacoff, E. (2021). Cell specific photoswitchable agonist for reversible control of endogenous dopamine receptors. *Nature Communications*, *12*(1), 4775. https://doi.org/10.1038/s41467-021-25003-w

Downes, G. B., & Gautam, N. (1999). The G Protein Subunit Gene Families. *Genomics*, *62*(3), 544–552. https://doi.org/10.1006/geno.1999.5992

Dror, R. O., Arlow, D. H., Maragakis, P., Mildorf, T. J., Pan, A. C., Xu, H., Borhani, D. W., & Shaw, D. E. (2011). Activation mechanism of the β2-adrenergic receptor. *Proceedings of the National Academy of Sciences*, *108*(46), 18684–18689. https://doi.org/10.1073/pnas.1110499108

Drube, J., Haider, R. S., Matthees, E. S. F., Reichel, M., Zeiner, J., Fritzwanker, S., Ziegler, C., Barz, S., Klement, L., Filor, J., Weitzel, V., Kliewer, A., Miess-Tanneberg, E., Kostenis, E., Schulz, S., & Hoffmann, C. (2022a). GPCR kinase knockout cells reveal the impact of individual GRKs on arrestin binding and GPCR regulation. *Nature Communications*, *13*(1), 540. https://doi.org/10.1038/s41467-022-28152-8

Drube, J., Haider, R. S., Matthees, E. S. F., Reichel, M., Zeiner, J., Fritzwanker, S., Ziegler, C., Barz, S., Klement, L., Filor, J., Weitzel, V., Kliewer, A., Miess-Tanneberg, E., Kostenis, E., Schulz, S., & Hoffmann, C. (2022b). GPCR kinase knockout cells reveal the impact of individual GRKs on arrestin binding and GPCR regulation. *Nature Communications*, *13*(1), 540. https://doi.org/10.1038/s41467-022-28152-8

Drugs@FDA: FDA-Approved Drugs. (n.d.). Retrieved March 21, 2022, from https://www.accessdata.fda.gov/scripts/cder/daf/index.cfm?event=overview.process&ApplNo=211939

Dunlay, R., & Hruska, K. (1990). PTH receptor coupling to phospholipase C is an alternate pathway of signal transduction in bone and kidney. *American Journal of Physiology-Renal Physiology*, *258*(2), F223–F231. https://doi.org/10.1152/ajprenal.1990.258.2.F223

Ehrenmann, J., Schöppe, J., Klenk, C., Rappas, M., Kummer, L., Doré, A. S., & Plückthun, A. (2018). High-resolution crystal structure of parathyroid hormone 1 receptor in complex with a peptide agonist. *Nature Structural & Molecular Biology*, 1. https://doi.org/10.1038/s41594-018-0151-4

EMA. (2022, March 21). *Medicines* [Text]. European Medicines Agency. https://www.ema.europa.eu/en/medicines

Evans, R., O'Neill, M., Pritzel, A., Antropova, N., Senior, A., Green, T., Žídek, A., Bates, R., Blackwell, S., Yim, J., Ronneberger, O., Bodenstein, S., Zielinski, M., Bridgland, A., Potapenko, A., Cowie, A., Tunyasuvunakool, K., Jain, R., Clancy, E., … Hassabis, D. (2021). *Protein complex prediction with AlphaFold-Multimer* (p. 2021.10.04.463034). bioRxiv. https://doi.org/10.1101/2021.10.04.463034

Evans, R., O'Neill, M., Pritzel, A., Antropova, N., Senior, A., Green, T., Žídek, A., Bates, R., Blackwell, S., Yim, J., Ronneberger, O., Bodenstein, S., Zielinski, M., Bridgland, A., Potapenko, A., Cowie, A., Tunyasuvunakool, K., Jain, R., Clancy, E., … Hassabis, D. (2022). *Protein complex prediction with AlphaFold-Multimer* (p. 2021.10.04.463034). bioRxiv. https://doi.org/10.1101/2021.10.04.463034

F, S., J, Z., M, J., J, Z., J, F., SF, O., Y, L., F, L., H, W., T, Y., Z, Y., Y, G., W, P., L, W., S, Z., J, D., D, L., M, X., AC, K., … Y, L. (2018). A Genetically Encoded Fluorescent Sensor Enables Rapid and Specific Detection of Dopamine in Flies, Fish, and Mice. *Cell*, *174*(2). https://doi.org/10.1016/j.cell.2018.06.042

Fahrenkrug, J., Goetzl, E. J., Gozes, I., Harmar, A., Laburthe, M., May, V., Pisegna, J. R., Said, S. I., Vaudry, D., Vaudry, H., & Waschek, J. A. (2019). VIP and PACAP receptors (version 2019.4) in the IUPHAR/BPS Guide to Pharmacology Database. *IUPHAR/BPS Guide to Pharmacology CITE*, *2019*(4), Article 4. https://doi.org/10.2218/gtopdb/F67/2019.4

Feinstein, T. N., Yui, N., Webber, M. J., Wehbi, V. L., Stevenson, H. P., King, J. D., Hallows, K. R., Brown, D., Bouley, R., & Vilardaga, J.-P. (2013). Noncanonical Control of Vasopressin Receptor Type 2 Signaling by Retromer and Arrestin *. *Journal of Biological Chemistry*, *288*(39), 27849–27860. https://doi.org/10.1074/jbc.M112.445098

Fenton, A. J., Kemp, B. E., Hammonds, R. G., JR., Mitchelhill, K., Moseley, J. M., Martin, T. J., & Nicholson, G. C. (1991). A POTENT INHIBITOR OF OSTEOCLASTIC BONE RESORPTION WITHIN A HIGHLY CONSERVED PENTAPEPTIDE REGION OF PARATHYROID HORMONE-RELATED PROTEIN; PTHrP[107–lll]. *Endocrinology*, *129*(6), 3424–3426. https://doi.org/10.1210/endo-129-6-3424

FENTON, A. J., KEMP, B. E., KENT, G. N., MOSELEY, J. M., ZHENG, M.-H., ROWE, D. J., BRITTO, J. M., MARTIN, T. J., & NICHOLSON, G. C. (1991). A Carboxyl-Terminal Peptide from the Parathyroid Hormone-Related Protein Inhibits Bone Resorption by Osteoclasts*. *Endocrinology*, *129*(4), 1762–1768. https://doi.org/10.1210/endo-129-4-1762

Ferguson, S. S. G., Zhang, J., Barakt, L. S., & Caron, M. G. (1998). Molecular mechanisms of G protein-coupled receptor desensitization and resensitization. *Life Sciences*, *62*(17), 1561–1565. https://doi.org/10.1016/S0024-3205(98)00107-6

Ferrandon, S., Feinstein, T. N., Castro, M., Wang, B., Bouley, R., Potts, J. T., Gardella, T. J., & Vilardaga, J.-P. (2009). Sustained cyclic AMP production by parathyroid hormone receptor endocytosis. *Nature Chemical Biology*, *5*(10), 734–742. https://doi.org/10.1038/nchembio.206

Ferrari, S. L., Behar, V., Chorev, M., Rosenblatt, M., & Bisello, A. (1999). Endocytosis of Ligand-Human Parathyroid Hormone Receptor 1 Complexes Is Protein Kinase C-dependent and Involves β-Arrestin2: REAL-TIME MONITORING BY FLUORESCENCE MICROSCOPY*. *Journal of Biological Chemistry*, *274*(42), 29968–29975. https://doi.org/10.1074/jbc.274.42.29968

Ferrari, S. L., Pierroz, D. D., Glatt, V., Goddard, D. S., Bianchi, E. N., Lin, F. T., Manen, D., & Bouxsein, M. L. (2005). Bone Response to Intermittent Parathyroid Hormone Is Altered in Mice Null for β-Arrestin2. *Endocrinology*, *146*(4), 1854–1862. https://doi.org/10.1210/en.2004-1282

Ferré, S., Casadó, V., Devi, L. A., Filizola, M., Jockers, R., Lohse, M. J., Milligan, G., Pin, J.-P., & Guitart, X. (2014). G Protein–Coupled Receptor Oligomerization Revisited: Functional and Pharmacological Perspectives. *Pharmacological Reviews*, *66*(2), 413–434. https://doi.org/10.1124/pr.113.008052

Fleetwood, O., Matricon, P., Carlsson, J., & Delemotte, L. (2020). Energy Landscapes Reveal Agonist Control of G Protein-Coupled Receptor Activation via Microswitches. *Biochemistry*, *59*(7), 880–891. https://doi.org/10.1021/acs.biochem.9b00842

Flock, T., Hauser, A. S., Lund, N., Gloriam, D. E., Balaji, S., & Babu, M. M. (2017). Selectivity determinants of GPCR-G-protein binding. *Nature*, *545*(7654), 317–322. https://doi.org/10.1038/nature22070

Förster, T. (1948). Zwischenmolekulare Energiewanderung und Fluoreszenz. *Annalen Der Physik*, *Wiley Online Library*. https://doi.org/10.1002/andp.19484370105

Foster, S. R., Roura, E., Molenaar, P., & Thomas, W. G. (2015). G protein-coupled receptors in cardiac biology: Old and new receptors. *Biophysical Reviews*, *7*(1), 77–89. https://doi.org/10.1007/s12551-014-0154-2

Fredriksson, R., Lagerström, M. C., Lundin, L.-G., & Schiöth, H. B. (2003). The G-Protein-Coupled Receptors in the Human Genome Form Five Main Families. Phylogenetic Analysis, Paralogon Groups, and Fingerprints. *Molecular Pharmacology*, *63*(6), 1256–1272. https://doi.org/10.1124/mol.63.6.1256

Furness, S. G. B., Liang, Y.-L., Nowell, C. J., Halls, M. L., Wookey, P. J., Dal Maso, E., Inoue, A., Christopoulos, A., Wootten, D., & Sexton, P. M. (2016). Ligand-Dependent Modulation of G Protein Conformation Alters Drug Efficacy. *Cell*, *167*(3), 739-749.e11. https://doi.org/10.1016/j.cell.2016.09.021

Gardella, T. J., & Vilardaga, J.-P. (2015). International Union of Basic and Clinical Pharmacology. XCIII. The Parathyroid Hormone Receptors—Family B G Protein–Coupled Receptors. *Pharmacological Reviews*, *67*(2), 310–337. https://doi.org/10.1124/pr.114.009464

Garelja, M. L., Au, M., Brimble, M. A., Gingell, J. J., Hendrikse, E. R., Lovell, A., Prodan, N., Sexton, P. M., Siow, A., Walker, C. S., Watkins, H. A., Williams, G. M., Wootten, D., Yang, S. H., Harris, P. W. R., & Hay, D. L. (2020). Molecular Mechanisms of Class B GPCR Activation: Insights from Adrenomedullin Receptors. *ACS Pharmacology & Translational Science*, *3*(2), 246–262. https://doi.org/10.1021/acsptsci.9b00083

Gelbert, L., Schipani, E., Jüppner, H., Abou-Samra, A. B., Segre, G. V., Naylor, S., Drabkin, H., & Heath, H., 3rd. (1994). Chromosomal localization of the parathyroid hormone/parathyroid hormone-related protein receptor gene to human chromosome 3p21.1-p24.2. *The Journal of Clinical Endocrinology & Metabolism*, *79*(4), 1046–1048. https://doi.org/10.1210/jcem.79.4.7962272

Gentry, P. R., Sexton, P. M., & Christopoulos, A. (2015). Novel Allosteric Modulators of G Protein-coupled Receptors. *The Journal of Biological Chemistry*, *290*(32), 19478–19488. https://doi.org/10.1074/jbc.R115.662759

George, S. R., O'Dowd, B. F., & Lee, S. P. (2002). G-Protein-coupled receptor oligomerization and its potential for drug discovery. *Nature Reviews Drug Discovery*, *1*(10), 808–820. https://doi.org/10.1038/nrd913

Gesty-Palmer, D., Chen, M., Reiter, E., Ahn, S., Nelson, C. D., Wang, S., Eckhardt, A. E., Cowan, C. L., Spurney, R. F., Luttrell, L. M., & Lefkowitz, R. J. (2006). Distinct β-Arrestin- and G Protein-dependent Pathways for Parathyroid Hormone Receptor-stimulated ERK1/2 Activation *. *Journal of Biological Chemistry*, *281*(16), 10856–10864. https://doi.org/10.1074/jbc.M513380200

Gesty-Palmer, D., Flannery, P., Yuan, L., Corsino, L., Spurney, R., Lefkowitz, R. J., & Luttrell, L. M. (2009). A β-Arrestin–Biased Agonist of the Parathyroid Hormone Receptor (PTH1R) Promotes Bone Formation Independent of G Protein Activation. *Science Translational Medicine*, *1*(1), 1ra1. https://doi.org/10.1126/scitranslmed.3000071

Gesty-Palmer, D., & Luttrell, L. M. (2011). 'Biasing' the parathyroid hormone receptor: A novel anabolic approach to increasing bone mass? *British Journal of Pharmacology*, *164*(1), 59–67. https://doi.org/10.1111/j.1476-5381.2011.01450.x

Gidon, A., Feinstein, T. N., Xiao, K., & Vilardaga, J.-P. (2016). Studying the regulation of endosomal cAMP production in GPCR signaling. *Methods in Cell Biology*, *132*, 109–126. https://doi.org/10.1016/bs.mcb.2015.10.007

Gilman, A. G. (1987). G Proteins: Transducers of Receptor-Generated Signals. *Annual Review of Biochemistry*, *56*(1), 615–649. https://doi.org/10.1146/annurev.bi.56.070187.003151

Godbole, A., Lyga, S., Lohse, M. J., & Calebiro, D. (2017). Internalized TSH receptors en route to the TGN induce local Gs-protein signaling and gene transcription. *Nature Communications*, *8*(1), 443. https://doi.org/10.1038/s41467-017-00357-2

Goedhart, J., von Stetten, D., Noirclerc-Savoye, M., Lelimousin, M., Joosen, L., Hink, M. A., van Weeren, L., Gadella, T. W. J., & Royant, A. (2012). Structure-guided evolution of cyan fluorescent proteins towards a quantum yield of 93%. *Nature Communications*, *3*(1), 1–9. https://doi.org/10.1038/ncomms1738

Goltzman, D. (1999). Interactions of PTH and PTHrP with the PTH/PTHrP Receptor and with Downstream Signaling Pathways: Exceptions That Provide the Rules. *Journal of Bone and Mineral Research*, *14*(2), 173–177. https://doi.org/10.1359/jbmr.1999.14.2.173

Gonzalez, F. A., Raden, D. L., & Davis, R. J. (1991). Identification of substrate recognition determinants for human ERK1 and ERK2 protein kinases. *Journal of Biological Chemistry*, *266*(33), 22159–22163. https://doi.org/10.1016/S0021-9258(18)54548-8

Grauschopf, U., Lilie, H., Honold, K., Wozny, M., Reusch, D., Esswein, A., Schäfer, W., Rücknagel, K. P., & Rudolph, R. (2000). The N-Terminal Fragment of Human Parathyroid Hormone Receptor 1 Constitutes a Hormone Binding Domain and Reveals a Distinct Disulfide Pattern. *Biochemistry*, *39*(30), 8878–8887. https://doi.org/10.1021/bi0001426

Gregorio, G. G., Masureel, M., Hilger, D., Terry, D. S., Juette, M., Zhao, H., Zhou, Z., Perez-Aguilar, J. M., Hauge, M., Mathiasen, S., Javitch, J. A., Weinstein, H., Kobilka, B. K., & Blanchard, S. C. (2017). Single-molecule analysis of ligand efficacy in β2AR–G-protein activation. *Nature*, *547*(7661), 68–73. https://doi.org/10.1038/nature22354

Grimm, J. B., English, B. P., Choi, H., Muthusamy, A. K., Mehl, B. P., Dong, P., Brown, T. A., Lippincott-Schwartz, J., Liu, Z., Lionnet, T., & Lavis, L. D. (2016). Bright photoactivatable fluorophores for single-molecule imaging. *Nature Methods*, *13*(12), 985–988. https://doi.org/10.1038/nmeth.4034

Grimm, J. B., Muthusamy, A. K., Liang, Y., Brown, T. A., Lemon, W. C., Patel, R., Lu, R., Macklin, J. J., Keller, P. J., Ji, N., & Lavis, L. D. (2017). A general method to fine-tune fluorophores for live-cell and in vivo imaging. *Nature Methods*, *14*(10), 987–994. https://doi.org/10.1038/nmeth.4403

Grimm, J. B., Tkachuk, A. N., Xie, L., Choi, H., Mohar, B., Falco, N., Schaefer, K., Patel, R., Zheng, Q., Liu, Z., Lippincott-Schwartz, J., Brown, T. A., & Lavis, L. D. (2020). A general method to optimize and functionalize red-shifted rhodamine dyes. *Nature Methods*, *17*(8), 815–821. https://doi.org/10.1038/s41592-020-0909-6

Grundmann, M., & Kostenis, E. (2017). Temporal Bias: Time-Encoded Dynamic GPCR Signaling. *Trends in Pharmacological Sciences*, *38*(12), 1110–1124. https://doi.org/10.1016/j.tips.2017.09.004

Grundmann, M., Merten, N., Malfacini, D., Inoue, A., Preis, P., Simon, K., Rüttiger, N., Ziegler, N., Benkel, T., Schmitt, N. K., Ishida, S., Müller, I., Reher, R., Kawakami, K., Inoue, A., Rick, U., Kühl, T., Imhof, D., Aoki, J., … Kostenis, E. (2018). Lack of beta-arrestin signaling in the absence of active G proteins. *Nature Communications*, *9*(1), 341. https://doi.org/10.1038/s41467-017-02661-3

Grushevskyi, E. O., Kukaj, T., Schmauder, R., Bock, A., Zabel, U., Schwabe, T., Benndorf, K., & Lohse, M. J. (2019). Stepwise activation of a class C GPCR begins with millisecond dimer rearrangement. *Proceedings of the National Academy of Sciences*, *116*(20), 10150–10155. https://doi.org/10.1073/pnas.1900261116

Gurevich, V. V., & Gurevich, E. V. (2019). GPCR Signaling Regulation: The Role of GRKs and Arrestins. *Frontiers in Pharmacology*, *10*. https://www.frontiersin.org/article/10.3389/fphar.2019.00125

Gusach, A., Maslov, I., Luginina, A., Borshchevskiy, V., Mishin, A., & Cherezov, V. (2020). Beyond structure: Emerging approaches to study GPCR dynamics. *Current Opinion in Structural Biology*, *63*, 18–25. https://doi.org/10.1016/j.sbi.2020.03.004

Harada, K., Ito, M., Wang, X., Tanaka, M., Wongso, D., Konno, A., Hirai, H., Hirase, H., Tsuboi, T., & Kitaguchi, T. (2017). Red fluorescent protein-based cAMP indicator applicable to optogenetics and in vivo imaging. *Scientific Reports*, *7*, 7351. https://doi.org/10.1038/s41598-017-07820-6

Harris, M., Mackie, D. I., Pawlak, J. B., Carvalho, S., Truong, T. T., Safitri, D., Yeung, H. Y., Routledge, S., Harper, M. T., Al-Zaid, B., Soave, M., Al-Sabah, S., Inoue, A., Poyner, D. R., Hill, S. J., Briddon, S. J., Sexton, P. M., Wootten, D., Zhao, P., … Ladds, G. (2021a). *RAMPs regulate signalling bias and internalisation of the GIPR* (p. 2021.04.08.436756). bioRxiv. https://doi.org/10.1101/2021.04.08.436756

Harris, M., Mackie, D. I., Pawlak, J. B., Carvalho, S., Truong, T. T., Safitri, D., Yeung, H. Y., Routledge, S., Harper, M. T., Al-Zaid, B., Soave, M., Al-Sabah, S., Inoue, A., Poyner, D. R., Hill, S. J., Briddon, S. J., Sexton, P. M., Wootten, D., Zhao, P., … Ladds, G. (2021b). *RAMPs regulate signalling bias and internalisation of the GIPR* (p. 2021.04.08.436756). bioRxiv. https://doi.org/10.1101/2021.04.08.436756

Harvey, C. D., Ehrhardt, A. G., Cellurale, C., Zhong, H., Yasuda, R., Davis, R. J., & Svoboda, K. (2008). A genetically encoded fluorescent sensor of ERK activity. *Proceedings of the National Academy of Sciences*, *105*(49), 19264–19269. https://doi.org/10.1073/pnas.0804598105

Hausdorff, W. P., Bouvier, M., O'Dowd, B. F., Irons, G. P., Caron, M. G., & Lefkowitz, R. J. (1989). Phosphorylation Sites on Two Domains of the β2-Adrenergic Receptor Are Involved in Distinct Pathways of Receptor Desensitization. *Journal of Biological Chemistry*, *264*(21), 12657–12665. https://doi.org/10.1016/S0021-9258(18)63907-9

Hauser, A. S., Attwood, M. M., Rask-Andersen, M., Schiöth, H. B., & Gloriam, D. E. (2017). Trends in GPCR drug discovery: New agents, targets and indications. *Nature Reviews Drug Discovery*, *16*(12), 829–842. https://doi.org/10.1038/nrd.2017.178

Hauser, A. S., Avet, C., Normand, C., Mancini, A., Inoue, A., Bouvier, M., & Gloriam, D. E. (2022). Common coupling map advances GPCR-G protein selectivity. *ELife*, *11*, e74107. https://doi.org/10.7554/eLife.74107

Hauser, A. S., Chavali, S., Masuho, I., Jahn, L. J., Martemyanov, K. A., Gloriam, D. E., & Babu, M. M. (2018). Pharmacogenomics of GPCR Drug Targets. *Cell*, *172*(1), 41-54.e19. https://doi.org/10.1016/j.cell.2017.11.033

Hauser, A. S., Kooistra, A. J., Munk, C., Heydenreich, F. M., Veprintsev, D. B., Bouvier, M., Babu, M. M., & Gloriam, D. E. (2021). GPCR activation mechanisms across classes and macro/microscales. *Nature Structural & Molecular Biology*, *28*(11), 879–888. https://doi.org/10.1038/s41594-021-00674-7

Hay, D. L., & Pioszak, A. A. (2016a). Receptor Activity-Modifying Proteins (RAMPs): New Insights and Roles. *Annual Review of Pharmacology and Toxicology*, *56*(1), 469–487. https://doi.org/10.1146/annurev-pharmtox-010715-103120

Hay, D. L., & Pioszak, A. A. (2016b). Receptor Activity-Modifying Proteins (RAMPs): New Insights and Roles. *Annual Review of Pharmacology and Toxicology*, *56*(1), 469–487. https://doi.org/10.1146/annurev-pharmtox-010715-103120

Hay, D. L., Walker, C. S., Gingell, J. J., Ladds, G., Reynolds, C. A., & Poyner, D. R. (2016). Receptor activity-modifying proteins; multifunctional G protein-coupled receptor accessory proteins. *Biochemical Society Transactions*, *44*(2), 568–573. https://doi.org/10.1042/BST20150237

Hay, D., Poyner, D. R., & Walker, C. S. (2021). Calcitonin receptors in GtoPdb v.2021.2. *IUPHAR/BPS Guide to Pharmacology CITE*, *2021*(2), Article 2. https://doi.org/10.2218/gtopdb/F11/2021.2

Hens, J. R., & Wysolmerski, J. J. (2005). Key stages of mammary gland development: Molecular mechanisms involved in the formation of the embryonic mammary gland. *Breast Cancer Research*, *7*(5), 220–224. https://doi.org/10.1186/bcr1306

Heydenreich, F. M., Marti-Solano, M., Sandhu, M., Kobilka, B. K., Bouvier, M., & Babu, M. M. (2021). *Dissecting the allosteric networks governing agonist efficacy and potency in G protein-coupled receptors* (p. 2021.09.14.460253). bioRxiv. https://doi.org/10.1101/2021.09.14.460253

Hilger, D., Kumar, K. K., Hu, H., Pedersen, M. F., O'Brien, E. S., Giehm, L., Jennings, C., Eskici, G., Inoue, A., Lerch, M., Mathiesen, J. M., Skiniotis, G., & Kobilka, B. K. (2020). Structural insights into differences in G protein activation by family A and family B GPCRs. *Science*, *369*(6503), eaba3373. https://doi.org/10.1126/science.aba3373

Hilger, D., Masureel, M., & Kobilka, B. K. (2018). Structure and dynamics of GPCR signaling complexes. *Nature Structural & Molecular Biology*, *25*(1), 4–12. https://doi.org/10.1038/s41594-017-0011-7

Hill, S. J. (2006). G-protein-coupled receptors: Past, present and future. *British Journal of Pharmacology*, *147*(Suppl 1), S27–S37. https://doi.org/10.1038/sj.bjp.0706455

Hlavackova, V., Zabel, U., Frankova, D., Bätz, J., Hoffmann, C., Prezeau, L., Pin, J.-P., Blahos, J., & Lohse, M. J. (2012). Sequential Inter- and Intrasubunit Rearrangements During Activation of Dimeric Metabotropic Glutamate Receptor 1. *Sci. Signal.*, *5*(237), ra59–ra59. https://doi.org/10.1126/scisignal.2002720

Hoare, S. R. J., Gardella, T. J., & Usdin, T. B. (2001). Evaluating the Signal Transduction Mechanism of the Parathyroid Hormone 1 Receptor: EFFECT OF RECEPTOR-G-PROTEIN INTERACTION ON THE LIGAND BINDING MECHANISM AND RECEPTOR CONFORMATION *. *Journal of Biological Chemistry*, *276*(11), 7741–7753. https://doi.org/10.1074/jbc.M009395200

Hoare, S. R. J., & Usdin, T. B. (2000). Tuberoinfundibular Peptide (7-39) [TIP(7-39)], a Novel, Selective, High-Affinity Antagonist for the Parathyroid Hormone-1 Receptor with No Detectable Agonist Activity. *Journal of Pharmacology and Experimental Therapeutics*, *295*(2), 761–770.

Hollenstein, K., de Graaf, C., Bortolato, A., Wang, M.-W., Marshall, F. H., & Stevens, R. C. (2014). Insights into the structure of class B GPCRs. *Trends in Pharmacological Sciences*, *35*(1), 12–22. https://doi.org/10.1016/j.tips.2013.11.001

Hüll, K., Morstein, J., & Trauner, D. (2018). *In Vivo Photopharmacology*. https://doi.org/10.1021/acs.chemrev.8b00037

Ichikawa-Shindo, Y., Sakurai, T., Kamiyoshi, A., Kawate, H., Iinuma, N., Yoshizawa, T., Koyama, T., Fukuchi, J., Iimuro, S., Moriyama, N., Kawakami, H., Murata, T., Kangawa, K., Nagai, R., & Shindo, T. (2008). The GPCR modulator protein RAMP2 is essential for angiogenesis and vascular integrity. *The Journal of Clinical Investigation*, *118*(1), 29–39. https://doi.org/10.1172/JCI33022

Igarashi, K., Sakurai, T., Kamiyoshi, A., Ichikawa-Shindo, Y., Kawate, H., Yamauchi, A., Toriyama, Y., Tanaka, M., Liu, T., Xian, X., Imai, A., Zhai, L., Owa, S., Koyama, T., Uetake, R., Ihara, M., & Shindo, T. (2014). Pathophysiological roles of adrenomedullin-RAMP2 system in acute and chronic cerebral ischemia. *Peptides*, *62*, 21–31. https://doi.org/10.1016/j.peptides.2014.08.013

Inoue, A., Raimondi, F., Kadji, F. M. N., Singh, G., Kishi, T., Uwamizu, A., Ono, Y., Shinjo, Y., Ishida, S., Arang, N., Kawakami, K., Gutkind, J. S., Aoki, J., & Russell, R. B. (2019). Illuminating G-Protein-Coupling Selectivity of GPCRs. *Cell*, *177*(7), 1933-1947.e25. https://doi.org/10.1016/j.cell.2019.04.044

Irannejad, R., Tomshine, J. C., Tomshine, J. R., Chevalier, M., Mahoney, J. P., Steyaert, J., Rasmussen, S. G. F., Sunahara, R. K., El-Samad, H., Huang, B., & von Zastrow, M. (2013). Conformational biosensors reveal GPCR signalling from endosomes. *Nature*, *495*(7442), 534–538. https://doi.org/10.1038/nature12000

Isberg, V., de Graaf, C., Bortolato, A., Cherezov, V., Katritch, V., Marshall, F. H., Mordalski, S., Pin, J.-P., Stevens, R. C., Vriend, G., & Gloriam, D. E. (2015). Generic GPCR Residue Numbers—Aligning Topology Maps Minding The Gaps. *Trends in Pharmacological Sciences*, *36*(1), 22–31. https://doi.org/10.1016/j.tips.2014.11.001

Isberg, V., Mordalski, S., Munk, C., Rataj, K., Harpsøe, K., Hauser, A. S., Vroling, B., Bojarski, A. J., Vriend, G., & Gloriam, D. E. (2016). GPCRdb: An information system for G protein-coupled receptors. *Nucleic Acids Research*, *44*(D1), D356–D364. https://doi.org/10.1093/nar/gkv1178

Işbilir, A., Möller, J., Arimont, M., Bobkov, V., Perpiñá-Viciano, C., Hoffmann, C., Inoue, A., Heukers, R., Graaf, C. de, Smit, M. J., Annibale, P., & Lohse, M. J. (2020a). Advanced fluorescence microscopy reveals disruption of dynamic CXCR4 dimerization by subpocket-specific inverse agonists. *Proceedings of the National Academy of Sciences*, *117*(46), 29144–29154. https://doi.org/10.1073/pnas.2013319117

Işbilir, A., Möller, J., Arimont, M., Bobkov, V., Perpiñá-Viciano, C., Hoffmann, C., Inoue, A., Heukers, R., Graaf, C. de, Smit, M. J., Annibale, P., & Lohse, M. J. (2020b). Advanced fluorescence microscopy reveals disruption of dynamic CXCR4 dimerization by subpocket-specific inverse agonists. *Proceedings of the National Academy of Sciences*, *117*(46), 29144–29154. https://doi.org/10.1073/pnas.2013319117

Işbilir, A., Serfling, R., Möller, J., Thomas, R., De Faveri, C., Zabel, U., Scarselli, M., Beck-Sickinger, A. G., Bock, A., Coin, I., Lohse, M. J., & Annibale, P. (2021). Determination of G-protein–coupled receptor oligomerization by molecular brightness analyses in single cells. *Nature Protocols*, *16*(3), 1419–1451. https://doi.org/10.1038/s41596-020-00458-1

J, F., C, Z., JE, L., M, J., J, Z., H, W., Y, Z., A, D., Z, W., H, W., W, C., P, Z., J, Z., SA, H., JJ, Z., G, C., D, L., J, D., & Y, L. (2019). A Genetically Encoded Fluorescent Sensor for Rapid and Specific In Vivo Detection of Norepinephrine. *Neuron*, *102*(4). https://doi.org/10.1016/j.neuron.2019.02.037

J Gingell, J., Simms, J., Barwell, J., Poyner, D. R., Watkins, H. A., Pioszak, A. A., Sexton, P. M., & Hay, D. L. (2016a). An allosteric role for receptor activity-modifying proteins in defining GPCR pharmacology. *Cell Discovery*, *2*(1), 1–14. https://doi.org/10.1038/celldisc.2016.12

J Gingell, J., Simms, J., Barwell, J., Poyner, D. R., Watkins, H. A., Pioszak, A. A., Sexton, P. M., & Hay, D. L. (2016b). An allosteric role for receptor activity-modifying proteins in defining GPCR pharmacology. *Cell Discovery*, *2*(1), 1–14. https://doi.org/10.1038/celldisc.2016.12

Jackson, J. A., Hungnes, I. N., Ma, M. T., & Rivas, C. (2020). Bioconjugates of Chelators with Peptides and Proteins in Nuclear Medicine: Historical Importance, Current Innovations, and Future Challenges. *Bioconjugate Chemistry*, *31*(3), 483–491. https://doi.org/10.1021/acs.bioconjchem.0c00015

Jeffrey Conn, P., Christopoulos, A., & Lindsley, C. W. (2009). Allosteric modulators of GPCRs: A novel approach for the treatment of CNS disorders. *Nature Reviews Drug Discovery*, *8*(1), 41–54. https://doi.org/10.1038/nrd2760

Jing, M., Zhang, P., Wang, G., Feng, J., Mesik, L., Zeng, J., Jiang, H., Wang, S., Looby, J. C., Guagliardo, N. A., Langma, L. W., Lu, J., Zuo, Y., Talmage, D. A., Role, L. W., Barrett, P. Q., Zhang, L. I., Luo, M., Song, Y., … Li, Y. (2018). A genetically encoded fluorescent acetylcholine indicator for in vitro and in vivo studies. *Nature Biotechnology*, *36*(8), 726–737. https://doi.org/10.1038/nbt.4184

Jonsson, K. B., Endocrine Unit (K.B.J., M. R. J., R. C. G. ,. T. J. G. ,. H. J.), Massachusetts General Hospital and Harvard Medical School, Boston, Massachusetts 02114, John, M. R., Endocrine Unit (K.B.J., M. R. J., R. C. G. ,. T. J. G. ,. H. J.), Massachusetts General Hospital and Harvard Medical School, Boston, Massachusetts 02114, Gensure, R. C., Endocrine Unit (K.B.J., M. R. J., R. C. G. ,. T. J. G. ,. H. J.), Massachusetts General Hospital and Harvard Medical School, Boston, Massachusetts 02114, Department of Medicine and Pediatric Endocrine Unit (R.C.G.), M. G. H. and H. M. S., Boston, Massachusetts 02114, MassGeneral Hospital for Children (R.C.G., H. J.), Massachusetts General Hospital and Harvard Medical School, Boston, Massachusetts 02114, Gardella, T. J., Endocrine Unit (K.B.J., M. R. J., R. C. G. ,. T. J. G. ,. H. J.), Massachusetts General Hospital and Harvard Medical School, Boston, Massachusetts 02114, Jüppner, H.,

Endocrine Unit (K.B.J., M. R. J., R. C. G. ,. T. J. G. ,. H. J.), Massachusetts General Hospital and Harvard Medical School, Boston, Massachusetts 02114, & MassGeneral Hospital for Children (R.C.G., H. J.), Massachusetts General Hospital and Harvard Medical School, Boston, Massachusetts 02114. (2021). Tuberoinfundibular Peptide 39 Binds to the Parathyroid Hormone(PTH)/PTH-Related Peptide Receptor, but Functions as an Antagonist*This work was supported by grants from the NIH, NIDDK (DK-11794), the Swedish Foundation for International Cooperation in Research and Higher Education (to K.B.J.), and the Deutsche Forschungsgemeinschaft (JO 315/1–2; to M.R.J.). *Endocrinology*, *142*(2), 704–709. https://doi.org/10.1210/endo.142.2.7945

Jonsson, K. B., John, M. R., Gensure, R. C., Gardella, T. J., & Jüppner, H. (2001). Tuberoinfundibular Peptide 39 Binds to the Parathyroid Hormone (PTH)/PTH-Related Peptide Receptor, but Functions as an Antagonist**This work was supported by grants from the NIH, NIDDK (DK-11794), the Swedish Foundation for International Cooperation in Research and Higher Education (to K.B.J.), and the Deutsche Forschungsgemeinschaft (JO 315/1–2; to M.R.J.). *Endocrinology*, *142*(2), 704–709. https://doi.org/10.1210/endo.142.2.7945

Jorgensen, R., Martini, L., Schwartz, T. W., & Elling, C. E. (2005). Characterization of Glucagon-Like Peptide-1 Receptor β-Arrestin 2 Interaction: A High-Affinity Receptor Phenotype. *Molecular Endocrinology*, *19*(3), 812–823. https://doi.org/10.1210/me.2004-0312

Josephs, T. M., Belousoff, M. J., Liang, Y.-L., Piper, S. J., Cao, J., Garama, D. J., Leach, K., Gregory, K. J., Christopoulos, A., Hay, D. L., Danev, R., Wootten, D., & Sexton, P. M. (2021a). Structure and dynamics of the CGRP receptor in apo and peptide-bound forms. *Science*. https://doi.org/10.1126/science.abf7258

Josephs, T. M., Belousoff, M. J., Liang, Y.-L., Piper, S. J., Cao, J., Garama, D. J., Leach, K., Gregory, K. J., Christopoulos, A., Hay, D. L., Danev, R., Wootten, D., & Sexton, P. M. (2021b). Structure and dynamics of the CGRP receptor in apo and peptide-bound forms. *Science*, *372*(6538), eabf7258. https://doi.org/10.1126/science.abf7258

Jouishomme, H., Whitfield, J. F., Gagnon, L., MacLean, S., Isaacs, R., Chakravarthy, B., Durkin, J., Neugebauer, W., Willick, G., & Rixon, R. H. (1994). Further definition of the protein kinase C activation domain of the parathyroid hormone. *Journal of Bone and Mineral Research*, *9*(6), 943–949. https://doi.org/10.1002/jbmr.5650090620

Juillerat, A., Gronemeyer, T., Keppler, A., Gendreizig, S., Pick, H., Vogel, H., & Johnsson, K. (2003). Directed Evolution of O6-Alkylguanine-DNA Alkyltransferase for Efficient Labeling of Fusion Proteins with Small Molecules In Vivo. *Chemistry & Biology*, *10*(4), 313–317. https://doi.org/10.1016/S1074-5521(03)00068-1

Jumper, J., Evans, R., Pritzel, A., Green, T., Figurnov, M., Ronneberger, O., Tunyasuvunakool, K., Bates, R., Žídek, A., Potapenko, A., Bridgland, A., Meyer, C., Kohl, S. A. A., Ballard, A. J., Cowie, A., Romera-Paredes, B., Nikolov, S., Jain, R., Adler, J., … Hassabis, D. (2021). Highly accurate protein structure prediction with AlphaFold. *Nature*, *596*(7873), 583–589. https://doi.org/10.1038/s41586-021-03819-2

Jüppner, H. (1994). Molecular cloning and characterization of a parathyroid hormone/parathyroid hormone-related peptide receptor: A member of an ancient family of G protein-coupled receptors. *Current Opinion in Nephrology and Hypertension*, *3*(4), 371–378.

Jüppner, H., Abou-Samra, A.-B., Freeman, M., Kong, X. F., Schipani, E., Richards, J., Kolakowski, L. F., Hock, J., Potts, J. T., Kronenberg, H. M., & Segre, G. V. (1991). A G Protein-Linked Receptor for Parathyroid Hormone and Parathyroid Hormone-Related Peptide. *Science*, *254*(5034), 1024–1026. https://doi.org/10.1126/science.1658941

Jüppner, H., Schipani, E., Bringhurst, F. R., McClure, I., Keutmann, H. T., Potts, J. T., Jr, Kronenberg, H. M., Abou-Samra, A. B., Segre, G. V., & Gardella, T. J. (1994). The extracellular amino-terminal region of the parathyroid hormone (PTH)/PTH-related peptide receptor determines the binding affinity for carboxyl-terminal fragments of PTH-(1-34). *Endocrinology*, *134*(2), 879–884. https://doi.org/10.1210/endo.134.2.8299582

Kadmiel, M., Fritz-Six, K. L., & Caron, K. M. (2012). Understanding RAMPs Through Genetically Engineered Mouse Models. In W. S. Spielman & N. Parameswaran (Eds.), *RAMPs* (pp. 49–60). Springer US. https://doi.org/10.1007/978-1-4614-2364-5_5

Kadmiel, M., Fritz-Six, K., Pacharne, S., Richards, G. O., Li, M., Skerry, T. M., & Caron, K. M. (2011a). Research Resource: Haploinsufficiency of Receptor Activity-Modifying Protein-2 (Ramp2) Causes Reduced Fertility, Hyperprolactinemia, Skeletal Abnormalities, and Endocrine Dysfunction in Mice. *Molecular Endocrinology*, *25*(7), 1244–1253. https://doi.org/10.1210/me.2010-0400

Kadmiel, M., Fritz-Six, K., Pacharne, S., Richards, G. O., Li, M., Skerry, T. M., & Caron, K. M. (2011b). Research Resource: Haploinsufficiency of Receptor Activity-Modifying Protein-2 (Ramp2) Causes Reduced Fertility, Hyperprolactinemia, Skeletal Abnormalities, and Endocrine Dysfunction in Mice. *Molecular Endocrinology*, *25*(7), 1244–1253. https://doi.org/10.1210/me.2010-0400

Kadmiel, M., Matson, B. C., Espenschied, S. T., Lenhart, P. M., & Caron, K. M. (2017). Loss of receptor activity-modifying protein 2 in mice causes placental dysfunction and alters PTH1R regulation. *PLOS ONE*, *12*(7), e0181597. https://doi.org/10.1371/journal.pone.0181597

Kawakami, K., Yanagawa, M., Hiratsuka, S., Yoshida, M., Ono, Y., Hiroshima, M., Ueda, M., Aoki, J., Sako, Y., & Inoue, A. (2022). Heterotrimeric Gq proteins act as a switch for GRK5/6 selectivity underlying β-arrestin transducer bias. *Nature Communications*, *13*(1), 487. https://doi.org/10.1038/s41467-022-28056-7

Kechele, D. O., Dunworth, W. P., Trincot, C. E., Wetzel-Strong, S. E., Li, M., Ma, H., Liu, J., & Caron, K. M. (2016). Endothelial Restoration of Receptor Activity–Modifying Protein 2 Is Sufficient to Rescue Lethality, but Survivors Develop Dilated Cardiomyopathy. *Hypertension*, *68*(3), 667–677. https://doi.org/10.1161/HYPERTENSIONAHA.116.07191

Kenakin, T. (2002). Drug Efficacy at G Protein–Coupled Receptors. *Annual Review of Pharmacology and Toxicology*, *42*(1), 349–379. https://doi.org/10.1146/annurev.pharmtox.42.091401.113012

Kenakin, T. (2019). Biased Receptor Signaling in Drug Discovery. *Pharmacological Reviews*, *71*(2), 267–315. https://doi.org/10.1124/pr.118.016790

Kenakin, T., & Christopoulos, A. (2013). Signalling bias in new drug discovery: Detection, quantification and therapeutic impact. *Nature Reviews Drug Discovery*, *12*(3), 205–216. https://doi.org/10.1038/nrd3954

Klarenbeek, J., Goedhart, J., van Batenburg, A., Groenewald, D., & Jalink, K. (2015). *Fourth-Generation Epac-Based FRET Sensors for cAMP Feature Exceptional Brightness, Photostability and Dynamic Range: Characterization of Dedicated Sensors for FLIM, for Ratiometry and with High Affinity*. https://doi.org/10.1371/journal.pone.0122513

Klein, K. R., Matson, B. C., & Caron, K. M. (2016). The expanding repertoire of receptor activity modifying protein (RAMP) function. *Critical Reviews in Biochemistry and Molecular Biology*, *51*(1), 65–71. https://doi.org/10.3109/10409238.2015.1128875

Kolakowski, L. F. (1994). GCRDb: A G-protein-coupled receptor database. *Receptors & Channels*, *2*(1), 1–7.

Kolb, P., Kenakin, T., Alexander, S. P. H., Bermudez, M., Bohn, L. M., Breinholt, C. S., Bouvier, M., Hill, S. J., Kostenis, E., Martemyanov, K. A., Neubig, R. R., Onaran, H. O., Rajagopal, S., Roth, B. L., Selent, J., Shukla, A. K., Sommer, M. E., & Gloriam, D. E. (2022). Community guidelines for GPCR ligand bias: IUPHAR review 32. *British Journal of Pharmacology*, *n/a*(n/a). https://doi.org/10.1111/bph.15811

Komolov, K. E., & Benovic, J. L. (2018). G protein-coupled receptor kinases: Past, present and future. *Cellular Signalling*, *41*, 17–24. https://doi.org/10.1016/j.cellsig.2017.07.004

Kooistra, A. J., Mordalski, S., Pándy-Szekeres, G., Esguerra, M., Mamyrbekov, A., Munk, C., Keserű, G. M., & Gloriam, D. E. (2021). GPCRdb in 2021: Integrating GPCR sequence, structure and function. *Nucleic Acids Research*, *49*(D1), D335–D343. https://doi.org/10.1093/nar/gkaa1080

Kooistra, A. J., Munk, C., Hauser, A. S., & Gloriam, D. E. (2021). An online GPCR structure analysis platform. *Nature Structural & Molecular Biology*, *28*(11), 875–878. https://doi.org/10.1038/s41594-021-00675-6

Kostyuk, A. I., Demidovich, A. D., Kotova, D. A., Belousov, V. V., & Bilan, D. S. (2019). Circularly Permuted Fluorescent Protein-Based Indicators: History, Principles, and Classification. *International Journal of Molecular Sciences*, *20*(17). https://doi.org/10.3390/ijms20174200

Kowalski-Jahn, M., Schihada, H., Turku, A., Huber, T., Sakmar, T. P., & Schulte, G. (n.d.). Frizzled BRET sensors based on bioorthogonal labeling of unnatural amino acids reveal WNT-induced dynamics of the cysteine-rich domain. *Science Advances*, *7*(46), eabj7917. https://doi.org/10.1126/sciadv.abj7917

Krasel, C., Bünemann, M., Lorenz, K., & Lohse, M. J. (2005). β-Arrestin Binding to the β2-Adrenergic Receptor Requires Both Receptor Phosphorylation and Receptor Activation*. *Journal of Biological Chemistry*, *280*(10), 9528–9535. https://doi.org/10.1074/jbc.M413078200

Kruse, K., & Schütz, C. (1993). Calcium metabolism in the jansen type of metaphyseal dysplasia. *European Journal of Pediatrics*, *152*(11), 912–915. https://doi.org/10.1007/BF01957529

Kuna, R. S., Girada, S. B., Asalla, S., Vallentyne, J., Maddika, S., Patterson, J. T., Smiley, D. L., DiMarchi, R. D., & Mitra, P. (2013). Glucagon-like peptide-1 receptor-mediated endosomal cAMP generation promotes glucose-stimulated insulin secretion in pancreatic β-cells. *American Journal of Physiology-Endocrinology and Metabolism*, *305*(2), E161–E170. https://doi.org/10.1152/ajpendo.00551.2012

Kunishima, N., Shimada, Y., Tsuji, Y., Sato, T., Yamamoto, M., Kumasaka, T., Nakanishi, S., Jingami, H., & Morikawa, K. (2000). Structural basis of glutamate recognition by a dimeric metabotropic glutamate receptor. *Nature*, *407*(6807), 971–977. https://doi.org/10.1038/35039564

Lambert, N. A., Johnston, C. A., Cappell, S. D., Kuravi, S., Kimple, A. J., Willard, F. S., & Siderovski, D. P. (2010). Regulators of G-protein Signaling accelerate GPCR signaling kinetics and govern sensitivity solely by accelerating GTPase activity. *Proceedings of the National Academy of Sciences*, *107*(15), 7066–7071. https://doi.org/10.1073/pnas.0912934107

Larráyoz, I. M., Martínez-Herrero, S., García-Sanmartín, J., Ochoa-Callejero, L., & Martínez, A. (2014). Adrenomedullin and tumour microenvironment. *Journal of Translational Medicine*, *12*(1), 339. https://doi.org/10.1186/s12967-014-0339-2

Larrue, C., Guiraud, N., Mouchel, P.-L., Dubois, M., Farge, T., Gotanègre, M., Bosc, C., Saland, E., Nicolau-Travers, M.-L., Sabatier, M., Serhan, N., Sahal, A., Boet, E., Mouche, S., Heydt, Q., Aroua, N., Stuani, L., Kaoma, T., Angenendt, L., … Sarry, J.-E. (2021). Adrenomedullin-CALCRL axis controls relapse-initiating drug tolerant acute myeloid leukemia cells. *Nature Communications*, *12*(1), 422. https://doi.org/10.1038/s41467-020-20717-9

Latorraca, N. R., Masureel, M., Hollingsworth, S. A., Heydenreich, F. M., Suomivuori, C.-M., Brinton, C., Townshend, R. J. L., Bouvier, M., Kobilka, B. K., & Dror, R. O. (2020). How GPCR Phosphorylation Patterns Orchestrate Arrestin-Mediated Signaling. *Cell*, *183*(7), 1813-1825.e18. https://doi.org/10.1016/j.cell.2020.11.014

Latorraca, N. R., Venkatakrishnan, A. J., & Dror, R. O. (2017). GPCR Dynamics: Structures in Motion. *Chemical Reviews*, *117*(1), 139–155. https://doi.org/10.1021/acs.chemrev.6b00177

Lefkowitz, R. J. (2000). The superfamily of heptahelical receptors. *Nature Cell Biology*, *2*(7), E133–E136. https://doi.org/10.1038/35017152

Lefkowitz, R. J., Rajagopal, K., & Whalen, E. J. (2006). New Roles for β-Arrestins in Cell Signaling: Not Just for Seven-Transmembrane Receptors. *Molecular Cell*, *24*(5), 643–652. https://doi.org/10.1016/j.molcel.2006.11.007

Lenhart, P. M., Broselid, S., Barrick, C. J., Leeb-Lundberg, L. M. F., & Caron, K. M. (2013a). G-protein Coupled Receptor 30 Interacts with Receptor Activity Modifying Protein 3 and Confers Sex-Dependent Cardioprotection. *Journal of Molecular Endocrinology*, *51*(1), 191–202. https://doi.org/10.1530/JME-13-0021

Lenhart, P. M., Broselid, S., Barrick, C. J., Leeb-Lundberg, L. M. F., & Caron, K. M. (2013b). G-protein-coupled receptor 30 interacts with receptor activity-modifying protein 3 and confers sex-dependent

cardioprotection. *Journal of Molecular Endocrinology*, *51*(1), 191–202. https://doi.org/10.1530/JME-13-0021

Liang, Y.-L., Belousoff, M. J., Fletcher, M. M., Zhang, X., Khoshouei, M., Deganutti, G., Koole, C., Furness, S. G. B., Miller, L. J., Hay, D. L., Christopoulos, A., Reynolds, C. A., Danev, R., Wootten, D., & Sexton, P. M. (2020a). Structure and Dynamics of Adrenomedullin Receptors AM $_1$ and AM $_2$ Reveal Key Mechanisms in the Control of Receptor Phenotype by Receptor Activity-Modifying Proteins. *ACS Pharmacology & Translational Science*, acsptsci.9b00080. https://doi.org/10.1021/acsptsci.9b00080

Liang, Y.-L., Belousoff, M. J., Fletcher, M. M., Zhang, X., Khoshouei, M., Deganutti, G., Koole, C., Furness, S. G. B., Miller, L. J., Hay, D. L., Christopoulos, A., Reynolds, C. A., Danev, R., Wootten, D., & Sexton, P. M. (2020b). Structure and Dynamics of Adrenomedullin Receptors AM1 and AM2 Reveal Key Mechanisms in the Control of Receptor Phenotype by Receptor Activity-Modifying Proteins. *ACS Pharmacology & Translational Science*, *3*(2), 263–284. https://doi.org/10.1021/acsptsci.9b00080

Liang, Y.-L., Belousoff, M. J., Fletcher, M. M., Zhang, X., Khoshouei, M., Deganutti, G., Koole, C., Furness, S. G. B., Miller, L. J., Hay, D. L., Christopoulos, A., Reynolds, C. A., Danev, R., Wootten, D., & Sexton, P. M. (2020c). Structure and Dynamics of Adrenomedullin Receptors AM1 and AM2 Reveal Key Mechanisms in the Control of Receptor Phenotype by Receptor Activity-Modifying Proteins. *ACS Pharmacology & Translational Science*, *3*(2), 263–284. https://doi.org/10.1021/acsptsci.9b00080

Liang, Y.-L., Belousoff, M. J., Zhao, P., Koole, C., Fletcher, M. M., Truong, T. T., Julita, V., Christopoulos, G., Xu, H. E., Zhang, Y., Khoshouei, M., Christopoulos, A., Danev, R., Sexton, P. M., & Wootten, D. (2020). Toward a Structural Understanding of Class B GPCR Peptide Binding and Activation. *Molecular Cell*, *77*(3), 656-668.e5. https://doi.org/10.1016/j.molcel.2020.01.012

Liang, Y.-L., Khoshouei, M., Deganutti, G., Glukhova, A., Koole, C., Peat, T. S., Radjainia, M., Plitzko, J. M., Baumeister, W., Miller, L. J., Hay, D. L., Christopoulos, A., Reynolds, C. A., Wootten, D., & Sexton, P. M. (2018). Cryo-EM structure of the active, G s -protein complexed, human CGRP receptor. *Nature*, *561*(7724), 492. https://doi.org/10.1038/s41586-018-0535-y

Liggett, S. B. (2011). Phosphorylation Barcoding as a Mechanism of Directing GPCR Signaling. *Science Signaling*. https://doi.org/10.1126/scisignal.2002331

Liu, X., Xu, X., Hilger, D., Aschauer, P., Tiemann, J. K. S., Du, Y., Liu, H., Hirata, K., Sun, X., Guixà-González, R., Mathiesen, J. M., Hildebrand, P. W., & Kobilka, B. K. (2019). Structural Insights into the Process of GPCR-G Protein Complex Formation. *Cell*, *177*(5), 1243-1251.e12. https://doi.org/10.1016/j.cell.2019.04.021

Lohse, M. J. (1993). Molecular mechanisms of membrane receptor desensitization. *Biochimica et Biophysica Acta (BBA) - Molecular Cell Research*, *1179*(2), 171–188. https://doi.org/10.1016/0167-4889(93)90139-G

Lohse, M. J., Benovic, J. L., Codina, J., Caron, M. G., & Lefkowitz, R. J. (1990). beta-Arrestin: A protein that regulates beta-adrenergic receptor function. *Science (New York, N.Y.)*, *248*(4962), 1547–1550.

Lohse, M. J., & Calebiro, D. (2013). Cell biology: Receptor signals come in waves. *Nature*, *495*(7442), 457–458. https://doi.org/10.1038/nature12086

Lorenzen, E., Dodig-Crnković, T., Kotliar, I. B., Pin, E., Ceraudo, E., Vaughan, R. D., Uhlèn, M., Huber, T., Schwenk, J. M., & Sakmar, T. P. (2019). Multiplexed analysis of the secretin-like GPCR-RAMP interactome. *Science Advances*. https://doi.org/10.1126/sciadv.aaw2778

Los, G. V., Encell, L. P., McDougall, M. G., Hartzell, D. D., Karassina, N., Zimprich, C., Wood, M. G., Learish, R., Ohana, R. F., Urh, M., Simpson, D., Mendez, J., Zimmerman, K., Otto, P., Vidugiris, G., Zhu, J., Darzins, A., Klaubert, D. H., Bulleit, R. F., & Wood, K. V. (2008). HaloTag: A Novel Protein Labeling Technology for Cell Imaging and Protein Analysis. *ACS Chemical Biology*, *3*(6), 373–382. https://doi.org/10.1021/cb800025k

Lu, P.-J., Zhou, X. Z., Shen, M., & Lu, K. P. (1999). Function of WW Domains as Phosphoserine- or Phosphothreonine-Binding Modules. *Science*. https://doi.org/10.1126/science.283.5406.1325

Luttrell, L. M., & Lefkowitz, R. J. (2002). The role of β-arrestins in the termination and transduction of G-protein-coupled receptor signals. *Journal of Cell Science*, *115*(3), 455–465. https://doi.org/10.1242/jcs.115.3.455

Lyga, S., Volpe, S., Werthmann, R. C., Götz, K., Sungkaworn, T., Lohse, M. J., & Calebiro, D. (2016). Persistent cAMP Signaling by Internalized LH Receptors in Ovarian Follicles. *Endocrinology*, *157*(4), 1613–1621. https://doi.org/10.1210/en.2015-1945

Lyu, P., Li, B., Li, P., Bi, R., Cui, C., Zhao, Z., Zhou, X., & Fan, Y. (2021). Parathyroid Hormone 1 Receptor Signaling in Dental Mesenchymal Stem Cells: Basic and Clinical Implications. *Frontiers in Cell and Developmental Biology*, *9*. https://www.frontiersin.org/article/10.3389/fcell.2021.654715

Mackie, D. I., Nielsen, N. R., Harris, M., Singh, S., Davis, R. B., Dy, D., Ladds, G., & Caron, K. M. (2019). RAMP3 determines rapid recycling of atypical chemokine receptor-3 for guided angiogenesis. *Proceedings of the National Academy of Sciences*. https://doi.org/10.1073/pnas.1905561116

Mahoney, J. P., & Sunahara, R. K. (2016). Mechanistic insights into GPCR–G protein interactions. *Current Opinion in Structural Biology*, *41*, 247–254. https://doi.org/10.1016/j.sbi.2016.11.005

Malecz, N., Bambino, T., Bencsik, M., & Nissenson, R. A. (1998). Identification of Phosphorylation Sites in the G Protein-Coupled Receptor for Parathyroid Hormone. Receptor Phosphorylation Is Not Required for Agonist-Induced Internalization. *Molecular Endocrinology*, *12*(12), 1846–1856. https://doi.org/10.1210/mend.12.12.0203

Manglik, A., Kim, T. H., Masureel, M., Altenbach, C., Yang, Z., Hilger, D., Lerch, M. T., Kobilka, T. S., Thian, F. S., Hubbell, W. L., Prosser, R. S., & Kobilka, B. K. (2015). Structural Insights into the Dynamic Process of β2-Adrenergic Receptor Signaling. *Cell*, *161*(5), 1101–1111. https://doi.org/10.1016/j.cell.2015.04.043

Manglik, A., & Kruse, A. C. (2017). Structural Basis for G Protein-Coupled Receptor Activation. *Biochemistry*, *56*(42), 5628–5634. https://doi.org/10.1021/acs.biochem.7b00747

Marti-Solano, M., Crilly, S. E., Malinverni, D., Munk, C., Harris, M., Pearce, A., Quon, T., Mackenzie, A. E., Wang, X., Peng, J., Tobin, A. B., Ladds, G., Milligan, G., Gloriam, D. E., Puthenveedu, M. A., & Babu, M. M. (2020). Combinatorial expression of GPCR isoforms affects signalling and drug responses. *Nature*, *587*(7835), 650–656. https://doi.org/10.1038/s41586-020-2888-2

Matthees, E. S. F., Haider, R. S., Hoffmann, C., & Drube, J. (2021). Differential Regulation of GPCRs—Are GRK Expression Levels the Key? *Frontiers in Cell and Developmental Biology*, *9*. https://www.frontiersin.org/article/10.3389/fcell.2021.687489

Maurel, D., Comps-Agrar, L., Brock, C., Rives, M.-L., Bourrier, E., Ayoub, M. A., Bazin, H., Tinel, N., Durroux, T., Prézeau, L., Trinquet, E., & Pin, J.-P. (2008). Cell-surface protein-protein interaction analysis with time-resolved FRET and snap-tag technologies: Application to GPCR oligomerization. *Nature Methods*, *5*(6), 561–567. https://doi.org/10.1038/nmeth.1213

Mayer, D., Damberger, F. F., Samarasimhareddy, M., Feldmueller, M., Vuckovic, Z., Flock, T., Bauer, B., Mutt, E., Zosel, F., Allain, F. H. T., Standfuss, J., Schertler, G. F. X., Deupi, X., Sommer, M. E., Hurevich, M., Friedler, A., & Veprintsev, D. B. (2019). Distinct G protein-coupled receptor phosphorylation motifs modulate arrestin affinity and activation and global conformation. *Nature Communications*, *10*(1), 1261. https://doi.org/10.1038/s41467-019-09204-y

McCudden, C. R., Hains, M. D., Kimple, R. J., Siderovski, D. P., & Willard, F. S. (2005). G-protein signaling: Back to the future. *Cellular and Molecular Life Sciences*, *62*(5), 551–577. https://doi.org/10.1007/s00018-004-4462-3

McGlone, E. R., Manchanda, Y., Jones, B., Pickford, P., Inoue, A., Carling, D., Bloom, S. R., Tan, T., & Tomas, A. (2021). Receptor Activity-Modifying Protein 2 (RAMP2) alters glucagon receptor trafficking in hepatocytes with functional effects on receptor signalling. *Molecular Metabolism*, *53*, 101296. https://doi.org/10.1016/j.molmet.2021.101296

McLatchie, L. M., Fraser, N. J., Main, M. J., Wise, A., Brown, J., Thompson, N., Solari, R., Lee, M. G., & Foord, S. M. (1998). RAMPs regulate the transport and ligand specificity of the calcitonin-receptor-like receptor. *Nature*, *393*(6683), 333–339. https://doi.org/10.1038/30666

Mehta, S., Zhang, Y., Roth, R. H., Zhang, J., Mo, A., Tenner, B., Huganir, R. L., & Zhang, J. (2018). Single-fluorophore biosensors for sensitive and multiplexed detection of signalling activities. *Nature Cell Biology*, *20*(10), 1215–1225. https://doi.org/10.1038/s41556-018-0200-6

Meral, D., Provasi, D., Prada-Gracia, D., Möller, J., Marino, K., Lohse, M. J., & Filizola, M. (2018). Molecular details of dimerization kinetics reveal negligible populations of transient μ-opioid receptor homodimers at physiological concentrations. *Scientific Reports*, *8*(1), 7705. https://doi.org/10.1038/s41598-018-26070-8

Merriam, L. A., Baran, C. N., Girard, B. M., Hardwick, J. C., May, V., & Parsons, R. L. (2013). Pituitary Adenylate Cyclase 1 Receptor Internalization and Endosomal Signaling Mediate the Pituitary Adenylate Cyclase Activating Polypeptide-Induced Increase in Guinea Pig Cardiac Neuron Excitability. *Journal of Neuroscience*, *33*(10), 4614–4622. https://doi.org/10.1523/JNEUROSCI.4999-12.2013

Meyrath, M., Palmer, C. B., Reynders, N., Vanderplasschen, A., Ollert, M., Bouvier, M., Szpakowska, M., & Chevigné, A. (2021). Proadrenomedullin N-Terminal 20 Peptides (PAMPs) Are Agonists of the Chemokine Scavenger Receptor ACKR3/CXCR7. *ACS Pharmacology & Translational Science*, *4*(2), 813–823. https://doi.org/10.1021/acsptsci.1c00006

Miller, P. D., Hattersley, G., Riis, B. J., Williams, G. C., Lau, E., Russo, L. A., Alexandersen, P., Zerbini, C. A. F., Hu, M., Harris, A. G., Fitzpatrick, L. A., Cosman, F., Christiansen, C., & for the ACTIVE Study Investigators. (2016). Effect of Abaloparatide vs Placebo on New Vertebral Fractures in Postmenopausal Women With Osteoporosis: A Randomized Clinical Trial. *JAMA*, *316*(7), 722–733. https://doi.org/10.1001/jama.2016.11136

Milligan, G., & Kostenis, E. (2006). Heterotrimeric G-proteins: A short history. *British Journal of Pharmacology*, *147*(S1), S46–S55. https://doi.org/10.1038/sj.bjp.0706405

Minoshima, M., & Kikuchi, K. (2017). Photostable and photoswitching fluorescent dyes for super-resolution imaging. *JBIC Journal of Biological Inorganic Chemistry*, *22*(5), 639–652. https://doi.org/10.1007/s00775-016-1435-y

Miyauchi, A., Dobre, V., Rickmeyer, M., Cole, J., Forte, L., & Hruska, K. A. (1990). Stimulation of transient elevations in cytosolic Ca2+ is related to inhibition of Pi transport in OK cells. *The American Journal of Physiology*, *259*(3 Pt 2), F485-493. https://doi.org/10.1152/ajprenal.1990.259.3.F485

Mizuno, N., & Itoh, H. (2009). Functions and Regulatory Mechanisms of Gq-Signaling Pathways. *Neurosignals*, *17*(1), 42–54. https://doi.org/10.1159/000186689

Mo, G. C. H., Ross, B., Hertel, F., Manna, P., Yang, X., Greenwald, E., Booth, C., Plummer, A. M., Tenner, B., Chen, Z., Wang, Y., Kennedy, E. J., Cole, P. A., Fleming, K. G., Palmer, A., Jimenez, R., Xiao, J., Dedecker, P., & Zhang, J. (2017). Genetically encoded biosensors for visualizing live-cell biochemical activity at super-resolution. *Nature Methods*, *14*(4), 427–434. https://doi.org/10.1038/nmeth.4221

Mohammad Nezhady, M. A., Rivera, J. C., & Chemtob, S. (2020). Location Bias as Emerging Paradigm in GPCR Biology and Drug Discovery. *IScience*, *23*(10), 101643. https://doi.org/10.1016/j.isci.2020.101643

Möller, J. (2020). *Mechanisms and consequences of μ-opioid receptor dimerization*. 140.

Möller, J., Isbilir, A., Sungkaworn, T., Osberg, B., Karathanasis, C., Sunkara, V., Grushevskyi, E. O., Bock, A., Annibale, P., Heilemann, M., Schütte, C., & Lohse, M. J. (2020a). Single-molecule analysis reveals agonist-specific dimer formation of μ-opioid receptors. *Nature Chemical Biology*, *16*(9), 946–954. https://doi.org/10.1038/s41589-020-0566-1

Möller, J., Isbilir, A., Sungkaworn, T., Osberg, B., Karathanasis, C., Sunkara, V., Grushevskyi, E. O., Bock, A., Annibale, P., Heilemann, M., Schütte, C., & Lohse, M. J. (2020b). Single-molecule analysis reveals agonist-

specific dimer formation of μ-opioid receptors. *Nature Chemical Biology*, *16*(9), 946–954. https://doi.org/10.1038/s41589-020-0566-1

Morfis, M., Tilakaratne, N., Furness, S. G. B., Christopoulos, G., Werry, T. D., Christopoulos, A., & Sexton, P. M. (2008). Receptor Activity-Modifying Proteins Differentially Modulate the G Protein-Coupling Efficiency of Amylin Receptors. *Endocrinology*, *149*(11), 5423–5431. https://doi.org/10.1210/en.2007-1735

Morstein, J., Romano, G., Hetzler, B. E., Plante, A., Haake, C., Levitz, J., & Trauner, D. (2022). Photoswitchable Serotonins for Optical Control of the 5-HT2A Receptor. *Angewandte Chemie International Edition*, *n/a*(n/a), e202117094. https://doi.org/10.1002/anie.202117094

Mullard, A. (2020). FDA approves first GPCR biased agonist. *Nature Reviews Drug Discovery*, *19*(10), 659–659. https://doi.org/10.1038/d41573-020-00159-0

Mullershausen, F., Zecri, F., Cetin, C., Billich, A., Guerini, D., & Seuwen, K. (2009). Persistent signaling induced by FTY720-phosphate is mediated by internalized S1P1 receptors. *Nature Chemical Biology*, *5*(6), 428–434. https://doi.org/10.1038/nchembio.173

Nagai, T., Sawano, A., Park, E. S., & Miyawaki, A. (2001). *Circularly permuted green fluorescent proteins engineered to sense Ca2+*. https://doi.org/10.1073/pnas.051636098

Nemec, K. (2017). *The role of EP4 prostaglandin receptor in patients with chronic lymphocytic leukemia* [Master thesis, University of Ljubljana]. https://www.ffa.uni-lj.si/docs/default-source/knjiznica-doc/magistrske/2017/nemec_katarina_mag_nal_2017.pdf?sfvrsn=2

Nemec, K., Schihada, H., Kleinau, G., Zabel, U., Grushevskyi, E. O., Scheerer, P., Lohse, M. J., & Maiellaro, I. (2021). *Functional modulation of PTH1R activation and signalling by RAMP2* (p. 2021.12.08.471790). bioRxiv. https://doi.org/10.1101/2021.12.08.471790

Nguyen, A. H., Thomsen, A. R. B., Cahill, T. J., Huang, R., Huang, L.-Y., Marcink, T., Clarke, O. B., Heissel, S., Masoudi, A., Ben-Hail, D., Samaan, F., Dandey, V. P., Tan, Y. Z., Hong, C., Mahoney, J. P., Triest, S., Little, J., Chen, X., Sunahara, R., … Lefkowitz, R. J. (2019). Structure of an endosomal signaling GPCR–G protein–β-arrestin megacomplex. *Nature Structural & Molecular Biology*, *26*(12), 1123–1131. https://doi.org/10.1038/s41594-019-0330-y

Nikolaev, V. O., Bünemann, M., Hein, L., Hannawacker, A., & Lohse, M. J. (2004). Novel Single Chain cAMP Sensors for Receptor-induced Signal Propagation*♦. *Journal of Biological Chemistry*, *279*(36), 37215–37218. https://doi.org/10.1074/jbc.C400302200

Nobles, K. N., Xiao, K., Ahn, S., Shukla, A. K., Lam, C. M., Rajagopal, S., Strachan, R. T., Huang, T.-Y., Bressler, E. A., Hara, M. R., Shenoy, S. K., Gygi, S. P., & Lefkowitz, R. J. (2011). Distinct Phosphorylation Sites on the β2-Adrenergic Receptor Establish a Barcode That Encodes Differential Functions of β-Arrestin. *Science Signaling*. https://doi.org/10.1126/scisignal.2001707

Northup, J. K., Sternweis, P. C., Smigel, M. D., Schleifer, L. S., Ross, E. M., & Gilman, A. G. (1980). Purification of the regulatory component of adenylate cyclase. *Proceedings of the National Academy of Sciences*, *77*(11), 6516–6520. https://doi.org/10.1073/pnas.77.11.6516

Noseda, R., & Burstein, R. (2013). Migraine pathophysiology: Anatomy of the trigeminovascular pathway and associated neurological symptoms, cortical spreading depression, sensitization, and modulation of pain. *PAIN*, *154*, S44. https://doi.org/10.1016/j.pain.2013.07.021

Nuber, S., Zabel, U., Lorenz, K., Nuber, A., Milligan, G., Tobin, A. B., Lohse, M. J., & Hoffmann, C. (2016). β-Arrestin biosensors reveal a rapid, receptor-dependent activation/deactivation cycle. *Nature*, *531*(7596), 661–664. https://doi.org/10.1038/nature17198

Nygaard, R., Frimurer, T. M., Holst, B., Rosenkilde, M. M., & Schwartz, T. W. (2009). Ligand binding and micro-switches in 7TM receptor structures. *Trends in Pharmacological Sciences*, *30*(5), 249–259. https://doi.org/10.1016/j.tips.2009.02.006

OctaFlow II – Automated Perfusion System – NPI Electronic. (n.d.). Retrieved March 22, 2022, from https://www.npielectronic.com/product/octaflow-ii/

Offermanns, S., Iida-Klein, A., Segre, G. V., & Simon, M. I. (1996). G alpha q family members couple parathyroid hormone (PTH)/PTH-related peptide and calcitonin receptors to phospholipase C in COS-7 cells. *Molecular Endocrinology (Baltimore, Md.)*, *10*(5), 566–574. https://doi.org/10.1210/mend.10.5.8732687

Ohta, Y., Furuta, T., Nagai, T., & Horikawa, K. (2018). Red fluorescent cAMP indicator with increased affinity and expanded dynamic range. *Scientific Reports*, *8*, 1866. https://doi.org/10.1038/s41598-018-20251-1

Øie, E., Vinge, L. E., Andersen, G. Ø., Yndestad, A., Krobert, K. A., Sandberg, C., Ahmed, M. S., Haug, T., Levy, F. O., Skomedal, T., & Attramadal, H. (2005). RAMP2 and RAMP3 mRNA levels are increased in failing rat cardiomyocytes and associated with increased responsiveness to adrenomedullin. *Journal of Molecular and Cellular Cardiology*, *38*(1), 145–151. https://doi.org/10.1016/j.yjmcc.2004.10.009

Ortiz Zacarías, N. V., Lenselink, E. B., IJzerman, A. P., Handel, T. M., & Heitman, L. H. (2018). Intracellular receptor modulation: Novel approach to target GPCRs. *Trends in Pharmacological Sciences*, *39*(6), 547–559. https://doi.org/10.1016/j.tips.2018.03.002

Ouyang, N., Li, H., Wang, M., Shen, H., Si, J., & Shen, G. (2020). The Transcription Factor Foxc1 Promotes Osteogenesis by Directly Regulating Runx2 in Response of Intermittent Parathyroid Hormone (1–34) Treatment. *Frontiers in Pharmacology*, *11*. https://doi.org/10.3389/fphar.2020.00592

Pandey, S., Kumari, P., Baidya, M., Kise, R., Cao, Y., Dwivedi-Agnihotri, H., Banerjee, R., Li, X. X., Cui, C. S., Lee, J. D., Kawakami, K., Maharana, J., Ranjan, A., Chaturvedi, M., Jhingan, G. D., Laporte, S. A., Woodruff, T. M., Inoue, A., & Shukla, A. K. (2021). Intrinsic bias at non-canonical, β-arrestin-coupled seven transmembrane receptors. *Molecular Cell*, *81*(22), 4605-4621.e11. https://doi.org/10.1016/j.molcel.2021.09.007

Pándy-Szekeres, G., Esguerra, M., Hauser, A. S., Caroli, J., Munk, C., Pilger, S., Keserű, G. M., Kooistra, A. J., & Gloriam, D. E. (2022). The G protein database, GproteinDb. *Nucleic Acids Research*, *50*(D1), D518–D525. https://doi.org/10.1093/nar/gkab852

Parfitt, A. M., Schipani, E., Rao, D. S., Kupin, W., Han, Z. H., & Jüppner, H. (1996). Hypercalcemia due to constitutive activity of the parathyroid hormone (PTH)/PTH-related peptide receptor: Comparison with primary hyperparathyroidism. *The Journal of Clinical Endocrinology & Metabolism*, *81*(10), 3584–3588. https://doi.org/10.1210/jcem.81.10.8855805

Patriarchi, T., Cho, J. R., Merten, K., Howe, M. W., Marley, A., Xiong, W.-H., Folk, R. W., Broussard, G. J., Liang, R., Jang, M. J., Zhong, H., Dombeck, D., Zastrow, M. von, Nimmerjahn, A., Gradinaru, V., Williams, J. T., & Tian, L. (2018). Ultrafast neuronal imaging of dopamine dynamics with designed genetically encoded sensors. *Science*, eaat4422. https://doi.org/10.1126/science.aat4422

Pazos, F., Ranea, J. A. G., Juan, D., & Sternberg, M. J. E. (2005). Assessing Protein Co-evolution in the Context of the Tree of Life Assists in the Prediction of the Interactome. *Journal of Molecular Biology*, *352*(4), 1002–1015. https://doi.org/10.1016/j.jmb.2005.07.005

Pearce, A., Redfern-Nichols, T., Harris, M., Poyner, D. R., Wigglesworth, M., & Ladds, G. (2022). Determining the Effects of Differential Expression of GRKs and β-arrestins on CLR-RAMP Agonist Bias. *Frontiers in Physiology*, *13*. https://www.frontiersin.org/article/10.3389/fphys.2022.840763

Phelps, E., Bezouglaia, O., Tetradis, S., & Nervina, J. M. (2005). Parathyroid hormone induces receptor activity modifying protein-3 (RAMP3) expression primarily via 3',5'-cyclic adenosine monophosphate signaling in osteoblasts. *Calcified Tissue International*, *77*(2), 96–103. https://doi.org/10.1007/s00223-004-0239-1

Picard, L.-P., Schönegge, A. M., Lohse, M. J., & Bouvier, M. (2018). Bioluminescence resonance energy transfer-based biosensors allow monitoring of ligand- and transducer-mediated GPCR conformational changes. *Communications Biology*, *1*(1), 1–7. https://doi.org/10.1038/s42003-018-0101-z

Pierce, K. L., Premont, R. T., & Lefkowitz, R. J. (2002). Seven-transmembrane receptors. *Nature Reviews Molecular Cell Biology*, *3*(9), 639–650. https://doi.org/10.1038/nrm908

Pines, M., Fukayama, S., Costas, K., Meurer, E., Goldsmith, P. K., Xu, X., Muallem, S., Behar, V., Chorev, M., Rosenblatt, M., Tashjian, A. H., & Suva, L. J. (1996). Inositol 1-,4-,5-trisphosphate-dependent Ca2+ signaling by the recombinant human PTH/PTHrP receptor stably expressed in a human kidney cell line. *Bone*, *18*(4), 381–389. https://doi.org/10.1016/8756-3282(96)00008-7

Ping, Y.-Q., Xiao, P., Yang, F., Zhao, R.-J., Guo, S.-C., Yan, X., Wu, X., Zhang, C., Lu, Y., Zhao, F., Zhou, F., Xi, Y.-T., Yin, W., Liu, F.-Z., He, D.-F., Zhang, D.-L., Zhu, Z.-L., Jiang, Y., Du, L., … Sun, J.-P. (2022). Structural basis for the tethered peptide activation of adhesion GPCRs. *Nature*, 1–8. https://doi.org/10.1038/s41586-022-04619-y

Pioszak, A. A., Parker, N. R., Gardella, T. J., & Xu, H. E. (2009). Structural Basis for Parathyroid Hormone-related Protein Binding to the Parathyroid Hormone Receptor and Design of Conformation-selective Peptides*. *Journal of Biological Chemistry*, *284*(41), 28382–28391. https://doi.org/10.1074/jbc.M109.022905

Pioszak, A. A., & Xu, H. E. (2008). Molecular recognition of parathyroid hormone by its G protein-coupled receptor. *Proceedings of the National Academy of Sciences*, *105*(13), 5034–5039. https://doi.org/10.1073/pnas.0801027105

Qi, X., Liu, H., Thompson, B., McDonald, J., Zhang, C., & Li, X. (2019). Cryo-EM structure of oxysterol-bound human Smoothened coupled to a heterotrimeric Gi. *Nature*, *571*(7764), 279–283. https://doi.org/10.1038/s41586-019-1286-0

Qiao, A., Han, S., Li, X., Li, Z., Zhao, P., Dai, A., Chang, R., Tai, L., Tan, Q., Chu, X., Ma, L., Thorsen, T. S., Reedtz-Runge, S., Yang, D., Wang, M.-W., Sexton, P. M., Wootten, D., Sun, F., Zhao, Q., & Wu, B. (2020). Structural basis of Gs and Gi recognition by the human glucagon receptor. *Science*, *367*(6484), 1346–1352. https://doi.org/10.1126/science.aaz5346

Qu, X., Qiu, N., Wang, M., Zhang, B., Du, J., Zhong, Z., Xu, W., Chu, X., Ma, L., Yi, C., Han, S., Shui, W., Zhao, Q., & Wu, B. (2022). Structural basis of tethered agonism of the adhesion GPCRs ADGRD1 and ADGRF1. *Nature*, 1–8. https://doi.org/10.1038/s41586-022-04580-w

Rajagopal, S., Kim, J., Ahn, S., Craig, S., Lam, C. M., Gerard, N. P., Gerard, C., & Lefkowitz, R. J. (2010). β-arrestin- but not G protein-mediated signaling by the "decoy" receptor CXCR7. *Proceedings of the National Academy of Sciences*, *107*(2), 628–632. https://doi.org/10.1073/pnas.0912852107

Rajagopal, S., Rajagopal, K., & Lefkowitz, R. J. (2010). Teaching old receptors new tricks: Biasing seven-transmembrane receptors. *Nature Reviews Drug Discovery*, *9*(5), 373–386. https://doi.org/10.1038/nrd3024

Ralston, StuartH. (1987). THE PATHOGENESIS OF HUMORAL HYPERCALCAEMIA OF MALIGNANCY. *The Lancet*, *330*(8573), 1443–1446. https://doi.org/10.1016/S0140-6736(87)91139-1

Rasmussen, S. G. F., Choi, H.-J., Rosenbaum, D. M., Kobilka, T. S., Thian, F. S., Edwards, P. C., Burghammer, M., Ratnala, V. R. P., Sanishvili, R., Fischetti, R. F., Schertler, G. F. X., Weis, W. I., & Kobilka, B. K. (2007). Crystal structure of the human β2 adrenergic G-protein-coupled receptor. *Nature*, *450*(7168), 383–387. https://doi.org/10.1038/nature06325

Ravotto, L., Duffet, L., Zhou, X., Weber, B., & Patriarchi, T. (2022). *Frontiers | A Bright and Colorful Future for G-Protein Coupled Receptor Sensors | Cellular Neuroscience*. https://doi.org/10.3389/fncel.2020.00067

Reiter, E., Ahn, S., Shukla, A. K., & Lefkowitz, R. J. (2012). Molecular Mechanism of β-Arrestin-Biased Agonism at Seven-Transmembrane Receptors. *Annual Review of Pharmacology and Toxicology*, *52*(1), 179–197. https://doi.org/10.1146/annurev.pharmtox.010909.105800

Rodbell, M., Birnbaumer, L., Pohl, S. L., & Krans, H. M. J. (1971). The Glucagon-sensitive Adenyl Cyclase System in Plasma Membranes of Rat Liver. *Journal of Biological Chemistry*, *246*(6), 1877–1882. https://doi.org/10.1016/S0021-9258(18)62390-7

Rodriguez, E. A., Campbell, R. E., Lin, J. Y., Lin, M. Z., Miyawaki, A., Palmer, A. E., Shu, X., Zhang, J., & Tsien, R. Y. (2017). The Growing and Glowing Toolbox of Fluorescent and Photoactive Proteins. *Trends in Biochemical Sciences*, *42*(2), 111–129. https://doi.org/10.1016/j.tibs.2016.09.010

Rosenbaum, D. M., Rasmussen, S. G. F., & Kobilka, B. K. (2009). The structure and function of G-protein-coupled receptors. *Nature*, *459*(7245), 356–363. https://doi.org/10.1038/nature08144

Rosenblatt, M., Callahan, E. N., Mahaffey, J. E., Pont, A., & Potts, J. T. (1977). Parathyroid hormone inhibitors. Design, synthesis, and biologic evaluation of hormone analogues. *Journal of Biological Chemistry*, *252*(16), 5847–5851. https://doi.org/10.1016/S0021-9258(17)40100-1

Ross, E. M., & Gilman, A. G. (1977). Resolution of some components of adenylate cyclase necessary for catalytic activity. *Journal of Biological Chemistry*, *252*(20), 6966–6969. https://doi.org/10.1016/S0021-9258(19)66920-6

Roth, B. L., & Chuang, D. M. (1987). Multiple mechanisms of serotonergic signal transduction. *Life Sciences*, *41*(9), 1051–1064. https://doi.org/10.1016/0024-3205(87)90621-7

Sanni, S., Hansen, J., Bonde, M., Speerschneider, T., Christensen, G., Munk, S., Gammeltoft, S., & Hansen, J. (2010). β-Arrestin 1 and 2 stabilize the angiotensin II type I receptor in distinct high-affinity conformations. *British Journal of Pharmacology*, *161*(1), 150–161. https://doi.org/10.1111/j.1476-5381.2010.00875.x

Sarkar, K., Joedicke, L., Westwood, M., Burnley, R., Wright, M., McMillan, D., & Byrne, B. (2019). Modulation of PTH1R signaling by an ECD binding antibody results in inhibition of β-arrestin 2 coupling. *Scientific Reports*, *9*(1), 14432. https://doi.org/10.1038/s41598-019-51016-z

Sato, T., Verma, S., Khatri, A., Dean, T., Goransson, O., Gardella, T. J., & Wein, M. N. (2021). Comparable Initial Engagement of Intracellular Signaling Pathways by Parathyroid Hormone Receptor Ligands Teriparatide, Abaloparatide, and Long-Acting PTH. *JBMR Plus*, *5*(5), e10441. https://doi.org/10.1002/jbm4.10441

Schihada, H. (2018). Novel optical methods to monitor G-protein-coupled receptor activation in microtiter plates [Julius-Maximilians-Universität Würzburg]. In *Biomedicine: Vol. Doctoral*. https://drive.google.com/drive/u/0/search?q=thesis

Schihada, H. (2021). *Bioluminescence in G Protein-Coupled Receptors Drug Screening Using Nanoluciferase and Halo-Tag Technology | SpringerLink*. https://doi.org/10.1007/978-1-0716-1221-7_9

Schihada, H., Kowalski-Jahn, M., Turku, A., & Schulte, G. (2021). Deconvolution of WNT-induced Frizzled conformational dynamics with fluorescent biosensors. *Biosensors & Bioelectronics*, *177*. https://doi.org/10.1016/j.bios.2020.112948

Schihada, H., Ma, X., Zabel, U., Vischer, H. F., Schulte, G., Leurs, R., Pockes, S., & Lohse, M. J. (2020). *Development of a Conformational Histamine H3 Receptor Biosensor for the Synchronous Screening of Agonists and Inverse Agonists*. https://doi.org/10.1021/acssensors.0c00397

Schihada, H., Shekhani, R., & Schulte, G. (2021). Quantitative assessment of constitutive G protein–coupled receptor activity with BRET-based G protein biosensors. *Science Signaling*. https://doi.org/10.1126/scisignal.abf1653

Schihada, H., Vandenabeele, S., Zabel, U., Frank, M., Lohse, M. J., & Maiellaro, I. (2018). A universal bioluminescence resonance energy transfer sensor design enables high-sensitivity screening of GPCR activation dynamics. *Communications Biology*, *1*(1), 1–8. https://doi.org/10.1038/s42003-018-0072-0

Schipani, E., Endocrine Unit, D. of M. (E. S., J. H. ,. H. J.), Boston, Massachusetts 02114, Langman, C., the Division of Nephrology, C. M. H. (C. L.), Chicago, Illinois 60614, Hunzelman, J., Endocrine Unit, D. of M. (E. S., J. H. ,. H. J.), Boston, Massachusetts 02114, Le Merrer, M., Hôpital Necker Enfants Malades (M.L.M.), P., Cedex 18 75870, France, Loke, K. Y., the Department of Pediatrics, N. U. H. (K. Y. L.), Singapore 119074, Dillon, M. J., Great Ormond Street Hospital for Children (M.J.D.), L., United Kingdom WC1N 3JH, Silve, C., INSERM, U.-426, Faculté de Médicine, Xavier Bichat (C. S.), and INSERM U.-393, Jüppner, H., Endocrine Unit, D. of M. (E. S., J. H. ,. H. J.), Boston, Massachusetts 02114, & Children's Service (H.J.), M. G. H. and H.

M. S., Boston, Massachusetts 02114. (1999). A Novel Parathyroid Hormone (PTH)/PTH-Related Peptide Receptor Mutation in Jansen's Metaphyseal Chondrodysplasia. *The Journal of Clinical Endocrinology & Metabolism*, *84*(9), 3052–3057. https://doi.org/10.1210/jcem.84.9.6000

Schipani, E., Endocrine Unit (E.S., G. S. J., J. P. ,. T. J. G. ,. H. J.), Department of Medicine, Boston, Massachusetts 02114, Jensen, G. S., Endocrine Unit (E.S., G. S. J., J. P. ,. T. J. G. ,. H. J.), Department of Medicine, Boston, Massachusetts 02114, Pincus, J., Endocrine Unit (E.S., G. S. J., J. P. ,. T. J. G. ,. H. J.), Department of Medicine, Boston, Massachusetts 02114, Nissenson, R. A., Department of Medicine (R.A.N.), V. A. M. C. and U. of C., San Francisco, California 94121-1545, Gardella, T. J., Endocrine Unit (E.S., G. S. J., J. P. ,. T. J. G. ,. H. J.), Department of Medicine, Boston, Massachusetts 02114, Jüppner, H., Endocrine Unit (E.S., G. S. J., J. P. ,. T. J. G. ,. H. J.), Department of Medicine, Boston, Massachusetts 02114, & Children's Service (H.J.), M. G. H. and H. M. S., Boston, Massachusetts 02114. (1997). Constitutive Activation of the Cyclic Adenosine 3',5'-Monophosphate Signaling Pathway by Parathyroid Hormone (PTH)/PTH-Related Peptide Receptors Mutated at the Two Loci for Jansen's Metaphyseal Chondrodysplasia. *Molecular Endocrinology*, *11*(7), 851–858. https://doi.org/10.1210/mend.11.7.9934

Schipani, E., Kruse, K., & Jüppner, H. (1995). A Constitutively Active Mutant PTH-PTHrP Receptor in Jansen-Type Metaphyseal Chondrodysplasia. *Science*, *268*(5207), 98–100. https://doi.org/10.1126/science.7701349

Schipani, E., Langman, C. B., Parfitt, A. M., Jensen, G. S., Kikuchi, S., Kooh, S. W., Cole, W. G., & Jüppner, H. (2009). Constitutively Activated Receptors for Parathyroid Hormone and Parathyroid Hormone–Related Peptide in Jansen's Metaphyseal Chondrodysplasia. *Http://Dx.Doi.Org/10.1056/NEJM199609053351004*. https://www.nejm.org/doi/full/10.1056/NEJM199609053351004

Scholler, P., Moreno-Delgado, D., Lecat-Guillet, N., Doumazane, E., Monnier, C., Charrier-Savournin, F., Fabre, L., Chouvet, C., Soldevila, S., Lamarque, L., Donsimoni, G., Roux, T., Zwier, J. M., Trinquet, E., Rondard, P., & Pin, J.-P. (2017). HTS-compatible FRET-based conformational sensors clarify membrane receptor activation. *Nature Chemical Biology*, *13*(4), 372–380. https://doi.org/10.1038/nchembio.2286

Sekar, R. B., & Periasamy, A. (2003). Fluorescence resonance energy transfer (FRET) microscopy imaging of live cell protein localizations. *The Journal of Cell Biology*, *160*(5), 629–633. https://doi.org/10.1083/jcb.200210140

Sengupta, D., & Chattopadhyay, A. (2015). Molecular dynamics simulations of GPCR–cholesterol interaction: An emerging paradigm. *Biochimica et Biophysica Acta (BBA) - Biomembranes*, *1848*(9), 1775–1782. https://doi.org/10.1016/j.bbamem.2015.03.018

Serafin, D. S., Harris, N. R., Nielsen, N. R., Mackie, D. I., & Caron, K. M. (2020). Dawn of a New RAMPage. *Trends in Pharmacological Sciences*, S0165614720300237. https://doi.org/10.1016/j.tips.2020.01.009

Serfling, R., Seidel, L., Bock, A., Lohse, M. J., Annibale, P., & Coin, I. (2019). Quantitative single-residue bioorthogonal labeling of G protein-coupled receptors in live cells. *ACS Chemical Biology*, acschembio.8b01115. https://doi.org/10.1021/acschembio.8b01115

Shaner, N. C., Steinbach, P. A., & Tsien, R. Y. (2005). A guide to choosing fluorescent proteins. *Nature Methods*, *2*(12), 905–909. https://doi.org/10.1038/nmeth819

Shao, L., Chen, Y., Zhang, S., Zhang, Z., Cao, Y., Yang, D., & Wang, M.-W. (2021). Modulating effects of RAMPs on signaling profiles of the glucagon receptor family. *Acta Pharmaceutica Sinica B*. https://doi.org/10.1016/j.apsb.2021.07.028

Shenoy, S. K., Drake, M. T., Nelson, C. D., Houtz, D. A., Xiao, K., Madabushi, S., Reiter, E., Premont, R. T., Lichtarge, O., & Lefkowitz, R. J. (2006). β-Arrestin-dependent, G Protein-independent ERK1/2 Activation by the β2 Adrenergic Receptor*. *Journal of Biological Chemistry*, *281*(2), 1261–1273. https://doi.org/10.1074/jbc.M506576200

Shimada, M., Chen, X., Cvrk, T., Hilfiker, H., Parfenova, M., & Segre, G. V. (2002). Purification and characterization of a receptor for human parathyroid hormone and parathyroid hormone-related peptide. *The Journal of Biological Chemistry*, *277*(35), 31774–31780. https://doi.org/10.1074/jbc.M204166200

Shimizu, M., Joyashiki, E., Noda, H., Watanabe, T., Okazaki, M., Nagayasu, M., Adachi, K., Tamura, T., Potts, J. T., Gardella, T. J., & Kawabe, Y. (2016). Pharmacodynamic Actions of a Long-Acting PTH Analog (LA-PTH) in Thyroparathyroidectomized (TPTX) Rats and Normal Monkeys. *Journal of Bone and Mineral Research*, *31*(7), 1405–1412. https://doi.org/10.1002/jbmr.2811

Shukla, A. K., Manglik, A., Kruse, A. C., Xiao, K., Reis, R. I., Tseng, W.-C., Staus, D. P., Hilger, D., Uysal, S., Huang, L.-Y., Paduch, M., Tripathi-Shukla, P., Koide, A., Koide, S., Weis, W. I., Kossiakoff, A. A., Kobilka, B. K., & Lefkowitz, R. J. (2013). Structure of active β-arrestin-1 bound to a G-protein-coupled receptor phosphopeptide. *Nature*, *497*(7447), 137–141. https://doi.org/10.1038/nature12120

Shukla, A. K., Violin, J. D., Whalen, E. J., Gesty-Palmer, D., Shenoy, S. K., & Lefkowitz, R. J. (2008). Distinct conformational changes in β-arrestin report biased agonism at seven-transmembrane receptors. *Proceedings of the National Academy of Sciences*, *105*(29), 9988–9993. https://doi.org/10.1073/pnas.0804246105

Singh, A. T. K., Gilchrist, A., Voyno-Yasenetskaya, T., Radeff-Huang, J. M., & Stern, P. H. (2005a). Gα12/Gα13 Subunits of Heterotrimeric G Proteins Mediate Parathyroid Hormone Activation of Phospholipase D in UMR-106 Osteoblastic Cells. *Endocrinology*, *146*(5), 2171–2175. https://doi.org/10.1210/en.2004-1283

Singh, A. T. K., Gilchrist, A., Voyno-Yasenetskaya, T., Radeff-Huang, J. M., & Stern, P. H. (2005b). Gα12/Gα13 Subunits of Heterotrimeric G Proteins Mediate Parathyroid Hormone Activation of Phospholipase D in UMR-106 Osteoblastic Cells. *Endocrinology*, *146*(5), 2171–2175. https://doi.org/10.1210/en.2004-1283

Smith, J. S., Lefkowitz, R. J., & Rajagopal, S. (2018). Biased Signalling: From Simple Switches to Allosteric Microprocessors. *Nature Reviews. Drug Discovery*, *17*(4), 243–260. https://doi.org/10.1038/nrd.2017.229

Smrcka, A. V. (2008). G protein βγ subunits: Central mediators of G protein-coupled receptor signaling. *Cellular and Molecular Life Sciences*, *65*(14), 2191–2214. https://doi.org/10.1007/s00018-008-8006-5

Soave, M., Briddon, S. J., Hill, S. J., & Stoddart, L. A. (2020). Fluorescent ligands: Bringing light to emerging GPCR paradigms. *British Journal of Pharmacology*, *177*(5), 978–991. https://doi.org/10.1111/bph.14953

Soave, M., Stoddart, L. A., White, C. W., Kilpatrick, L. E., Goulding, J., Briddon, S. J., & Hill, S. J. (2021). Detection of genome-edited and endogenously expressed G protein-coupled receptors. *The FEBS Journal*, *288*(8), 2585–2601. https://doi.org/10.1111/febs.15729

Soki, F. N., Park, S. I., & McCauley, L. K. (2012). The multifaceted actions of PTHrP in skeletal metastasis. *Future Oncology*, *8*(7), 803–817. https://doi.org/10.2217/fon.12.76

Specht, E. A., Braselmann, E., & Palmer, A. E. (2017). A Critical and Comparative Review of Fluorescent Tools for Live-Cell Imaging. *Http://Dx.Doi.Org/10.1146/Annurev-Physiol-022516-034055*. https://doi.org/10.1146/annurev-physiol-022516-034055

Spongier, D., Waeber, C., Pantaloni, C., Holsboer, F., Bockaert, J., Seeburgt, P. H., & Journot, L. (1993). Differential signal transduction by five splice variants of the PACAP receptor. *Nature*, *365*(6442), 170–175. https://doi.org/10.1038/365170a0

Staus, D. P., Wingler, L. M., Choi, M., Pani, B., Manglik, A., Kruse, A. C., & Lefkowitz, R. J. (2018). Sortase ligation enables homogeneous GPCR phosphorylation to reveal diversity in β-arrestin coupling. *Proceedings of the National Academy of Sciences*, *115*(15), 3834–3839. https://doi.org/10.1073/pnas.1722336115

Sun, D., Fan, X., Shi, Y., Zhang, H., Huang, Z., Cheng, B., Tang, Q., Li, W., Zhu, Y., Bai, J., Liu, W., Li, Y., Wang, X., Lei, X., & Chen, X. (2020). Click-ExM enables expansion microscopy for all biomolecules. *Nature Methods*, *18*(1), 107–113. https://doi.org/10.1038/s41592-020-01005-2

Sungkaworn, T., Jobin, M.-L., Burnecki, K., Weron, A., Lohse, M. J., & Calebiro, D. (2017). Single-molecule imaging reveals receptor–G protein interactions at cell surface hot spots. *Nature*, *advance online publication*. https://doi.org/10.1038/nature24264

Sutkeviciute, I., Clark, L. J., White, A. D., Gardella, T. J., & Vilardaga, J.-P. (2019). PTH/PTHrP Receptor Signaling, Allostery, and Structures. *Trends in Endocrinology & Metabolism*, *30*(11), 860–874. https://doi.org/10.1016/j.tem.2019.07.011

Sutkeviciute, I., Lee, J. Y., White, A. D., Maria, C. S., Peña, K. A., Savransky, S., Doruker, P., Li, H., Lei, S., Kaynak, B., Tu, C., Clark, L. J., Sanker, S., Gardella, T. J., Chang, W., Bahar, I., & Vilardaga, J.-P. (2021). Precise druggability of the PTH type 1 receptor. *Nature Chemical Biology*, 1–9. https://doi.org/10.1038/s41589-021-00929-w

Sutkeviciute, I., & Vilardaga, J.-P. (2020). Structural insights into emergent signaling modes of G protein–coupled receptors. *Journal of Biological Chemistry*, *295*(33), 11626–11642. https://doi.org/10.1074/jbc.REV120.009348

Syme, C. A., Friedman, P. A., & Bisello, A. (2005). Parathyroid Hormone Receptor Trafficking Contributes to the Activation of Extracellular Signal-regulated Kinases but Is Not Required for Regulation of cAMP Signaling*. *Journal of Biological Chemistry*, *280*(12), 11281–11288. https://doi.org/10.1074/jbc.M413393200

Tang, X., Wang, Y., Li, D., Luo, J., & Liu, M. (2012). Orphan G protein-coupled receptors (GPCRs): Biological functions and potential drug targets. *Acta Pharmacologica Sinica*, *33*(3), 363–371. https://doi.org/10.1038/aps.2011.210

Tella, S. H., Kommalapati, A., & Correa, R. (n.d.). Profile of Abaloparatide and Its Potential in the Treatment of Postmenopausal Osteoporosis. *Cureus*, *9*(5), e1300. https://doi.org/10.7759/cureus.1300

Tesmer, V. M., Kawano, T., Shankaranarayanan, A., Kozasa, T., & Tesmer, J. J. G. (2005). Snapshot of Activated G Proteins at the Membrane: The Gαq-GRK2-Gßγ Complex. *Science*, *310*(5754), 1686–1690. https://doi.org/10.1126/science.1118890

Thomas, R. (2019). Development of novel positive cAMP FRET reporters. In *Department of Biotechnology: Vol. Master of Biotechnology*. University of Technology Berlin.

Thompson, M. D., Cole, D. E. C., Capra, V., Siminovitch, K. A., Rovati, G. E., Burnham, W. M., & Rana, B. K. (2014). Pharmacogenetics of the G Protein-Coupled Receptors. In Q. Yan (Ed.), *Pharmacogenomics in Drug Discovery and Development* (pp. 189–242). Springer. https://doi.org/10.1007/978-1-4939-0956-8_9

Thomsen, A. R. B., Plouffe, B., Cahill, T. J., Shukla, A. K., Tarrasch, J. T., Dosey, A. M., Kahsai, A. W., Strachan, R. T., Pani, B., Mahoney, J. P., Huang, L., Breton, B., Heydenreich, F. M., Sunahara, R. K., Skiniotis, G., Bouvier, M., & Lefkowitz, R. J. (2016). GPCR-G Protein-β-Arrestin Super-Complex Mediates Sustained G Protein Signaling. *Cell*, *166*(4), 907–919. https://doi.org/10.1016/j.cell.2016.07.004

Tilakaratne, N., Christopoulos, G., Zumpe, E. T., Foord, S. M., & Sexton, P. M. (2000). Amylin Receptor Phenotypes Derived from Human Calcitonin Receptor/RAMP Coexpression Exhibit Pharmacological Differences Dependent on Receptor Isoform and Host Cell Environment. *Journal of Pharmacology and Experimental Therapeutics*, *294*(1), 61–72.

Tobin, A. B. (2008). G-protein-coupled receptor phosphorylation: Where, when and by whom. *British Journal of Pharmacology*, *153*(S1), S167–S176. https://doi.org/10.1038/sj.bjp.0707662

Tobin, A. B., Butcher, A. J., & Kong, K. C. (2008). Location, location, location…site-specific GPCR phosphorylation offers a mechanism for cell-type-specific signalling. *Trends in Pharmacological Sciences*, *29*(8), 413–420. https://doi.org/10.1016/j.tips.2008.05.006

Tohgo, A., Choy, E. W., Gesty-Palmer, D., Pierce, K. L., Laporte, S., Oakley, R. H., Caron, M. G., Lefkowitz, R. J., & Luttrell, L. M. (2003). The Stability of the G Protein-coupled Receptor-β-Arrestin Interaction Determines the Mechanism and Functional Consequence of ERK Activation *. *Journal of Biological Chemistry*, *278*(8), 6258–6267. https://doi.org/10.1074/jbc.M212231200

Topaz, N., Mojib, N., Chande, A. T., Kubanek, J., & Jordan, I. K. (2017). RampDB: A web application and database for the exploration and prediction of receptor activity modifying protein interactions. *Database*, *2017*, bax067. https://doi.org/10.1093/database/bax067

Tunyasuvunakool, K., Adler, J., Wu, Z., Green, T., Zielinski, M., Žídek, A., Bridgland, A., Cowie, A., Meyer, C., Laydon, A., Velankar, S., Kleywegt, G. J., Bateman, A., Evans, R., Pritzel, A., Figurnov, M., Ronneberger, O., Bates, R., Kohl, S. A. A., … Hassabis, D. (2021). Highly accurate protein structure prediction for the human proteome. *Nature*, *596*(7873), 590–596. https://doi.org/10.1038/s41586-021-03828-1

Turku, A., Schihada, H., Kozielewicz, P., Bowin, C.-F., & Schulte, G. (2021). Residue 6.43 defines receptor function in class F GPCRs. *Nature Communications*, *12*(1), 3919. https://doi.org/10.1038/s41467-021-24004-z

Udawela, M., Christopoulos, G., Morfis, M., Christopoulos, A., Ye, S., Tilakaratne, N., & Sexton, P. M. (2006). A Critical Role for the Short Intracellular C Terminus in Receptor Activity-Modifying Protein Function. *Molecular Pharmacology*, *70*(5), 1750–1760. https://doi.org/10.1124/mol.106.024257

Udawela, M., Christopoulos, G., Morfis, M., Tilakaratne, N., Christopoulos, A., & Sexton, P. M. (2008). The effects of C-terminal truncation of receptor activity modifying proteins on the induction of amylin receptor phenotype from human CTb receptors. *Regulatory Peptides*, *145*(1), 65–71. https://doi.org/10.1016/j.regpep.2007.08.003

Uhlén, M., Fagerberg, L., Hallström, B. M., Lindskog, C., Oksvold, P., Mardinoglu, A., Sivertsson, Å., Kampf, C., Sjöstedt, E., Asplund, A., Olsson, I., Edlund, K., Lundberg, E., Navani, S., Szigyarto, C. A.-K., Odeberg, J., Djureinovic, D., Takanen, J. O., Hober, S., … Pontén, F. (2015). Tissue-based map of the human proteome. *Science*, *347*(6220), 1260419. https://doi.org/10.1126/science.1260419

Uhlen, M., Oksvold, P., Fagerberg, L., Lundberg, E., Jonasson, K., Forsberg, M., Zwahlen, M., Kampf, C., Wester, K., Hober, S., Wernerus, H., Björling, L., & Ponten, F. (2010). Towards a knowledge-based Human Protein Atlas. *Nature Biotechnology*, *28*(12), 1248–1250. https://doi.org/10.1038/nbt1210-1248

Urban, J. D., Clarke, W. P., Zastrow, M. von, Nichols, D. E., Kobilka, B., Weinstein, H., Javitch, J. A., Roth, B. L., Christopoulos, A., Sexton, P. M., Miller, K. J., Spedding, M., & Mailman, R. B. (2007). Functional Selectivity and Classical Concepts of Quantitative Pharmacology. *Journal of Pharmacology and Experimental Therapeutics*, *320*(1), 1–13. https://doi.org/10.1124/jpet.106.104463

Ureña, P., Kong, X. F., Abou-Samra, A. B., Jüppner, H., Kronenberg, H. M., Potts, J. T., Jr, & Segre, G. V. (1993). Parathyroid hormone (PTH)/PTH-related peptide receptor messenger ribonucleic acids are widely distributed in rat tissues. *Endocrinology*, *133*(2), 617–623. https://doi.org/10.1210/endo.133.2.8393771

Valli, J., Garcia-Burgos, A., Rooney, L. M., Vale de Melo e Oliveira, B., Duncan, R. R., & Rickman, C. (2021). Seeing beyond the limit: A guide to choosing the right super-resolution microscopy technique. *Journal of Biological Chemistry*, *297*(1), 100791. https://doi.org/10.1016/j.jbc.2021.100791

Varadi, M., Anyango, S., Deshpande, M., Nair, S., Natassia, C., Yordanova, G., Yuan, D., Stroe, O., Wood, G., Laydon, A., Žídek, A., Green, T., Tunyasuvunakool, K., Petersen, S., Jumper, J., Clancy, E., Green, R., Vora, A., Lutfi, M., … Velankar, S. (2022). AlphaFold Protein Structure Database: Massively expanding the structural coverage of protein-sequence space with high-accuracy models. *Nucleic Acids Research*, *50*(D1), D439–D444. https://doi.org/10.1093/nar/gkab1061

Varela, A., Chouinard, L., Lesage, E., Guldberg, R., Smith, S. Y., Kostenuik, P. J., & Hattersley, G. (2017). One year of abaloparatide, a selective peptide activator of the PTH1 receptor, increased bone mass and strength in ovariectomized rats. *Bone*, *95*, 143–150. https://doi.org/10.1016/j.bone.2016.11.027

Vázquez, R., Riveiro, M. E., Berenguer-Daizé, C., O'Kane, A., Gormley, J., Touzelet, O., Rezai, K., Bekradda, M., & Ouafik, L. (2021). Targeting Adrenomedullin in Oncology: A Feasible Strategy With Potential as Much More Than an Alternative Anti-Angiogenic Therapy. *Frontiers in Oncology*, *10*. https://www.frontiersin.org/article/10.3389/fonc.2020.589218

Venkatakrishnan, A. J., Deupi, X., Lebon, G., Heydenreich, F. M., Flock, T., Miljus, T., Balaji, S., Bouvier, M., Veprintsev, D. B., Tate, C. G., Schertler, G. F. X., & Babu, M. M. (2016). Diverse activation pathways in class A GPCRs converge near the G-protein-coupling region. *Nature*, *536*(7617), 484–487. https://doi.org/10.1038/nature19107

Vernall, A. J., Hill, S. J., & Kellam, B. (2014). The evolving small-molecule fluorescent-conjugate toolbox for Class A GPCRs. *British Journal of Pharmacology*, *171*(5), 1073–1084. https://doi.org/10.1111/bph.12265

Vilardaga, J.-P., Bünemann, M., Krasel, C., Castro, M., & Lohse, M. J. (2003a). Measurement of the millisecond activation switch of G protein–coupled receptors in living cells. *Nature Biotechnology*, *21*(7), 807–812. https://doi.org/10.1038/nbt838

Vilardaga, J.-P., Bünemann, M., Krasel, C., Castro, M., & Lohse, M. J. (2003b). Measurement of the millisecond activation switch of G protein–coupled receptors in living cells. *Nature Biotechnology*, *21*(7), 807–812. https://doi.org/10.1038/nbt838

Vilardaga, J.-P., Frank, M., Krasel, C., Dees, C., Nissenson, R. A., & Lohse, M. J. (2001). Differential Conformational Requirements for Activation of G Proteins and the Regulatory Proteins Arrestin and G Protein-coupled Receptor Kinase in the G Protein-coupled Receptor for Parathyroid Hormone (PTH)/PTH-related Protein. *Journal of Biological Chemistry*, *276*(36), 33435–33443. https://doi.org/10.1074/jbc.M011495200

Vilardaga, J.-P., Gardella, T. J., Wehbi, V. L., & Feinstein, T. N. (2012). Non-canonical signaling of the PTH receptor. *Trends in Pharmacological Sciences*, *33*(8), 423–431. https://doi.org/10.1016/j.tips.2012.05.004

Vilardaga, J.-P., Krasel, C., Chauvin, S., Bambino, T., Lohse, M. J., & Nissenson, R. A. (2002). Internalization Determinants of the Parathyroid Hormone Receptor Differentially Regulate β-Arrestin/Receptor Association *. *Journal of Biological Chemistry*, *277*(10), 8121–8129. https://doi.org/10.1074/jbc.M110433200

Vilardaga, J.-P., Nikolaev, V. O., Lorenz, K., Ferrandon, S., Zhuang, Z., & Lohse, M. J. (2008). Conformational cross-talk between α2A-adrenergic and μ-opioid receptors controls cell signaling. *Nature Chemical Biology*, *4*(2), 126–131. https://doi.org/10.1038/nchembio.64

Vilardaga, J.-P., Romero, G., Friedman, P. A., & Gardella, T. J. (2011). Molecular basis of parathyroid hormone receptor signaling and trafficking: A family B GPCR paradigm. *Cellular and Molecular Life Sciences : CMLS*, *68*(1), 1–13. https://doi.org/10.1007/s00018-010-0465-9

Wachten, S., Masada, N., Ayling, L.-J., Ciruela, A., Nikolaev, V. O., Lohse, M. J., & Cooper, D. M. F. (2010). Distinct pools of cAMP centre on different isoforms of adenylyl cyclase in pituitary-derived GH3B6 cells. *Journal of Cell Science*, *123*(1), 95–106. https://doi.org/10.1242/jcs.058594

Wan, J., Peng, W., Li, X., Qian, T., Song, K., Zeng, J., Deng, F., Hao, S., Feng, J., Zhang, P., Zhang, Y., Zou, J., Pan, S., Shin, M., Venton, B. J., Zhu, J. J., Jing, M., Xu, M., & Li, Y. (2021). A genetically encoded sensor for measuring serotonin dynamics. *Nature Neuroscience*, *24*(5), 746–752. https://doi.org/10.1038/s41593-021-00823-7

Wang, X., Cheng, X., Zhao, L., Wang, Y., Ye, C., Zou, X., Dai, A., Cong, Z., Chen, J., Zhou, Q., Xia, T., Jiang, H., Xu, H. E., Yang, D., & Wang, M.-W. (2021). *Molecular insights into differentiated ligand recognition of the human parathyroid hormone receptor 2*. https://doi.org/10.1073/pnas.2101279118

Wang, Y., & Townsend, P. D. (2012). Common mistakes in luminescence analysis. *Journal of Physics: Conference Series*, *398*, 012003. https://doi.org/10.1088/1742-6596/398/1/012003

Warne, T., Edwards, P. C., Doré, A. S., Leslie, A. G. W., & Tate, C. G. (2019). Molecular basis for high-affinity agonist binding in GPCRs. *Science*. https://doi.org/10.1126/science.aau5595

Weckmann, M. T., Gröne, A., Capen, C. C., & Rosol, T. J. (1997). Regulation of Parathyroid Hormone-Related Protein Secretion and mRNA Expression in Normal Human Keratinocytes and a Squamous Carcinoma Cell Line. *Experimental Cell Research*, *232*(1), 79–89. https://doi.org/10.1006/excr.1997.3481

Wehbi, V. L., Stevenson, H. P., Feinstein, T. N., Calero, G., Romero, G., & Vilardaga, J.-P. (2013). Noncanonical GPCR signaling arising from a PTH receptor–arrestin–Gβγ complex. *Proceedings of the National Academy of Sciences*, *110*(4), 1530–1535. https://doi.org/10.1073/pnas.1205756110

Weidler, M., Marx, U. C., Seidel, G., Schäfer, W., Hoffmann, E., Eßwein, A., & Rösch, P. (1999). The structure of human parathyroid hormone-related protein(1–34) in near-physiological solution. *FEBS Letters*, *444*(2–3), 239–244. https://doi.org/10.1016/S0014-5793(98)01658-5

Weis, W. I., & Kobilka, B. K. (2018). The Molecular Basis of G Protein–Coupled Receptor Activation. *Annual Review of Biochemistry*, *87*(1), 897–919. https://doi.org/10.1146/annurev-biochem-060614-033910

Westhuizen, E. T. van der, Valant, C., Sexton, P. M., & Christopoulos, A. (2015). Endogenous Allosteric Modulators of G Protein–Coupled Receptors. *Journal of Pharmacology and Experimental Therapeutics*, *353*(2), 246–260. https://doi.org/10.1124/jpet.114.221606

Weston, C., Lu, J., Li, N., Barkan, K., Richards, G. O., Roberts, D. J., Skerry, T. M., Poyner, D., Pardamwar, M., Reynolds, C. A., Dowell, S. J., Willars, G. B., & Ladds, G. (2015). Modulation of Glucagon Receptor Pharmacology by Receptor Activity-modifying Protein-2 (RAMP2)*. *Journal of Biological Chemistry*, *290*(38), 23009–23022. https://doi.org/10.1074/jbc.M114.624601

Whalen, E. J., Rajagopal, S., & Lefkowitz, R. J. (2011). Therapeutic potential of β-arrestin- and G protein-biased agonists. *Trends in Molecular Medicine*, *17*(3), 126–139. https://doi.org/10.1016/j.molmed.2010.11.004

White, A. D., Fang, F., Jean-Alphonse, F. G., Clark, L. J., An, H.-J., Liu, H., Zhao, Y., Reynolds, S. L., Lee, S., Xiao, K., Sutkeviciute, I., & Vilardaga, J.-P. (2019). Ca2+ allostery in PTH-receptor signaling. *Proceedings of the National Academy of Sciences*, 201814670. https://doi.org/10.1073/pnas.1814670116

White, A. D., Jean-Alphonse, F. G., Fang, F., Peña, K. A., Liu, S., König, G. M., Inoue, A., Aslanoglou, D., Gellman, S. H., Kostenis, E., Xiao, K., & Vilardaga, J.-P. (2020). Gq/11-dependent regulation of endosomal cAMP generation by parathyroid hormone class B GPCR. *Proceedings of the National Academy of Sciences*, *117*(13), 7455–7460. https://doi.org/10.1073/pnas.1918158117

White, A. D., Peña, K. A., Clark, L. J., Maria, C. S., Liu, S., Jean-Alphonse, F. G., Lee, J. Y., Lei, S., Cheng, Z., Tu, C.-L., Fang, F., Szeto, N., Gardella, T. J., Xiao, K., Gellman, S. H., Bahar, I., Sutkeviciute, I., Chang, W., & Vilardaga, J.-P. (2021). Spatial bias in cAMP generation determines biological responses to PTH type 1 receptor activation. *Science Signaling*. https://doi.org/10.1126/scisignal.abc5944

White, C. W., Caspar, B., Vanyai, H. K., Pfleger, K. D. G., & Hill, S. J. (2020). CRISPR-Mediated Protein Tagging with Nanoluciferase to Investigate Native Chemokine Receptor Function and Conformational Changes. *Cell Chemical Biology*, *27*(5), 499-510.e7. https://doi.org/10.1016/j.chembiol.2020.01.010

Wootten, D., Lindmark, H., Kadmiel, M., Willcockson, H., Caron, K., Barwell, J., Drmota, T., & Poyner, D. (2013). Receptor activity modifying proteins (RAMPs) interact with the VPAC2 receptor and CRF1 receptors and modulate their function. *British Journal of Pharmacology*, *168*(4), 822–834. https://doi.org/10.1111/j.1476-5381.2012.02202.x

Wright, S. C., Kozielewicz, P., Kowalski-Jahn, M., Petersen, J., Bowin, C.-F., Slodkowicz, G., Marti-Solano, M., Rodríguez, D., Hot, B., Okashah, N., Strakova, K., Valnohova, J., Babu, M. M., Lambert, N. A., Carlsson, J., & Schulte, G. (2019). A conserved molecular switch in Class F receptors regulates receptor activation and pathway selection. *Nature Communications*, *10*(1), 667. https://doi.org/10.1038/s41467-019-08630-2

Xiao, P., Guo, S., Wen, X., He, Q.-T., Lin, H., Huang, S.-M., Gou, L., Zhang, C., Yang, Z., Zhong, Y.-N., Yang, C.-C., Li, Y., Gong, Z., Tao, X.-N., Yang, Z.-S., Lu, Y., Li, S.-L., He, J.-Y., Wang, C., … Yu, X. (2022). Tethered peptide activation mechanism of the adhesion GPCRs ADGRG2 and ADGRG4. *Nature*, 1–8. https://doi.org/10.1038/s41586-022-04590-8

Xu, C., Peter, M., bouquier, nathalie, ollendorff, vincent, Villamil, I., Liu, J., Fagni, L., & Perroy, J. (2013). REV, A BRET-Based Sensor of ERK Activity. *Frontiers in Endocrinology*, *4*. https://www.frontiersin.org/article/10.3389/fendo.2013.00095

Yarwood, R. E., Imlach, W. L., Lieu, T., Veldhuis, N. A., Jensen, D. D., Herenbrink, C. K., Aurelio, L., Cai, Z., Christie, M. J., Poole, D. P., Porter, C. J. H., McLean, P., Hicks, G. A., Geppetti, P., Halls, M. L., Canals, M., & Bunnett, N. W. (2017). Endosomal signaling of the receptor for calcitonin gene-related peptide mediates pain

transmission. *Proceedings of the National Academy of Sciences*, *114*(46), 12309–12314. https://doi.org/10.1073/pnas.1706656114

Yin, Y., de Waal, P. W., He, Y., Zhao, L.-H., Yang, D., Cai, X., Jiang, Y., Melcher, K., Wang, M.-W., & Xu, H. E. (2017). Rearrangement of a polar core provides a conserved mechanism for constitutive activation of class B G protein-coupled receptors. *Journal of Biological Chemistry*, *292*(24), 9865–9881. https://doi.org/10.1074/jbc.M117.782987

Zacharias, D. A., Violin, J. D., Newton, A. C., & Tsien, R. Y. (2002). *Partitioning of Lipid-Modified Monomeric GFPs into Membrane Microdomains of Live Cells*. https://doi.org/10.1126/science.1068539

Zhang, J., Campbell, R. E., Ting, A. Y., & Tsien, R. Y. (2002). Creating new fluorescent probes for cell biology. *Nature Reviews Molecular Cell Biology*, *3*(12), 906–918. https://doi.org/10.1038/nrm976

Zhang, Q., Huang, H., Zhang, L., Wu, R., Chung, C.-I., Zhang, S.-Q., Torra, J., Schepis, A., Coughlin, S. R., Kornberg, T. B., & Shu, X. (2018). Visualizing Dynamics of Cell Signaling In Vivo with a Phase Separation-Based Kinase Reporter. *Molecular Cell*, *69*(2), 334-346.e4. https://doi.org/10.1016/j.molcel.2017.12.008

Zhao, L.-H., Ma, S., Sutkeviciute, I., Shen, D.-D., Zhou, X. E., Waal, P. W. de, Li, C.-Y., Kang, Y., Clark, L. J., Jean-Alphonse, F. G., White, A. D., Yang, D., Dai, A., Cai, X., Chen, J., Li, C., Jiang, Y., Watanabe, T., Gardella, T. J., … Zhang, Y. (2019). Structure and dynamics of the active human parathyroid hormone receptor-1. *Science*, *364*(6436), 148–153. https://doi.org/10.1126/science.aav7942

Zhao, P., Liang, Y.-L., Belousoff, M. J., Deganutti, G., Fletcher, M. M., Willard, F. S., Bell, M. G., Christe, M. E., Sloop, K. W., Inoue, A., Truong, T. T., Clydesdale, L., Furness, S. G. B., Christopoulos, A., Wang, M.-W., Miller, L. J., Reynolds, C. A., Danev, R., Sexton, P. M., & Wootten, D. (2020). Activation of the GLP-1 receptor by a non-peptidic agonist. *Nature*, *577*(7790), 432–436. https://doi.org/10.1038/s41586-019-1902-z

Zheng, M. H., McCaughan, H. B., Papadimitriou, J. M., Nicholson, G. C., & Wood, D. J. (1994). Tartrate resistant acid phosphatase activity in rat cultured osteoclasts is inhibited by a carboxyl terminal peptide (osteostatin) from parathyroid hormone-related protein. *Journal of Cellular Biochemistry*, *54*(2), 145–153. https://doi.org/10.1002/jcb.240540203

Zheng, Q., Ayala, A. X., Chung, I., Weigel, A. V., Ranjan, A., Falco, N., Grimm, J. B., Tkachuk, A. N., Wu, C., Lippincott-Schwartz, J., Singer, R. H., & Lavis, L. D. (2019). *Rational Design of Fluorogenic and Spontaneously Blinking Labels for Super-Resolution Imaging*. https://doi.org/10.1021/acscentsci.9b00676

Zhou, Q., Yang, D., Wu, M., Guo, Y., Guo, W., Zhong, L., Cai, X., Dai, A., Jang, W., Shakhnovich, E. I., Liu, Z.-J., Stevens, R. C., Lambert, N. A., Babu, M. M., Wang, M.-W., & Zhao, S. (2019). Common activation mechanism of class A GPCRs. *ELife*, *8*, e50279. https://doi.org/10.7554/eLife.50279

Zindel, D., Engel, S., Bottrill, A. R., Pin, J.-P., Prézeau, L., Tobin, A. B., Bünemann, M., Krasel, C., & Butcher, A. J. (2016). Identification of key phosphorylation sites in PTH1R that determine arrestin3 binding and fine-tune receptor signaling. *Biochemical Journal*, *473*(22), 4173–4192. https://doi.org/10.1042/BCJ20160740

CURRICULUM VITAE

ACKNOWLEDGEMENTS

I took up the challenge to pursue PhD in Biomedicine with my whole body and soul in late 2017. I subscribed to Nature and engaged in literature seminars to understand the scientific conception of the world, and went to as many conferences as possible to hear about the contemporary interpretations of pharmacology. I loved to philosophize about the hypotheses and predict unique molecular mechanisms to dissect novel roles in the molecular universe of GPCRs, which tried to explain the basis for a plethora of physiological processes. The fact that I was a rather short-distance runner needed to be readjusted for, so far, the longest project of my life. This marathon would not have been possible without the tremendous support of my supervisors, colleagues, family, and friends.

First, I would like to express my deepest gratitude to my primary supervisor Prof. Dr. Martin J. Lohse, for giving me an exceptional opportunity to conduct research under his supervision and complete my doctoral studies in his outstanding laboratory. His broad and profound knowledge of pharmacology, many years of expertise in the research environment, original ideas, and strategic planning contributed profoundly to the accomplishment of my project. I am grateful for his patience with me and, his ongoing enthusiasm, his support during manuscript preparation and submission. He granted me the opportunity of attending numerous conferences and foster collaborations, which contributed immensely to my knowledge about the field and increased my network inside the GPCR community. Sincere gratitude for his financial support in the last months of my doctorate.

Second, a huge thank you to my scientific mother, Dr. Isabella Maiellaro, for her enduring support in the challenging moments, her critical mind while evaluating the data, and her tolerance with wild me. From her I learned about rigorous experimental design, how to defend my data and present my results in the comprehensive and engaging way. She was always responsive and through numerous discussions contributed immensely to my scientific and personal growth.

I want to thank Prof. Dr. Manfred Schartl for being my second supervisor. His wide projection of my data during the committee meetings put my results in a broader perspective and inspired me to think outside the field. Moreover, his guidance was of great help in critically reassessing the experiments and defending them with scientific reasoning.

An extraordinary acknowledgment goes to my third supervisor, Prof. Dr. Kathleen Caron, one of the most significant people I met throughout my PhD. I genuinely admire her continuous encouragement and her insightful and field-relevant thoughts. Our discussions were extremely valuable for the success of some of the critical experiments. They helped to shape my understanding of the GPCR-RAMP universe, and finally, led to the decision that I continue research in the field.

Many thanks go to all the members of my lab family - AG Lohse/Receptor signaling lab, where I spent four and half years of vivid life. Life in the lab would be way more challenging without my lab sister, Dr. Selma Anton. She was an irreplaceable friend, who assisted with initial setup, showed me how to work efficiently, and, most importantly – helped to live in a testosterone-overloaded lab. Thanks for numerous scientific debates, personal reassessments, and shared adventures. Next, most sincere gratitude goes to my lab brothers Dr. Ali Isbilir, Dr. Hannes Schihada, Dr. Eugene Grushevskyi and Dr. Jan Möller. I will be eternally thankful for what was the most essential for my scientific growth during my doctoral studies - their unselfish advice and support with methodology, analysis, insights from the literature, critical thinking-activation, and all funny hours which we spent inside or outside of the lab. Thanks to Ali for his thoughtful ideas, infinite pieces of advice for experiments and numerous plasmids from his magic boxes. Thanks to Hannes, with whom I learned how to set up precise experiments, thanks for his ongoing support and all the decisive & enlightened debates we had. Thanks to Eugene for sharp suggestions based on his theoretical and practical expertise, and for showing me how to evaluate data and look at it from all possible angles. Thanks to Jan for numerous pragmatic advice, well-argument criticism, and sincere considerations of my work.

Furthermore, thanks to everybody in the lab, who created a good spirit and helped to overcome everyday struggles. Thanks to Dr. Andreas Bock and Dr. Paolo Annibale for helpful discussions during the lab meetings and navigating the AG Receptor signaling in the last two years. Thanks to our kind technicians, Bärbel Pohl, Marlies Grieben, Ruth Pareja, Nicole Grunert, and Victoria Prochnow, who often relieved my workload, which allowed me to focus on the actual experiments. Many thanks also to the other lab members; Philipp Gmach, Dr. Atakan Aydin, Dr. Charlotte Kayser, Romy Thomas, Lisa Martin, Iqra Sohail, Ziming Wang, Alexei Sirbu, Dr. Marc Bathe-Peter, Dr. Jean-Yves Tano, and all other friendly people who were guests in our lab in recent years.

There was also a branch of the lab in Würzburg, which was very helpful throughout my studies - thanks to Dr. Ulrike Zabel and Monika Frank for help with the cloning and Christine Salomon for her assistance in administrative matters.

In this place, I want to thank our collaborators and group members who facilitated materials & methods development, data collection, and thus contributed to the publication of my first paper: Dr. Hannes Schihada, Dr. Ulrike Zabel, Dr. Gunnar Kleinau, Dr. Eugene Grushevskyi, Dr. Patrick Scheerer.

Thanks to sci-hub, which enabled that knowledge was reachable. Big gratitude goes to the DAAD fellowship, which enabled my stay in Nottingham, and both graduate schools (MDC, GSLS) that facilitated my research ad study and participation in various courses. Thanks to Dr. Selma Anton, Dr. Katarina Stefanic, Melina Kraus, Dr. Russel Hodge, and Dr. Sergei Kobzak for proofreading parts of my thesis.

A sincere thanks to the people without whom this work would never have ended – to my family and friends. Although not physically present but of undeniable importance in this story were my parents. They deserve the most fundamental acknowledgment. From an early age, I inherited good working habits, a sense of helping people, and an appreciation of the sciences – my mother, was elementary in growing my awareness of mathematics, physics, logic, and my father of sociology, psychology, medicine, history, and geography. The broad range of disciplines appreciated in my surroundings, and my inceptive curiosity resulted in my interest in different subjects. Finally, I fell somewhere in the middle – towards the interdisciplinary pharmacy. Thanks to my unique brothers, Peter and Aleksander, which were irreplaceable comrades on the way to adulthood. They were brilliant companions, fantastic entertainers, and eloquent critics of my life path. Since recently, my life has been more vivid also because of my nephew Niko & sister-in-law Valentina. And thanks to my godmother Dr. Branislava Belović, which was my first scientific role model, entertaining educator, and lifelong family friend. Finally, thanks to my love and best friend Aleksandar for his support, patience, and tenderness, especially in the last phases of my doctoral studies.

There is a massive list of people who supported me during my PhD. My friends from home or abroad, from Murska Sobota, Ljubljana, Baška, and Berlin, from studies, exchanges, and adventures. I wouldn´t be here without you!

Neskončna hvala mojima dragima staršema ter bratoma Petru in Aleksandru, ki so verjeli vame.
Hvala vsem prijateljem od blizu in daleč, ki so mi pomagali prehoditi to pot.

Thank you!
Hvala!

"**Every science begins as philosophy and ends as art;**
it arises in hypothesis and flows into achievement."

William James Durant,
The Story of Philosophy